Multi-Section Mode-Locked Semiconductor Lasers

by

Dennis James Derickson

ECE Technical Report 92-13

Department of Electrical and Computer Engineering

University of California, Santa Barbara

July 31, 1992

University of California
Santa Barbara

Multi-Section Mode-Locked Semiconductor Lasers

A Dissertation submitted in partial satisfaction of the
requirements for the degree of

Doctor of Philosophy
in
Electrical and Computer Engineering
by

Dennis James Derickson

Committee in charge:

Professor John E. Bowers
Professor Larry A. Coldren
Professor Nadir Dagli
Professor Mark J. W. Rodwell

July 1992

The dissertation of Dennis James Derickson

is approved:

_____

_____

_____

_____

Committee Chairperson

July 1992

Multi-Section Mode-Locked Semiconductor Lasers

Electrical and Computer Engineering Department
University of California
Santa Barbara, CA 93106

July 30, 1992

Copyright © by
Dennis James Derickson
All rights reserved
1992

Acknowledgements

This dissertation on multi-section mode-locked semiconductor lasers has been aided by many people. John Bowers is the person behind the effort and has been very supportive technically and financially. Roger Helkey, Alan Mar, and Wenbin Jiang have given me ideas and direction since they are also working in the mode-locked semiconductor laser area. Judy Karin has been very helpful by providing photodetector calibrations and saturable absorber measurements for the mode-locking effort. Paul Humphrey has provided computer interface programs to take data from the measurement instrumentation. Tom Reynolds has been extremely helpful in producing laser coatings and for providing laboratory assistance. Radha Nagarajan, Jim Dudley, Yih Guei Wey, Pat Corvini, Gary Wang, and Dan Tauber are always willing to give advice on technical subjects. Thanks to Rajiv Ram and Dubravko Babic for help in understanding noise in semiconductor lasers.

Some of the biggest thanks goes to the people that have provided devices for this work. John Wasserbauer has been incredibly generous to me by working for hours on mask layout and device fabrication. Tawee Tanbun-Ek and co-workers at AT&T Bell Laboratories were very generous in supplying long wavelength material to our group. Thanks go to Robert Thornton at Xerox for providing me with the GaAs lasers that got the multi-section project started.

I wish to thank Al Goodman at the Office of Naval Research for supporting the project the last four years. Hewlett Packard Company provided financial support and sponsored my leave of absence for these four years.

I would finally like to thank Sara Derickson for help in preparation of this dissertation and for in general being such a nice person to be around.

To Sara Derickson

Vita

Dennis Derickson

July 17, 1959: Born, Westbrook, Minnesota.

May, 1981: B.S., Electrical Engineering, South Dakota State University. Brookings, South Dakota.

December, 1982: M.S., Electrical Engineering, University of Wisconsin, Madison, Wisconsin.

February, 1983-September, 1988: Member of Technical Staff, Hewlett Packard Co., Santa Rosa, CA.

Fall, 1988-Spring, 1992: Research Assistant, ECE Dept., University of California, Santa Barbara.

Publications

1. D. J. Derickson, R. J. Helkey, J. R. Karin, A. Mar, and J. E.Bowers, "Multi-segment mode-locked semiconductor lasers,",(invited paper) IEEE J. Quantum Electron. ,**QE-28**, 1992.

2. D. J. Derickson, R. J. Helkey, J. R. Karin, A. Mar, W. B. Jiang, and J. E. Bowers, "Mode-locked semiconductor lasers, short pulse small package!" Optical Society of America Optics and Photonics News, **3**, pp. 15-19, 1992.

3. D. J. Derickson, R. J. Helkey, A. Mar, J. E. Bowers, "Suppression of multiple pulse formation in external cavity mode-locked semiconductor lasers using intra-waveguide saturable absorbers", IEEE Photonics Technology Letters, **4**, pp. 333-335, 1992.

4. D. J. Derickson, J. G. Wasserbauer, R. J. Helkey, A. Mar, J. E. Bowers, "A comparison of colliding pulse and self-colliding pulse monolithic cavity mode-locked semiconductor lasers", Optical Fiber Conference, San Jose, CA., Paper ThB3, 1992.

5. D. J. Derickson, R.L. Thornton, J. E. Bowers "A comparison of timing jitter in external and monolithic cavity mode-locked semiconductor lasers", Applied Physics Letters, **59**,. pp. 3372-3374 , 1991.

6. D. J. Derickson , R. J. Helkey, A. Mar, J. E. Bowers, "Design of mult-element mode-locked semiconductor lasers with intra-waveguide saturable absorbers", 1992 OSA Integrated Photonics Research Topical Meeting, New Orleans, LA., Paper WC3, pp. 270-271, 1992.

7. D. J. Derickson, R. J. Helkey, A. Mar, J. E. Bowers, "Microwave and millimeter wave signal generation using mode-locked semiconductor lasers with intra-waveguide saturable absorbers", 1992 IEEE Microwave Theory and Technolgy Symposium, Albuquerque, NM, Paper V-2, pp. 753-756, 1992.

8. D. J. Derickson, R. J. Helkey, A. Mar, R.L. Thornton, and J. E. Bowers, "The benefits of intra-waveguide saturable absorbers in external cavity mode-locked semiconductor lasers", 1991 Optical Society of America Annual Meeting, San Jose, CA, Paper MG-5, pp.6, 1991.

9. D. J. Derickson, A. Mar, J. E. Bowers, " Absolute and residual timing jitter in actively mode-locked semiconductor lasers", 1990 International Semiconductor Conference, Davos, Switzerland, 1990.

10. D. J. Derickson, A. Mar, J. E. Bowers, "Residual and absolute timing jitter in actively mode-locked semiconductor lasers", Electronics Letters, **26**, pp. 2026-2027, 1990.

11. D. J. Derickson, R.S. Geels, G. Jia, R.L. Thornton, J. E. Bowers, "Monolithic cavity 0.85 μm mode-locked semiconductor lasers", 1991 Integrated Photonics Research Meeting, Monterey, CA., 1991.

12. D. J. Derickson, J. E. Bowers, R. L. Thornton, "Residual and absolute timing jitter in monolithic and external cavity mode-locked semiconductor lasers" (invited talk) 1991 High Speed, High Frequency Optoelectronics Engineering Foundation Conference, Palm Coast, FL., 1992.

13. D. J. Derickson, R. J. Helkey, A. Mar, P. A. Morton, J. E. Bowers, "Self mode-locking of a semiconductor laser using positive feedback", Applied Phyics Letters, **56** ,pp. 7-9, 1990.

14. D. J. Derickson, R. J. Helkey, A. Mar, J. E. Bowers " Self mode-locking of a semiconductor laser using positive feedback." 1989 LEOS annual meeting, Orlando, FL., 1989.

15. R. J. Helkey, D. J. Derickson, A. Mar, J. E. Bowers "Colliding Pulse effects in passively mode-locked semiconductor lasers" 1992 Conference on Lasers and Electrooptics, Anaheim, CA., Paper JThB2, 1992.

16. D. J. Derickson, C. M. Miller, R. L. Van Tuyl " A 22 GHz bandwidth instrumentation photoreceiver", 1988 International Microwave Symposium, New York, NY, Paper 00-1, pp. 1063-1066, 1988.

17. A. Mar, D. J. Derickson, R. J. Helkey, and J. E. Bowers, "1.4 ps pulses directly generated using a tandem-contact actively mode-locked 1.3 μm semiconductor laser", 1991 IEEE LEOS annual meeting1991, San Jose, CA., Paper SDL14.1, 1991.

18. J. E. Bowers, D. J. Derickson, A. Mar, P.A. Morton, and M. J. W. Rodwell, "Phase noise in actively mode-locked semiconductor lasers" Seventh International Conference on Integrated Optics and Optical Fiber Communications, Kobe, Japan, 1989.

19. P. A. Morton, J. E. Bowers, R. J. Helkey, and D. J. Derickson, "High Speed Lasers and applications in sub-picosecond mode-locking", 1989 LEOS annual meeting, Orlando, FL., 1989.

20. R.J. Simes, R.H. Ran, C.C. Barron, D.G. Lishan, J. Karin, L.A. Coldren, M. Rodwell, S. Elliot, D. J. Derickson, and B. Hughes, "High-frequency electrooptic Fabrey-Perot modulators", IEEE Photonics Technology Letters, 3, pp. 513-515, 1991.

21. S. Sloan, D. Braun, J. L. Russell, M. Zurakowski, M. Lightner, F. Kellert, G. Patterson, R. Koo, D. Derickson, and J. E. Bowers, " Efficient single-heterostructure AlGaAs/GaAs p-i-n photodiodes with 22 GHz bandwidth" , IEEE Trans. Electron Devices, pp. 1968, 1991.

Abstract

Multi-Section Mode-Locked Semiconductor Lasers

by

Dennis James Derickson

When the microwave community discusses broadband electrical amplifiers, they speak of devices with tens of GHz of bandwidth using MESFET or HEMT transistors. When the optical community discusses broadband optical amplifiers, they speak of semiconductor laser diode devices with *thousands* of GHz of bandwidth. This dissertation describes new methods to take advantage of the THz bandwidth in semiconductor laser amplifiers by mode-locking techniques. Mode-locked semiconductor lasers are devices that produce short optical pulses in which the pulsewidth is limited only by the tremendous bandwidth of the laser amplifiers.

This Dissertation focusses on advancements in the field of mode-locked semiconductor lasers that are the result of using laser diodes which use multiple pumping contacts instead of the single contact devices which were commonly used in previous research. With a multiple contact process, the functions of gain, gain modulation, saturable absorption, repetition rate tuning, and photodetection can be integrated together on a single monolithic chip. For repetition rates above 5 GHz (limited by fabrication technology), the entire optical cavity can be monolithically integrated together on a single chip forming a very compact source of optical pulses. The most important component in multiple segment mode-locked lasers is the saturable aborber. A large section of this dissertation is devoted to the study of the optimization of this component.

As a result of this work and that of others, the pulsewidths that are directly achievable from mode-locked lasers have dropped from 5-10 ps down to the 1-3 ps range. This will soon drop into the subpicosecond range as researchers develop phase compensation filters in the optical cavity. Mode-locked semiconductor lasers are becoming increasingly important for optical and optoelectronic applications. They will see widespread use in high-speed

telecommunications systems, optoelectronic measurement systems, microwave signal generation, and distribution applications.

This dissertation takes a very practical approach to the analysis and design of mode-locked lasers. The approach is to identify those characteristics which would be important to a designer who wants to incorporate a mode-locked laser into his system. The characteristics of amplitude noise, phase noise, pulsewidth, pulse energy, optical spectral width, and repetition rate tunability of the pulse streams are measured. These characteristics are then connected to the device design parameters of segment lengths, active region design, electrical parasitics, and waveguiding characteristics so that the optimal design can be obtained.

Table of Contents

1. Introduction. 1

1.1 Mode-locked semiconductor lasers and their applications. 1

1.2 Progress in mode-locked semiconductor lasers. 5

1.3 Organization of the following chapters. 11

2 External cavity mode-locked semiconductor lasers. 15

2.1 Active mode-locked single and two-section lasers. 15

2.2 Self mode locking of single section semiconducor lasers. 30

2.3 Passive mode locking with excitonic saturable absorbers. 39

2.4 Two-section passive mode locking with waveguide saturable absorbers. 53

2.5 Hybrid mode locking using two and three section designs. 75

3. Monolithic cavity mode-locked semiconductor lasers. 81

3.1 Device configurations. 81

3.2 Colliding pulse versus self-colliding pulse designs. 95

4. Comparison of device performance. 108

4.1 Pulsewidth. 108

4.2 Spectral width. 112

4.3 Pulse energy. 118

4.4 Repetition rate. 125

4.5 Phase and amplitude noise. 134

4.6 self-pulsation instabilities. 161

5. Optimization of multiple-segment designs. 165

5.1 Optimization parameters. 165

5.2 Model for analysis. 172

5.3 Pulse shortening in waveguide saturable absorbers. 184

5.4 Pulse shortening by active gain modulation. 203

5.5 Self phase modulation due to gain and absorption saturation. 216

5.6 Pulse widening in semiconductor laser amplifiers. 226

5.7 Laser structure design. 236

5.8 Limits on the achievable pulsewidth. 244

6. Analysis of timing jitter in mode-locked semiconductor lasers.

6.1 Introduction. 253

6.2 The noise sources responsible for timing jitter. 257

6.3 Noise source to timing jitter relationships. 267

6.4 Calculation of timing jitter from the noise source spectral densities and the sensitivity factors. 283

6.5 Results of the timing jitter and phase noise theory. 289

7. Future directions for the field and conclusions. 296

8. References. 303

List of Symbols

A	square root of power ($W^{0.5}$)
$A_{Cross\ Section}$	cross-sectional area (cm^2)
$A_{in}(t)$	input electric field ($W^{0.5}$)
$A_{in}(\omega)$	Fourier transform of $A_{in}(t)$
A_{out}	ouput electric field ($W^{0.5}$)
a	linewidth enhancement factor (unitless)
α	differential gain (cm^2)
α_{int}	internal waveguide loss (cm^{-1})
β_2	group velocity dispersion parameter ($s^2\ m^{-1}$)
β_{eff}	effective group velocity dispersion parameter ($s^2\ m^{-1}$)
B_o	optical bandwidth (Hz)
β_{sp}	fraction of spontaneous emission into lasing mode (unitless)
C	chirp parameter (s^{-2})
c	speed of light (m/s)
D_e	optical delay time (s)
D_o	electrical delay time (s)
d	T_o/t_2 time normalized to the bandwidth parameter (unitless)
$\Delta\lambda$	change in optical wavelength (cm^{-1})
δF_N	sinusoidal variation in the carrier number noise
δF_p	sinusoidal variation in the photon number noise
δF_ϕ	sinusoidal variation in the phase noise
δN	sinusoidal variation in the photon number
δP	sinusoidal variation in the photon number

δt	deviation in time (s)
$\delta \nu$	deviation in optical frequency from the gain maximum (Hz)
$\delta \phi$	sinusoidal variation in the phase (radians)
$\delta \phi_{max}$	maximum phase deviation (radians)
E	Energy (J)
E_{main}	energy of the main pulse (J)
$E_{out\ main}$	output energy for the main pulse (J)
$E_{out\ sec}$	output energy for the secondary pulse (J)
E_{pulse}	energy of the optical pulse (J)
E_{sat}	saturation energy (J)
E_{sec}	energy of the secondary pulse (J)
η	differential quantum efficiency (unitless)
η_{sp}	effective inversion factor (unitless)
F_N	carrier number noise source (s^{-1})
F_P	photon number noise source (s^{-1})
F_ϕ	phase noise source (s^{-1})
F^{-1}	inverse Fourier transform
f	frequency (Hz)
f_c	conduction band fermi function (unitless)
f_{cavity}	resonant frequency of the optical cavity (Hz)
f_{high}	upper frequency limit of integration (Hz)
f_{low}	lower limit of integration (Hz)
f_{mod}	modulation frequency (Hz)
f_{rep}	repetition frequency of the pulse stream (Hz)
f_v	valence band Fermi function (unitless)
Φ_{in}	input optical phase (radians)

Φ_{out}	output optical phase (radians)
G_e	energy gain (unitless)
G_n	differential gain coefficient (s^{-1})
G_o	unsaturated gain (unitless)
G_p	nonlinear gain coefficient (s^{-1})
G_{rt}	round trip energy gain for the main pulse (unitless)
G_{rts}	round trip energy gain for the secondary pulse (unitless)
G_1	first pass energy gain for the main pulse (unitless)
G_{1s}	first pass energy gain for the secondary pulse (unitless)
G_2	second pass energy gain for the main pulse (unitless)
G_{2s}	second pass energy gain for the secondary pulse (unitless)
g	gain coefficient (cm^{-1})
g'	gain coefficient including confinement factor (cm^{-1})
g_{goal}	achievable gain with no stimulated emission (cm^{-1})
$g(\omega)$	frequency dependence of the gain (cm^{-1})
g_p	peak gain (cm^{-1})
Γ_N	damping constant (Hz)
Γ_P	damping constant (Hz)
Γ_R	damping constant (Hz)
Γ_t	transverse confinement factor (unitless)
Γ_1	longitudinal fill fraction, gain to the total cavity length (unitless)
Γ_2	total confinement factor $\Gamma_1\Gamma_t$ (unitless)
γ	1/(photon lifetime) (s^{-1})
γ_e	1/(carrier lifetime) (s^{-1})
h	Planck's constant (J s)
h_a	height of the active region (μm)

h_{eff}	integrated gain factor (unitless)
I	optical intensity (W m^{-2})
I	pumping current (A)
I_o	pumping current at transparency (A)
K	Peterman K factor (unitless)
k_o	2π / (free space wavelength) (cm^{-1})
L	length parameter (cm)
L(f)	single sideband phase noise normalized to 1 Hz (dBc/Hz)
L_a	length of the absorber segment (cm)
L_g	length of the gain segment (cm)
L_m	length of the modulation segment (cm)
L_{seg}	length of a segment (cm)
λ	optical wavelength (cm)
M_{if}	momentum matrix element between state i and j
m	integer
N	carrier number
n	carrier density (cm^{-3})
n_g	group index of refraction
n_{in}	index of refraction
n_o	low intensity index of refraction
n_{tr}	carrier density at transparency (cm^{-3})
n_2	nonlinear index coefficient (cm^2/W)
ν	optical frequency (Hz)
O_{ea}	sensitivity factor (ps/J)
O_{ep}	sensitivity factor (ps/J)
O_{ga}	sensitivity factor (ps cm)

O_{gp}	sensitivity factor (ps cm)
O_{na}	sensitivity factor (ps/ps)
O_{np}	sensitivity factor (ps/ps)
Ω_R	relaxation resonance frequency (radians/s)
ω	optical frequency (radians/s)
ω_o	optical frequency at gain maximum (radians/s)
P	photon number
ρ_c	conduction band density of states (cm^{-3})
P_{in}	power input (W)
$P_{in\ eff}$	effective input noise power to an amplifier (W)
P_{noise}	noise power (W)
P_{out}	power output (W)
P_p	pulse position (s)
ρ_v	valence band density of states (cm^{-3}
Q	quality factor (unitless)
q	electronic charge (Coulombs)
$R_{\phi\phi}$	autocorrelation of phase noise source ($radians^2$)
R_{ext}	effective external cavity reflectivity (unitless)
R_{oe}	responsivity (A/W)
R_{NN}	autocorrelation of carrier number noise source
R_{PN}	crosscorrelation of photon number noise
R_{PP}	autocorrelation of photon number noise source
R_{sp}	spontaneous emission rate into the lasing mode
R_2	output facet power reflectivity (unitless)
S	photon density (cm^{-3})

S_{in}	spectral density of the index of refraction fluctuations (Hz^{-1})
$S_{\phi\phi}$	spectral density of the phase fluctuations (Hz^{-1})
S_N	spectral density of the carrier density flucturations (Hz^{-1})
S_{NN}	spectral density of the Langevin carrier noise source (Hz^{-1})
S_{PN}	cross spectral density (Hz^{-1})
S_P	spectral density of the photon fluctuations (Hz^{-1})
S_{PP}	spectral density of the photon Langevin noise source (Hz^{-1})
σ_x	generalized standard deviation value
T_{ab}	transmission through saturable absorber (unitless)
T_e	electrical pulsewidth (s)
T_o	optical pulsewidth (s)
T_{oab}	unsaturated transmission through saturable absorber
T_{rt}	round trip time in the laser cavity (s)
t	time (s)
t_{rt}	round trip time in the laser diode (s)
t_2	optical bandwidth parameter (s)
τ	time relative to the center of the optical pulse (s)
τ_{ab}	carrier lifetime in the saturable absorber (s)
τ_c	carrier lifetime (s)
U_{in}	energy factor (J)
V	volume of the active region (cm^3)
v_g	group velocity (m/s)
w_a	width of the active region (μm)
z	distance coordinate (cm)

Chapter 1
Introduction

1.1 Mode-locked semiconductor lasers and their applications

Researchers have long recognized the potential for short pulse generation using the semiconductor laser medium. Soon after room temperature CW operation in semiconductor lasers was obtained, the first reported mode-locking results occurred in the early 1970's [1]. Like dye lasers or Ti:Sapphire lasers, the gain-bandwidth of semiconductor lasers can span many THz, allowing the generation of femtosecond optical pulses. Because of their small size, electrical pumping convenience, and ease of use, they will supplant solid-state and dye lasers in many applications. With the use of semiconductor materials, mode locked lasers are now attractive for many applications which were previously not feasible or uneconomical. Semiconductor lasers interface well with high-speed electronics. Epitaxial growth technology using compound semiconductor materials allows emission wavelengths to be chosen from the infrared into the visible spectrum. Mode-locked semiconductor lasers can be integrated monolithically or hybridly together with electronic components resulting in small, easy to use sources. The repetition rates available from semiconductor lasers extend from rf to sub-millimeter wave frequencies. These devices can also be used as electronic signal sources because electrical signals are generated as a by-product of the optical pulse generation process. The design of the laser itself is also considerably simplified compared to other laser systems. Dye laser

systems require gain and saturable absorber dye jet hardware along with a cw or synchronous optical pumping source. With semiconductor lasers, the functions of the optical cavity, mirror, gain, saturable absorption, gain modulation, and wavelength tunability have been integrated together on a single monolithic chip that is only a few millimeters long. The major drawback of mode-locked semiconductor lasers is their moderate output power, however, the achievable power levels have been increasing with the use of semiconductor and fiber amplifiers. With the advent of erbium doped fiber amplifiers, power levels comparable to compressed YAG laser systems and dye laser systems are possible.

The small size, low power requirements, and ease of use of these multi-function devices allow the possibility of applications which would not be practical using other lasers. Figure 1.1 illustrates several of the important applications that make use of mode-locked semiconductor lasers (MLSL). In high speed optical fiber telecommunication systems, mode-locked semiconductor lasers are being used for systems using time division multiplexing as shown in Figure 1.1a. In the time-division multiplexing scheme, several mode-locked semiconductor lasers are driven from the same electronic source. The outputs from the three mode-locked lasers are thus synchronized with respect to each other. Because the optical pulses are short and controlled by a single electronic oscillator, many mode-locked laser pulse outputs can be interleaved together at multi-Gigabit/s data rates with very little timing jitter between adjacent pulse streams [2]. Information is then modulated onto the mode-locked bit stream with optical modulators and the bit streams are then interleaved allowing several low data rate channels to be combined into one multi-Gbit/s stream. The modulator and pulse source have also been combined

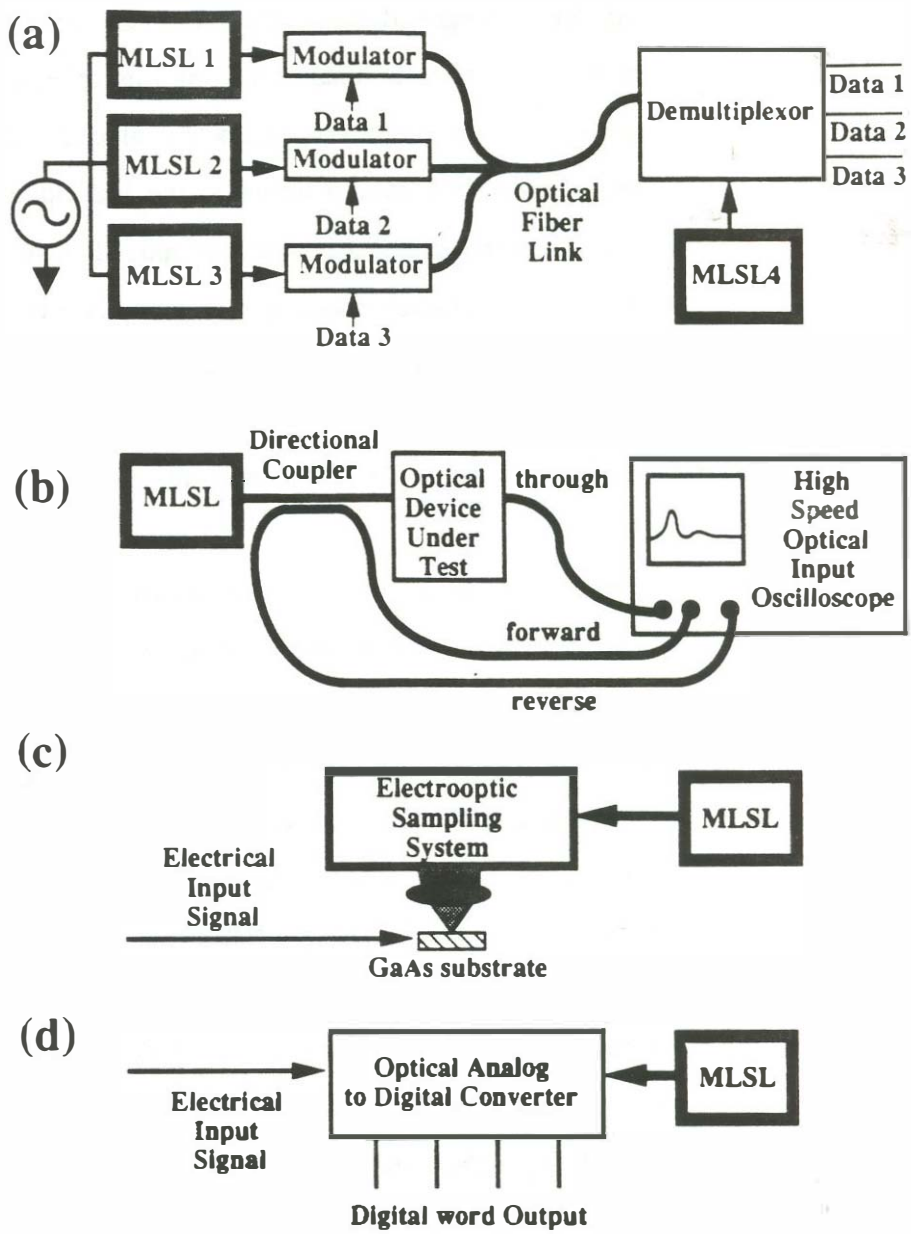

Figure 1.1 Application examples for mode-locked semiconductor lasers (MLSL). (a) Telecommunications system using time-division multiplexing. (b) Impulse response testing and high resolution optical time domain reflectometry. (c) Electro-optic sampling of electronic signals. (d) Analog to digital (A/D) conversion of electrical signals.

together to form a completely integrated transmitter. Andrekson et al. [3] have accomplished 64 Gbit/s communication channels using this scheme. At the receiving end of the system, mode-locked lasers are also useful in de-multiplexing the multi-Gbit/s data stream down to the individual slower channels. Mode-locked lasers are used as the source for optically driven optical switches. Optical demultiplexing switches have been accomplished using non-linear loop fiber mirrors [4], four-wave mixing in optical fibers [5] and gain saturation effects in semiconductor amplifiers [6]. Mode-locked semiconductor lasers are also convenient pulse sources for soliton transmission in optical fibers [7].

Mode-locked optical pulse sources are useful in optoelectronic measurement systems. Impulse response testing of photodetectors and optical to electrical converters with short optical pulses allows the magnitude and phase response of the system to be measured (Figure 1.1b). Since pulses as short as 1 ps have been directly generated using semiconductor lasers, the bandwidth from the pulses is much wider than most commonly available photoreceivers. The impulses can also be used for high resolution optical time domain reflectometry with better than 1 mm resolution.

Electrooptic sampling of electronic signals has been demonstrated using semiconductor lasers instead of a YAG laser source with fiber and pulse compressor [8] (Figure 1.1b). The semiconductor laser is much more stable than a compressed YAG laser. The YAG laser depends on the nonlinearity in an optical fiber to generate sufficient bandwidth for short pulse operation. Small changes in the power to the fiber result in dramatic changes in the compressed pulse shape. In semiconductor lasers, the devices have sufficient bandwidth to directly generate stable picosecond pulses. Helkey et al. have

demonstrated 0.5 ps pulses using a compressed semiconductor laser pulse [9]. The compressed output of the semiconductor laser is much more stable than the output of a compressed YAG laser because the compressor for the semiconductor laser consists of only a diffraction grating pair and doesn't require the fiber non-linearity.

Electrical input analog to digital (A/D) converters with ps time resolution have been demonstrated using optical sampling pulses from mode-locked semiconductor lasers (Figure 1.1d) [10]. Since mode-locked semiconductor lasers can achieve 1-3 ps pulses routinely at very high repetition rates, the digitization rate of optically based A/D converters exceeds that of all electronic A/D converters. There are a host of other applications for mode-locked semiconductor lasers such as gyroscopes [11], optical computing [12], and sensor applications.

1.2 Progress in mode-locked semiconductor lasers

1.2.1 Single pumping contact structures

There are many techniques that can be used to induce short pulse generation in semiconductor lasers. This dissertation focuses on active, passive, and hybrid active-passive mode-locking techniques. Early experiments with mode-locked semiconductor lasers involved anti-reflection coating one facet of a single-section semiconductor laser and coupling it into an external cavity as is shown in Figure 1.2. The external cavity contains a focussing lens, a mirror, and possibly a wavelength control filter to provide optical feedback. The device is then actively mode-locked by applying a repetitive electrical pulse stream with a period nearly equal to the round trip time in the entire laser cavity. Each time

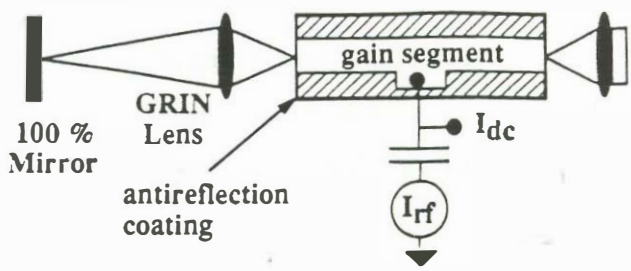

Figure 1.2 The cavity configuration used for *active* mode-locking of an *external* cavity single contact semiconductor laser. The laser diode is driven by electrical pulses which have a period nearly equal to the roundtrip time of the laser cavity.

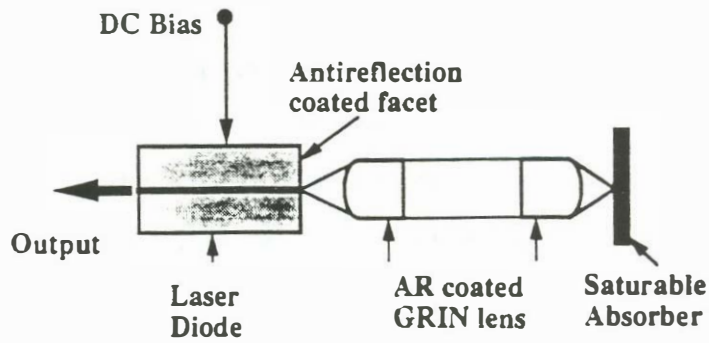

Figure 1.3 An example of an *external* cavity *passive* mode-locked semiconductor laser. In passive mode-locking, only DC bias currents are required for the semiconductor laser to produce short optical pulses. The key component in passive mode-locking is the saturable absorber. The saturable absorber is a non-linear element that selectively passes high intensity portions of an optical pulse.

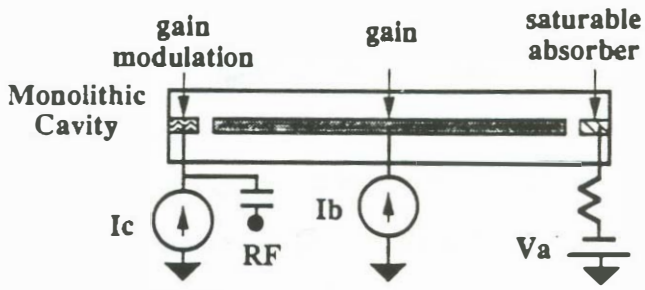

Figure 1.4 An example of a *monolithic* cavity *hybrid* mode-locked semiconductor laser using multiple top-contacts. The left hand segment is used for gain modulation. The center section is for providing the overall gain for the laser. The right hand segment is a waveguide saturable absorber.

an optical pulse enters the laser diode from the external cavity, the electrical pump signal increases the gain in the device, shortening the width of the optical pulse. In order to get very short optical pulses from the device, the electrical modulation pulses driving the laser must be narrow and of large amplitude in order to create a very short time window of net gain in the device. The laser must also have small electrical parasitics so that the high frequency content of the electrical pulse is not attenuated. Early attempts at single-section passive mode-locking produced optical pulsewidths in the 5-30 ps range [13,14,15]. The first sub-picosecond pulses generated by active mode-locking used a 27 dBm sinusoidal signal at a frequency of 16 GHz [16]. The first key to the success of the experiment of Reference 16 was the low parasitic laser structure that had a capacitance of 1 pF and a parasitic resistance of 5 Ω allowing for efficient high-frequency modulation of the gain. The second key to success of the experiment was the use of very short electrical modulation pulses (a 16 GHz sinusoid). **The drawback of this single section experiment was that although sub-picosecond pulses were formed, multiple pulses spaced at the round trip time of the laser diode were also generated.** Although the individual pulses obtained from this experiment were short, multiple pulses are usually a problem in practical applications of mode-locked semiconductor lasers. These secondary pulse outputs from the mode-locked laser are initiated by the imperfect anti-reflection coating on the laser diode and are amplified over many round trips to have an energy that is significant compared to the main pulse. Simulations have shown that reflection coefficients as small as 10^{-5} can cause multiple pulse formation in single segment external cavity lasers [17]. **A major thrust of this dissertation**

is to obtain *single* short pulses instead of the multiple short pulses produced in earlier experiments.

Passive mode-locking techniques are commonly used in many laser systems to generate short optical pulses. Figure 1.3 illustrates a typical configuration used to accomplish passive mode-locking. The key component necessary for passive mode-locking is a suitable saturable absorber. The saturable absorbers used in most semiconductor laser systems are called slow saturable absorbers [18]. This means that the leading edge of the optical pulse is absorbed and the trailing edge of the optical pulse is unattenuated during the passage of the optical pulse through the saturable absorber. Slow saturable absorption works in conjunction with gain saturation during the trailing edge of the optical pulse leading to a net pulsewidth narrowing on each transit around the mode-locked laser cavity. For successful passive mode-locking, the energy required to saturate the saturable absorber must be lower than the pulse energy that is available from the gain medium. Suitable saturable absorbers can be made with semiconductor laser materials. The saturation energy of semiconductor saturable absorbers can be small due to the higher differential gain in a low carrier density saturable absorber region as compared with the lower differential gain in the high carrier density gain regions [19]. The reduction in differential gain with increased carrier density can be particularly large in quantum well lasers.

The saturable absorber must also recover to its original large value of absorption very quickly after the passage of the optical pulse. The absorption recovery time due to spontaneous emission recombination, typically 1 ns, is too long for effective absorption recovery in semiconductor materials. This has

led researchers to introduce damage into the material in order to decrease the nonradiative lifetime of the material. Proton and nitrogen bombardment of laser diode facets have been successful in producing passive mode-locking results [20,21]. A disadvantage of these techniques which rely on damage to the active region is the questionable long-term reliability of the damage centers under high photon density conditions. Saturable absorbers using the excitonic absorption feature of multi-quantum well samples along with proton bombardment have also been used to achieve passive mode-locking [22]. Single pulses in the 5 ps range have been generated using the excitonic saturable absorber technique.

1.2.2 Multiple pumping contact structures

In 1983, Harder et al. introduced a technique of non-uniform current injection to produce passive mode-locking [23]. In Harder's experiment, the top pumping contact was separated so that different forward bias currents could be applied to each segment. Harder et al. produced 30 ps wide pulses using this technique. Several years later (1987-89), the concept of two-segment passive mode-locking was improved by shortening the length of one segment and introducing reverse bias to form a waveguide photodetector-saturable absorber segment [24-27].

This dissertation extends the work of researchers using reverse-biased sections. Multi-segment structures have been fabricated, tested, and analyzed to get the best performance from the semiconductor laser. The dissertation introduces new functionality that is available from two, three, and four segment mode-locked laser and amplifier structures.

The external cavity structures that have been discussed so far must be constructed on stable bases and considerable mechanical engineering has to be accomplished in order to obtain a device that performs well against temperature, shock, and vibration. The cost for external cavity devices will always be relatively high thereby limiting the applicability to low volume, relatively high cost applications. The disadvantage of external cavities can be addressed with the use of multi-segment monolithic cavity devices such as that shown in Figure 1.4. Monolithic cavities offer advantages in ease of use, compactness, and mechanical stability. Monolithic cavity devices are limited in their lowest possible repetition rate since they are fabricated from a single semiconductor die. The first reported monolithic cavity device was published by Tucker [28]. The device had a repetition rate of 40 GHz, was actively mode-locked, and produced a pulsewidth of 4 ps. Morton et al. produced pulses in the 3-5 ps range using a two-section active mode-locked laser at 15 GHz [24]. Sanders et al. reported the first passive mode-locking of a monolithic cavity device with repetition rates as high as 108 GHz [29]. Y. K. Chen, M. C. Wu et al. produced pulses as short as 0.6 ps using a colliding pulse linear cavity geometry [30]. **This dissertation also concentrates on the optimization of these monolithic cavity devices and the operation of the devices down to lower repetition rates that are required for most applications.**

Figure 1.5 shows examples of the multiple-segment designs that have been produced for the research presented in this dissertation. Devices have been fabricated and tested at the three important optical fiber communication wavelengths of 0.85 μm, 1.3 μm, and 1.55 μm. With a simple laser process, many types of multi-segment devices can be fabricated. The main focus of this

work is on external and monolithic cavity mode-locked lasers. Other devices such as gain switched lasers, Q-switched lasers, superluminescent light emitting diodes, waveguide photodetectors, pre-amplified waveguide photodetectors, and optimized optical pulse amplifiers are also addressed.

1.3 Organization of the following chapters

This dissertation starts out discussing the experimental results that have been obtained using the multiple-segment structures. In Chapter 2 external cavity devices are discussed starting with an explanation of single-section semiconductor laser mode-locking techniques. The problems with single-section lasers are illustrated and the following sections of the chapter demonstrate how many of the single section limitations can be overcome.

Chapter 3 discusses the monolithic cavity devices that overcome the mechanical problems associated with external cavities. The chapter outlines typical performance characteristics and geometries which produce the best mode-locking performance.

Chapter 4 examines the pulse characteristics that are important for a designer who may wish to incorporate a mode-locked laser into his system. A comparison of pulsewidth, spectral width, pulse energy, repetition rate, and noise is undertaken for both monolithic and external cavity devices.

Chapter 5 analyzes the pulse formation process in multi-segment mode-locked lasers. The goal of the section is to understand why mode-locked semiconductor lasers typically achieve pulsewidths in the 1-3 ps range instead of the < 0.1 ps range. The strength of the pulse shortening mechanisms and the

pulse widening mechanisms that determine the achievable pulsewidth are examined. It will be found that the linewidth enhancement factor is a very important parameter in mode-locked semiconductor lasers.

Chapter 6 discusses the origin of timing jitter in multi-segment mode-locked lasers. The extensive experimental comparison of the jitter properties given in Chapter 4 can be understood using this theory. Spontaneous emission and its effect on gain, pulse energy, and the index of refraction is used to explain the timing jitter differences for the various mode-locking techniques.

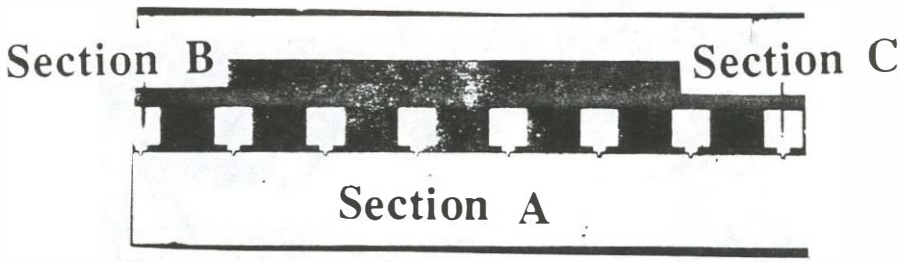

(a)

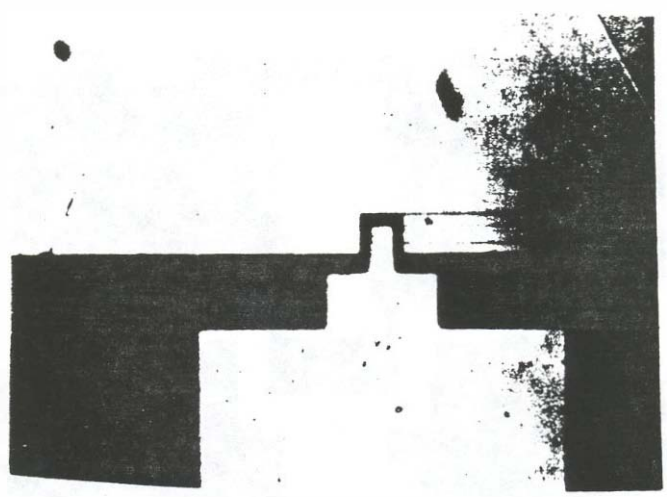

(b)

Figure 1.5 (a) A three section 0.85 μm monolithic cavity mode-locked laser with gain segment A, gain modulation segment B, and saturable absorber segment, C. The basic laser structure design is such that a short segment is introduced every 250 μm. This allows monolithic and external cavity designs to be cleaved from the same wafer. (b) A close up of the short saturable absorber or gain modulation segment is shown. Saturable absorber lengths of 4 μm, 8 μm, and 16 μm were fabricated. The area between contacts has been proton bombarded to increase inter-contact resistance to MΩ levels.

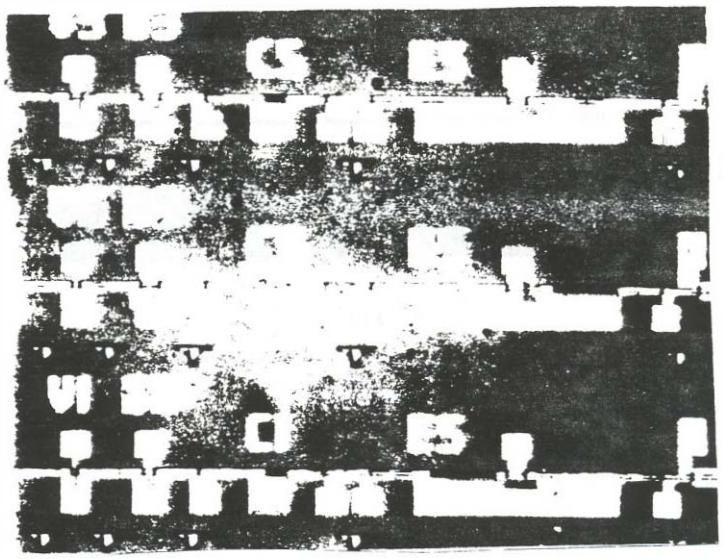

(c)

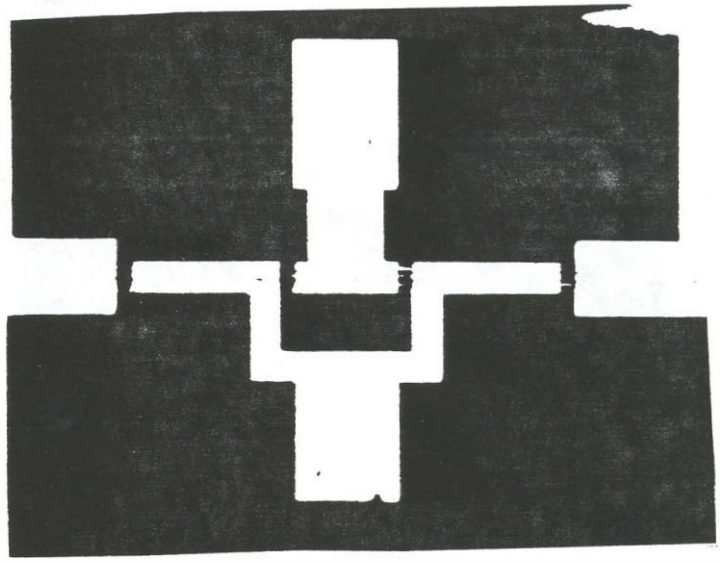

(d)

Figure 1.5 (c) An example 1.55 μm mode-locked laser design. The basic laser process is a semi-insulating re-grown buried heterostructure process. Etched cleave marks have been incorporated to give accurate cleave locations. (d) This is a close-up of a colliding pulse geometry saturable absorber and the adjacent gain modulation segment.

Chapter 2
External cavity mode-locked lasers

2.1 Active mode-locking of single-section and two-section external cavity semiconductor lasers

2.1.1 Single section actively mode-locked external cavity lasers

This section describes the simplest and most commonly used technique to mode-lock semiconductor lasers. Figure 2.1 shows the experimental configuration that was used to actively mode-lock a single-segment semiconductor laser in an external cavity. One facet of the laser is anti-reflection coated and coupled into an external cavity with a 0.22 pitch graded index lens. The light from the antireflection coated facet is either collimated or focussed onto an external mirror. The collimated case has the advantage of simple cavity length adjustments with a linear translation stage. The focussed or "cat's eye" configuration is less sensitive to angular rotation of the mirror and provides a more stable cavity against positional fluctuations of the external cavity.

Active mode-locking is accomplished by modulating the gain of the semiconductor laser with an electrical pulse stream having a period nearly equal to the round trip time in laser cavity. In order to obtain short optical pulses from active mode-locked semiconductor lasers, it is important to use short electrical modulation pulsewidths. The short electrical pulses form a narrow time window of net gain in the device that narrows the optical pulse on each pass through the laser diode. The width and amplitude of the modulation

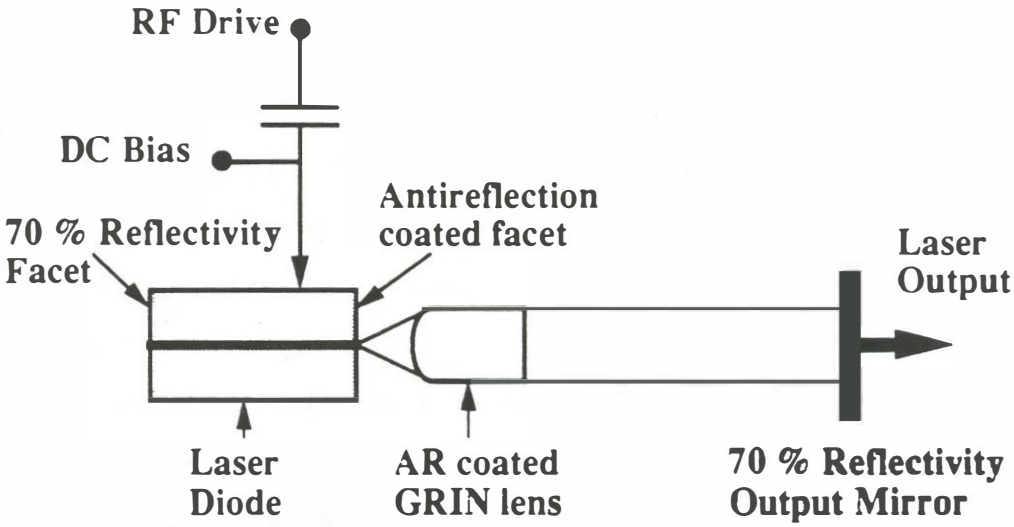

Figure 2.1 The simplest configuration for mode-locking a semiconductor laser. A single section laser is coated on one facet and coupled to an external cavity. A graded index (GRIN) lens is used to collimate the light onto a mirror. The output can be taken through the mirror or through the laser facet. The device is active mode-locked by applying electrical modulation pulses with a period nearly equal to the round trip time in the external cavity laser.

current determines how much narrowing the optical pulse receives on each pass through the laser. At high frequencies (> 5 GHz) ,sinusoids can be used as the active modulation signal since only the positive portion of the sinusoid causes forward conduction in the laser diode [16]. At lower repetition rates, step recovery diodes can provide electrical pulsewidths as narrow as 30 ps [31]. Recently, non-linear transmission line circuits have produced even shorter (<10 ps) high amplitude pulses [32]. State of the art semiconductor lasers have electrical parasitic corner frequencies on the order of 20 GHz. Electrical modulation pulses shorter than about 20 ps due not improve the active gain modulation effectiveness due to the low-pass filter operation of the device parasitics.

The optical pulsewidth decreases on each pass until the optical pulse becomes very much narrower than the electrical modulation pulse. The amount of pulsewidth narrowing on each pass decreases as the width of the optical pulse becomes very much narrower than the electrical modulation pulse. The final pulsewidth is obtained when pulse broadening effects in the gain medium equal the pulsewidth narrowing effects due to active gain modulation and the pulse reproduces itself on each round trip. Ideally, this final pulsewidth would reach sub-picosecond levels since the gain bandwidth of semiconductor lasers can be many THz.

Single-section active mode-locked lasers, at present, have achieved ***single*** optical pulsewidths of 4 ps [33] and sub-picosecond pulse bursts with an over-all envelope width of 7 ps [16]. There are several reasons why single sub-picosecond widths have not been achieved in single-section active mode-locked lasers.

Imperfect anti-reflection coatings applied to the semiconductor laser diode

facet can have a detrimental effect on the performance of single-section actively mode-locked lasers. The effects of imperfect antireflection coatings manifest themselves by the situation of mode-locking in clusters and by multiple pulse generation from the laser. Single layer anti-reflection coating values of 10^{-4} are obtainable if the index of refraction can be held to within 0.02 of the target index value. Even with this tight control of index, the effects of imperfect antireflection coatings are still very important.

2.1.1a Mode-locking in clusters

Figure 2.2 illustrates the concept of mode-locking in clusters. In the case of perfect anti-reflection coatings, the gain medium displays a broad gain versus wavelength function for entering optical pulses. If the antireflection coating is poor, reflections between the front and back facets of the laser diode cause a ripple in the effective gain versus wavelength function. The mode-locked laser cavity is now a coupled cavity laser. The ripple frequency spacing is equal to 1 over the round trip time in the laser diode. The set of longitudinal modes found within one ripple is referred to as a cluster of modes. In mode-locking in clusters, the longitudinal mode phases within each cluster of modes lock together, but the phases between each of the clusters do not lock together. This situation results in having several different phase locked optical pulses overlapped in time (by associating a mode-locked pulse with each cluster) with the phase relationship between the pulses slowly wandering in time. The pulses are relatively broad with a pulsewidth determined by the narrow bandwidth of the cluster and not the over-all wide bandwidth of the semiconductor laser. The resultant pulses have considerable temporal sub-structure. If an infinite bandwidth oscilloscope could time resolve the optical pulses individually, there

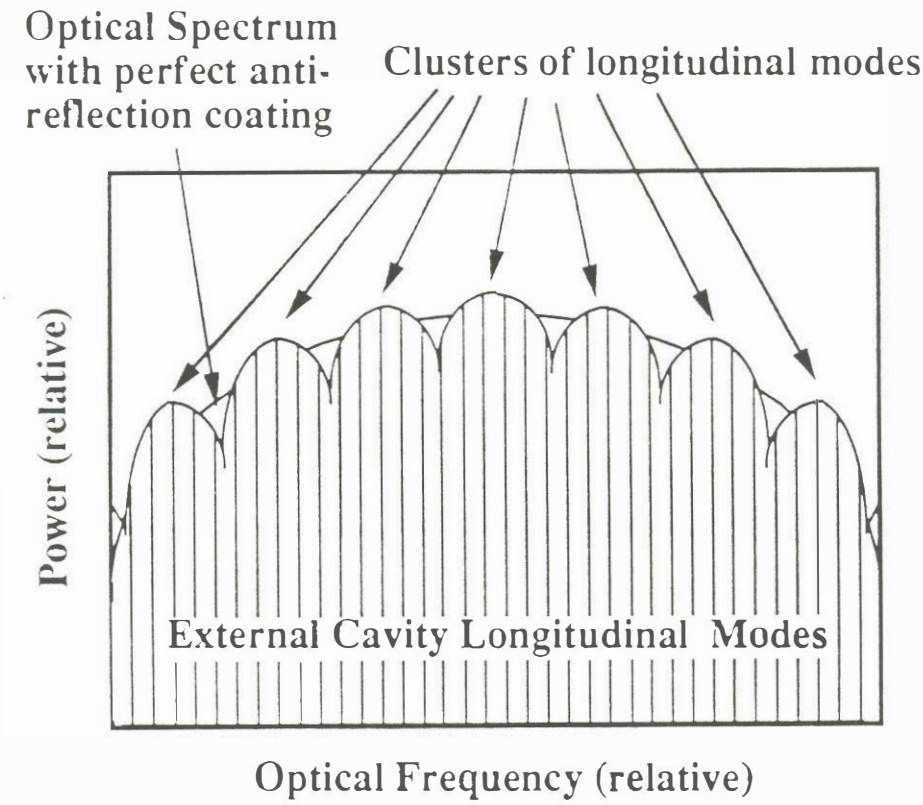

Figure 2.2 This figure illustrates the concept of mode-locking in clusters. The figure plots power versus frequency for a hypothetical mode-locked laser. The smooth line shows what the envelope of the optical spectrum should look like if there were a perfect antireflection coating on the laser diode facet. If the antireflection coating is not perfect, a ripple occurs in the optical spectrum. The frequency spacing of the ripple is $1/t_{rt}$. A cluster of modes is the group of external cavity modes that are associated with one ripple. When a laser is mode-locked in clusters, the phases within one cluster are locked together but the phases between the clusters may be slowly wandering in time. Pulses which are mode-locked in clusters have considerable pulse sub-structure. Substructure means that the pulses do not have a smooth envelope and have very fast ripples in time (on the sub-picosecond time scale).

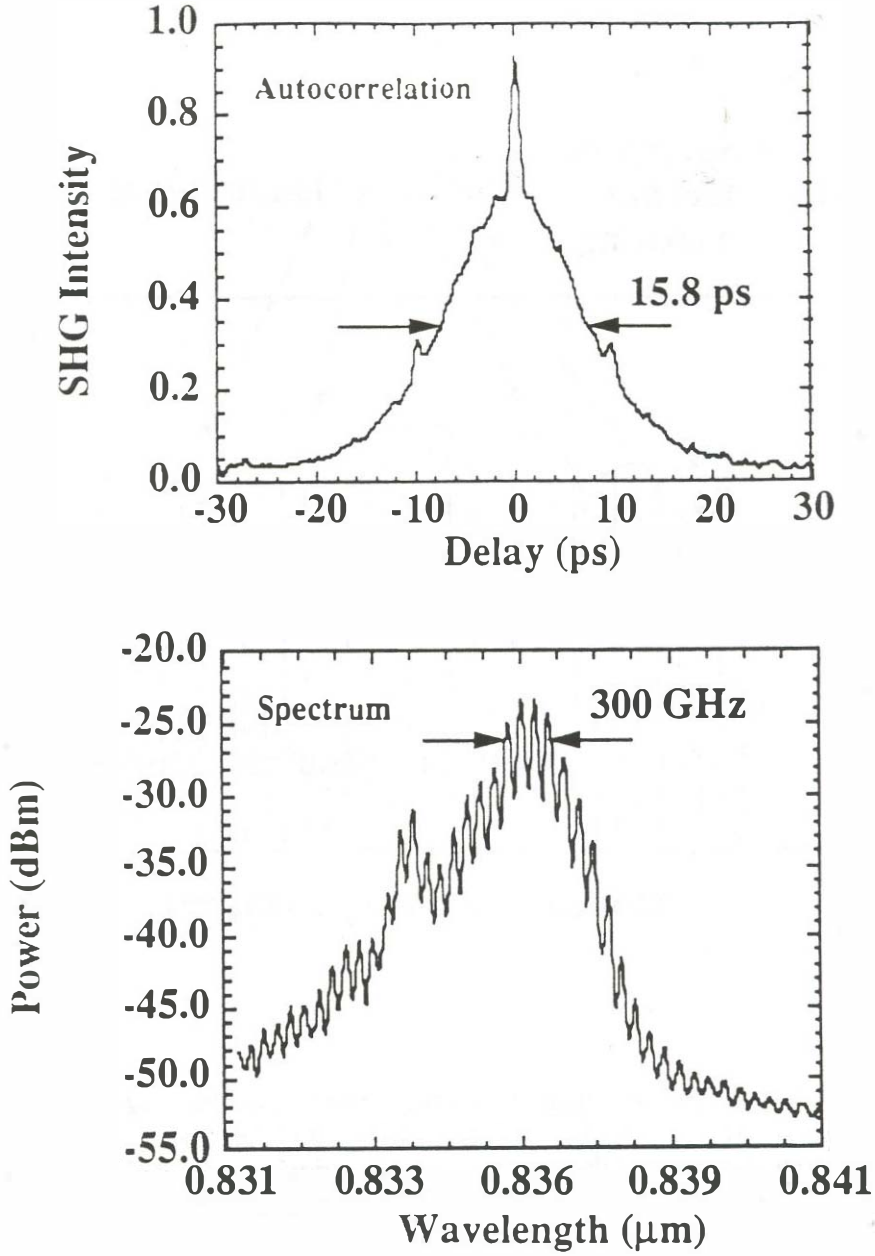

Figure 2.3 A typical autocorrelation and optical spectrum for a laser that is mode-locked in clusters. The autocorrelation shows a large coherence spike which is a sign of unmode-locked spectrum and pulse sub-structure. The optical spectrum shows deep ripples (>5 dB) which constitute the clusters of external cavity modes.

would be very fast envelope variations on a relatively broad pulse. The fast variations within the optical pulse vary slowly from one pulse to the next. Although the clusters are not-mode-locked together, the relative phases between clusters are only slowly drifting. Figure 2.3 shows an experimentally observed mode-locked laser that exhibits mode-locking in clusters. The laser is a 0.35 mm long multi-quantum well laser with an estimated residual facet power reflectivity of 5×10^{-3}. The laser is driven by a 5 GHz, 24 dBm sinusoidal drive signal. The optical spectrum shows 5-8 dB ripples caused by the imperfect anti-reflection coatings. The autocorrelation of the pulse shows a large coherence spike caused by pulse substructure and unmode-locked spectrum. The resulting pulsewidth is 10 ps which is consistent with the spectral bandwidth for 1 cluster of modes.

The situation also arises in which only one cluster of modes is excited. This situation can be induced in the laser by using a bandwidth-limiting element into the cavity such as a diffraction grating, an etalon, or a birefringent tuning filter. The situation may also occur naturally under certain drive signal levels and detuning of the modulation frequency from the cavity resonance frequency (usually detuning to a lower modulation frequency). With the addition of bandwidth limiting elements, a single cluster may be selected. Single cluster operation eliminates the pulse substructure problems of multiple cluster operation. Figure 2.4 shows an example of a mode-locked laser operating in one cluster. The laser diode is a 4 quantum well device actively mode-locked at 5 GHz. The pulsewidth is similar to that of the multiple cluster example of Figure 2.3. The autocorrelation shows no coherence spike indicating that the pulse is well mode locked and that pulse substructure is eliminated. Single cluster operation is an important case of mode-locked laser operation that is

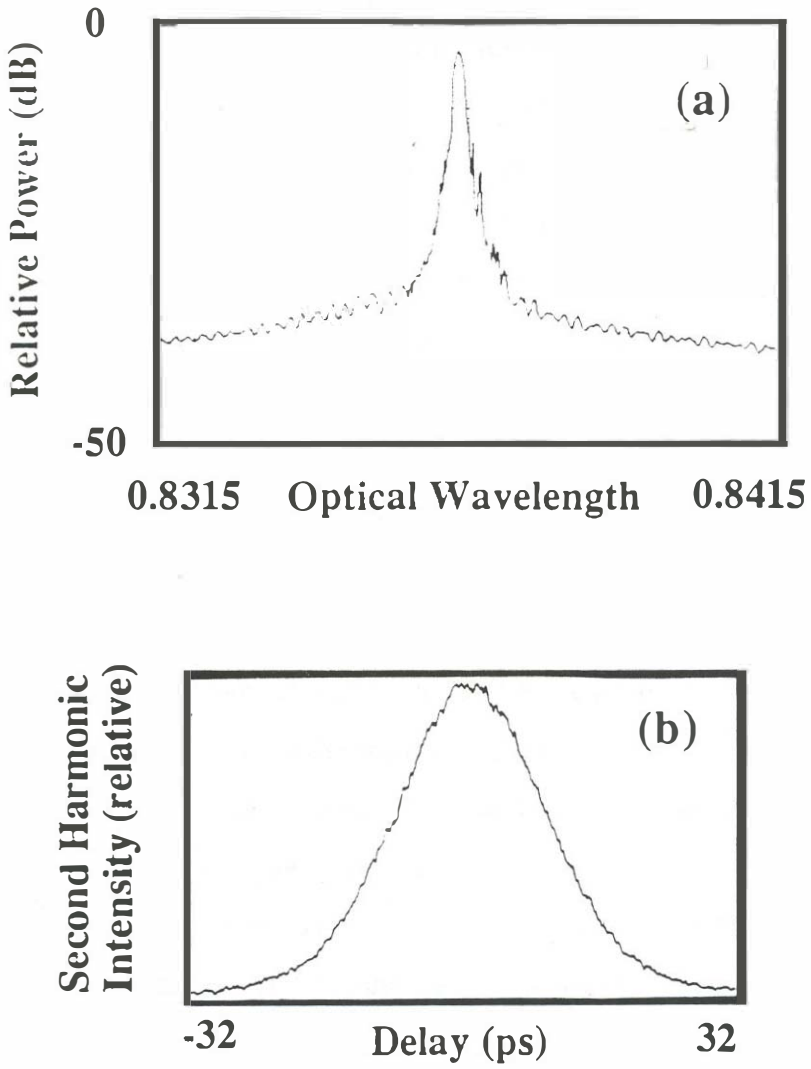

Figure 2.4 This is an example of operation in only one cluster of external cavity modes. The figure shows both the optical spectrum (a) and the autocorrelation (b). Note that the autocorrelation function contains no coherence spike and the optical spectrum has only one main cluster of modes. The pulsewidth is wide in this case because of the narrow optical spectrum that is available from one cluster width.

useful in applications which do not require extremely short optical pulses. The best way to accomplish single cluster operation is to use intentional bandwidth limiting elements. The pulses generated with bandwidth limiting elements in the cavity tend to have smaller time-bandwidth products because the semiconductor medium is not the main bandwidth limiting element. Pulses as short as 4 ps have been generated by Marshal et al. [34] by aligning the center frequency of a diffraction grating with the null in the spectrum between clusters. In this way, two clusters can be combined to give an over-all flat spectral response covering a two cluster bandwidth and allowing a shorter optical pulse. This technique of adding bandwidth limiting elements also limits the achievable pulsewidth and is a severe disadvantage if very short optical pulses are desired

2.1.1b Multiple pulse generation due to imperfect antireflection coatings

If the ripples in the optical spectrum are not too severe, and if the active modulation strength is large enough, the modes between clusters in Figure 2.2 can be locked together. The ripple in the frequency domain is still present though. A ripple in the frequency domain spectrum with mode-locking between clusters corresponds to multiple pulses in the time domain spaced by 1 over the ripple frequency spacing. This phenomena can also be described completely in the time domain which gives a more clear explanation for the origin of the multiple pulse outputs. The time domain illustration is shown in Figure 2.5. When a pulse enters the laser diode from the external cavity, the pulse is amplified and actively gain modulated in the laser. When the pulse leaves the diode and enters the external cavity, the imperfect antireflection coating causes a

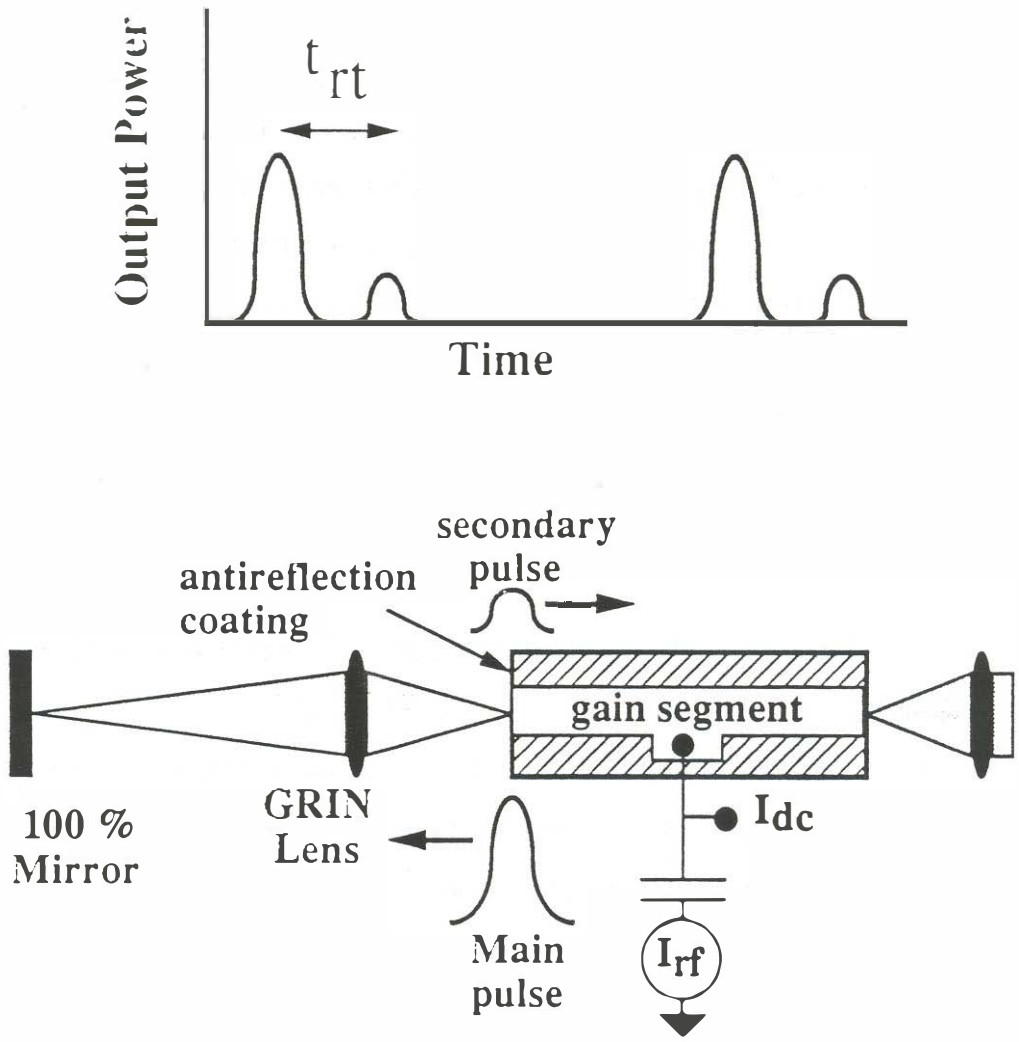

Figure 2.5 This is an illustration of the phenomena of multiple pulse formation in external cavity mode-locked lasers. The problem will be first illustrated in the time domain. As main pulse leaves the laser diode to go into the external cavity, a secondary pulse is reflected back into the laser diode by the imperfect antireflection coating. If the gain is substantial for the secondary pulse, the small reflected pulse will start to grow with each round trip in the laser. The gain for the secondary pulse is a result of incomplete gain saturation by the main pulse and by new gain introduced by the fact that the pump is still adding carriers. In the frequency domain view point (see Figure 2.2 also), the individual clusters of modes are now phase locked together, but the large ripple in the spectrum corresponds to multiple pulses in the time domain.

pulse to be reflected back toward the laser diode. The main pulse does not fully deplete the gain leaving residual gain for the secondary pulse. If the electrical modulation pulse has not ended its pumping interval, the gain rises again for the secondary pulse. Although the anti-reflection coating value may be very small, the secondary pulse can experience gain. Over many round trips, the secondary pulse amplitude builds up until the pulse energy is large enough to saturate the gain.

Figure 2.6 shows an experimentally observed case of multiple pulse formation in active mode-locked external cavity semiconductor lasers. The device length is 0.75 mm giving a round-trip time of 18 ps. The autocorrelation shows a strong secondary pulse spaced at the round trip time in the laser diode from the main pulse. The optical spectrum shows strong ripple but the phases are locked between clusters as is evidenced by the multiple output pulses. The problem is seen more clearly in the work of Bowers et al. [16] where three pulses were generated due to the multiple-reflection phenomena.

In summary, ***single*** section ***actively*** mode-locked lasers have the following characteristics which are of concern.

1. Imperfect anti-reflection coatings can either cause:

a. mode-locking in clusters

b. single cluster operation with poor coatings, intentional bandwidth control elements, or modulation frequency detuning.

c. multiple pulse outputs spaced at the round trip time of the laser diode

2. In order to produce short optical pulses, **very short electrical pulses are necessary** and very low electrical parasitic devices are necessary. The

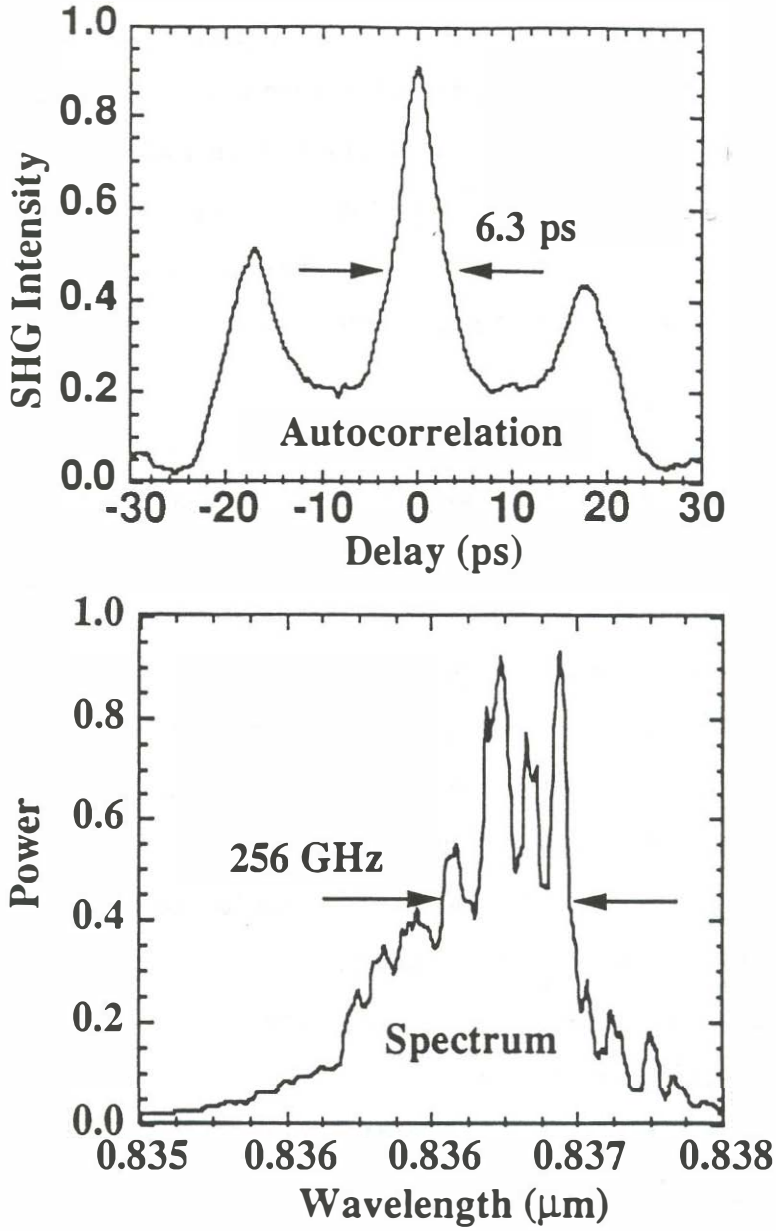

Figure 2.6 An example of multiple pulse formation in a single-section active mode-locked external cavity laser. The multiple pulses occur with a time interval equal to the round-trip time in the semiconductor laser.

pulsewidth shortening function becomes weak as the optical pulsewidth becomes very much narrower than the electrical modulation pulse.

2.1.2 Two-section active mode-locked external cavity lasers

The functions of gain and gain modulation are accomplished in the same segment in the device of Figure 2.1. By separating the gain and gain modulation functions into two separate locations as in Figure 2.7, the multiple pulsation problem can be reduced. The long segment is forward biased with a DC current to provide the over-all gain for the device. Since the gain modulation segment is not supplying the device gain, it can be reverse biased. Reverse-biased laser segments behave as p-i-n photodetectors and are highly absorbing. The DC reverse biased segment is driven by the gain modulation pulse. The electrical modulation pulse for this experiment is a 24 dBm sinusoid at 5 GHz. Since the modulation segment is nominally reverse biased, only the peak of the modulation cycle injects charge into the short segment resulting in a shorter effective pumping interval and more effective pulse shortening. After the modulation pulse ends, the modulation segment returns to the reverse bias condition after the stored charge is removed. The section is still operating as a photodetector and removes carriers from the active region of the short segment. The recovery of the absorption in the modulator segment results in a very high loss condition for secondary pulses. It is important to use a laser diode which has a round trip time comparable to the electrical modulation signal pulsewidth. Figure 2.7 shows an autocorrelation result for a two-segment active mode-locked semiconductor laser with a length of 500 μm. For this 500 μm long diode, the round trip time of 13 ps in the laser diode is sufficient for the modulation pulse to decay and allow the short segment to recover to a high loss

condition before the arrival of the reflected pulse. The resulting pulsewidth was 5 ps for the experiment. The secondary pulses at 13 ps delay are partially suppressed in the autocorrelation. Mar et al. [35] have used this design technique to produce single pulses as short as 1.4 ps and Werner et al. [36] produced 4 ps pulses with 3.5 pJ of energy in a similar experimental configuration .

The following sections in Chapter 2 demonstrate other methods to address the problems of multiple pulse formation and shorter pulse generation. The goal will be to eliminate some of the problems with anti-reflection coatings so that very short *single* optical pulses can be generated for reasonable values of anti-reflection coatings and for electrical modulation pulsewidths and pulse amplitudes that are easy to generate.

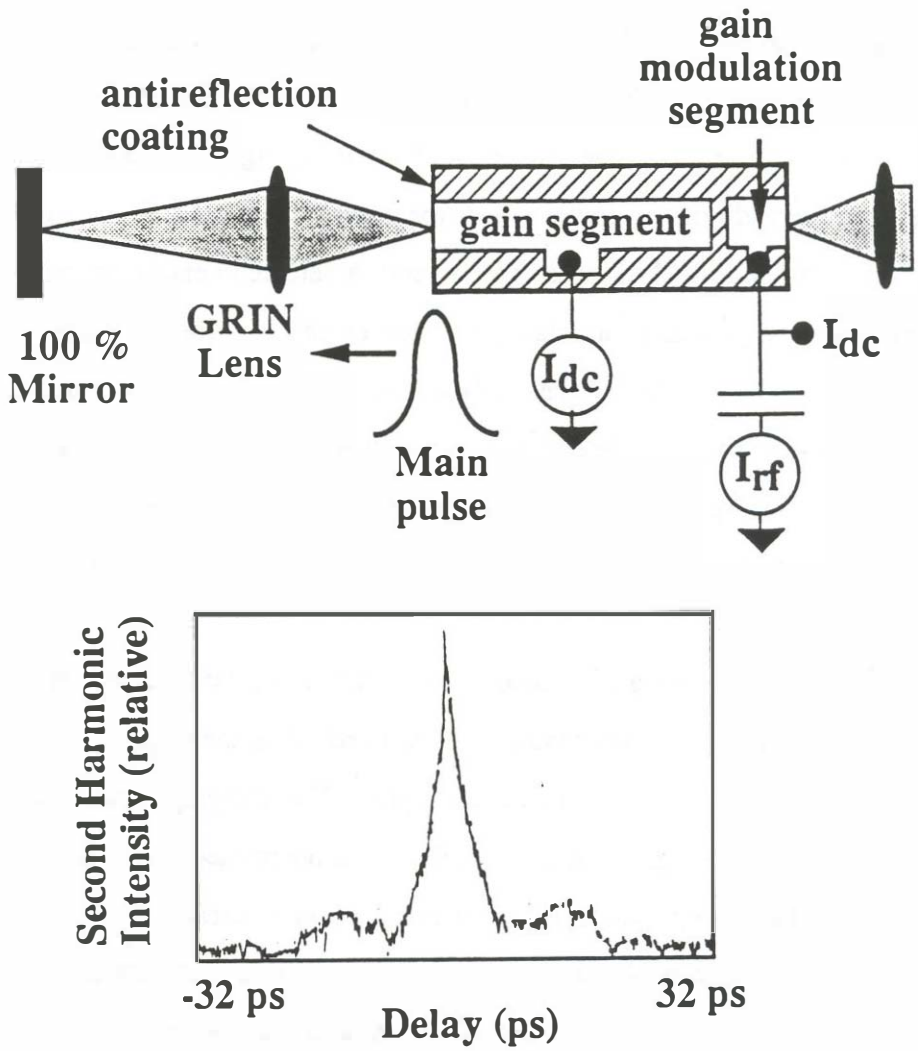

Figure 2.7 The diagram of a two-section active mode-locked external cavity laser. In this device, the functions of modulation and gain are separated. The modulation signal is a 5 GHz sinusoidal signal with a power of 24 dBm. The modulation segment length is 16 μm and is unbiased for this measurement. The active region has an $Al_{.04}Ga_{.96}As$ composition with an 80 nm thickness. The barriers are $Al_{.4}Ga_{.6}As$. The overall diode length is 500 μm. The autocorrelation shows one central peak with suppressed secondary pulses at the roundtrip time of the laser diode.

2.2 Self mode Locking of a single-segment semiconductor laser using positive feedback

In order to get very short optical pulses from active mode-locked lasers, it is important to use short electrical modulation pulses. Traditional sources of short pulses are from high frequency sinusoidal driving signals (> 5 GHz) or from step recovery diodes at lower repetition rates (<5 GHz). Since the optical pulses from mode-locked lasers are so short, a detected version of these pulses may serve as a potential candidate for a short electrical pulse modulation source. A new mode-locking technique, self mode-locking, is described in this section. Self-mode-locking uses detected optical pulses from the mode-locked laser as the active driving source. This technique forms narrow-width mode-locked optical pulses at low repetition rates without the use of a separate microwave synthesizer.

Active mode locking of semiconductor lasers has produced optical pulses as short as 0.58 ps [16]. This result was achieved using the positive portion of a 16 GHz sinusoid as an electrical drive signal. For many applications, such as electro-optic sampling, it is more useful to have the mode-locked optical pulses at a much lower repetition rate. This requires an electrical drive source that produces short electrical pulses at this lower rate. Step recovery diodes can be used, but they typically have pulse widths greater than 50 ps. Since the mode-locked optical pulses themselves are short, they are good candidates to drive the mode-locking action. Self mode locking uses a high speed optical to electrical (O/E) converter in a positive feedback configuration to convert the output optical pulses back into electrical drive signals to initiate the mode-

locking in a regenerative process. Previous authors [37], [38] have used positive feedback in a self gain-switching configuration. Self mode locking is different in that *both* coordinated optical and electrical feedback are involved and much shorter pulses can be obtained using mode-locking techniques. Advances in high speed electrical components allow short optical pulses to generate short electrical drive pulses. Photodetectors have been shown to be capable of producing impulse responses of less than 5 ps with 1 Volt peak amplitude into a 50 Ω load [39]. Since the detected photocurrent is too small to directly drive the laser, an amplifier is necessary to boost the feedback signal. Broadband distributed amplifiers using GaAs MESFETs have produced 3 dB bandwidths of over 30 GHz [40] and new device technologies promise to extend this bandwidth even further. Consequently, this technique can produce short mode-locked pulses at lower repetition rates, and it can do this without the need for an external electrical drive source.

The block diagram of the self mode-locked semiconductor laser experiment is shown in Figure 2.8. A semiconductor laser is placed in an external ring cavity configuration with a round trip delay time of 2 ns. The laser is a high speed 1300 nm semi-insulating planar buried heterostructure laser [41] with anti-reflection coatings on both facets. The light from the laser is collimated with the use of two anti-reflection coated GRIN lenses. The O/E converter [42] consists of a high-speed PIN photodetector and a 4 stage MESFET distributed amplifier. The O/E converter has an overall responsivity of 20 amps per watt. Impulse response measurements of the O/E converter were made using 1060 nm, 3 ps optical pulses from a pulse-compressed YAG laser. The resulting impulse response is shown in Figure 2.9. The O/E converter is capable of producing 50 ps full width at half maximum (FWHM) electrical pulses with a

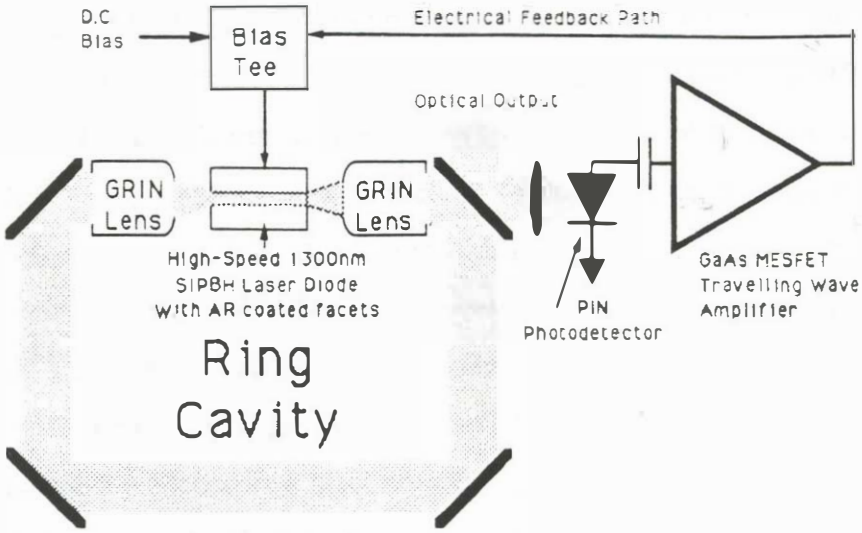

Figure 2.8 The configuration used for self-mode-locking of a semiconductor laser. The semiconductor laser is antireflection coated on both facets and coupled into an external ring cavity with two graded index lenses. One output of the laser is coupled into a high speed optical to electrical (O/E) converter. The 0/E converter converts the short optical pulse into a short electrical pulse. The short electrical pulse is then applied to the current modulation input of the laser to produce active mode-locking in a regenerative manner.

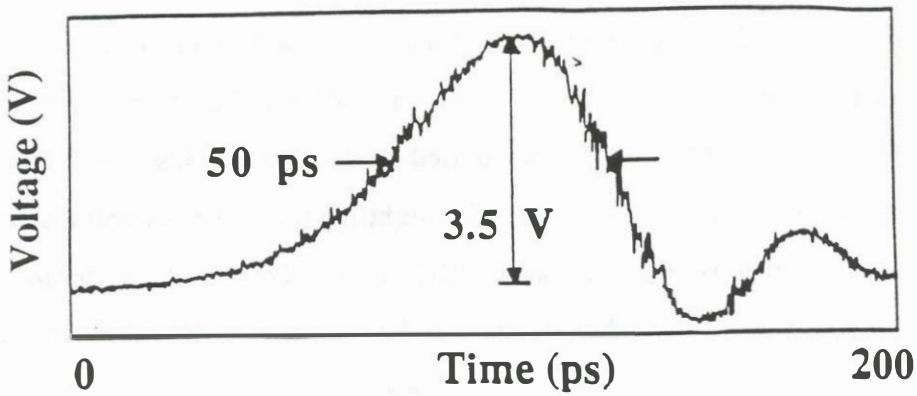

Figure 2.9 The measured impulse response of the high speed optical to electrical converter of Figure 2.8. The impulse response was measured by applying a 2 ps optical pulse from a compressed YAG laser and measuring the electrical output with a high speed sampling oscilloscope. The measured impulse response full width at half of maximum (FWHM) is 50 ps and the peak amplitude was 3.5 volts into a 50Ω load.

peak amplitude of 3.5 volts into a 50 ohm load.

The process of self mode-locking is described as follows: The external cavity laser is first biased above the CW lasing threshold. Counter-propagating optical signals start to build up in the ring cavity. One of the two output signals is fed into an O/E converter. This optical signal is then converted into an electrical drive signal and applied to the direct modulation input of the diode laser. If the round trip delay of the optical cavity and the round trip delay of the signal that goes through the O/E converter are properly chosen, a regenerative process will build up a mode-locked pulse stream in the laser. In order for self mode-locking to occur, the loop gain of the O/E converter feedback path, must be greater than one.

$$R_{oe}\eta h\nu/q>1 \tag{2.1}$$

where R_{oe} is the O/E converter responsivity, η is the laser differential quantum efficiency, h is Planck's constant, ν is the optical frequency, and q is the electronic charge.

The other condition necessary for self mode locking is that the optical path time delay, D_o, must be related to the electrical path time delay, D_e, by the expression:

$$\frac{D_o}{n} = \frac{D_e}{m} \tag{2.2}$$

where n and m are integers. This condition forces the electrical pulses and the optical pulses to arrive in the gain section of the laser at the same time. For

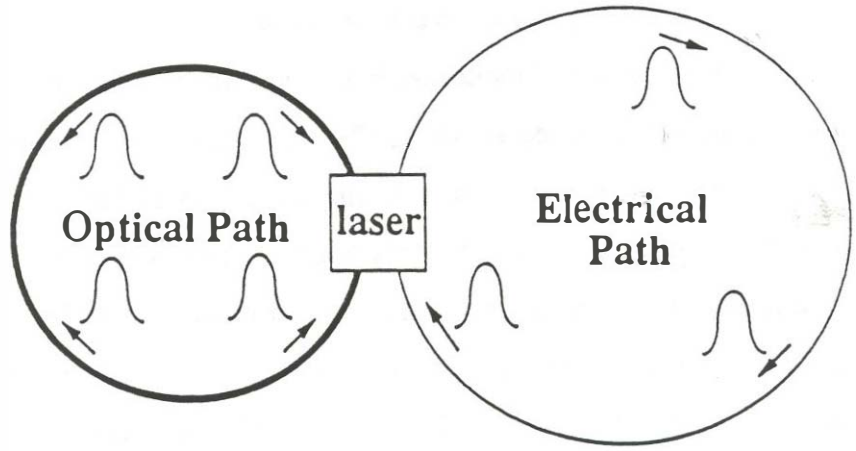

Figure 2.10 An illustration of the timing of the electrical and optical pulses in a self-mode-locked laser. There are two feedback paths in a self-mode-locked laser, the optical laser cavity and the optoelectronic feedback cavity. In order for the regenerative mode-locking process to begin, the time delay between pulses in the optical cavity must equal the time delay between the pulses in the optoelectronic feedback path. The shows illustration is the case for n=2 and m=3.

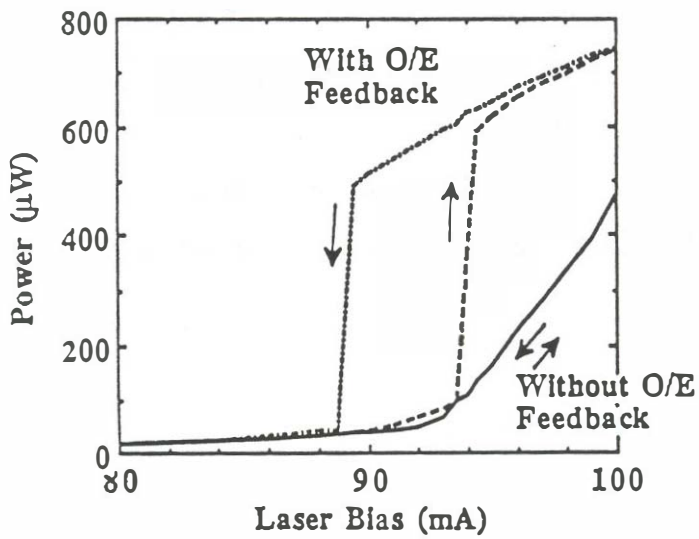

Figure 2.11 The hystersesis characteristics found in self-mode-locked lasers. When the laser drive current is increased, at a certain current the laser will digitally go into the mode-locking condition. After the mode-locked condition is reached, the bias current can be lowered to a current lower than the original turn-on threshold while still maintaining lasing.

stable operation, the electrical delay time must be shortened slightly to allow the carrier density to rise before the arrival of the optical pulse. Figure 2.10 illustrates this timing relationship for the case of n=2 and m=3. The electrical path delay is 1.5 times the optical path delay. The optical cavity has 2 sets of counter-propagating pulses and the electrical cavity has 3 propagating pulses. The time between the successive pulses in both loops is nearly identical. The pulse repetition frequency of the self mode-locked laser is $f_{rep} = n/T_{\sigma}$. Figure 2.11 shows the measured average power versus DC current drive of the self mode-locked laser for the case of n=3 and m=10. Curve A in the figure shows the response without O/E converter feedback. When feedback is added (Curve B), the laser breaks into pulsation just above the CW lasing threshold. For this particular system, the laser amplitude limits when the peak feedback current available from the O/E converter is reached. Curve B shows that the average power of the self mode-locked laser increases with laser bias but with a lower differential quantum efficiency than for the CW condition. Curve C shows that once self mode locking has been established, the laser can be biased below the CW lasing threshold and mode-locking will continue. The hysteresis shown is possible because the O/E converter supplies the extra current necessary to maintain the oscillation below the CW lasing threshold. Using the system of Figure 2.8, pulse repetition frequencies from 500 MHz (n=1,m=3) to 6 GHz (n=12,m=37) have been measured. The pulse rate is adjusted by substituting in various lengths of coaxial transmission line delays and changing the length of the optical ring cavity for fine length adjustments. It has been found experimentally that if two solutions of Equation 2.2 result in nearly the same cavity lengths, the mode with the lowest value of n actually occurs. Figure 2.12 shows a plot of the second harmonic intensity autocorrelation of a 1.5 GHz

(n=3,m=10) pulse train. If a hyperbolic secant squared pulse shape is assumed, the autocorrelation gives an optical pulse FWHM of 8 ps. The width of the optical pulse is very sensitive to the relative lengths of the optical and electrical feedback loops. Figure 2.13 shows a plot of the optical pulse FWHM versus changes in the optical path delay with the electrical path delay held constant for a 1.5 Ghz (n=3,m=10) case. The left hand side of the plot shows the condition of the electrical pulse arriving at the laser 30 ps earlier than the optical pulse. By shortening the optical cavity (or by lengthening the electrical cavity), the pulse width narrows until the optical pulse starts to arrive too late at the laser to achieve significant optical gain and the optical pulsewidth rises dramatically.

Figure 2.13 also shows the theoretical detuning behavior which agrees qualitatively with the experimental data. The theoretical results are based on a partial integration solution of the traveling wave rate equations [43]. The modeled current drive for the system has a DC bias plus a component due to the O/E feedback. This O/E feedback current is digitally bandwidth filtered and amplitude limited to match the measured impulse response and saturation characteristics of the O/E converter (Figure 2.12).

In summary, a new type of mode locking in which an external electronic oscillator is not needed was demonstrated. This self mode-locking process uses the output of the laser itself to drive the mode-locking action. The system can be made to pulse at harmonics of the fundamental cavity frequency by proper choice of feedback delays. The pulse repetition rate of the system can be made lower than the drive rates usually used for short pulse generation in actively mode-locked semiconductor lasers. Self mode-locking would also work with hybrid mode-locked lasers [44]. The saturable absorber current could be used

to drive the feedback amplifier directly, eliminating the need for an external photodetector (see Section 2.4).

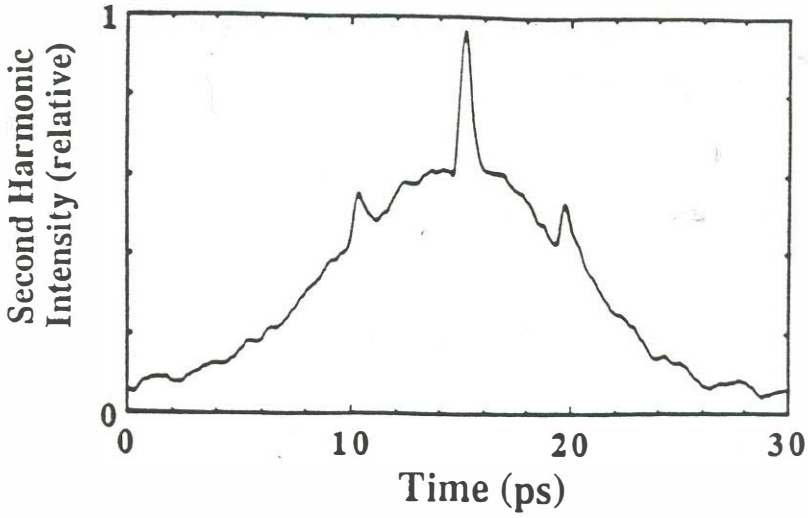

Figure 2.12 An autocorrelation trace from the self-mode-locked laser of Figure 2.8. The repetition rate is 1.5 GHz with n=3 and m=10.

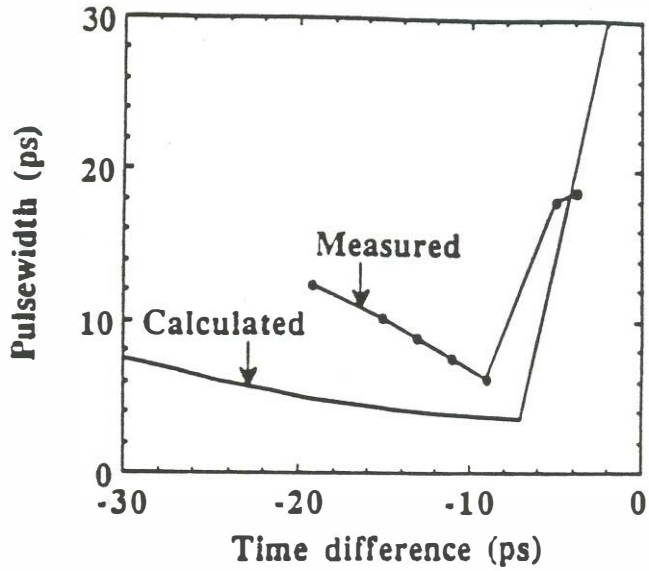

Figure 2.13 The pulsewidth versus change in the optical cavity length together with computer simulations of the response. The laser has a wide range of delays with short optical pulsewidths if the electrical pulse arrives in the laser sooner than the optical pulse. When the electrical pulse arrives in the laser diode too late, the optical pulsewidth rises very quickly. The pulses are unstable in time and amplitude if the electrical pump pulses arrives too early with respect to the optical pulse.

2.3 Passive mode-locking of semiconductor lasers using excitonic saturable absorbers

Passive mode-locking is a widely used technique for producing short optical pulses from lasers. The key component in a passive mode-locked laser is the saturable absorber. The saturable absorber is a nonlinear gain modulation element that narrows the width of an input pulse after passage through the device as is illustrated in Figure 2.14. The leading edge of the pulse is attenuated due to absorption. The absorbed photons create carriers in the saturable absorber which eventually reduce the attenuation. In this manner one obtains a preferential attenuation of the leading edge of the pulse.

In order to get this desired pulse shaping [18], the change in gain per unit carrier density change in the saturable absorber must be larger than this same ratio in the laser amplifier (for equal spot sizes in the laser amplifier and the absorber). Alternatively, the spot size in the absorber can be made smaller than the spot size in the laser (for the same material in both cases) . This requirement can be met in dye laser systems by having different types of dye for the laser and the absorber or by changing the spot size in the absorber and laser. For semiconductor lasers the spot size is already quite small and it would be hard to get a smaller spot size on the absorber.

Passive gain modulation has inherent advantages over active gain modulation. In passive gain modulation, the pulsewidth reduction on each pass around the laser cavity is a constant, independent of input pulsewidth (assuming a constant pulse energy). Active gain modulation produces large pulse narrowing for wide input pulsewidths, but the effectiveness of active gain

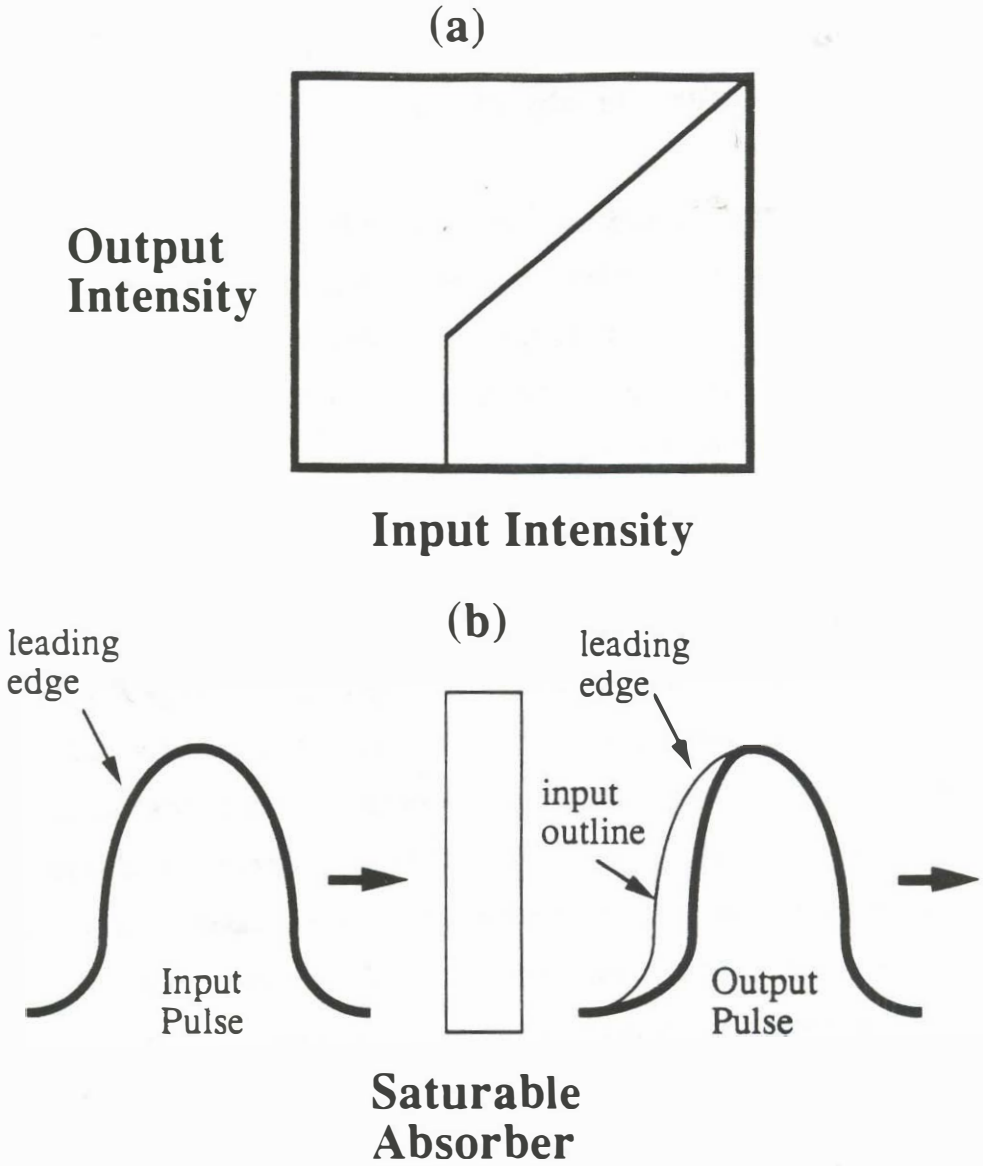

Figure 2.14 The input-output characteristics of a saturable absorber. (a) The static input output relationships of a fast saturable absorber. The fast saturable absorber has an intensity dependent transmission that favors the transmission of the high intensity portions of an optical pulse. (b) The input and output pulse for a slow saturable absorber. The leading edge of the pulse is absorbed and the trailing edge is passed with little attenuation. A fast saturable absorber would have both the leading edge and the trailing edge attenuated.

modulation is reduced as the input pulsewidth becomes narrow with respect to the electrical modulation pulsewidth. **With passive gain modulation, the need for short electrical modulation pulses is reduced since passive gain modulation is much more effective in obtaining short optical pulses.**

A suitable material for a saturable absorber in semiconductor lasers has been found in the excitonic non-linearity of multi-quantum well semiconductor samples which has been developed by Silverberg and Smith [45]. Excitonic absorption is a feature that is found just below the bandgap in semiconductor materials. Excitons are bound hole-electron pairs. In quantum well samples, the formation of excitonic features is more pronounced than in bulk active region semiconductor samples. This enhancement is due to the confining potential of the quantum well which confines the hole-electron pair in one dimension thereby increasing the hole-electron binding energy. The hole-electron binding energy for bulk active region samples is much smaller and excitonic features are not as pronounced because the binding energy is less than the thermal energy of the carriers.

Figure 2.15 shows an epitaxial layer structure fabricated for excitonic saturable absorbers experiments. This structure has an advantage over that used by Silverberg and Smith in that an integrated Bragg reflector has been grown epitaxially, eliminating the need for the more complex epitaxial lift-off procedure. The structure consists sixty 10 nm GaAs quantum wells with 10 nm $Al_{.3}Ga_{.7}As$ barriers.

The excitonic absorption peak is found several meV below the bound state energy level minimums in quantum wells. A typical low intensity absorption versus wavelength measurement is given in Figure 2.16 . This plot is given for

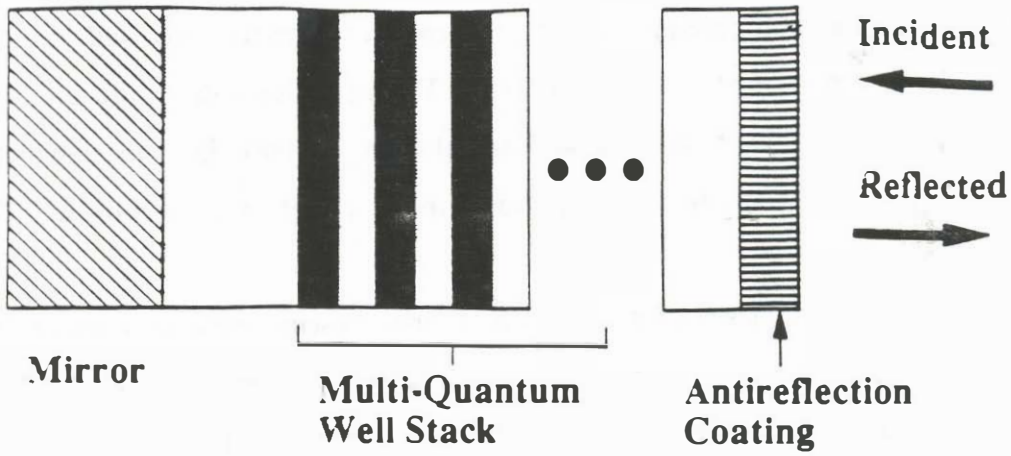

Figure 2.15 The typical structure of an excitonic saturable absorber. A series of quantum wells are grown epitaxially. In our case a Bragg reflector mirror is also grown below the quantum wells. The top of the structure is antireflection coated and the input light comes in perpendicular to the wells and is reflected back.

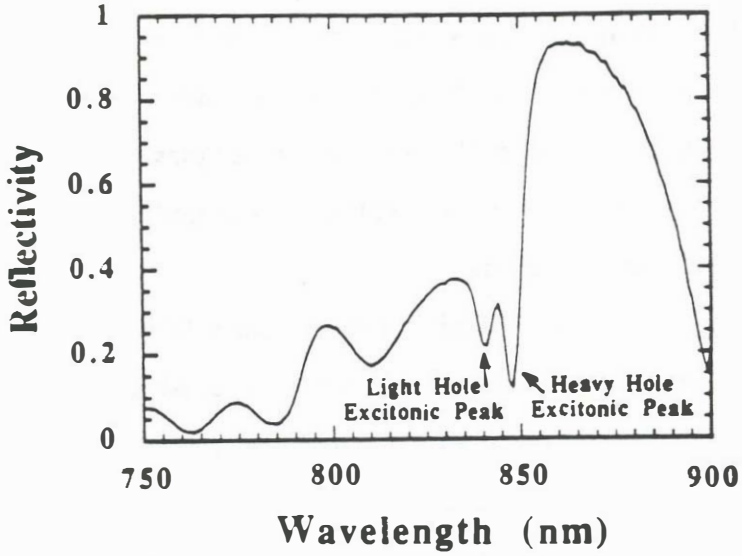

Figure 2.16 The reflectivity versus wavelength for the structure of Figure 2.15. The GaAs quantum well thickness is 10 nm, with 10 nm thick $Al_{.3}Ga_{.7}As$ barriers. The Bragg reflector is a 15.5 period $Al_{.3}Ga_{.7}As$/AlAs stack.

the GaAs/$Al_{.3}Ga_{.7}As$ saturable absorber of Figure 2.15. The GaAs/AlGaAs system is useful for lasers operating in the 0.8 to 0.87 μm range. Both the heavy-hole and the light-hole absorption features are clearly found in the reflection spectrum. The calculated low intensity absorption coefficient for the heavy hole excitonic peak is 18,000 cm^{-1}.

As mentioned earlier, it is desirable to have a saturable absorber in which the change in attenuation for a given change in carrier density is large. This is accomplished for the multi-quantum well devices because the bleaching energy for the excitonic absorption feature is much smaller than the bleaching energy for the above bandgap absorption processes [46]. The bleaching energy refers to the amount of energy it takes to bring the saturable absorber from the high loss condition to the transparency condition. The reduced bleaching energy is due to the fact the excitons can destroy themselves when the density of excitons is such that nearest neighbor distance between excitons becomes comparable to the excitonic pair diameter. The coulombic interaction of neighboring bound hole-electronic pairs reduces the binding energy of the excitons. This crowding of exciton concept is illustrated in Figure 2.17. The bleaching energy of excitons can be 10 times lower than the above bandgap bleaching energy.

For proper operation, saturable absorbers of the slow type (pulse shaping occurs only at the leading edge of the pulse), the absorption must quickly reset to a high value after passage of the optical pulse through the saturable absorber. The natural spontaneous decay constant for these quantum wells is over 1 ns and is too long for mode-locking operation. The lifetime can be shortened in these materials by using a small dose of proton bombardment to introduce extra recombination sites [22]. The proton bombardment reduces the carrier lifetime but also reduces the magnitude of the excitonic absorption features. Figure

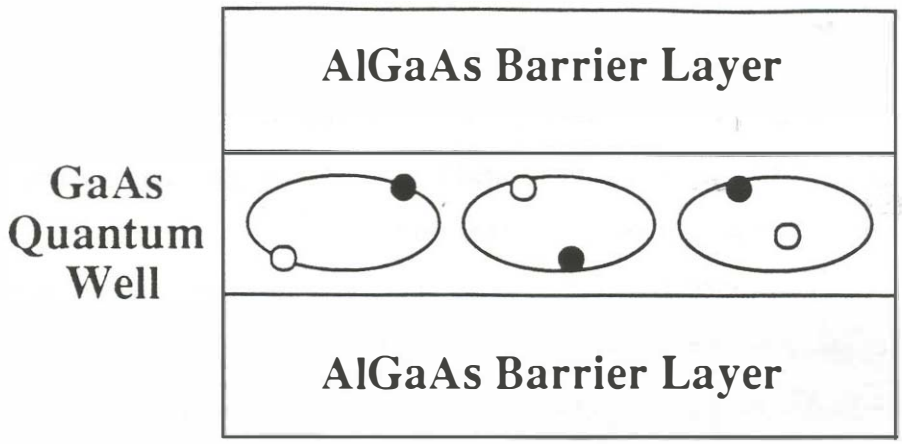

Figure 2.17 The absorption at the excitonic peak is bleached much easier than the absorption above the bandgap. This figure illustrates what causes exciton saturation. When the density of excitons becomes large enough so that the bound hole-electron pairs start to see the coulomb potential of each other, the binding energy of the exciton decreases, an optical phonon is absorbed and the carrier are promoted to free holes and electrons.

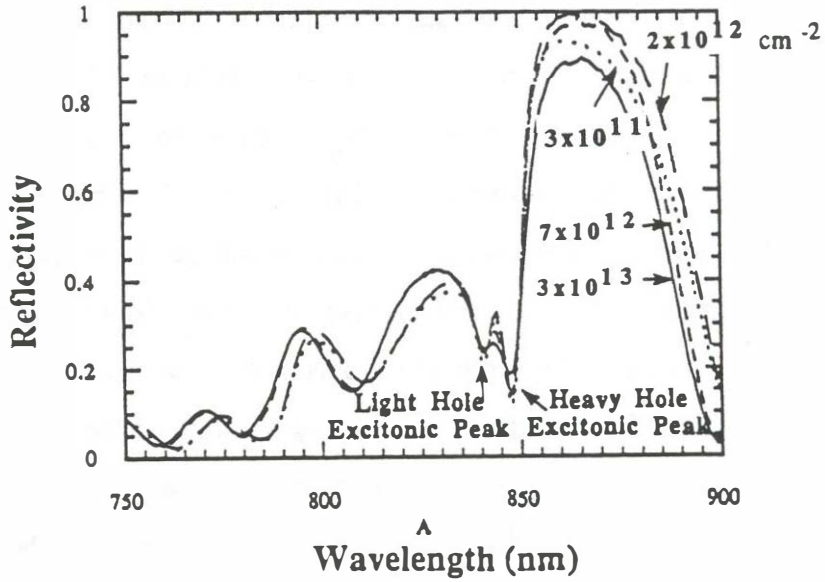

Figure 2.18 The absorption level versus proton bombardment level for the structure of Figure 2.16. The introduction of damage into the structure reduces the carrier lifetime. Reduced carrier lifetimes are necessary so that the saturable absorber can recover on each round trip through the laser. Increased proton bombardment levels also decrease the strength of the excitonic absorption since excitons due not live long near defect centers.

2.18 shows the low intensity absorption versus wavelength for various levels of proton bombardment. The samples do not show a significant change in excitonic absorption up to levels of 10^{12} cm^{-2}. The carrier lifetime for proton bombarded samples at the 10^{13} cm^{-2} level has been measured to be 60 ps [22].

Excitonic absorption effects can be enhanced using the concept of periodic loss. The periodic loss concept involves re-arranging the position of the quantum well layers in the device to make more efficient use of the quantum well absorption. Figure 2.19 shows the layer structure and standing wave patterns for a uniform well-spacing saturable absorber and one that uses the concept of periodic loss. In both structures, epitaxial dielectric mirrors have been constructed to simplify processing of these devices for the user. In the uniform spacing structure, some of the wells fall into standing wave nulls and contribute less to the absorption process. In the periodic loss structure, the quantum wells are all located next to the standing wave peaks leading to enhanced absorption over the uniform spaced case [47].

The absorption versus optical intensity for uniform and periodic loss samples was measured using the set-up shown in Figure 2.20. An Argon-ion laser was used to pump a tunable Ti:sapphire laser. The optical intensity and wavelength were varied to produce the absorber saturation curves shown in Figure 2.21. The plots show absorption versus wavelength at different incident optical powers for both uniform and periodic quantum well configurations. The plot shows that for a given optical power, the periodic loss absorber saturates more quickly than the uniform loss absorber, which is the desirable case for improved mode-locking. The contrast is actually greater than that shown in the figure because the mirror on the periodic saturable absorber was grown slightly off from the desired center frequency leading to a reduction in the absorption

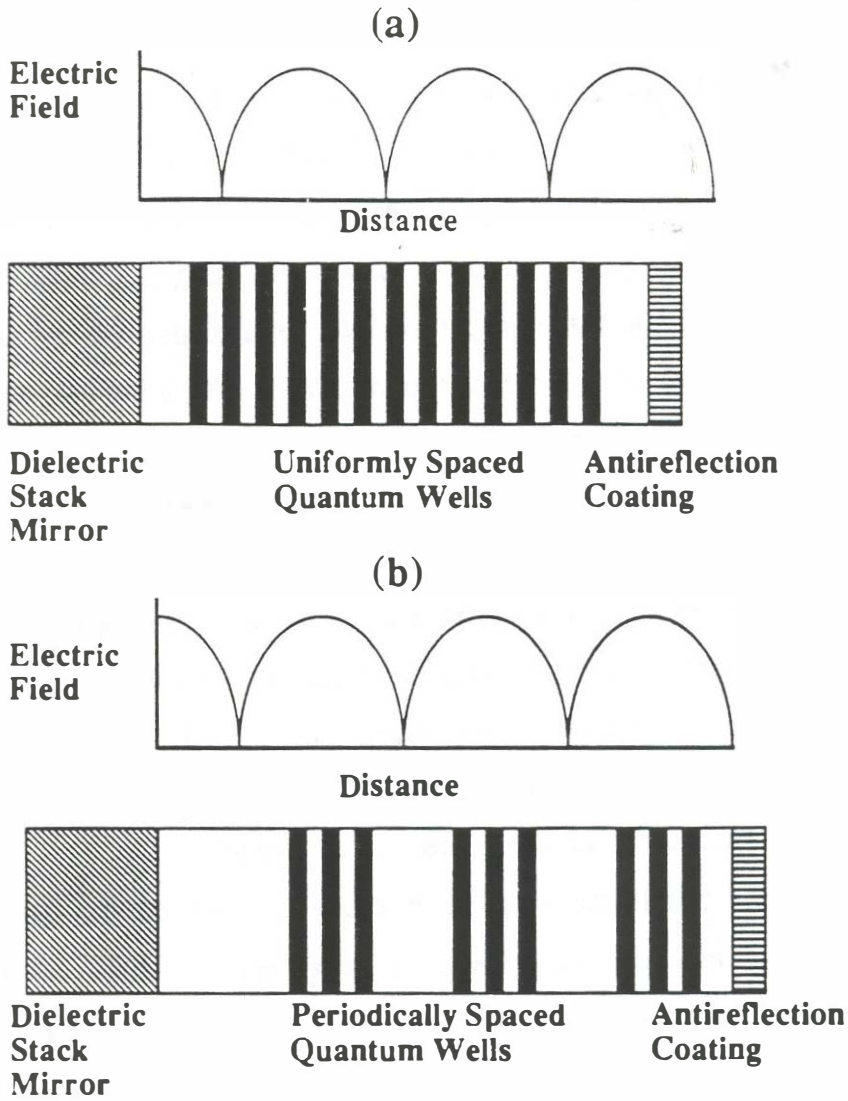

Figure 2.19 An illustration of the differences between an excitonic saturable absorber with (a) uniform and (b) periodic loss. In the uniform loss case, those wells that are located at the standing wave minimums do not initially contribute much to the absorption. The wells at the standing wave minimum are eventually filled up after a period of time which leads to a reduction in the pulse shortening per pass. In the periodic loss case, the wells at the standing wave minimum are removed, leading to the same absorption with fewer quantum wells. Both absorber types are examples of self-colliding pulse saturable absorbers. The uniform gain sample was described in Figure 2.16. The periodic sample has 11 periods of 3 quantum wells per period. The quantum wells were 8.5 nm thick.

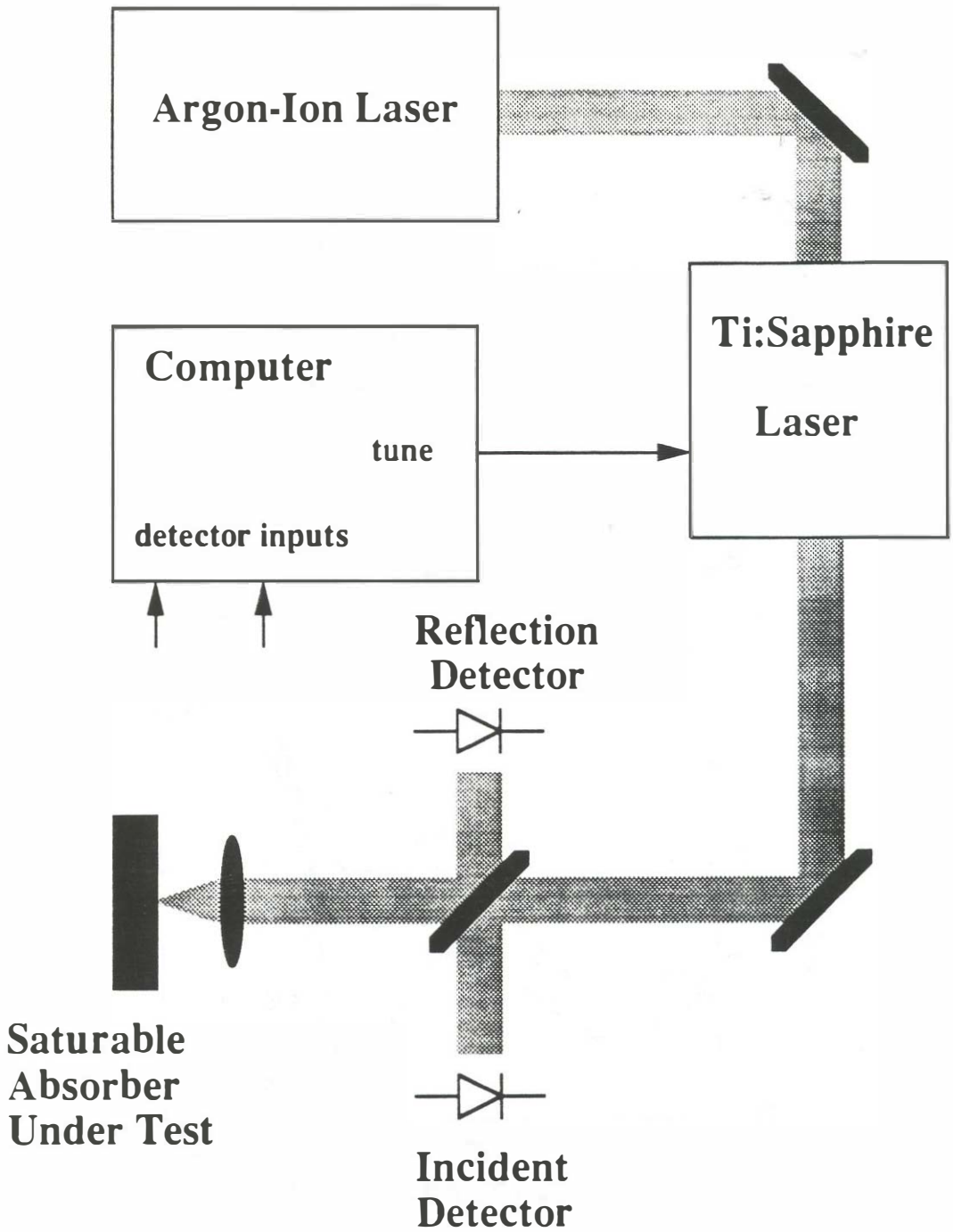

Figure 2.20 The measurement set-up used for measuring the absorption versus wavelength and the saturation characteristics of the excitonic saturable absorbers. A tunable Ti:Sapphire laser is focussed onto the samples.

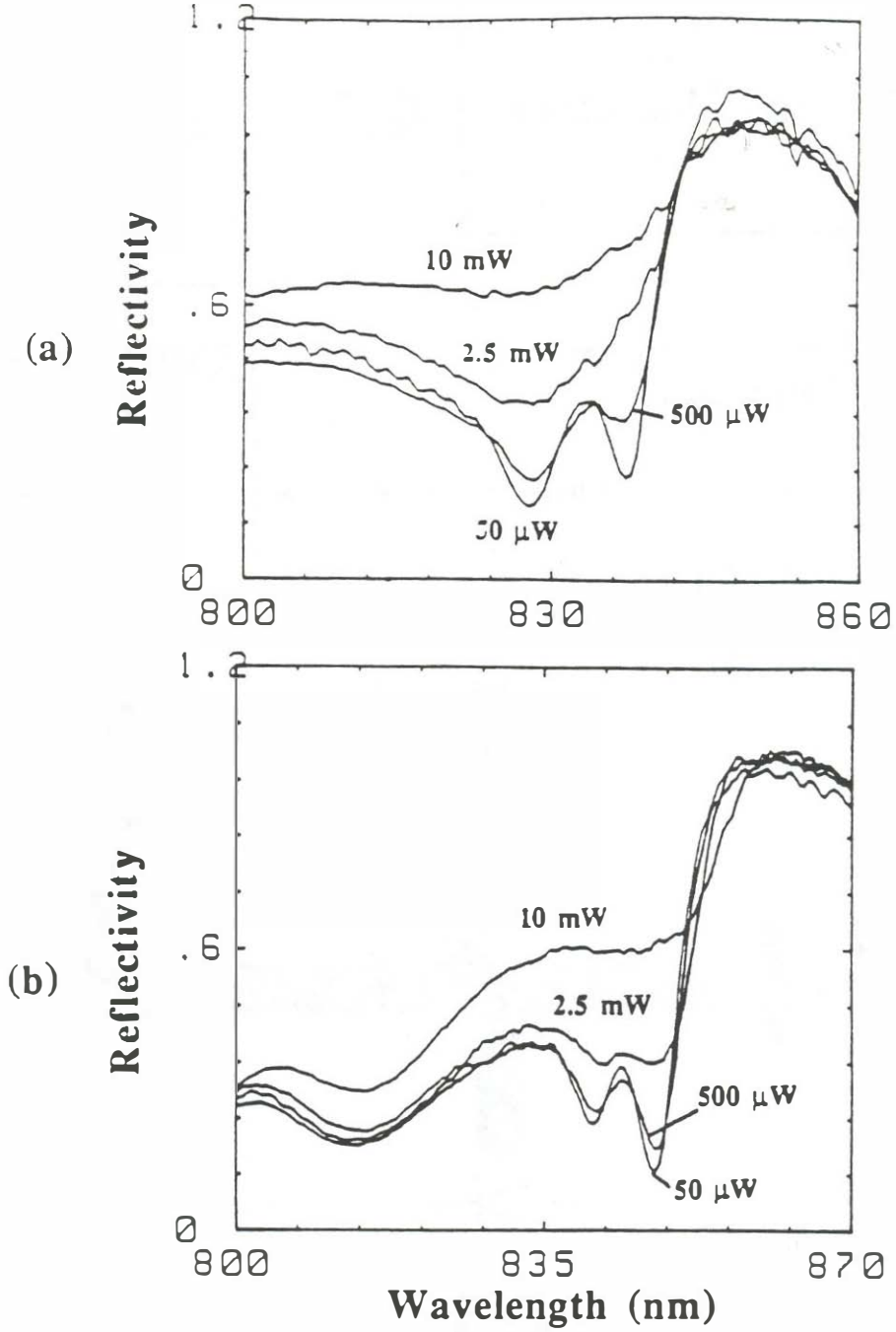

Figure 2.21 The reflectivity versus wavelength for various values of the input optical intensity for the measurement set-up of Figure 2.20. (a) The reflectivity for the periodic loss case. (b) The reflectivity for the uniform loss case. The sample compositions were described in Figure 2.19 and Figure 2.16.

enhancement. Note that the low intensity absorption coefficient for a 33 well periodic loss sample is nearly the same as that for a 60 well uniform loss sample. This points out again the improved absorption efficiency for the periodic loss design.

The excitonic saturable absorbers discussed up to this point have been investigated near 0.85 μm with the GaAs/AlGaAs system. For many applications in telecommunications and other areas it would be desirable to have a passively mode-locked laser at the 1.3μm and 1.55 μm wavelengths. The excitonic properties in the GaAs/AlGaAs system are particularly strong because the excitons have a high probability of spending their time in the binary composition, GaAs, of the quantum well. 1.3 μm and 1.55μm lasers are typically are fabricated in the InGaAsP/InP or InGaAs/InP material systems. The quantum wells in this system would have quaternary or ternary composition wells which do not give large excitonic features due to higher levels of alloy scattering in the semiconductor. The approach taken here is to use the InGaAs/InP system for the quantum wells. In this case the well is a ternary material and improved excitonic features should exist as compared to the quaternary well system.

To investigate the question of excitonic saturable absorbers in the long wavelength system, saturable absorbers were constructed using multi-quantum wells in the InGaAs/InP system. Quantum well samples were fabricated with lattice matched InGaAs wells and InP barriers using gas-source MBE [48]. The sample layer specifications are shown in Figure 2.22. The well and barrier dimensions were 9.3 nm and 11.9 nm respectively for the 1.55 μm absorber. The well and barrier dimensions for the 1.3 μm absorber were 2.7 nm and 11.9

nm respectively. Figure 2.23 shows the measured transmission versus wavelength for both samples. The excitonic features at 1.3 μm are much stronger than those at 1.55 μm. This is thought to be a result of the fact that for small barrier widths, the exciton has a much higher probability of spending time in the barrier, InP, which is a binary. The small quantum wells still serve to localize the excitons and the relatively large probability of the exciton being in the barrier reduces the alloy scattering level. The excitonic absorption peaks in both samples were found to show smaller exciton features than the GaAs/AlGaAs system.

In summary, an improved 0.85 μm excitonic saturable absorber has been developed. The concept of periodic loss is used to increase the change in absorption per unit change in carrier density that is beneficial for good mode-locking. By placing the quantum wells near the standing wave peak, the absorption coefficient is enhanced up to a factor of nearly two and the saturation energy is also reduced. Experimental results verify that this indeed happens. The device structures also offer improvement in that dielectric mirrors are grown epitaxially reducing the processing requirements of the devices.

Long wavelength excitonic saturable absorbers were fabricated for the first time. Exctionic features were found both at 1.3 μm and 1.55 μm. The excitonic features were found to be stronger for the narrow well width 1.3 μm samples.

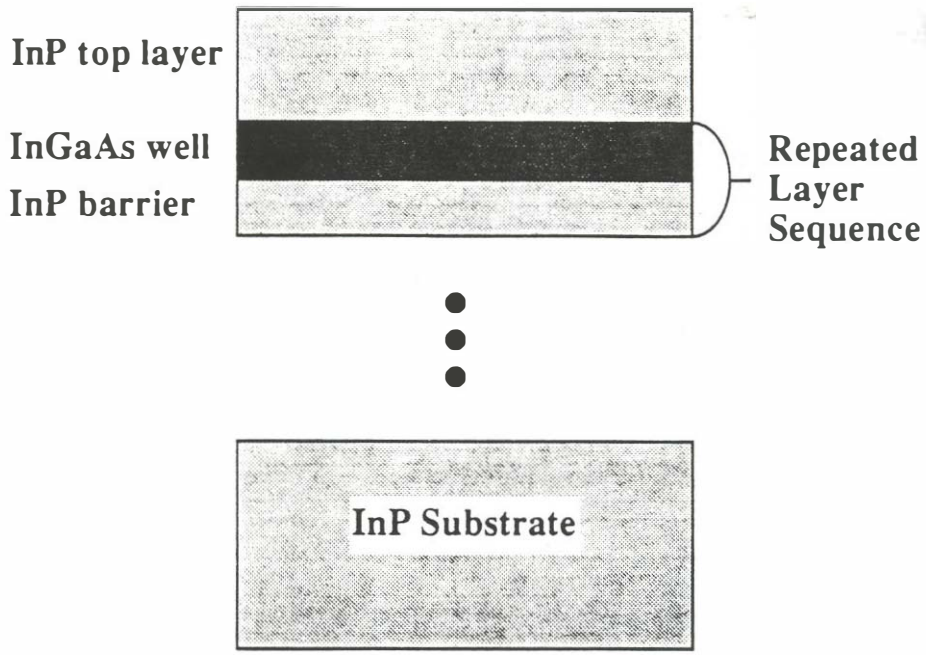

Wavelength	Well Width (A)	Barrier Width (A)	well number
1300 nm	27	119	130
1550 nm	93	119	50

Figure 2.22 The design parameters for 1.3 μm and 1.55 μm uniform gain quantum well samples. The samples were grown using gas-source MBE. The wells are InGaAs lattice matched to InP.

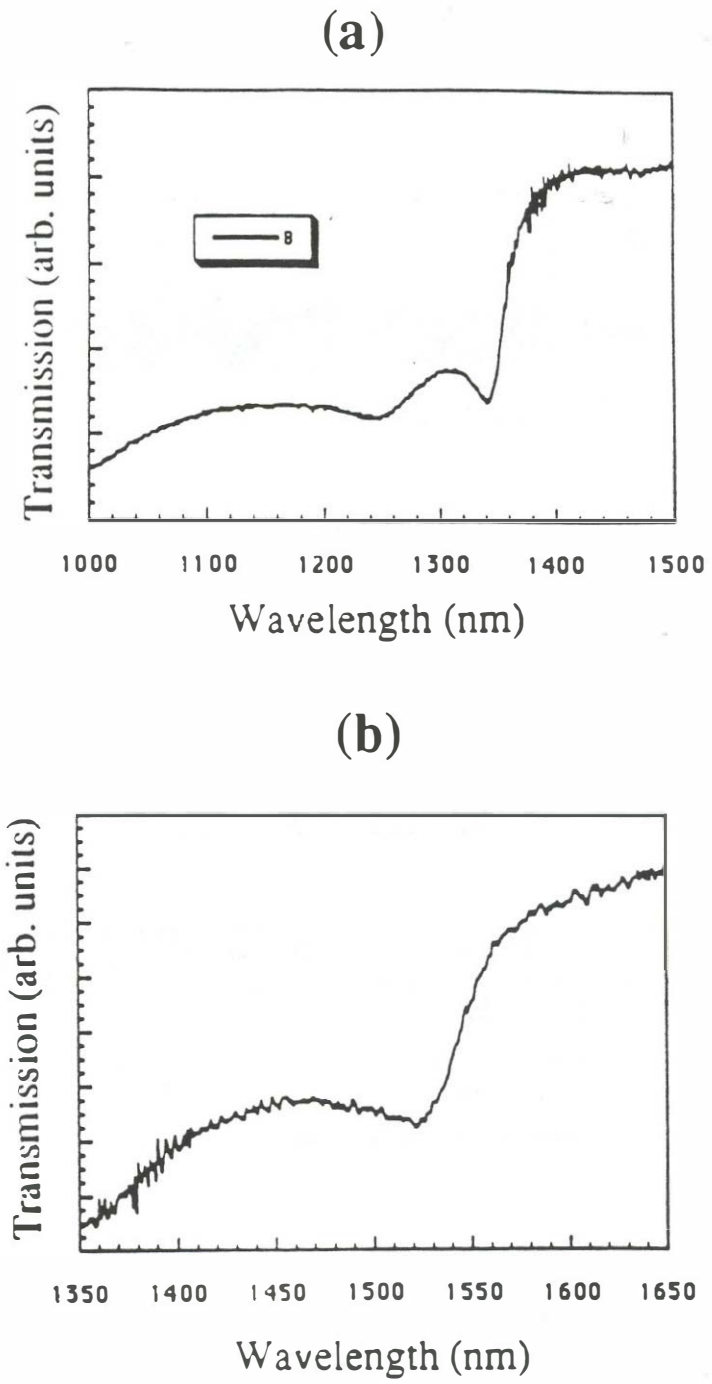

Figure 2.23 The transmission versus wavelength for the 1.3 μm and 1.55 μm quantum well saturable absorber samples as described in Figure 2.22.

2.4 Multi-section mode-locked semiconductor lasers using waveguide saturable absorbers

Section 2.3 described the advantages of passive mode locking. The pulse shortening strength of passive gain modulation is much stronger than that of active gain modulation. This reduces the need for very short electrical modulation pulsewidths. This section describes the use of waveguide saturable absorbers that are much easier to use than excitonic saturable absorbers. In addition, the technique is applicable to bulk or quantum well semiconductor material since the excitonic absorption peak is not a dominant contributor to the absorption non-linearity. The incorporation of waveguide saturable absorbers will also be shown to be effective in eliminating the problems of imperfect anti-reflection coatings as discussed in section 2.1. Single pulse outputs of less than 1.9 ps and and energies as high as 0.7 pJ are obtained using mode-locked lasers with waveguide saturable absorbers. Results will be given for both quantum well and bulk active region lasers.

2.4.1 Waveguide saturable absorbers

The band diagram versus distance for a typical bulk active region GaAs/AlGaAs laser structure at zero bias is shown in Figure 2.24. The laser structure was formed by impurity induced disordering with Si [50]. In forward bias, current is injected into the intrinsic (usually undoped) active region of a p-i-n double heterostructure to provide gain. In reverse bias, the laser has the same basic structure as is seen in a high speed p-i-n waveguide photodetector [51]. Even for small amounts of reverse bias, the electric field in the intrinsic region is large enough to produce saturated carrier velocity. The reverse-biased

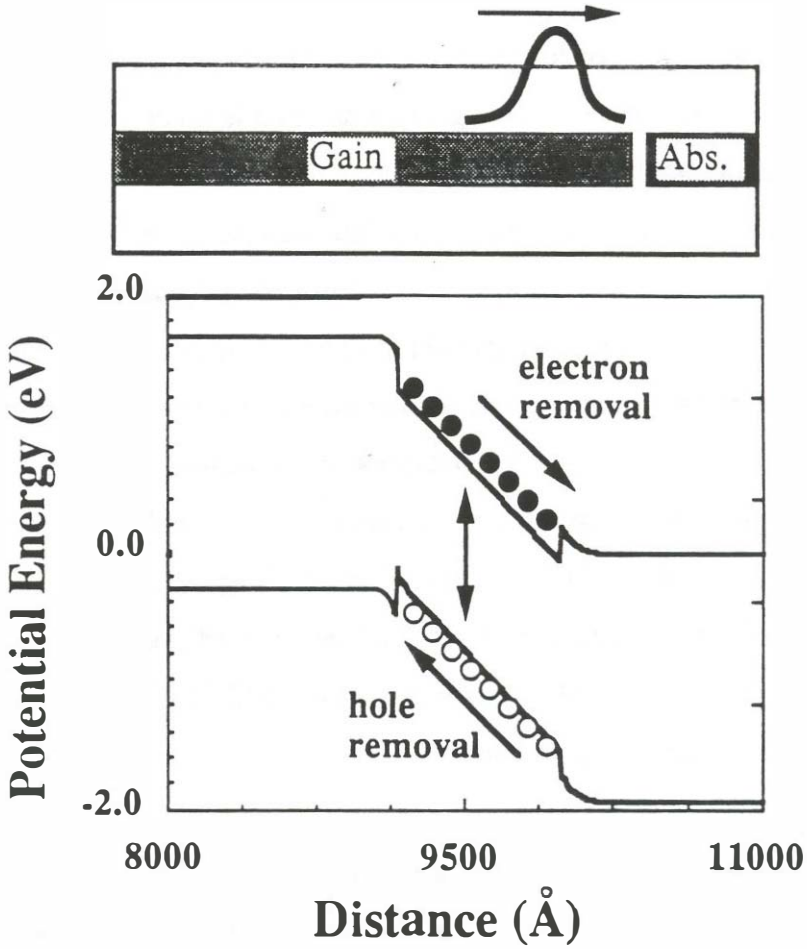

Figure 2.24 Potential versus distance for a zero biased laser structure. The active region is a 80 nm thick GaAs layer with $Al_{.4}Ga_{.6}As$ regions alongside. When forward biased, the structure is a laser. When reverse biased, the structure is a p-i-n waveguide photodetector. The illustration shows the generated hole-electron pairs when operated as a photodetector. The structure is also useful as a waveguide saturable absorber when reverse biased. The input optical pulse saturates the absorption of the GaAs by bringing the carrier density level up to transparency. The electric fields then sweep out the carriers so that the device recovers to the absorbing state.

photodetector can be saturated for an input optical pulse with enough energy to bring the detector carrier density to transparency levels. The electric fields will then remove the carriers due to electric field aided carrier sweep-out. The impulse response of the p-i-n waveguide photodetector of Figure 2.24 was measured for both small and high energy optical input pulses and the results are shown in Figure 2.25a and 2.25b. After the carriers are generated in the i region, the electric field sweeps the charge into the bond pad and junction capacitance where the stored charge is discharged into the 50 Ω load of the sampling oscilloscope. This analysis assumes that the capacitive portion of the photodetector response is dominant, which was clearly true for the detectors that were tested. When a large input pulse with enough energy to bleach the saturable absorber is applied to the waveguide photodetector, the device photocurrent response widens. This widening of the photocurrent response is due to saturation effects in the saturable absorber. As the holes and electrons separate to their respective collection ends, they create an electric field that opposes that of the built-in photodetector field, causing a reduction in the net field in the i-region. The reduced electric field slows removal of the carriers and increases the time it takes to remove all of the carriers from the i-region. In section 2.3 it was stated that it is important to recover the loss of a saturable absorber back to the high attenuation state very quickly after the passage of the optical pulse through the saturable absorber. In the excitonic saturable absorbers, this is accomplished by proton bombardment induced damage to the material in order to decrease the non-radiative lifetime in the material. In waveguide photodetectors, this is accomplished by removal of carriers by the electric fields. The question arises, does the capacitance of a waveguide saturable absorber segment affect the absorption recovery time of the saturable

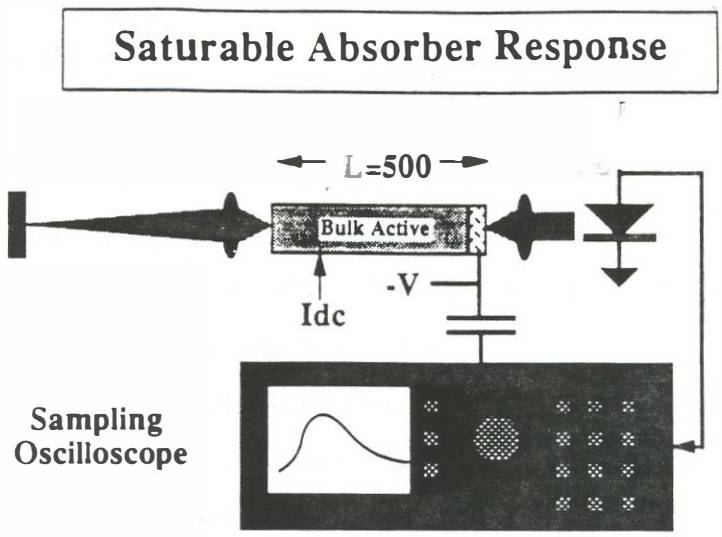

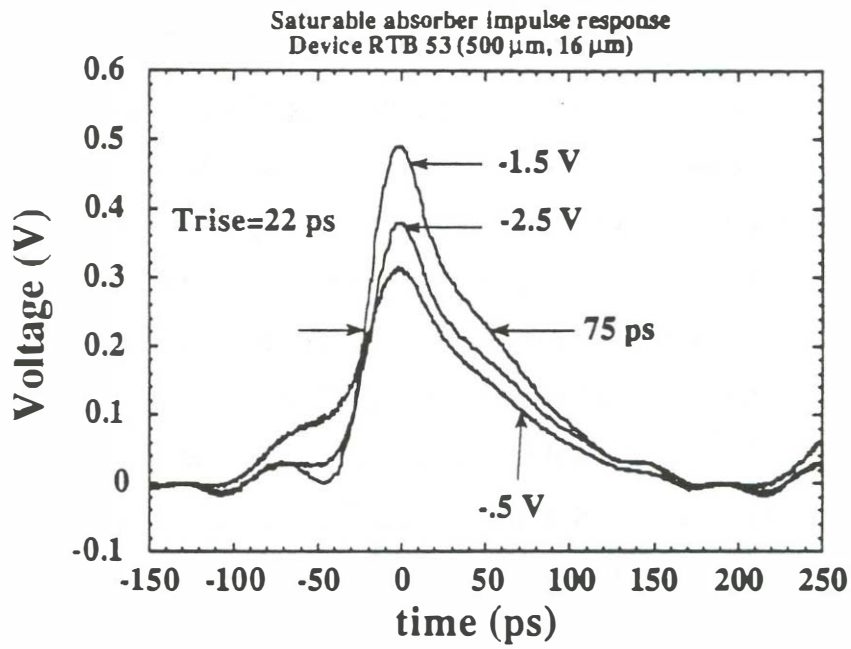

Figure 2.25a Saturable absorber/photodetector response in a saturation condition. Here the impulse response of the saturable absorber is measured using a high speed sampling oscilloscope. The response is given for several values of the reverse bias for a 16 µm long waveguide detector segment. The active region for this structure was described in Figure 2.24.

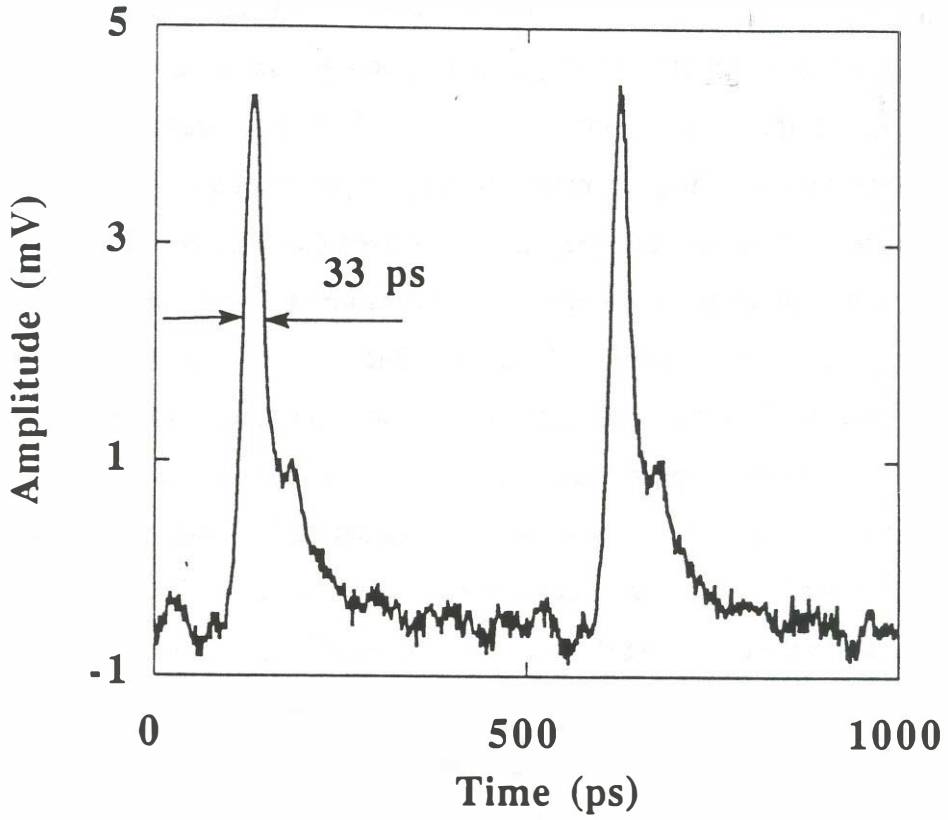

Figure 2.25b The photodetector response in the non-saturating condition. This measurement is done for an 8 μm long waveguide detector segment for pulse energies that do not cause saturation. The impulse response in this case is mainly limited by the bondpad capacitance of the device.

absorber ? The initial answer would be no. The transit time response removes all of the carriers into the capacitors where it is eventually drained off into a bleeding resistance. It is still important to bleed the charge off of the capacitor on each round trip but in terms of absorption recover times, the transit time response is the most important. In order to look at the transit time response (and the corresponding absorption recovery response) of a saturated waveguide photodetector, Karin et al. [52] have performed pump-probe measurements of the absorption recovery process in the waveguide saturable absorber structure of Figure 2.24. Figure 2.26 shows one result from the pump-probe experiments. Negative time refers to the case of the small probe pulse arriving before the large pump pulse and the transmission value at negative time shows the low-intensity transmission through this saturable absorber sample. The input optical pulse for this measurement was 100 fs, which is essentially an impulse for the time scale shown here. The wavelength of the pump and probe signals were chosen to be the same as that during actual mode-locking experiments. At zero time, the large pump pulse bleaches the saturable absorber and brings the carrier density in the device to the transparency level. The transmission level then quickly decays due to electric field aided sweep-out of the carriers. In less than 15 ps, the absorption of the saturable absorber has recovered to its original state. This very fast absorption recovery time has many consequences in mode-locked laser design, and is one of the key advantages of the use of waveguide saturable absorbers in mode locking of semiconductor lasers. The same measurement was done for a quantum well sample with similar results. In summary waveguide saturable absorbers have many advantages over excitonic saturable absorbers.

1. The external cavity mode-locked laser configuration is simplified.

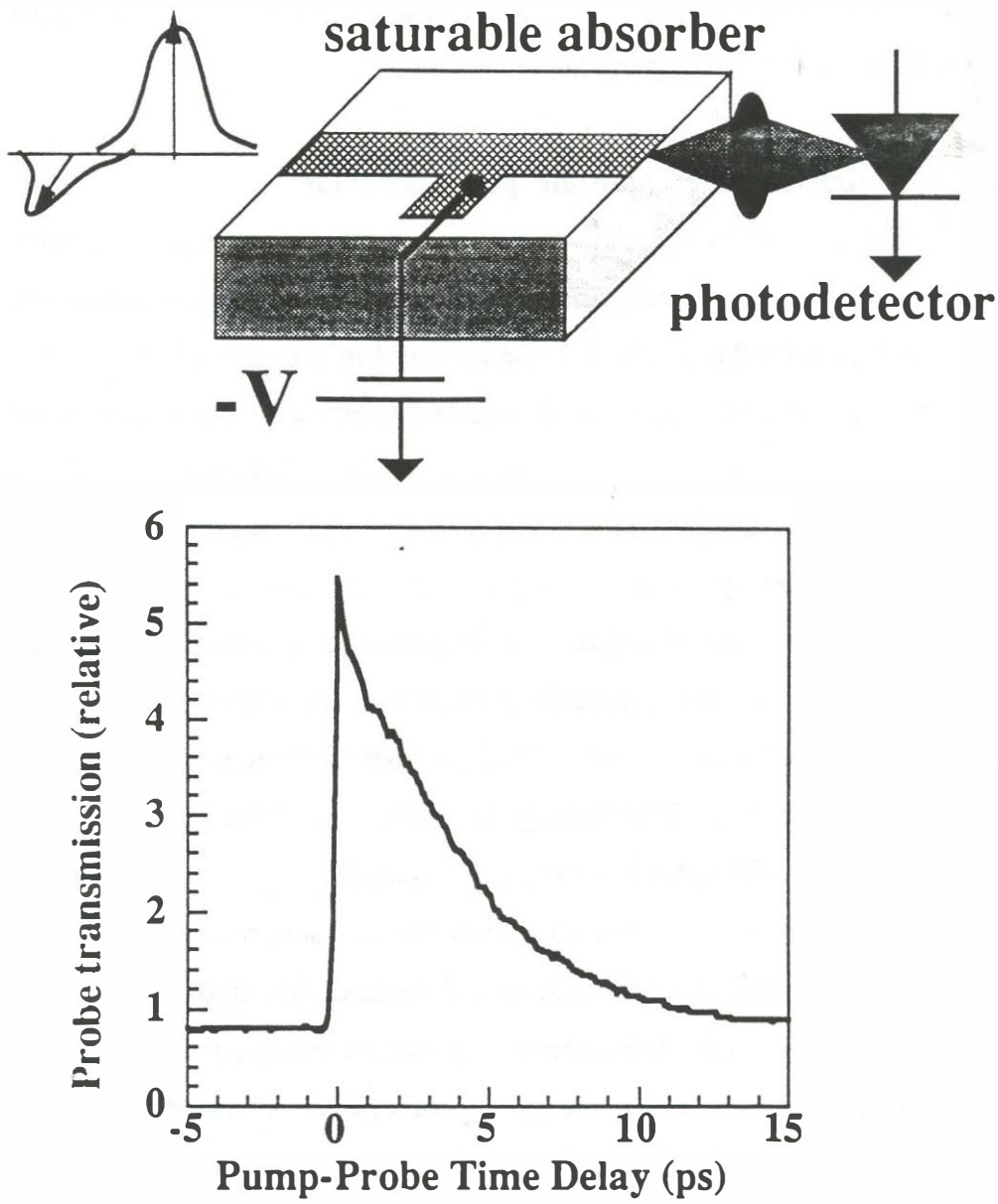

Figure 2.26 The absorption recovery time in a waveguide photodetector as measured with a pump-probe technique. A large pump pulse bleaches the absorption of an 80 μm long waveguide saturable absorber. A weak probe pulse follows the pump to measure the absorption recovery characteristics of the device. The active region has four 20 nm GaAs quantum wells. The reverse bias voltage for the device is 1V. The important conclusion from this measurement is that the absorption can recover to its unsaturated level very quickly.

2. Waveguide saturable absorbers have a wider absorption bandwidth.

3. Since damage is not introduced into the structure, the long term reliability of waveguide saturable absorbers should be improved.

2.4.2 Suppression of multiple pulse behavior

The problem of multiple pulse formation discussed in Section 2.1 can be reduced with the use of waveguide saturable absorbers. The active region layer structures used for the devices in these experiments are shown in Figure 2.27. Both bulk active and quantum well structures were used. The passive mode-locked laser structure used in the experiments is shown in Figure 2.28. The top contacts of the laser diode are separated to allow sections of the laser to be biased independently. The long segment provides the overall gain for the device. The reverse biased segment acts as a waveguide saturable absorber and p-i-n photodetector. One facet of the laser diode is antireflection coated with a residual power reflectivity of 10^{-3}. The light from the facet is focussed onto an external cavity mirror. The coatings are composed of nitrogen rich silicon nitride (index = 1..83) deposited by reactive sputtering.

To illustrate how the saturable absorber can suppress multiple pulse formation, the propagation of a pulse around the mode-locked cavity is outlined in Figure 2.28. The modeled device is a two section laser with a 500 μm overall length. The saturation energy, E_{sat}, of a gain or an absorbing segment is defined as [53]

$$E_{sat} = \frac{h \nu A_{\text{Cross Section}}}{\frac{\partial g}{\partial n}} \tag{2.3}$$

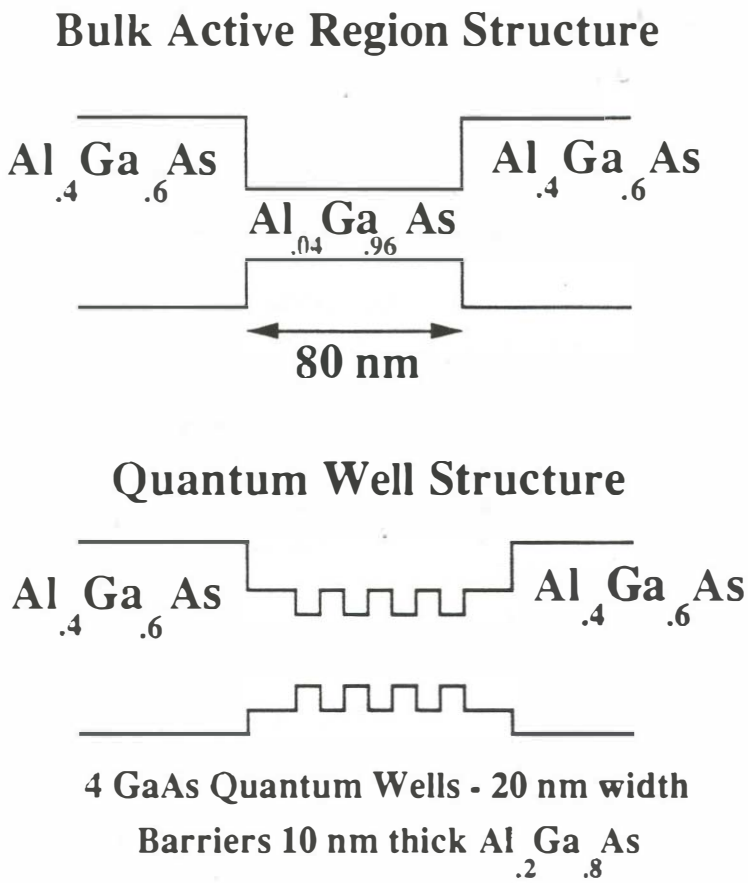

Figure 2.27 The GaAs active region compositions used for mode-locked laser experiments. Figure 3.3 shows the doping concentrations and details of the impurity induced disordering process to form the index guide.

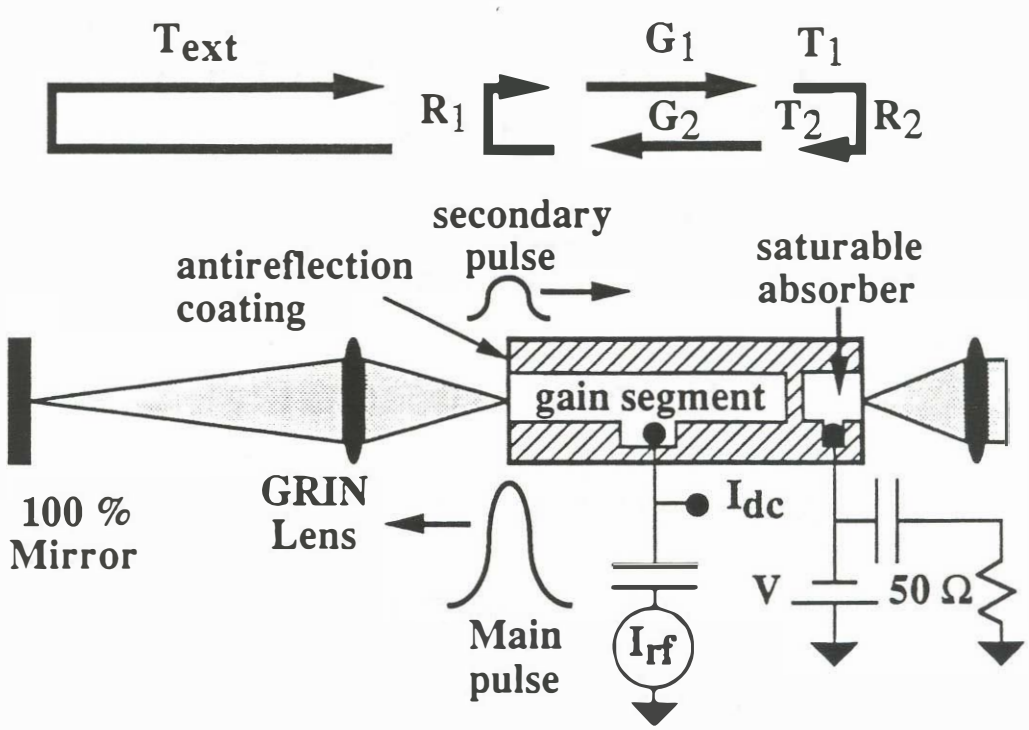

Figure 2.28 An illustration of the external cavity passive mode-locked structures used to suppress multiple pulse formation. As the main pulse leaves the external cavity, a secondary pulse is reflected back through the laser diode. If the saturable absorber can recover its absorption in a time less than the round trip time in the laser diode, the secondary pulse will not have enough energy to bleach the saturable absorber and it will be highly attenuated.

where hv is the photon energy, dg/dn is the differential gain and $A_{Cross\ Section}$ is the mode cross sectional area. The saturation energy is a measure of the energy required to saturate the gain of a gain section or the absorption of an absorber segment.

The E_{sat} of the gain section is 2.1 pJ and the E_{sat} of the absorber is 0.7 pJ in this simulation. The unsaturated energy gain of an amplifier segment is 17 (on a one way pass through the gain region for a total unsaturated gain of 289 on both passes) and the unsaturated transmission through the absorber is 0.05 (including both passes through the saturable absorber).

Figure 2.29 shows rate equation simulations (using the theory as presented in Chapter 5) of the pulse energy versus distance for the main pulse as the pulse enters from the external cavity and propagates through the gain and absorber segments on the forward and reverse transits. The large signal energy gain through the first gain segment transit, G_1, is only 8.5 due to large gain saturation. The pulse then encounters the saturable absorber where the leading edge of the pulse is absorbed and the pulse is narrowed. The mirror returns R_2=0.30 of the energy in the opposite direction. On the return trip through the gain section, the pulse experiences a gain, G_2, of only 5.0 due to the initial gain depletion from the first gain section transit. The pulse then passes into the external cavity which returns R_{ext} = 0.15 of the energy back again to the gain section. The round trip energy gain, G_{rt}, for the main pulse around the cavity is:

$$G_{rt} = G_1 T_1 R_2 T_2 G_2 R_{ext} = 1 \qquad (2.4)$$

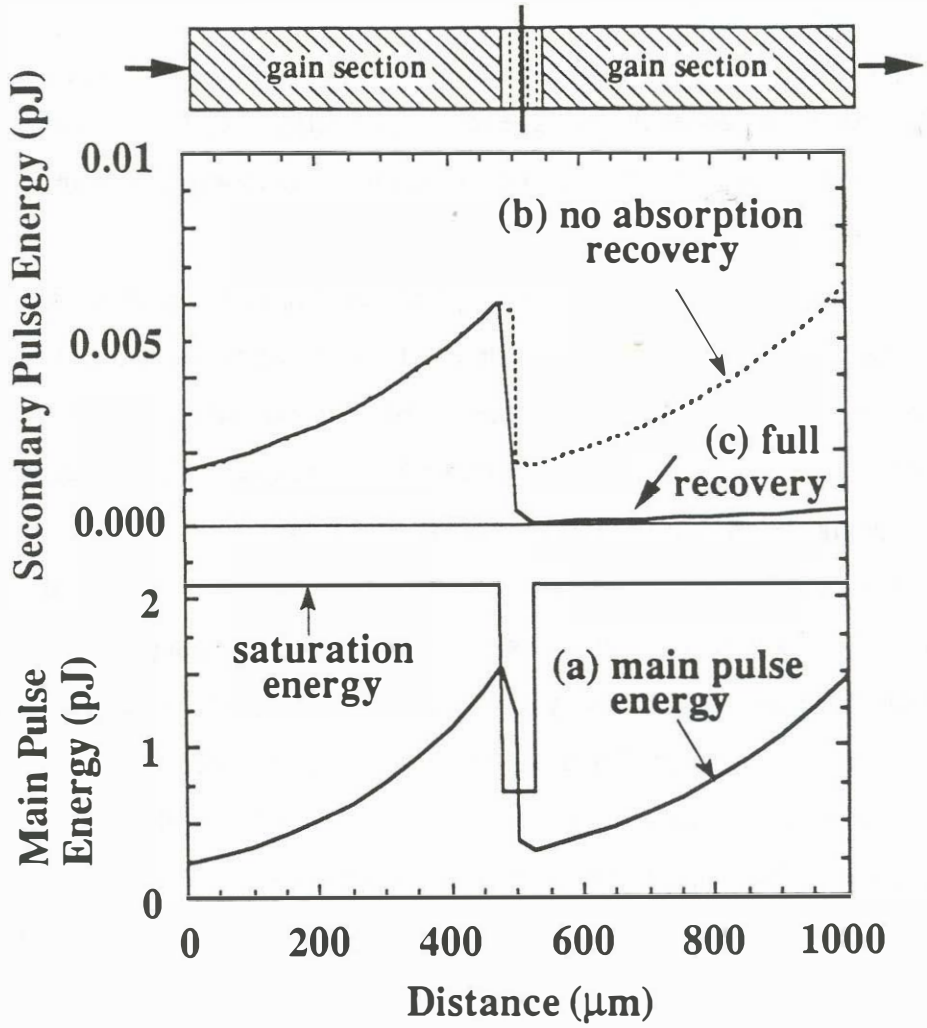

Figure 2.29 Pulse energy versus distance on the two passes through a two-section passive mode-locked semiconductor laser. (a) The main pulse energy versus distance. The pulse is first amplified and then shortened in the saturable absorber. 30% of the power is reflected back through the saturable absorber and then re-amplified before leaving to the external cavity. (b) A secondary pulse is introduced into the cavity by the imperfect antireflection coating. Because the main pulse does not fully deplete the gain and because continued pumping steadily drives the gain higher, the secondary pulse experiences gain. If the absorber does not recover (b), the secondary pulse will have a small loss in the saturable absorber and the amplitude of the secondary pulse can increase. If the saturable absorber recovers its absorption (c), the secondary pulse is highly attenuated leading to suppression of multiple pulse formation.

where T_1 and T_2 are the forward and back transmissions through the saturable absorber. A secondary pulse is initiated by the anti-reflection coated facet (10^{-3} power reflectivity) as the main pulse leaves the laser diode. The energy versus distance for the secondary pulse is shown in Figure 2.29b, and 2.29c for the cases of no saturable absorber recovery and complete saturable absorber recovery respectively. In Figure 2.29b, the absorption does not recover leading to an overall gain of 4.8 through the laser diode. The saturable absorber energy transmission, T_{ab}, decreases with time as:

$$T_{ab}(t)=T_{oab}\, e^{\left[\ln\left(\frac{1}{T_{oab}}\right) e^{\left(\frac{-t}{\tau_{ab}}\right)}\right]} \tag{2.5}$$

where T_{oab} is the unsaturated loss through the absorber, t_{ab} is the carrier density decay constant and t is the time measured with respect to the passage of the main pulse through the saturable absorber. If the absorber completely recovers, as seen in Figure 2.29c, the secondary pulse is partially absorbed, and the round trip gain for the secondary pulse, G_{rts}, is reduced from 0.72 to 0.036. This stops the secondary pulse from building up. If the pulse energies are assumed to add incoherently, the secondary pulse energy, E_{sec}, at the R_2 facet builds up as:

$$E_{sec}(I) = E_{main}\, R_1 + G_{rts}\, E_{sec}(I-1) \tag{2.6}$$

where I is the round trip index and E_{main} is the main pulse energy incident on the R_1 facet. If G_{rts} is less than unity, the ratio of the main pulse to secondary

pulse energies at the laser output is:

$$\frac{E_{out\ main}}{E_{out\ sec}} = \left(\frac{G_1 T_1(0)}{G_{1s}}\right) \frac{R_{ext}(1-G_{rts})}{T_1(t_{rt})R_1} \approx \frac{R_{ext}(1-G_{rts})}{T_1(t_{rt})R_1} \tag{2.7}$$

where t_{rt} is the laser diode round trip time. For the examples of Figure 2.29b and 2.29c, the ratio of pulse energies would be 40 for no absorption recovery, and 680 for full absorption recovery. The example of Figure 2.29 illustrates that significant secondary pulse build-up can occur if the saturable absorber does not recover in the diode round trip time, t_{rt}. If G_{rts} is greater than one, the pulse will continually build up until the energy of the secondary pulse saturates the gain enough to reduce the round trip gain back to one. For very short laser diode lengths, three effects increase G_{rts}:

a) The absorption can not recovery significantly in t_{rt}.

b) The pump is still increasing the gain.

c) The gain for the secondary pulses increases because the main pulse has not fully depleted the gain before the secondary pulse is initiated.

For very long laser diode lengths, the gain for the secondary pulse recovers significantly from the saturated gain values during the secondary pulse transit leading to a G_{rts} greater than one.

To test the saturable absorber's ability to suppress secondary pulses, bulk active region devices with gain section lengths of 150 μm, 250 μm, and 500 μm and absorber lengths of 8 μm and 16 μm are tested. These lengths correspond to a t_{rt} of 4.5, 7.5 and 15 ps respectively, and estimated T_o values of 0.05 and 0.22 respectively. The devices used in the experiment were the bulk active region structures of Figure 2.27 and Figure 2.28. The devices are

passively mode-locked at 5 GHz with -1.5 V on the saturable absorber and gain section currents of 48 mA, 49 mA and 52 mA for the 150 μm, 250 μm and 500 μm devices respectively. The pulses are measured by second harmonic autocorrelation and the resulting traces shown in Figure 2.30. This figure shows that for very short device lengths, secondary pulse generation is hard to suppress due to the small absorption recovery in the laser diode round trip time. The autocorrelation trace for the 150 μm device shows partially defined secondary pulses, the 250 μm device showed highly suppressed secondary pulses and the 500 μm device had no detectable secondary pulse. The fact that the 500 μm long device did not show multiple-pulse formation agrees with the measured absorption recovery time of approximately 10 ps in the pump-probe experiment of Figure 2.26. The propagation time around the 500 μm long device is 13 ps. In the frequency domain, multiple pulse generation manifests itself as ripple in the optical spectrum. The ripple frequency spacing is $1/t_{rt}$. Figure 2.31 shows the progressive reduction in spectral ripple as the laser diode length is increased. The 500 μm device produced a 4.4 ps autocorrelation width. If a $sech^2(t)$ pulse shape is assumed, the pulses are 2.9 ps wide with a peak power of 0.25 W. The experimental results of Figure 2.30 and 2.31 show that it is very important to have the round trip time in the diode laser at least as long as the absorption recovery time of the waveguide saturable absorber in order to suppress multiple pulse formation. It is also important to have enough unsaturated absorption in the saturable absorber so that the secondary pulses encounter high levels of absorption. Figure 2.32 shows autocorrelations and optical spectra for a comparison between saturable absorber lengths of 8 and 16 μm. The over-all laser diode lengths are 500 μm long in each case. The 16 μm long saturable absorber shows nearly complete suppression of secondary

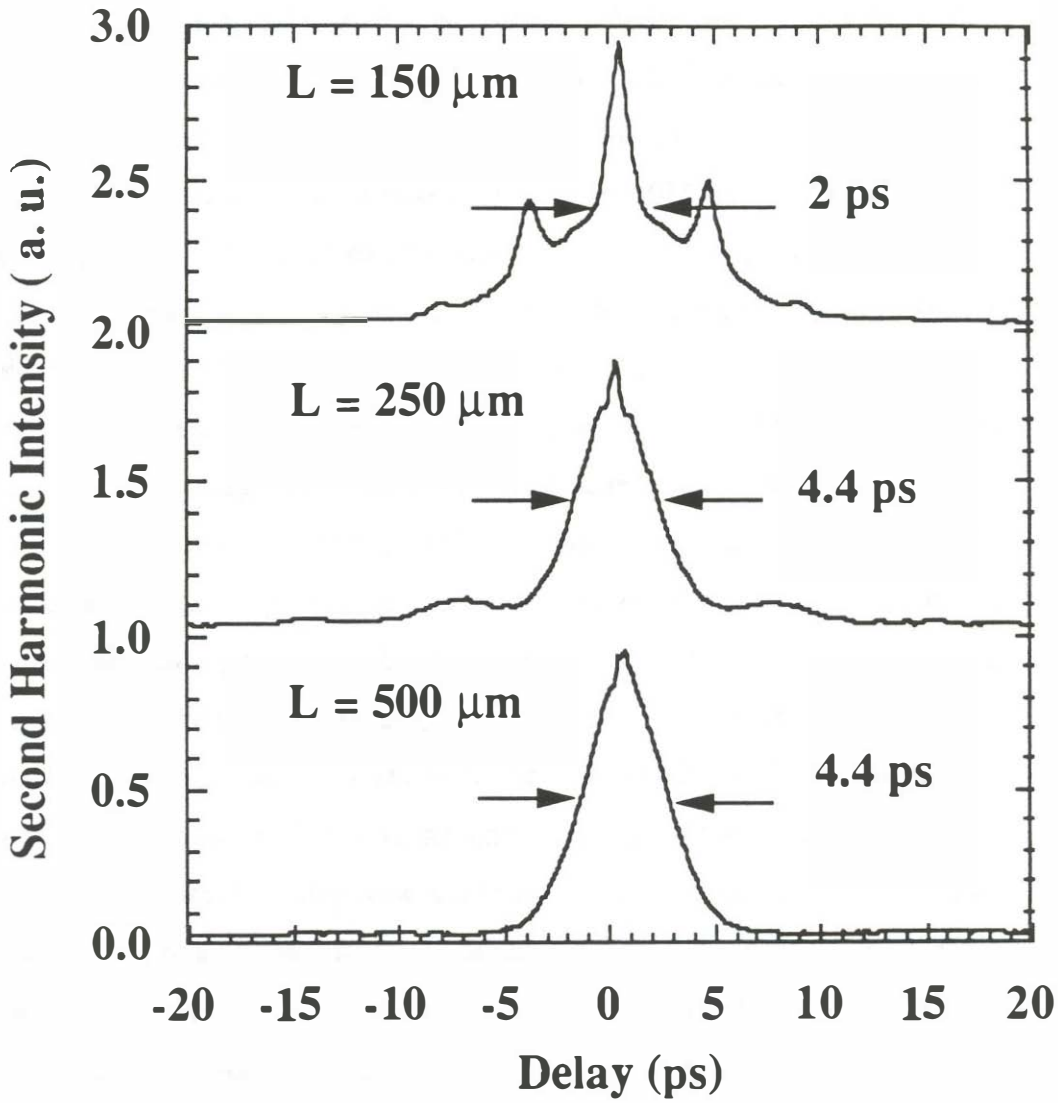

Figure 2.30 Autocorrelation traces for three lengths of the gain segment. The active region for the devices is described in Figure 2.24. The plot shows the improved suppression of the secondary pulses as the roundtrip time in the laser diode is increased.

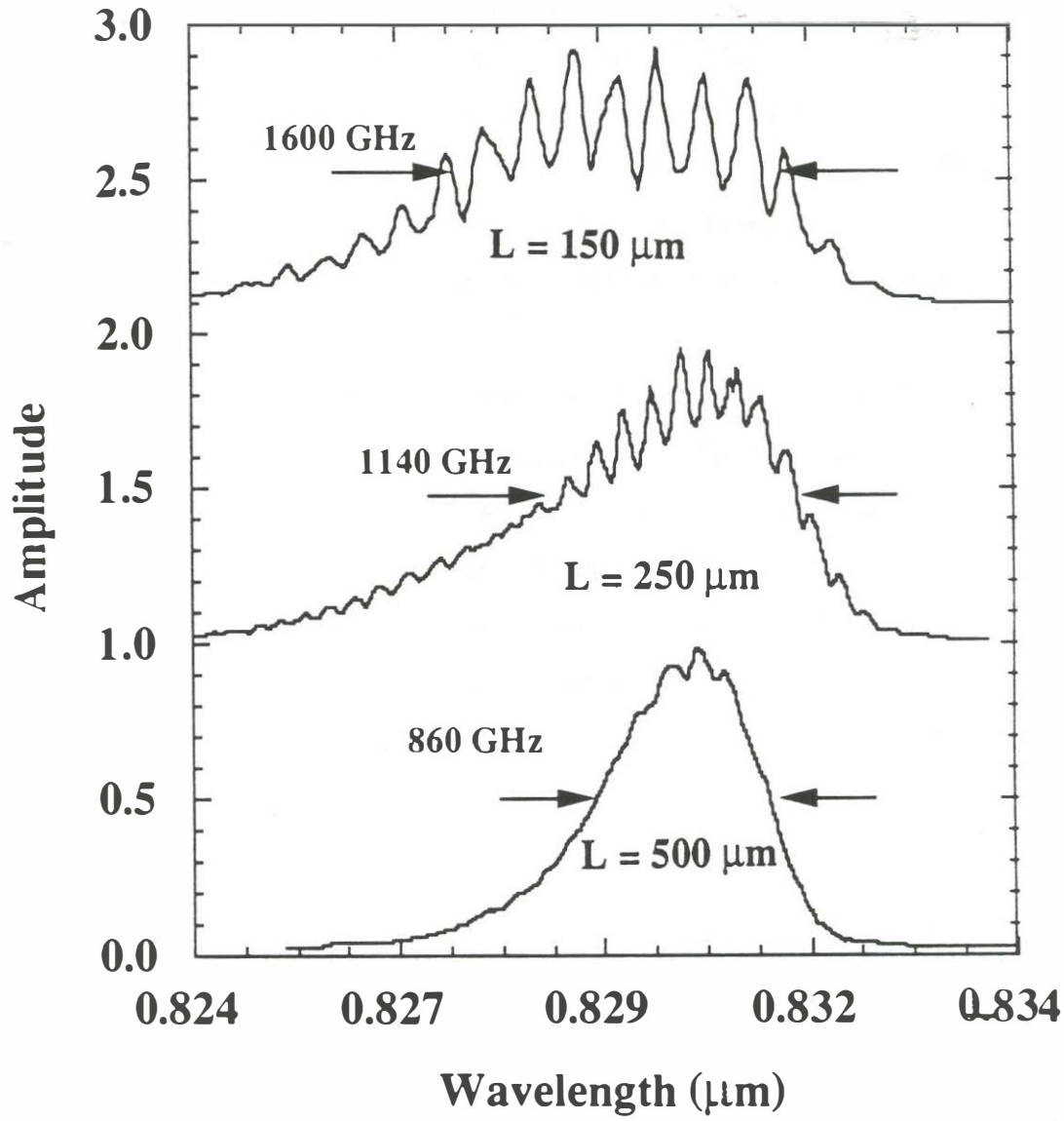

Figure 2.31 Optical spectrum for the three autocorrelation traces of Figure 2.30. The optical spectrum shows a ripple with a frequency spacing equal to 1/(round trip time in the laser diode). The trend shows that longer laser diode lengths have reduced ripple which corresponds to reduced secondary pulse level in the time domain.

pulses. The 8 μm saturable absorber s
pulsewidth with a partially suppressed s
2.32 is that there are two requirements f

1. There should be sufficient r
allow the saturable absorber to r
GaAs/AlGaAs devices).
2. There must be sufficient
saturable absorber to highly atten

A two section quantum-well laser
over-all device length was 500 μm wit
The results are shown in Figure 2.33 al
region device. The device showed an o
energy of 0.7 pJ. **An important poi**
mode-locking can be accomplish
devices.

shown in Figure 2.34. The photocurre
the charge is removed from the capac
mostly due to capacitance effects of t
absorption of secondary pulses. Figure
1.6 mm long quantum well device wi

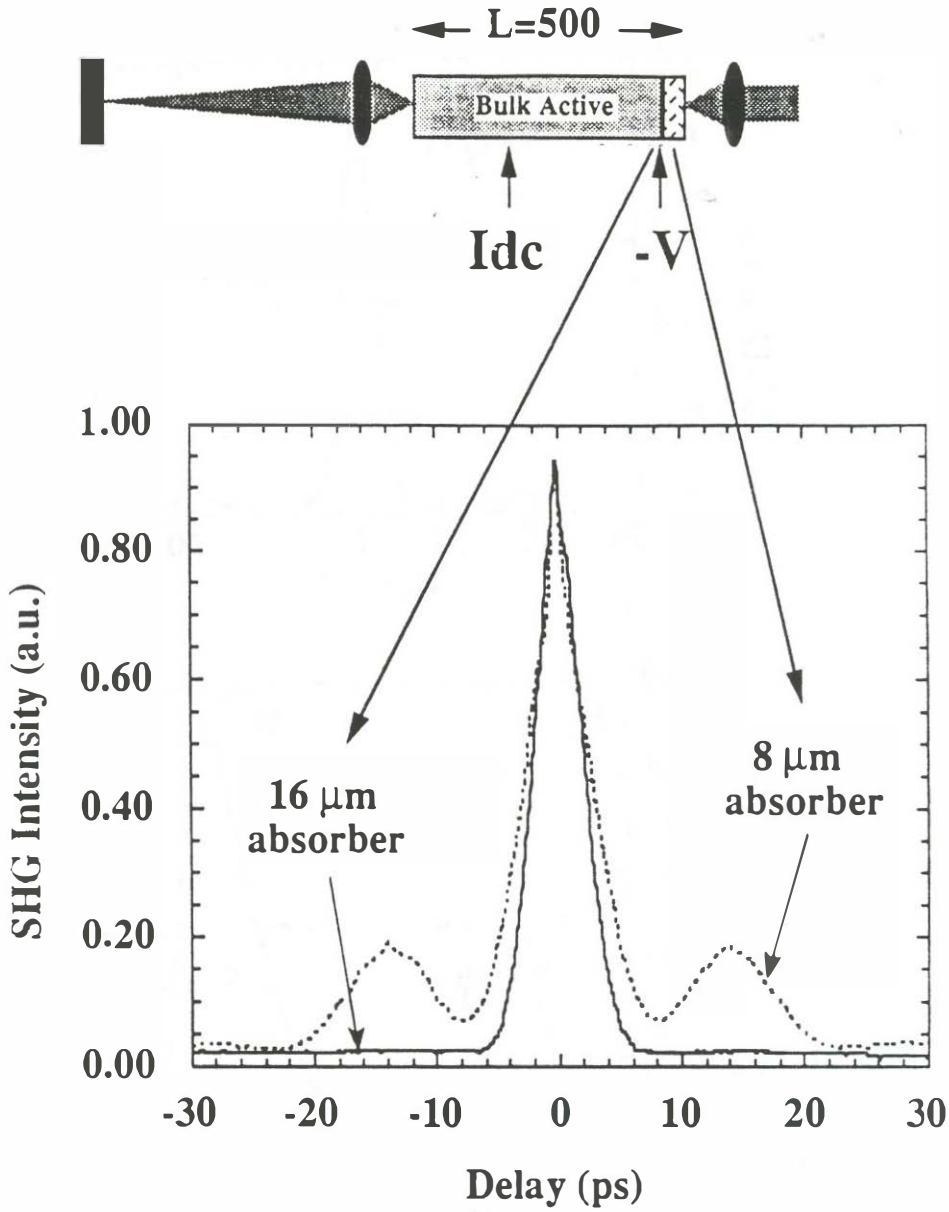

Figure 2.32 Performance of a two-section passive mode-locked laser as a function of the length of the saturable absorber. The saturable absorber lengths were 16 μm and 8 μm. The active region for the device was described in Figure 2.24. The gain section length was 500 μm in both cases. The 8 μm saturable absorber produced slightly wider pulsewidths and also showed reduced suppression of the secondary pulses compared with the 16 μm saturable absorber case.

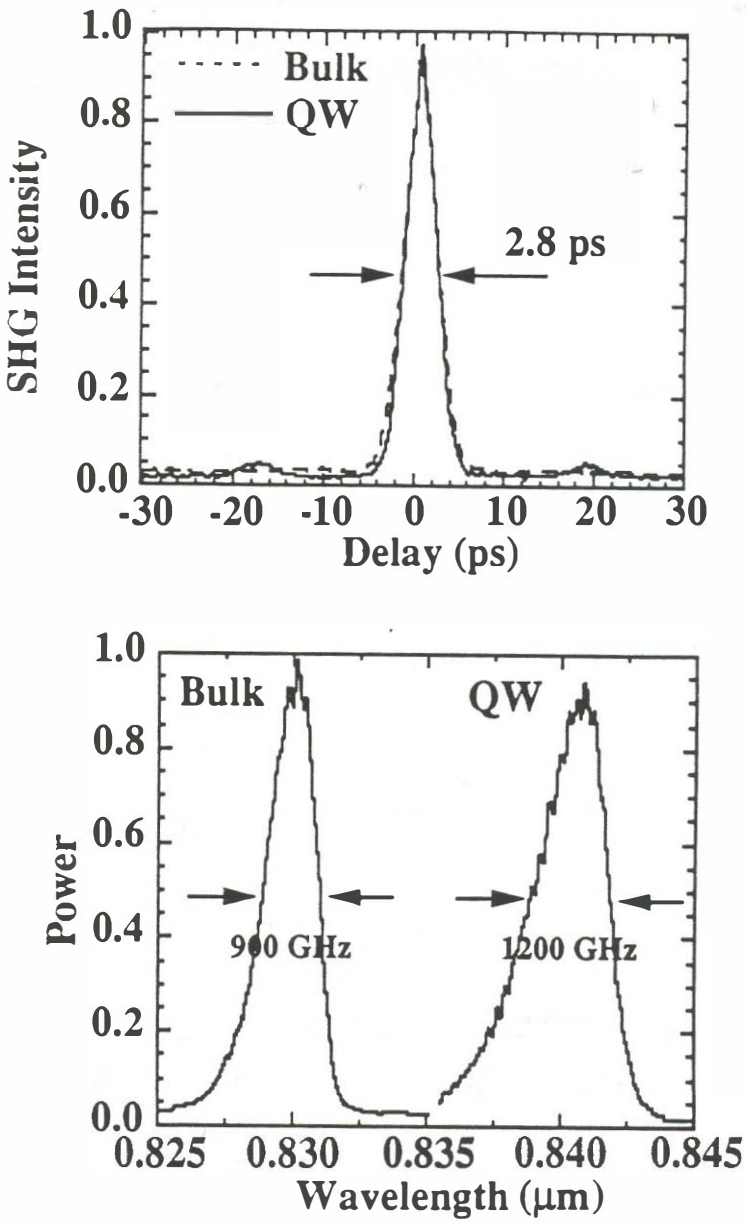

Figure 2.33 A comparison of the performance of a two section passive mode-locked laser using a GaAs bulk and GaAs quantum well active region. The quantum well structure was described in Figure 2.26 and the bulk active region structures was described in Figure 2.24. The point of the figure is to show that laser structures of both bulk and quantum well types are suitable for incorporation into multi-segment mode-locked laser structures.

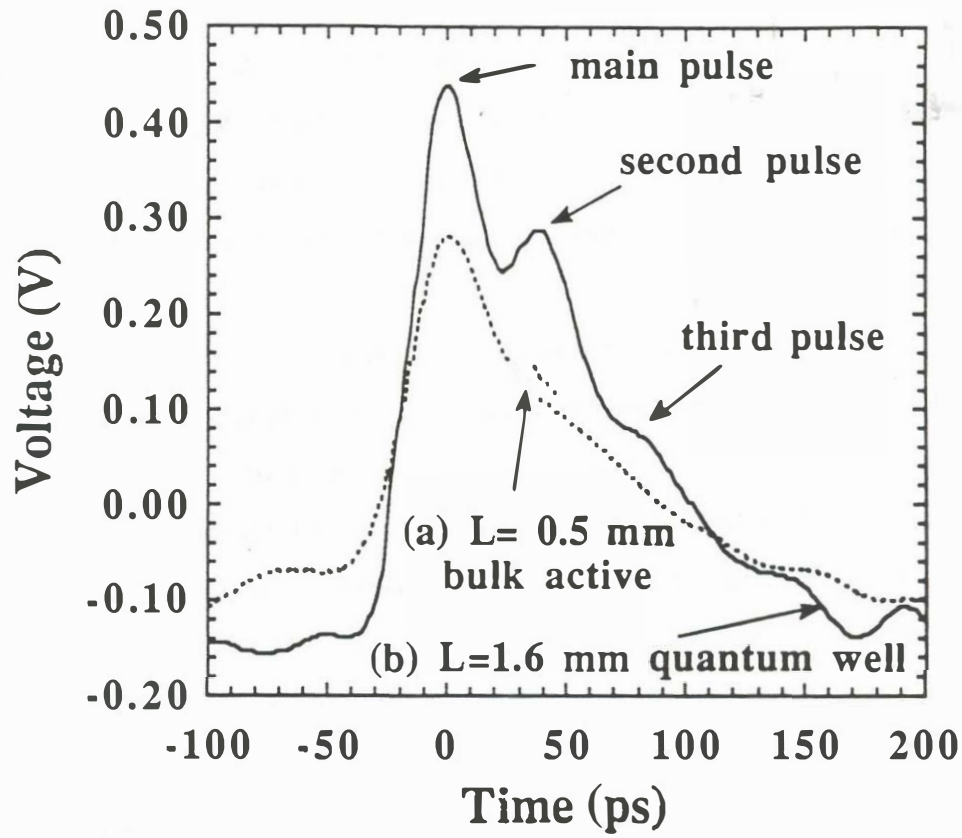

Figure 2.34 Photocurent from a saturable absorber during passive mode-locked laser operation. (a) The photocurrent from a 16 μm long bulk active region absorber with diode length of 500 μm. (b) The photocurrent from an 80 μm long quantum well saturable absorber with diode length of 1.6 mm. The 1.6 mm long device has a round trip time delay large enough so that the absorption of the secondary pulses becomes clearly evident. For the 500 μm long device, the secondary pulse absorption peaks are not clearly visible.

photocurrent shows clear absorption peaks spaced at t_{rt}. The first pulse is created by the leading edge of the main pulse. The second and third peaks are due to partial absorption of secondary pulses. An external detector measurement of the optical output showed that the energy of the secondary pulse was 15% of the main pulse. The cause of the secondary pulses in this case is presumably due to significant gain recovery during the secondary pulse transit in this long device.

In summary, it has been shown that multiple pulse behavior can be suppressed with the inclusion of intra-waveguide saturable absorbers into the mode-locked laser. The saturable absorber recovery time constant, the laser diode round trip time, and the unsaturated absorption level are important parameters in the effectiveness of the suppression. The saturable absorption mechanism can produce short pulses with energies approaching the saturation energy of the gain section without the need for fast electrical pumping waveforms. This technique is applicable to lasers with bulk or quantum well active regions and incorporates easily into many existing laser processes. Waveguide saturable absorbers are superior to the excitonic saturable absorbers of Section 2.3. Integrated waveguide saturable absorbers result in a much simpler cavity configuration. Since the laser and saturable absorber are fabricated together, their characteristics are well matched. The laser amplifier can more easily saturate a waveguide saturable absorber since there is no coupling loss between the amplifier and the waveguide saturable absorber.

2.5 Hybrid mode-locked multi-section external cavity lasers

Section 2.4 described the use of waveguide saturable absorbers to accomplish passive mode-locking. The use of the waveguide saturable absorber provided two important benefits over single-section active mode-locking techniques. 1) It suppressed the problems associated with imperfect anti-reflection coatings. 2) It reduced the need to have extremely short electrical gain modulation pulses since passive gain modulation is a stronger pulse shortening mechanism than active gain modulation.

For many applications, it is desirable to have the optical pulse output from the mode-locked laser coordinated to an electronic system. Passive mode-locked lasers have an electrical output timing reference from the photocurrent in the waveguide saturable absorber, but the electronic system would then have to be coordinated to the mode-locked laser. It has also been found that the timing stability of passive mode-locked lasers is inferior to that of active gain modulation (this point will be discussed in Chapter 4). The solution to this problems is to add active gain modulation along with passive gain modulation to accomplish hybrid mode-locking (a combination of active and passive). In hybrid mode-locking, passive gain modulation has the primary responsibility to form the short optical pulsewidths. Active modulation has the primary responsibility to stabilize the pulse stream in amplitude and in time and a secondary responsibility to shorten the optical pulsewidth.

The two configurations used to implement hybrid mode locking are shown in Figure 2.35. The first implementation uses a two-section passive mode-

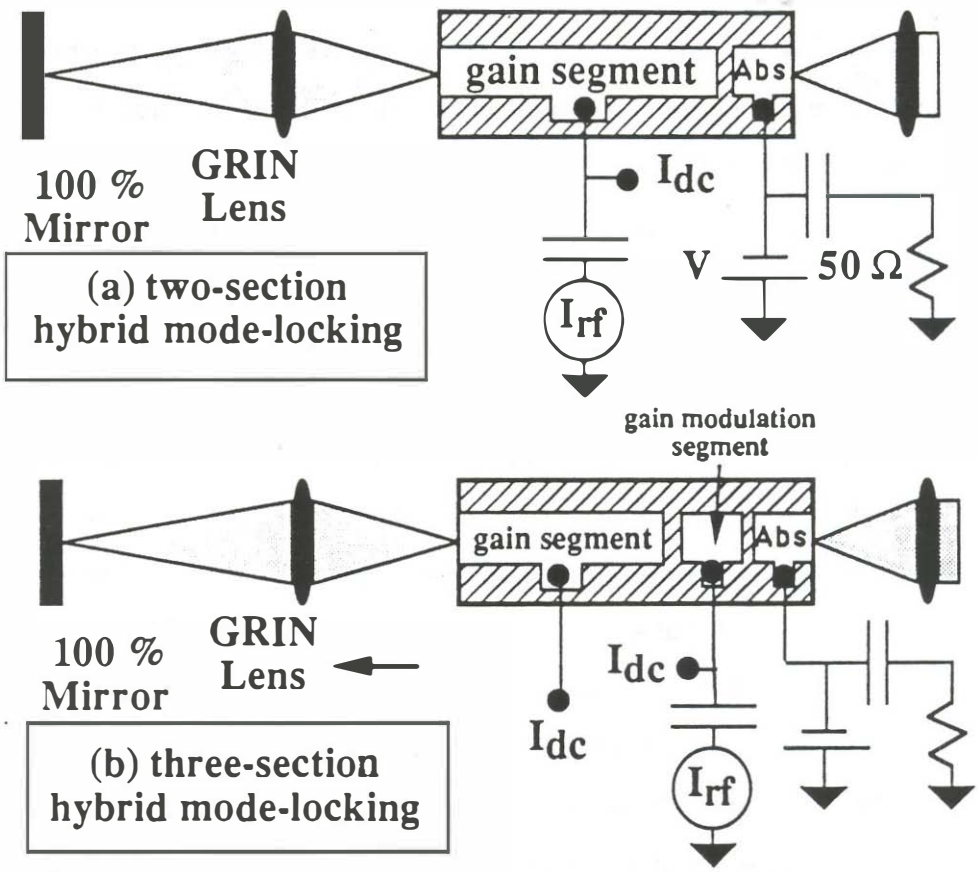

Figure 2.35 Methods of hybrid (combination active/passive) mode-locking an external cavity mode-locked semiconductor laser. (a) A two section laser in which the functions of gain and gain modulation are combined into the long segment. (b) A three section laser in which the functions of gain, gain modulation, and saturable absorption are separated into individual segments.

locked laser as studied in Section 2.4 with a modulation signal added to the long segment. In this design, the functions of gain and gain modulation are accomplished in the same segment. A two section quantum well laser was hybrid mode-locked with the experimental arrangement of Figure 2.35a. The long segment was modulated with a 24 dBm sinusoid at 5 GHz. The resulting autocorrelation and spectrum is shown in Figure 2.36. The deconvolved optical pulse width is 2.6 ps. The same device when passively mode locked produced a 2.5 ps pulse. This experimental comparison of active and passive mode-locking shows that the saturable absorber for this experiment is almost completely responsible for pulse shortening. The noise characteristics of the hybrid mode-locked devices are drastically improved compared with passive mode-locked devices (see Chapter 4).

The second implementation of external cavity hybrid mode-locking involves separating the functions of gain and gain modulation by creating a third segment as is shown in Figure 2.35b. The gain modulation segment is short and does not provide substantial gain for the device. This allows the gain modulation segment to be nominally DC reverse biased. The DC reverse biased segment is highly absorbing due to the photodetector-like operation as was described for waveguide saturable absorbers is Section 2.4. When a gain modulation pulse is added to the segment, the peak of the signal causes forward bias current injection. Since only the peak of the pulse is actually injecting current, the effective gain modulation pulsewidth is narrowed and the active gain modulation becomes more effective. Figure 2.37 shows experimental results for a hybrid mode-locked 3-section laser. The device had a 70 % high reflectivity coating at the output facet and was actively gain modulated with at 24 dBm 6 GHz sinusoid. The device is the bulk active region laser operating of

Figure 2.27. The resulting deconvolved pulsewidth is 1.9 ps with 0.18 pJ of energy. The same laser when operated as a 2 section passively mode-locked laser (the modulation signal was turned off and the gain modulation segment was connected to the gain segment) produced 2.6 ps pulses. This comparison shows that when the gain modulation segment is separated from the gain segment, more effective gain modulation results. Active gain modulation is not playing the dominant roll in pulse shaping but it is making a noticeable contribution.

It should be noted that the multi-segment structures used in Sections 2.4 and 2.5 are done with laser processes that were not originally designed for high modulation bandwidth operation. The cut-off frequency for the gain modulation segments due to device parasitics is estimated to be 5 GHz in the bulk active region design of Figure 2.27. Since passive gain modulation is doing most of the gain modulation (and the saturable absorber operation is relatively insensitive to bond-pad capacitance), the active gain modulation segment need not be a dominant player for pulse shortening. This illustrates the versatility of hybrid mode-locking as the easiest way to get high performance mode-locking results. Many existing laser processes can be converted to a mode-locked laser process simply by the separation of the top contacts of the material, and proper design of the segment lengths.

In summary, three section hybrid mode-locked lasers are the culmination of the progression of multi-section external cavity mode-locked lasers shown in Chapter 2. By separating the functions of gain, gain modulation, and saturable absorption into a single integrated structure, significant device performance increase is obtained.

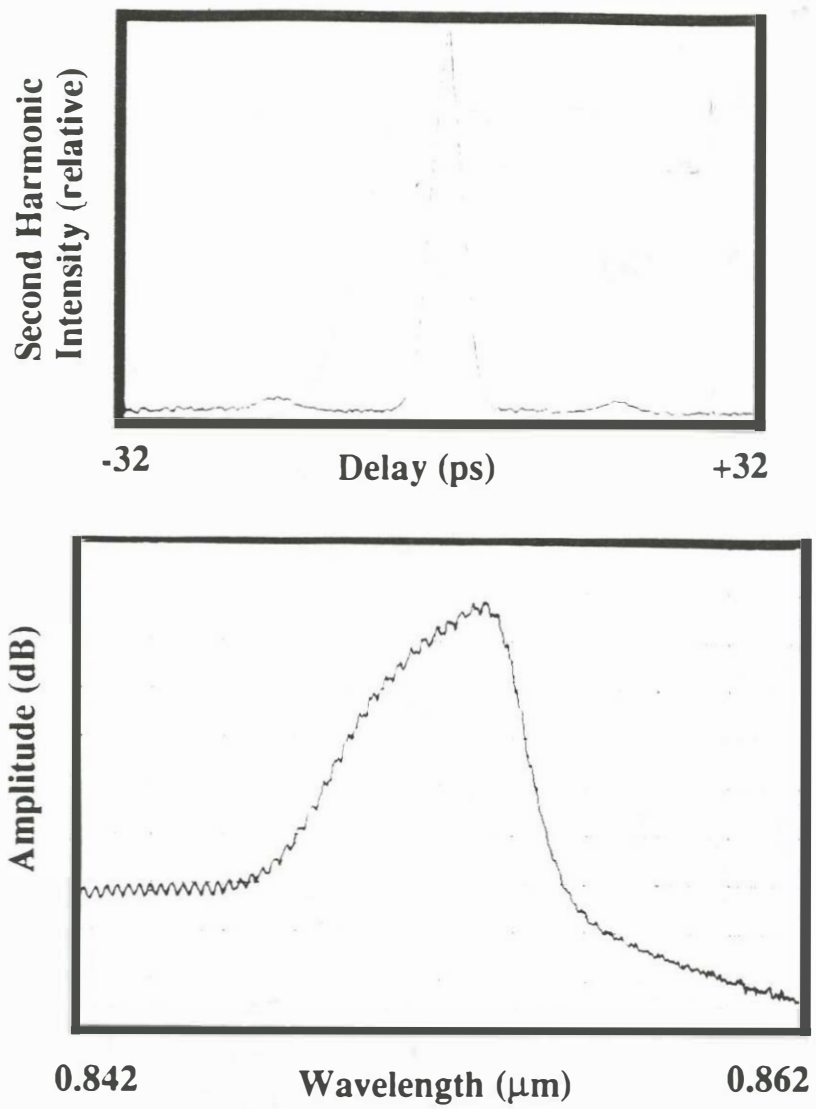

Figure 2.36 Autocorrelation and optical spectrum results for a two-section hybrid mode-locked quantum well external cavity laser operating at a repetition rate of 5 GHz. The absorber length is 80 μm and the diode length is 500 μm.

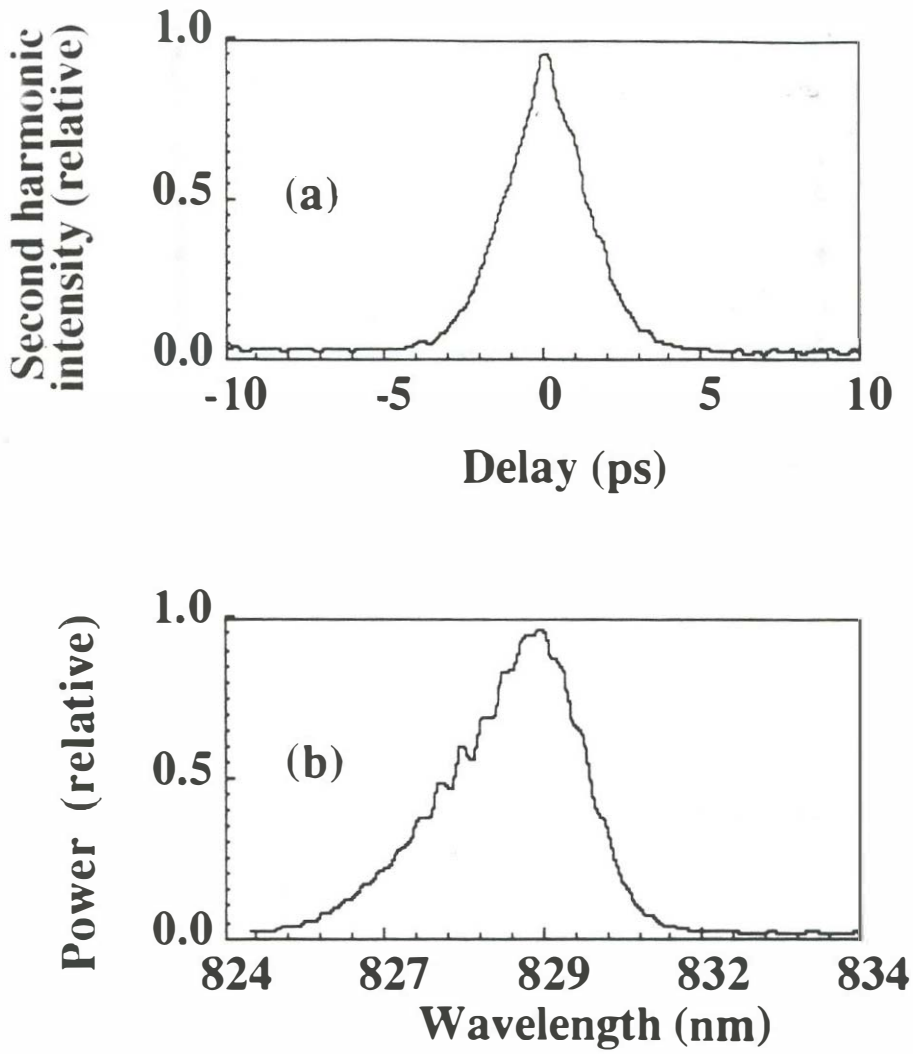

Figure 2.37 Autocorrelation and optical spectrum result for a three-section hybrid mode-locked bulk active region external cavity laser operating at a repetition rate of 6 GHz. The saturable absorber length is 16 μm and the diode length is 500 μm.

Chapter 3
Monolithic cavity mode-locked semiconductor lasers.

3.1 Multi-section monolithic cavity devices

Chapter 2 discussed the evolution of external cavity mode-locked lasers from single-segment to multiple-segment designs. The simplest configuration was the active mode-locked single section lasers as is shown in Figure 3.1a. Two-section active mode-locked lasers (Figure 3.1b) showed improved performance due to the separation of the functions of gain and gain modulation. Two section passive mode-locked lasers (Figure 3.1c) showed improved performance since passive gain modulation is a stronger pulse shortening mechanism than active gain modulation. The last improvement was to combine active and passive gain modulation into a hybrid mode-locked laser with three segments (Figure 3.1d). The experiments with multi-segment external-cavity mode-locked lasers have shown that all of the necessary functions for passive, active, and hybrid mode-locked lasers can be implemented together on a single semiconductor chip.

For the next step, the entire external cavity can be replaced with a semiconductor waveguide resulting in an integrated monolithic cavity mode-locked laser structure such as that shown in Figure 3.1e. If the entire cavity is one continuous semiconductor waveguide, the problems of multiple pulse formation due to intracavity reflections are eliminated (see Section 2.4). Monolithic cavity devices are very small and do not have the mechanical

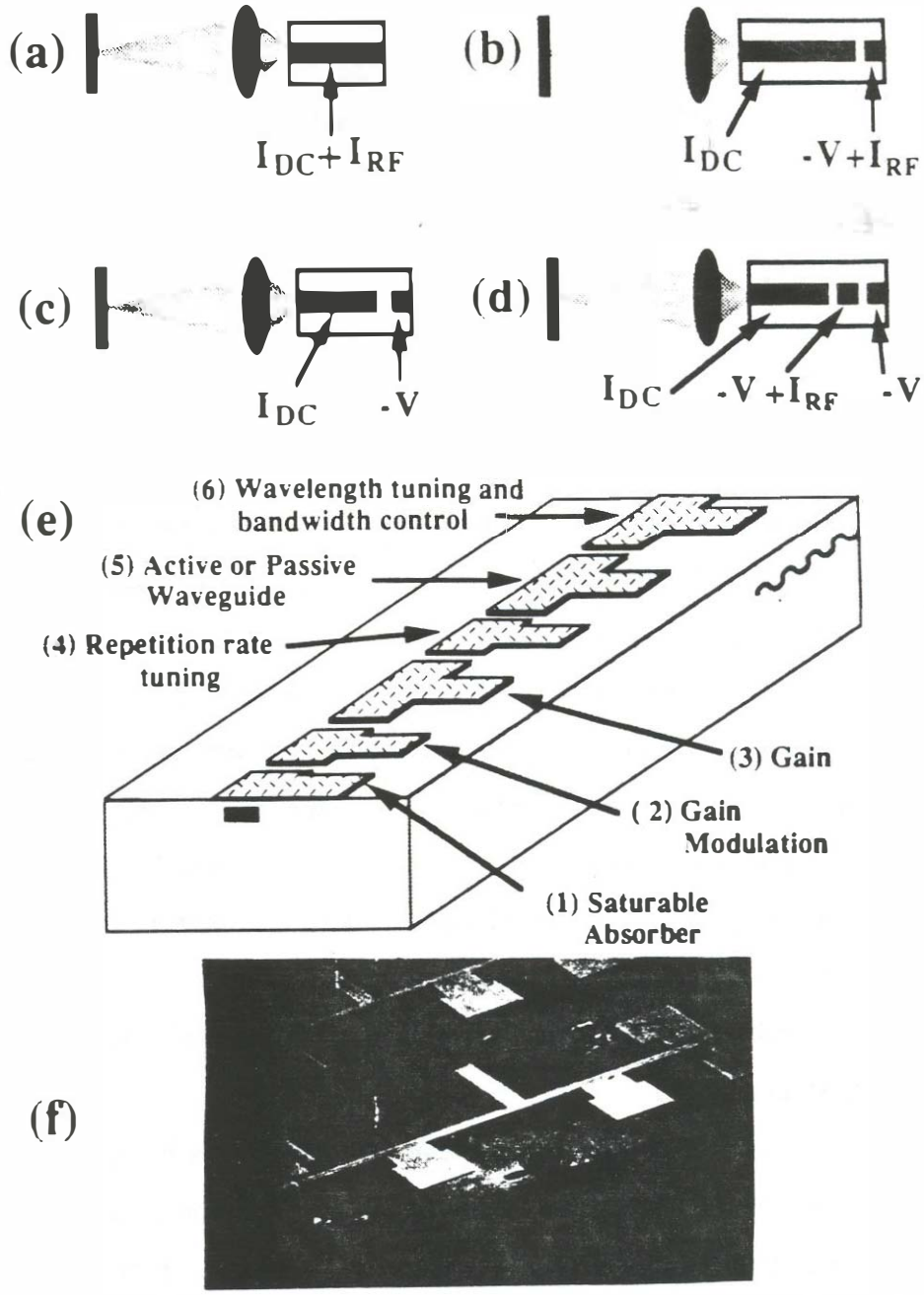

Figure 3.1 Multi-segment mode-locked semiconductor laser configurations and the evolution to a monolithic cavity structure. (a) Single-segment external cavity active mode-locking, (b) two-segment external cavity active mode-locking, (c) two-segment external cavity passive mode-locking, (d) three-segment external cavity hybrid mode-locking, (e) functionality in a monolithic cavity mode-locked laser structure, and (f) scanning electron micrograph of a multiple-segment mode-locked laser structure.

instabilities associated with the optical elements in an external cavity. Figure 3.1f shows a scanning electron micrograph of a monolithic cavity structure with multiple-segments. Figure 3.1e illustrates the wide range of functionality that is possible from a process that incorporates separated top contacts for non-uniform electrical biasing and a continuous waveguide along the entire device length. In this simple process, six distinct functions can be performed:

i) Section 1 is reverse-biased to act as a waveguide saturable absorber/photodetector for passive and hybrid mode-locking.

ii) Section 2 is the gain modulation segment.

iii) Section 3 is forward biased and provides the overall gain necessary for lasing.

iv) Section 4 is a segment that allows for electrical tuning of the repetition rate by adjusting the carrier density.

v) Section 5 is the active or passive waveguide section which provides the delay necessary for achieving a specific repetition rate. Active waveguides are the easiest to fabricate in a laser process. Low-loss passive waveguides can be integrated with a more complex processing sequence [54,55]. Multiple pulsation effects can be a problem if there is a reflection at the active-to-passive waveguide transition. Reflection problems caused by imperfect active-passive transitions can be suppressed using the multi-segment external-cavity laser techniques outlined in Sections 2.4 and 2.5.

vi) Section 6 incorporates Bragg wavelength filters to control the center wavelength and bandwidth of the laser [56]. Control of the laser bandwidth is very important for optical fiber communication system applications.

Monolithic cavity designs have been demonstrated with overall lengths between 7 mm and 0.25 mm corresponding to a repetition rate as low as 5.5

GHz [49] and as high as 350 GHz [30]. The low end of the repetition rates is limited by fabrication technology limits for very long devices. Such high repetition rates in the sub-millimeter wave range are truly amazing and have only been observed in semiconductor laser systems. These high repetition rates are seen only for passively mode-locking techniques. The high repetition rate is partially made possible by the very fast absorption recovery times of waveguide saturable absorbers as was discussed in section 2.4. If the absorption did not recover on each round trip of the pulse around the laser cavity, the saturable absorber would not be effective. The sub-10 ps absorption recovery time measured by the pump-probe technique of Karin [52] shows that passive mode-locking above 100 GHz is not limited by the absorption recovery time.

The three basic techniques used to mode-lock these monolithic cavity devices are shown in Figure 3.2. The monolithic cavity device is broken up into three different sections. The first section is the gain modulation segment, the second is the gain section, and the third is the gain modulation segment. In active mode-locking, the modulation segment is driven by the electrical modulation signal and the saturable absorber section is connected to the gain region. In passive mode-locking, the modulation segment is connected to the gain region, and the saturable absorber section is reverse biased. In hybrid mode-locking, both the gain modulation segment and the saturable absorber are used.

A three section monolithic cavity mode-locked laser with overall length of 7 mm was fabricated to characterize the performance of a monolithic cavity mode-locked lasers at very low repetition rates. The repetition rate for these long devices is 5.5 GHz, which is the lowest repetition rate monolithic cavity device fabricated to date. Low repetition rates for monolithic cavity devices are

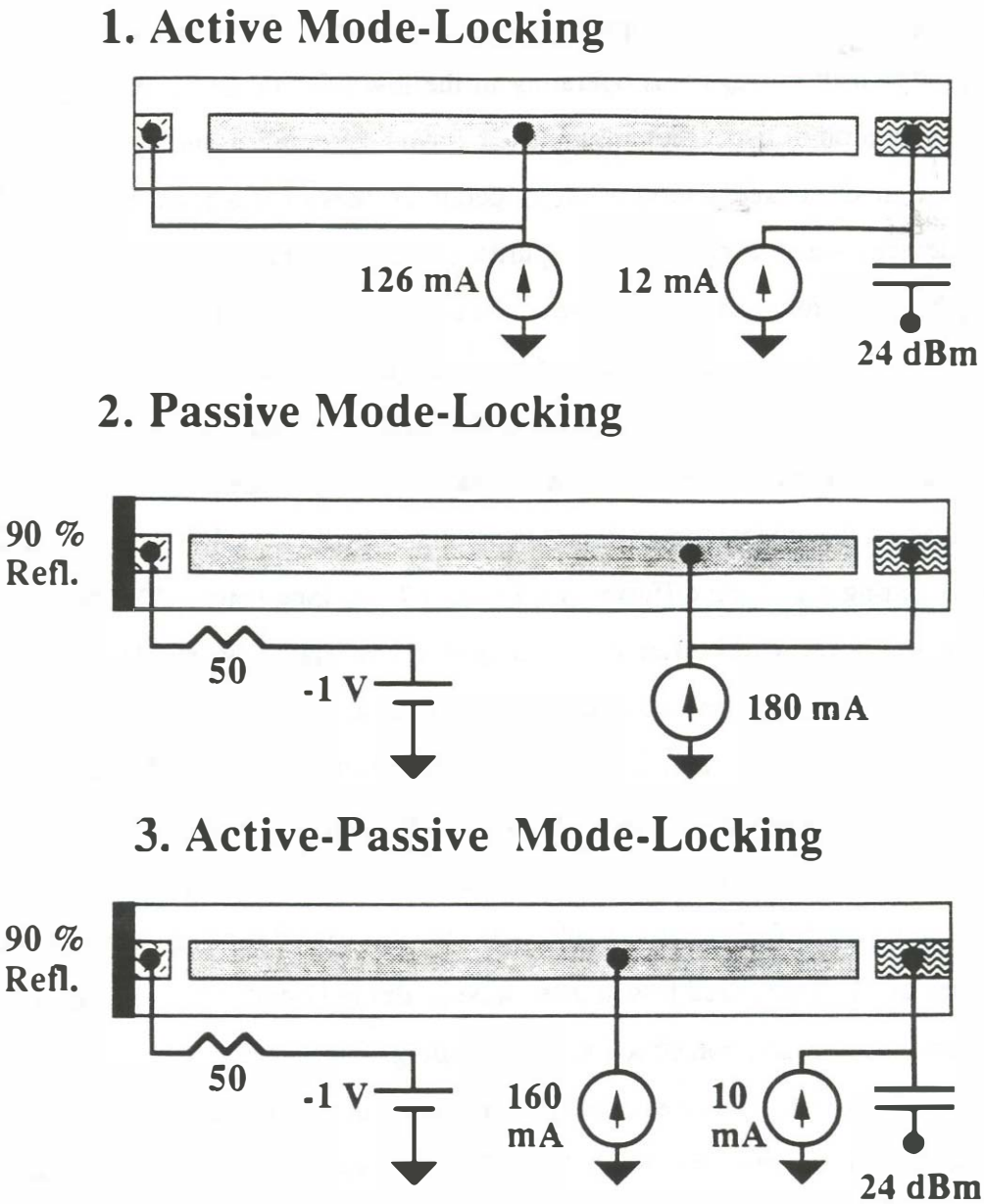

Figure 3.2 The three types of operation of a monolithic cavity mode-locked laser structure. (a) Active mode-locking is accomplished by connecting the saturable absorber to the gain region and applying the electrical modulation pulses to the gain modulation segment. (b) Passive mode-locking is accomplished by connecting the gain modulation segment to the gain region and reverse biasing the saturable absorber segment. (c) Hybrid mode-locking is accomplished by simultaneously applying current modulation to the modulation segment and by reverse biasing the saturable absorber. Both (b) and (c) take advantage of colliding pulse effects in the saturable absorber.

important because most applications of mode-locked lasers require an interface with electronic systems operating in the low GHz range. Present and next generation time-division multiplexed optical communications systems (which use mode-locked lasers) usually operate at rates of less than 20 GHz. The devices were fabricated by impurity induced disordering [50]. Figure 3.3 shows the four quantum well structure used in these monolithic cavity devices. The lateral index guide is formed by the diffusion enhanced intermixing of the four 20 nm GaAs quantum wells and the higher bandgap 8 nm wide $Al_{.4}Ga_{.6}As$ barriers. The finest feature in the process is the 4 μm wide diffusion mask layer making the process more tolerant to defects in the lithography. The critical step is getting a uniform diffusion mask over a 7 mm long length. The final stripe lasing stripe width after disordering is 2 μm leading to single lateral and transverse mode operation. Impurity induced disordering is an excellent high yield process for making very long semiconductor devices. The disordering process can also produce passive waveguides along with the active waveguides with no additional processing steps. The passive waveguide is formed by using a narrower diffusion mask width so that the disordered regions just meet in the center. The measured loss in these waveguides is 17 cm^{-1} which is high due to free carrier absorption effects and band-tailing effects.

Figure 3.4 shows the optical power versus current curves for the 7 mm long lasers. L-I curves for both the 75% active waveguide and 100 % active waveguide structures are shown. The 75% active waveguide structures show higher thresholds and lower quantum efficiencies due to the lossy passive waveguide sections. The threshold current for the 7 mm long device is 60 mA with a differential quantum efficiency of 5 % from each facet. The relatively low quantum efficiency is due to the fact that the internal loss of the laser

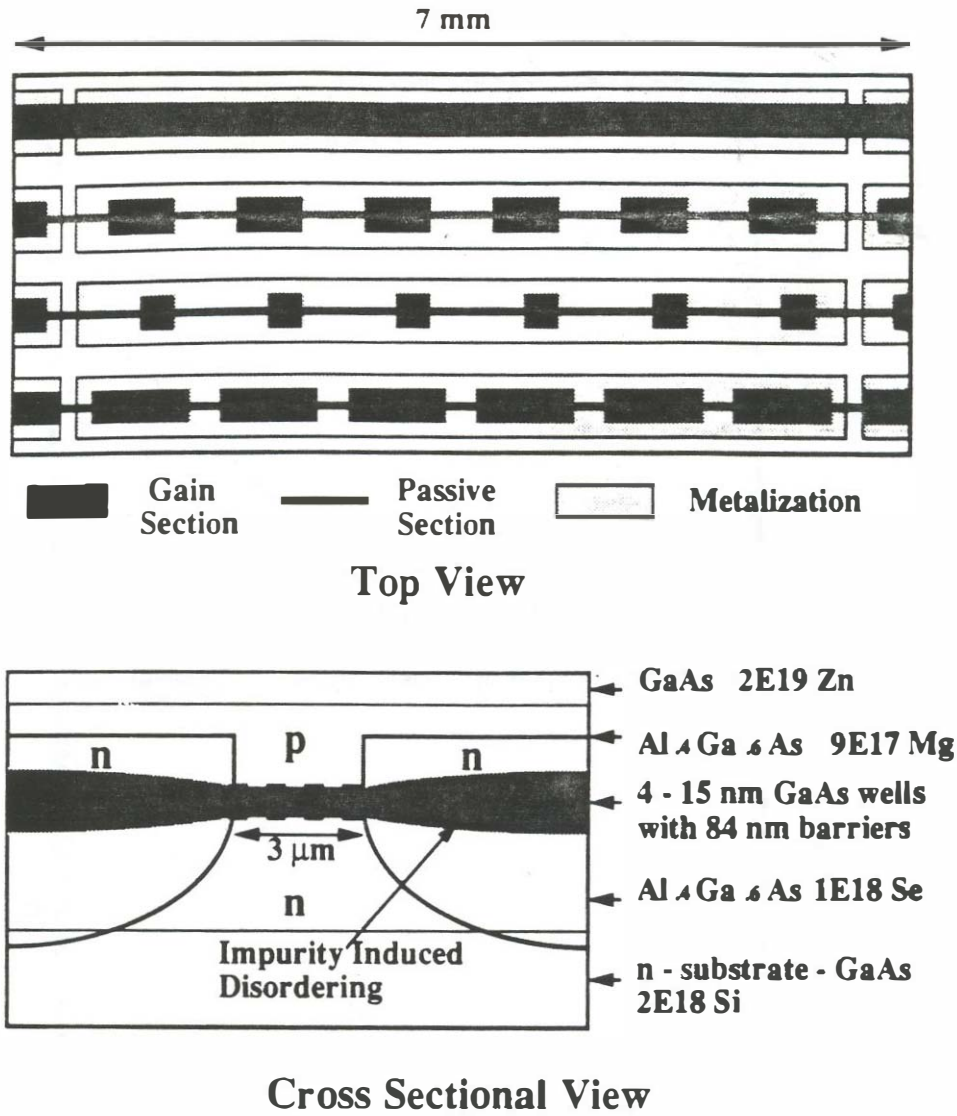

Figure 3.3 (a) The top view of the 7 mm long monolithic cavity mode-locked laser structures. The saturable absorber lengths are 80 µm and the gain modulation segments are 200 µm. (b) The active region cross section of the device is shown. The lateral index guide is formed by impurity induced disordering with silicon. Passive waveguide sections can be formed by allowing the disordered regions to just touch in the middle. The passive waveguide sections are measured to have a loss of 17 cm^{-1}. This relatively large amount of loss is partially caused by free carrier absorption due to the large levels of N-type doing in these passive waveguides.

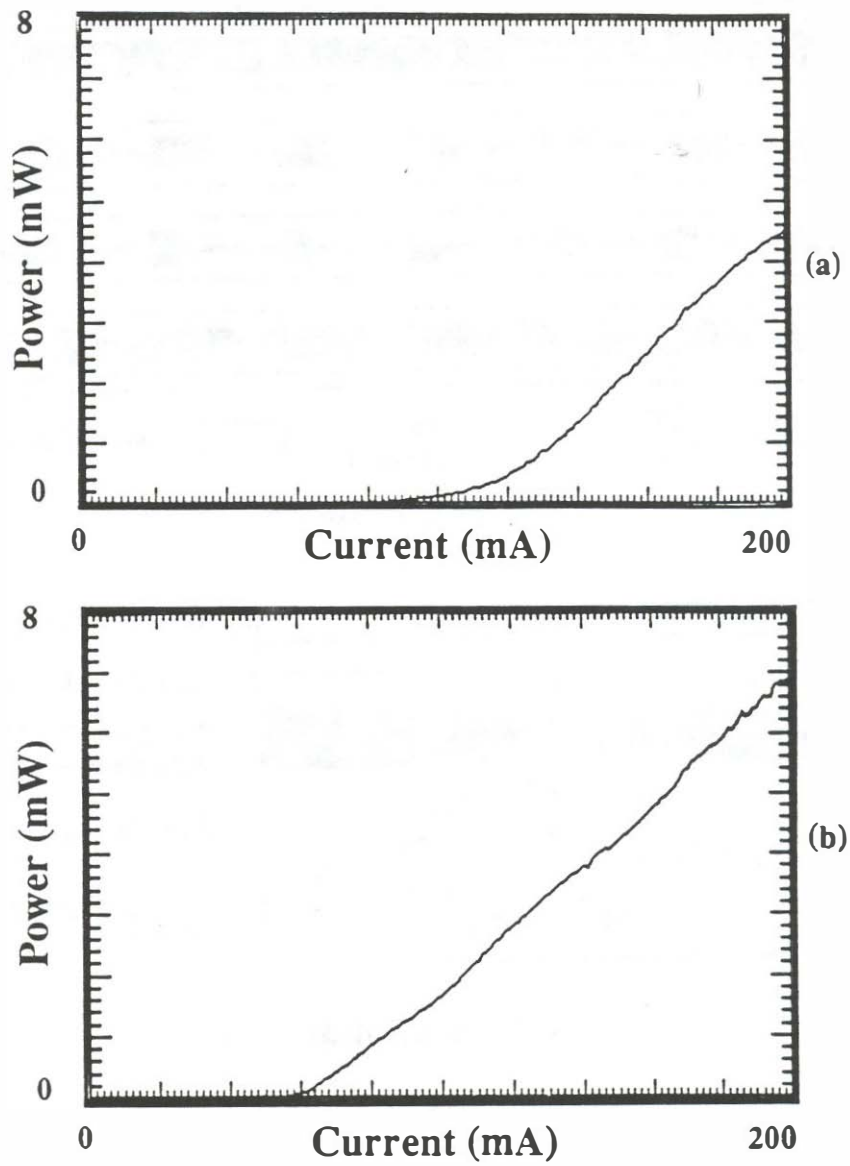

Figure 3.4 The light versus current curve for the 7 mm long lasers of Figure 3.3. L-I curves are given for both the (a) 75 % active waveguide and (b) for the device with 100 % active waveguide. The 75 % passive waveguide device shows a lower quantum efficiency. Lasers of this length in general have a low quantum efficiency because the waveguide loss is large compared to the mirror loss.

dominates over the mirror loss. The waveguide loss in the structure was measured by testing the light-current characteristics of several different length lasers and was found to be 7.5 cm^{-1}. The distributed mirror loss for the 7 mm long device is 0.85 cm^{-1}. The calculated external differential quantum efficiency is therefore 10.2 % assuming 100% internal quantum efficiency.

Figure 3.5a, 3.5b, and 3.5c show typical autocorrelation results using the active, passive, and hybrid mode-locking techniques described in Figure 3.2. For the active and hybrid mode-locking case, the electrical modulation signal was a 24 dBm sinusoid at a nominal frequency of 5.5 GHz. The gain modulation segment was 250 μm long and the saturable absorber section was 80 μm.

The pulsewidth is found to reduce as more pulse shortening mechanisms are added to the mode-locked laser system. Active mode-locking produced a 12 ps pulsewidth, passive mode-locking produced a 10 ps pulsewidth, and hybrid mode-locking produced a 6.5 ps pulsewidth. The spectral width in each case is much wider than the Fourier transform limit indicating that there is a substantial chirping on the optical pulse. The autocorrelations also show coherence spikes due to spontaneous emission noise, and unmode-locked spectrum.

There are significant spontaneous emission levels in a laser of this length. Because of the internal loss in the device and the extremely long length, the amplifier has to overcome a total waveguide loss of $\exp(7.5\ cm^{-1} \times 1.4\ cm) = 36{,}000$. The loss in the mirrors would only dictate a required gain of 9. Because of the large amount of loss in the laser, the amplifier gain width is also narrowed resulting in larger pulsewidths. A more desirable situation for these long mode-locked lasers is to use lower-loss passive waveguides to provide the

majority of the cavity time delay for low repetition rate monolithic cavity devices. Passive waveguide is a much more ideal propagation medium for optical pulses since spontaneous emission noise is not present and the optical bandwidth of passive waveguides is much larger.

A 3.5 mm long passively mode-locked device with an 80 μm saturable absorber was also fabricated from the same material as the 7 mm long 0.85 μm devices of Figure 3.3. The repetition rate of the device was 11 GHz. The resulting autocorrelation and spectral width is shown in Figure 3.6. The passive mode-locked pulsewidth for this device is 6 ps, a large improvement from the 10 ps of the 7 mm long device. A passive mode-locked laser from the same material with an 80 μm saturable absorber and a 1.6 mm length (25 GHz repetition rate) was also tested. The device did not mode lock and only a self-pulsation mode of operation with an approximate frequency of 2 GHz was observed. It is believed that the 80 μm length of the saturable absorber was too long in these designs for optimal operation, especially at higher repetition rates. Even with the 7 mm long device, at large reverse biases it was difficult to obtain passive mode-locking.

In summary, monolithic cavity mode-locked semiconductor lasers with record low repetition rates (5.5 GHz) were fabricated and tested. The devices were divided into three sections to accomplish the functions of gain, gain modulation, and saturable absorption. Hybrid mode-locking techniques give the shortest optical pulsewidth of 6.5 ps.

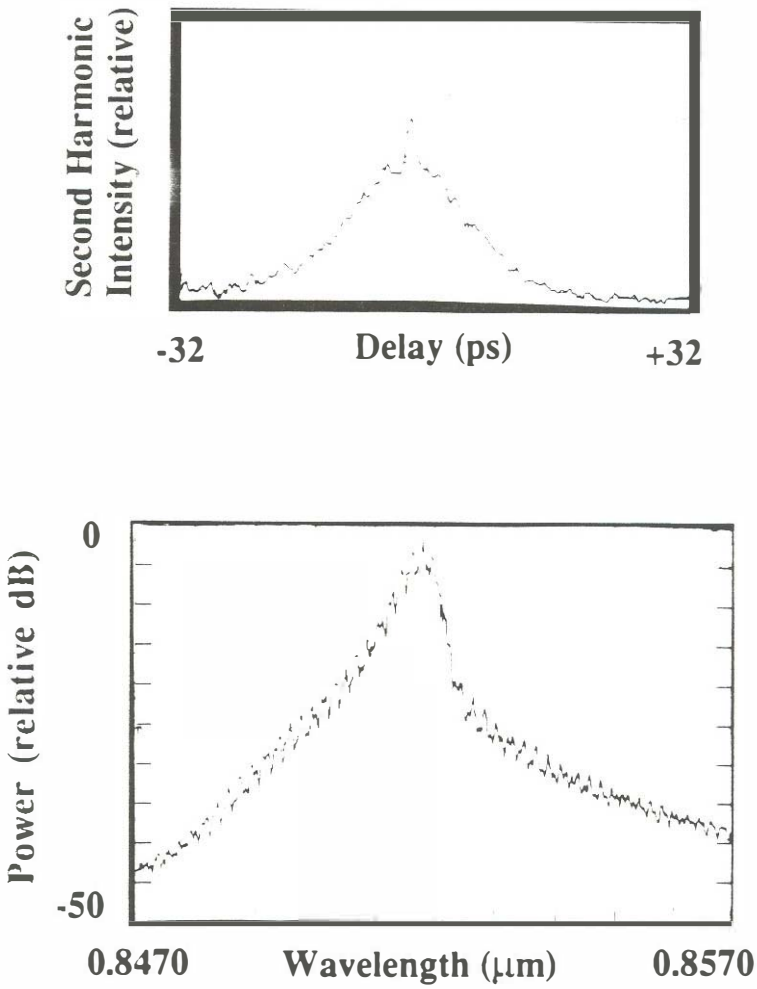

Figure 3.5a The spectrum and autocorrelation results for the 7 mm long monolithic cavity mode-locked laser for active mode-locking The output power was held at 1 mW in all cases. The electrical modulation signal is a 24 dBm sinusoid at a nominal repetition rate of 5.5 GHz. The gain segment current is 85 mA with a modulation section current of 0.3 mA. The optical pulsewidth is 11.5 ps and the spectral width is 480 GHz.

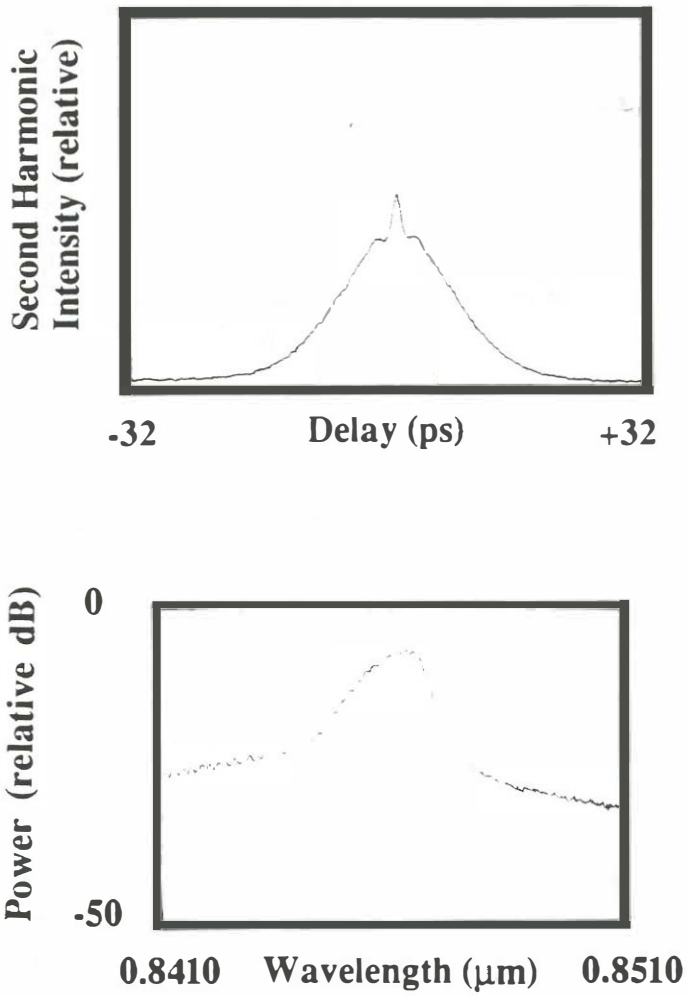

Figure 3.5b The spectrum and autocorrelation results for the 7 mm long monolithic cavity mode-locked laser for passive mode-locking. The saturable absorber reverse bias is 1 V, the gain section current is 170 mA. The output power is 1.9 mW. The pulsewidth is 10.5 ps and the spectral width is 500 GHz.

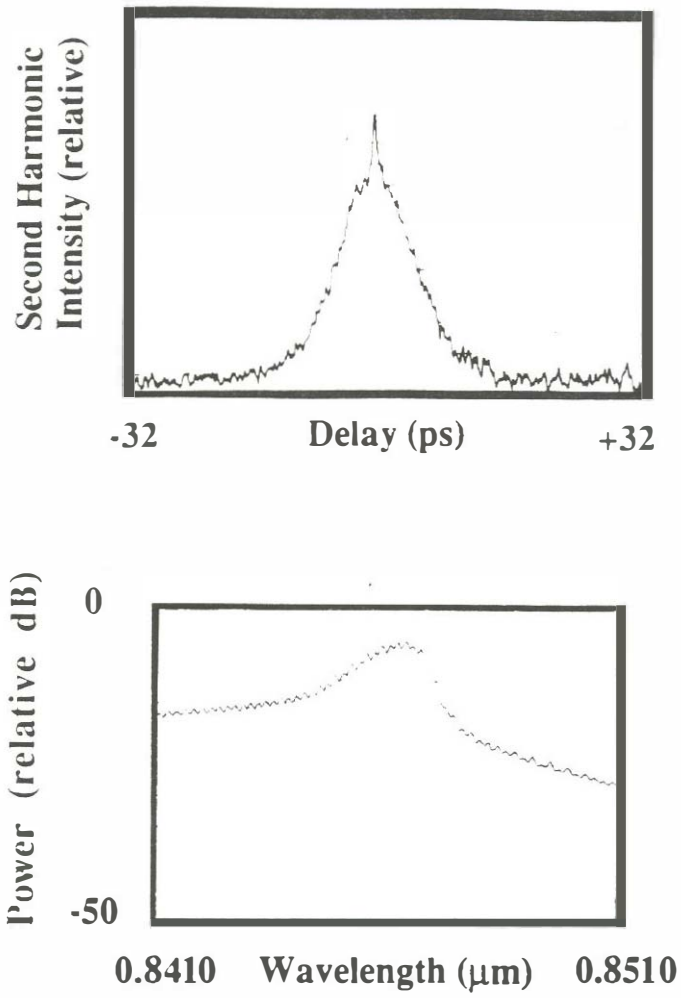

Figure 3.5c The spectrum and autocorrelation results for the 7 mm long monolithic cavity mode-locked laser for hybrid mode-locking. The output power was held at 1 mW in all cases. The electrical modulation signal is a 24 dBm sinusoid at a nominal repetition rate of 5.5 GHz. The saturable absorber reverse bias was 1 V for the passive and hybrid mode-locking cases. The gain section current is 149 mA and the modulation section current is 10 mA. The optical pulsewidth is 6.5 ps and the spectral width is 520 GHz.

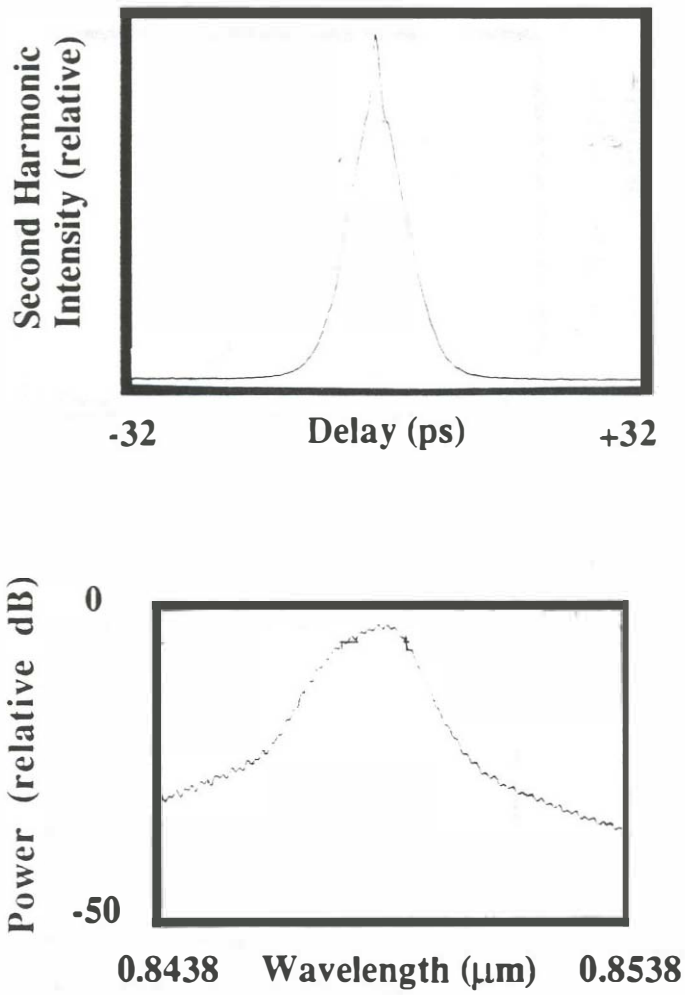

Figure 3.6 The spectrum and autocorrelation results for a 3.5 mm long passive mode-locked laser (the laser of Figure 3.5 cleaved in half). The repetition rate is 11.5 GHz. The saturable absorber bias is -0.7 volts with a gain section current of 146 mA. The output power is 2.95 mW, the pulsewidth is 5.9 ps, and the spectral width is 550 GHz.

3.2 Comparison of colliding pulse and self-colliding pulse monolithic cavity mode-locked semiconductor lasers

In passive and hybrid mode-locked lasers systems, the performance of the saturable absorber can be improved by using saturable absorber configurations which use the colliding pulse mode-locking (CPM) effect . The colliding pulse effect is illustrated in Figure 3.7. When two pulses coming from opposite directions meet in a saturable absorber, electric field standing waves are formed. The carrier generation rate due to absorption will be largest in the standing wave peaks and smallest in the standing wave minimums. In colliding pulse operation, the carrier density does not have to be brought everywhere to transparency in order for the pulses to pass with low loss. This means that it takes much less optical pulse energy to achieve bleaching compared to the case with no standing wave effects. The lower bleaching energy allows the mode-locked laser to operate at a lower pulse energy level and achieve smaller self-phase modulation levels (self-phase modulation is discussed in Chapter 4). Alternately, the saturable absorber can be designed to be longer in order to obtain more pulse shortening in the saturable absorber. The colliding pulse effect is reduced for very long saturable absorbers. If the pulsewidth is much shorter than the propagation time through the saturable absorber, standing waves will only formed near the mirror in Figure 3.7. The effects of standing waves are reduced for saturable absorbers with very high initial absorption levels. Large initial absorption levels mean that the standing wave will only be strong near the mirror in Figure 3.7. It should be noted that saturable absorbers in semiconductor laser systems typically are designed with less than 20 %

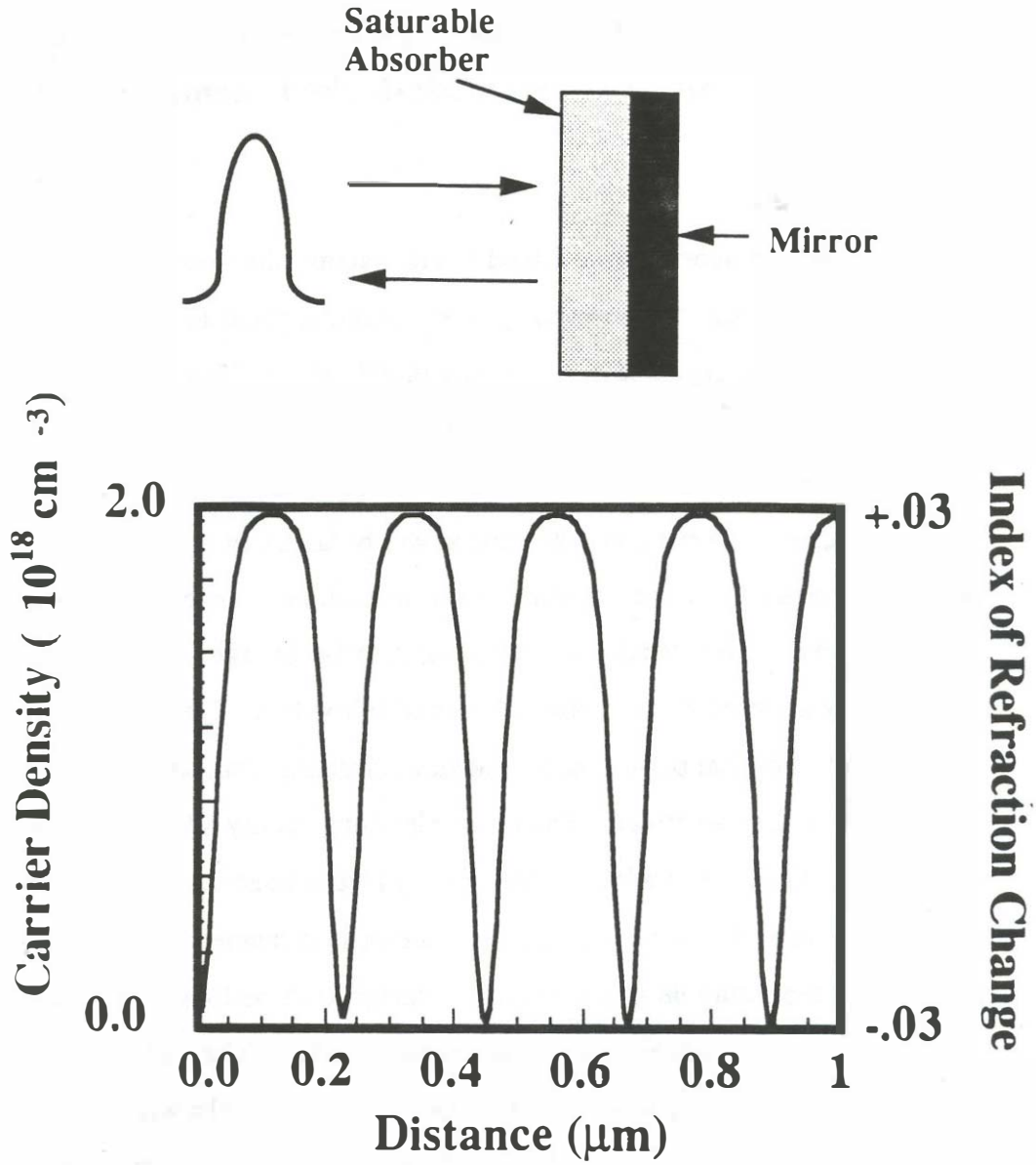

Figure 3.7 An illustration of the concept of colliding pulses in a semiconductor saturable absorber. The input pulse is reflected from the mirror and collides with itself in the saturable absorber. A standing wave is formed when there are oppositely directed portions of the pulse in the saturable absorber. The carrier generation rate is largest at the standing wave maximum and the carrier generation rate at the standing wave minimum is small. Since carriers do not have to be generated everywhere in the saturable absorber, less energy is required to bleach the saturable absorber.

unsaturated transmission so the effects of colliding pulses will be reduced. Semiconductor lasers also have large carrier diffusion effects which tend to continuously fill in the carrier grating while it is being formed.

The colliding pulse effect also has a more complicated phenomena involved. When the standing wave pattern of the colliding pulse forms the carrier density variations, an absorption grating is formed. The absorption grating causes the individual pulses to reflect energy back in the opposite direction. This reflection is caused by index of refraction modulation across the absorber due to gain-phase coupling, and also due to reflection from a gain grating. The grating can reduce frequency chirp in the mode-locked laser if the optical pulsewidth is comparable to the transit time through the absorber. Those portions of the two colliding pulses which collide and have non-equal zero-crossing spacings under the pulse envelope will not efficiently form the carrier density grating. **Thus pulses with frequency chirp will encounter a higher loss in the saturable absorber compared with unchirped pulses.**

The concepts of colliding pulse saturable absorbers were developed originally in dye laser systems, with a ring cavity configuration [57]. Y. K. Chen, M. C. Wu et al. [30] applied the principles of colliding pulse saturable absorber operation to the semiconductor laser system with a center-symmetric linear cavity configuration. In this section, the center symmetric colliding pulse mode-locked semiconductor (CPM) lasers are compared to a much simpler implementation called the self-colliding pulse mode-locked (SCPM) configuration.

The geometries of the CPM configuration and the SCPM configuration are compared in Figure 3.8. In CPM, two separate pulses of energy E collide in the center saturable absorber. The SCPM configuration is obtained by halving

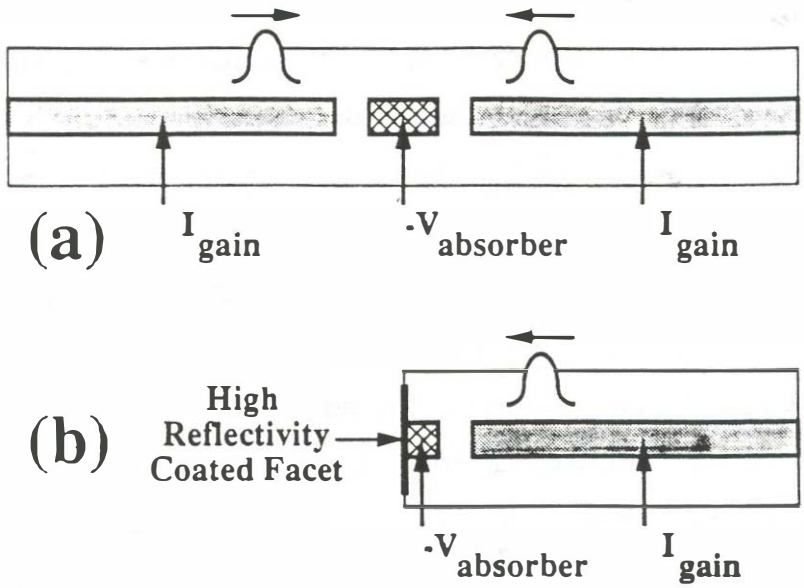

Figure 3.8 (a)The colliding pulse mode-locking saturable absorber (CPM) and (b) the self-colliding pulse mode-locking saturable absorber (SCPM). A comparison between the two configuration shows that the two should be nearly identical from symmetry arguments.

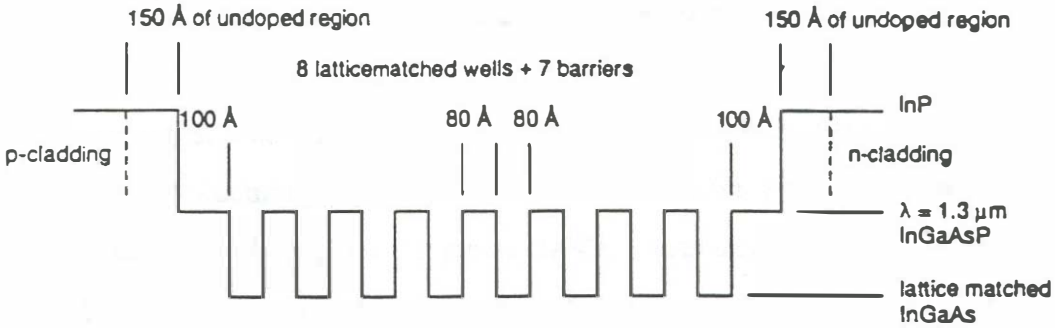

Figure 3.9 The active region composition for the 1.55 μm monolithic cavity mode-locked laser experiments. The structure is a semi-insulating buried heterostructure (SIPBH) with a quantum well active region consisting of InGaAs quantum wells.

the CPM configuration, and placing a high reflectivity coating on the saturable absorber facet. In SCPM, a pulse of energy E collides with itself in the half-length absorber. The performance of the two devices should be nearly identical due to the mirror symmetry of the two configurations. Both structures should therefore take equal advantage of the colliding pulse benefits [58,59]. The advantages of the CPM configuration are the lack of optical coatings and two identical output ports. SCPM, however, requires only half of the device length and half of the current drive requirement for a given repetition rate. The CPM device performance is found to be very sensitive to asymmetrical cleave lengths or asymmetrical gain with respect to the center saturable absorber, whereas SCPM devices have this symmetry inherently.

SCPM and CPM geometry devices with repetition rates of 36 GHz and 42 GHz respectively and a 1.59 μm wavelength were fabricated from the same wafer. Semi-insulating planar buried heterostructure laser structures (SIPBH) are used for these devices. The active region composition for these monolithic cavity devices is illustrated in Figure 3.9. The SCPM device has a 2 pair silicon nitride/silicon mirror sputtered on the saturable absorber facet to give a power reflectivity of 90%. The CPM absorber width is 80 μm and the SCPM absorber width is 37 μm. The CPM and SCPM devices have thresholds of 30 mA and 18 mA respectively, and the single output facet differential quantum efficiency of the SCPM device is approximately twice that of the CPM device. Both devices were passively mode-locked by applying a reverse bias to the saturable absorber segment and forward biasing the gain segments.

Figure 3.10 shows the pulse width performance versus average output power for the CPM and SCPM structures. The devices show very similar

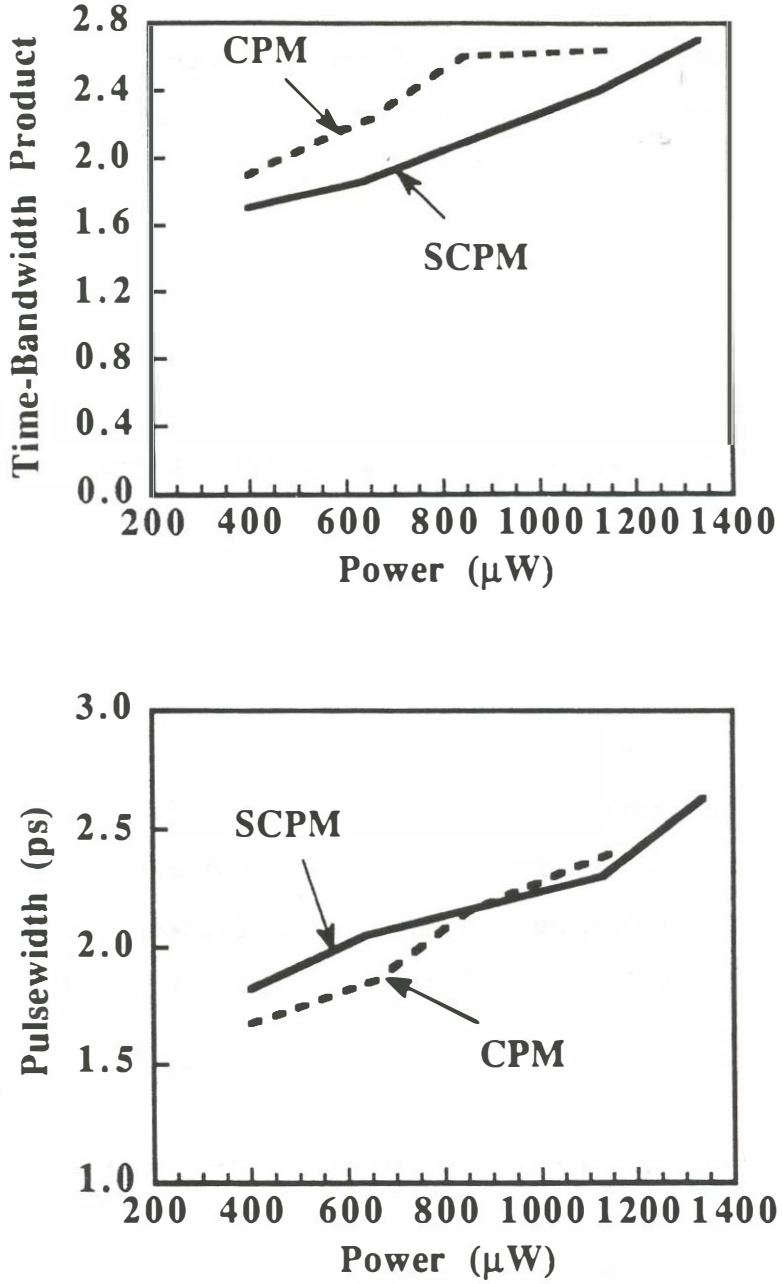

Figure 3.10 The pulsewidth and the time-bandwidth product versus the output power for the CPM and SCPM structures of Figure 3.8. The nominal repetition rate for both devices is 39 GHz. The saturable absorber length for the CPM structure is 80 μm and the saturable absorber length for the SCPM device is 37 μm.

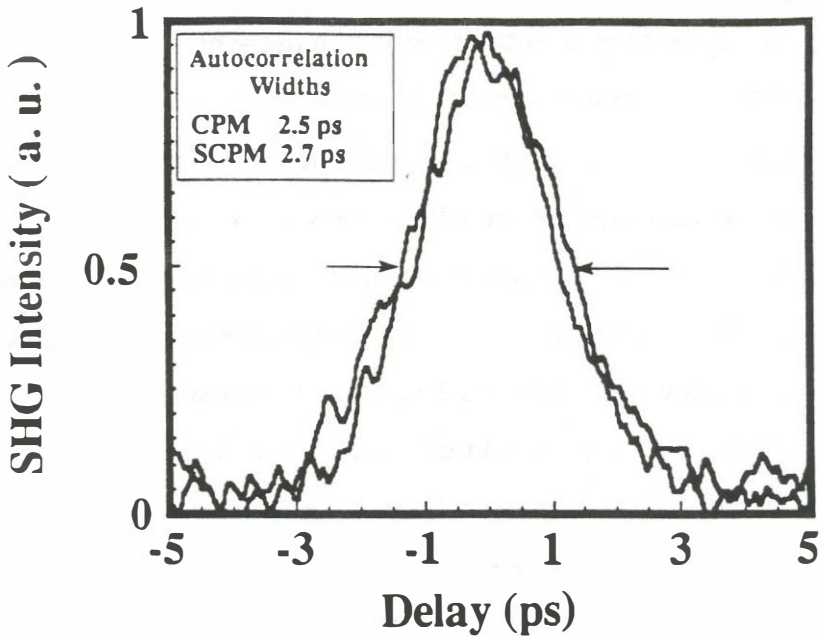

Figure 3.11 A comparison of the autocorrelation for the CPM and SCPM devices of Figure 3.10 for an output pulse energy of 13 fJ.

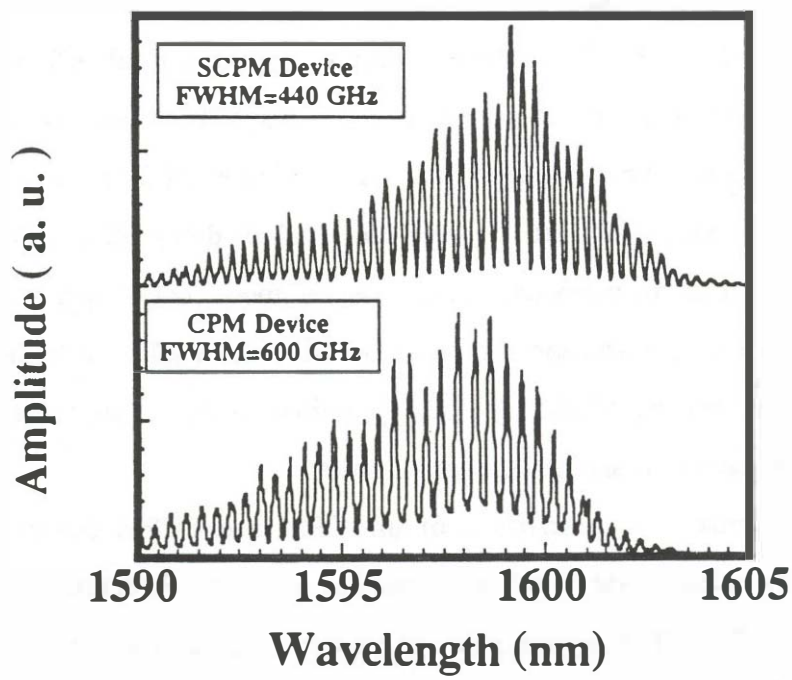

Figure 3.12 A comparison of the optical spectrum for the CPM and SCPM devices of Figure 3.10 for an output pulse energy of 13 fJ.

performance at low pulse energies. At very large pulse energies, the SCPM device tends to have a shorter optical pulsewidth. Figure 3.11 shows autocorrelation traces and Figure 3.12 shows the optical spectra for an output pulse energy of 13 fJ. A 2.5 ps autocorrelation width with a spectral width of 560 GHz was measured for the CPM case whereas the SCPM device had an autocorrelation width and spectral width of 2.7 ps and 470 GHz respectively. The longitudinal mode spacing for the 1.2 mm SCPM device is 36 GHz. The longitudinal mode spacing for the 2 mm long CPM device is 21 GHz but since two pulses are travelling around the cavity out of optical phase, every other longitudinal mode is suppressed in this case by 20 dB.

The autocorrelations and spectral widths at a higher pulse energy (35 fJ) are shown in Figures 3.13 and 3.14 respectively. At higher pulse energies, both the SCPM and the CPM device show pulsewidth and spectral width broadening due to self-phase modulation in the gain and saturable absorber segments (see Section 4.2). The CPM device shows two additional effects: (i) Poor suppression of every other mode in the optical spectrum. (ii) Coherence peaks on the autocorrelation for zero delay and multiples of 50 ps, and the lack of coherence peaks in the cross-correlation at 25 ps delay offsets. This lack of phase coherence between sets of pulses and unmode-locked spectrum results in a poor on-off contrast ratio and wider optical pulse width. At higher energies the SCPM device, which has no longitudinal modes to suppress, produced shorter pulsewidths and better contrast ratios.

In summary, a comparison of the CPM and SCPM device structures showed similar pulse width and spectral width performance at low pulse energies. The CPM device does not require a high reflectivity coating. The SCPM device has a shorter device length, lower current drive requirements,

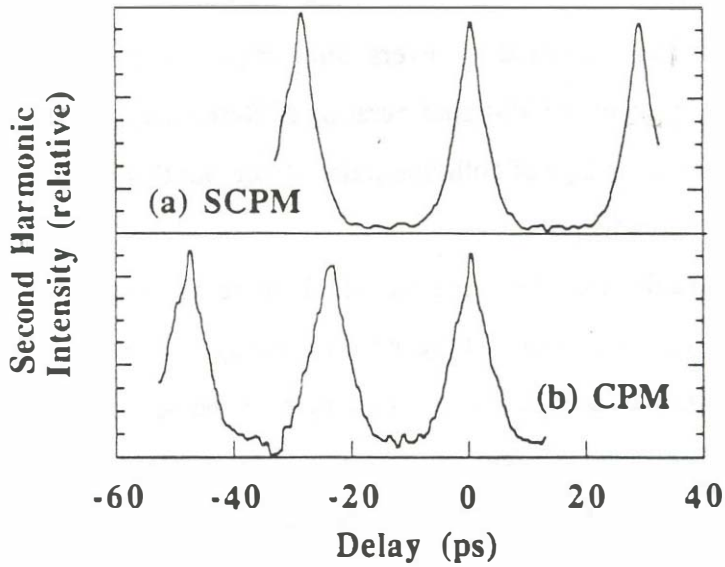

Figure 3.13 A comparison of the autocorrelation for the CPM and SCPM devices of Figure 3.10 for an output pulse energy of 35 fJ.

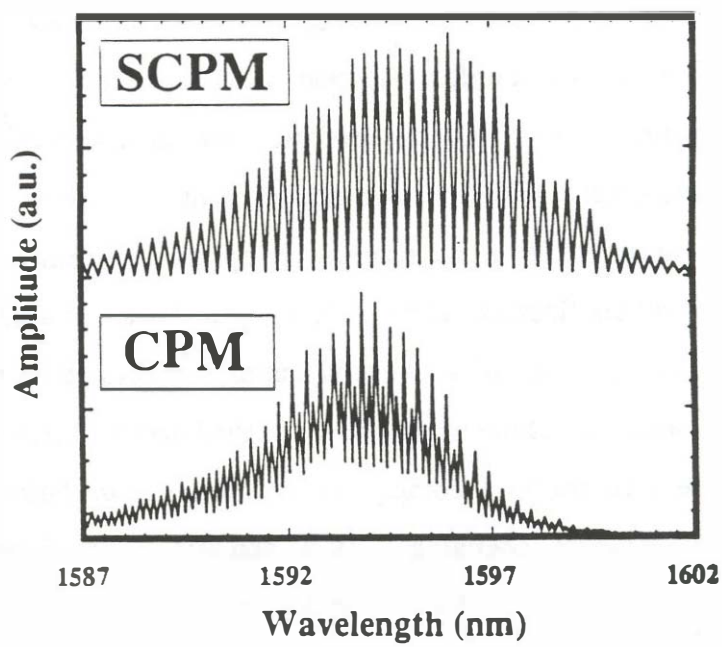

Figure 3.14 A comparison of the optical spectrum for the CPM and SCPM devices of Figure 3.10 for an output pulse energy of 35 fJ.

guaranteed device symmetry, and better performance at high pulse energies when compared to the CPM device. In should be noted that the SCPM configuration had been used by several authors [24,25] before the introduction of the center-symmetric CPM configuration of Reference 30. The devices were already taking advantage of colliding pulse effect, but this point was simply not brought out in the discussion.

The saturable absorber lengths which were used for the SCPM/CPM comparison were found to be longer than the length which was found to give the shortest optical pulses. When the length of the saturable absorber in the CPM configuration was lowered from 80 μm to 50 μm, the achievable pulsewidth went from 1.7 ps to 1.3 ps. The autocorrelation and spectral measurement results for a CPM device with 50 μm length are shown in Figure 3.15. It should be noted that the propagation times through the 50 μm and 80 μm saturable absorbers are 1.4 and 2.2 ps respectively. The propagation time through the saturable absorber matches well with the measured optical pulsewidth in both cases. Further reduction in the saturable absorber length for the same structure is not fruitful because the unsaturated saturable absorption level will be too small to initiate passive mode-locking. An alternate path to take is to add more quantum wells and increases the optical confinement factor. The increased optical confinement factor will allow a shorter saturable absorber transit time to be achieved with a high total unsaturated absorption level.

1.55 μm monolithic cavity structures were tested over a variety of repetition rates. Figure 3.16 shows a comparison of the autocorrelation traces for monolithic cavity devices operating at 20, 40, and 80 GHz repetition rates. The 20 GHz device used the SCPM configuration and the 40 and 80 GHz designs used the CPM configuration.

In conclusion, it has been found that monolithic cavity devices are an especially convenient way to generated short optical pulses. Segmentation of the top contact allows active, passive, and hybrid mode-locking to be accomplished in the same structure. The self-colliding pulse hybrid mode-locked arrangement gives the best performance in terms of pulsewidth, amplitude, and timing stability. A wide range of repetition rates are possible with rates from 5.5 GHz to 80 GHz demonstrated in this chapter.

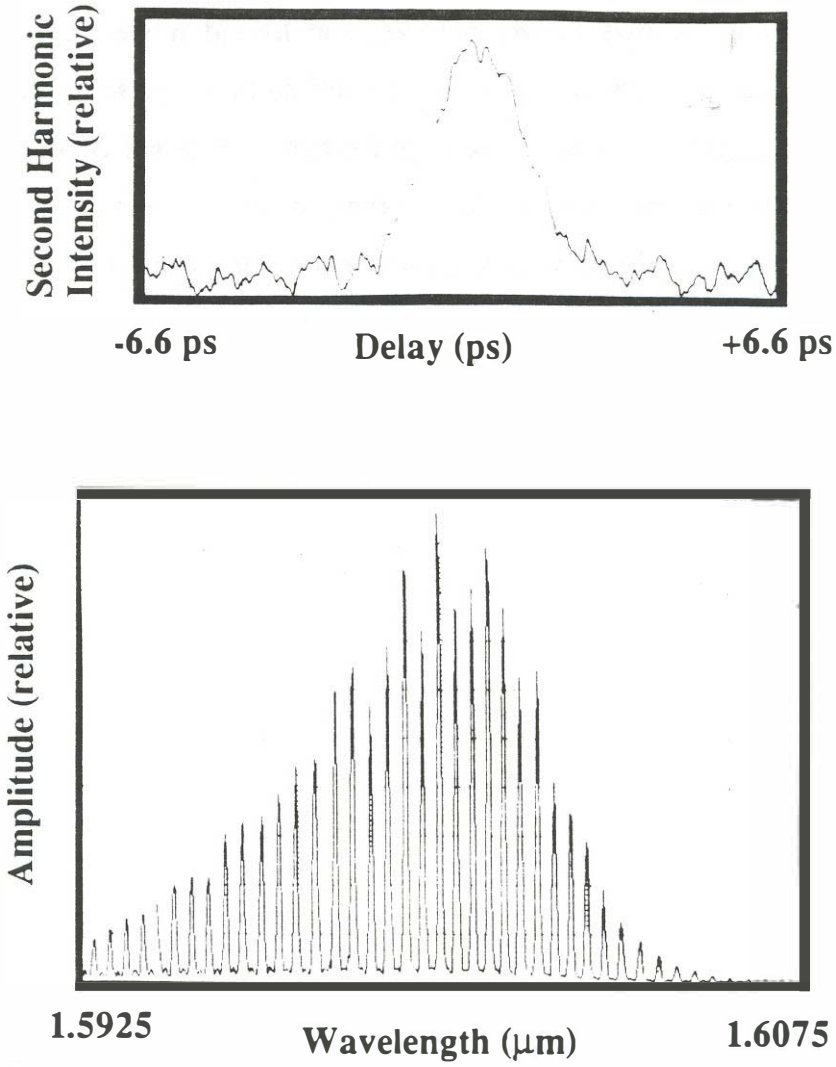

Figure 3.15 Autocorrelation traces and spectral characteristics of a CPM device with 50 μm saturable absorber. The shorter saturable absorber length (50 μm versus 80 μm) resulted in considerable improvement in device performance. The measured pulsewidth for this example is 1.4 ps. The repetition rate is 42 GHz (2mm long CPM device). The gain section current is 75.3 mA, the saturable absorber voltage is -0.72 V, and the average power is 0.53 mW.

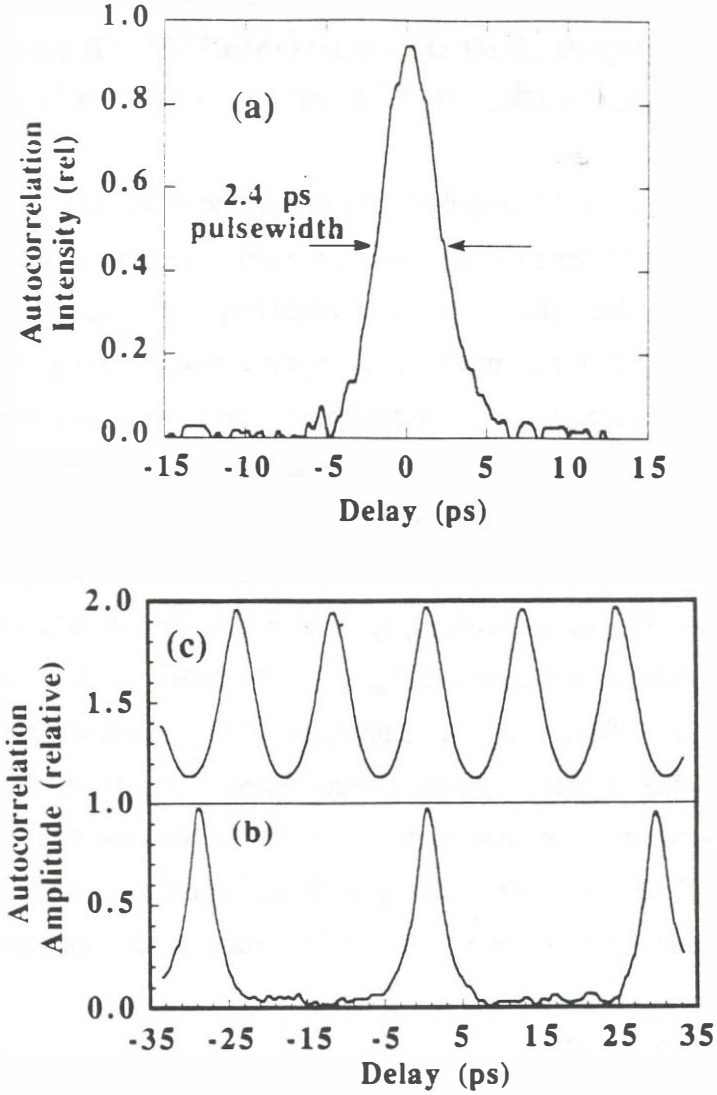

Figure 3.16 A comparison of device performance with respect to repetition rate. (a) Autocorrelation for a 2 mm long SCPM device (21GHz repetition rate) with 35 μm long saturable absorber. (b) Autocorrelation for a 2 mm long CPM device (42 GHz repetition rate) device with 50 μm long saturable absorber. (c) Autocorrelation for a 1mm long CPM device (84 GHz repetition rate) with 35 μm long saturable absorber length.

Chapter 4
Comparison of multi-section mode-locked semiconductor laser device performance

Chapters 2 and 3 described the external and monolithic cavity multi-segment mode-locked laser structures which are being studied in this dissertation. The description focussed on ways of achieving short, single pulses from these devices using active, passive, and hybrid mode-locking techniques. In this section, a more thorough discussion of the pulse characteristics from these devices are made. The section is intended to show the relative merits of active, passive, and hybrid gain modulation techniques. A performance comparison between monolithic and external cavity devices is also made. The relevant characteristics of pulsewidth, spectral width, time-bandwidth product, pulse energy, repetition rate, active region composition, and noise are included in the comparison. Table 1 lists a comparison of the performance characteristics for many of the multiple-segment devices tested in this work. Figure 4.1 illustrates the device structures which are tested for clarification of Table 4.1. From the results listed in Table 1 along with additional experiments which are not included in the table, there are many important trends which can be identified.

4.1 Pulsewidth

The pulsewidths that have been demonstrated for multi-segment external cavity mode-locked semiconductor lasers with single pulse outputs are typically in the 1 - 3 ps range for the active, passive or hybrid mode-locking techniques. The general trends found from Table 1 are as follows:

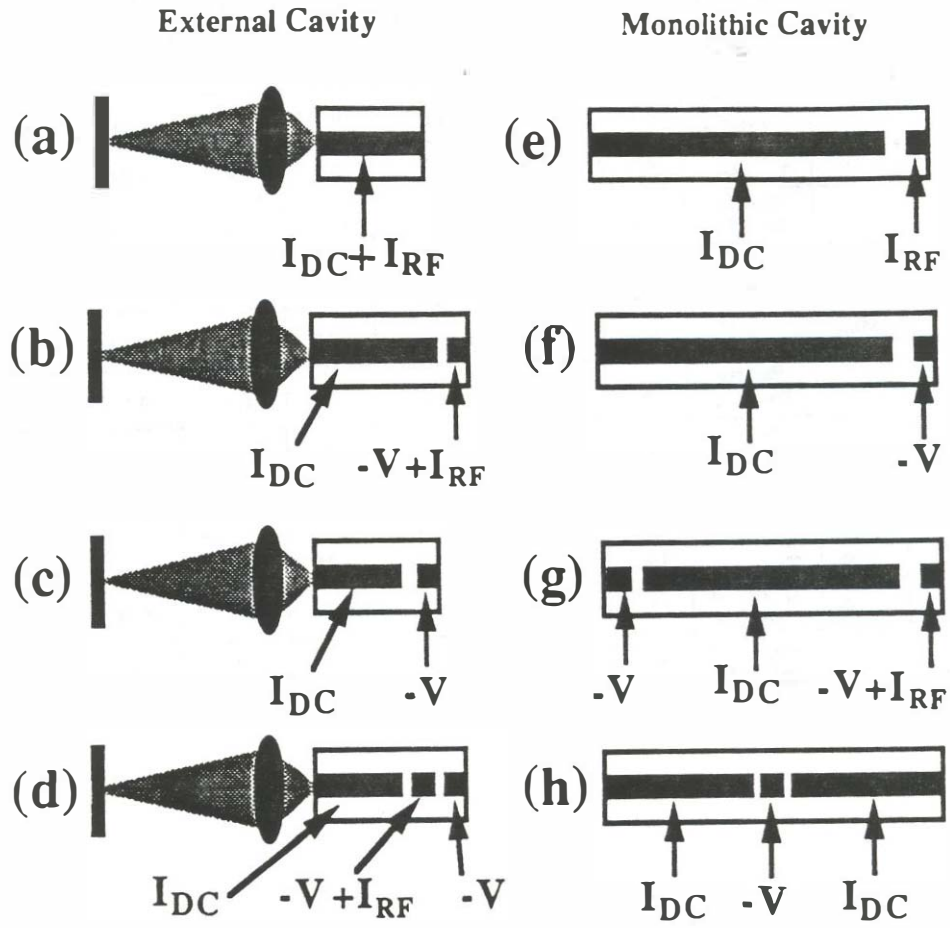

Figure 4.1 The structures compared in this section. **External cavity devices**: (a) single-section active, (b) two-section active, (c) three-section active, (d) two-section passive, (e) and **monolithic cavity devices** (f) two section active, (g) two-section passive, (h) three-section hybrid, (i) three-section passive.

Table 4.1 Comparison of multi-segment structure performance

Cavity Type	Modulation Technique	Pulse Width (ps)	Spectral Width (GHz)	Time-Bandwidth Product	Pulse Energy (pJ)	Repetition Rate (GHz)	Wave-Length (μm)	Active-Region
Ext.	Active Two-Seg.	5	342	1.5	0.28	5	0.83	Bulk
Ext.	Passive Two-Seg.	2.5	720	1.8	0.7	5	0.84	4 QW
Ext.	Hybrid Two-Seg.	2.5	1000	2.5	0.8	5	0.84	4 QW
Ext.	Hybrid Three-Seg.	1.9	900	1.71	0.18	6	0.83	Bulk
Mon.	Active Two-Seg.	13	330	4.3	0.19	5.5	0.84	4 QW
Mon.	Hybrid Three -Seg.	6.5	540	3.5	0.18	5.5	0.84	4 QW
Mon.	Passive Two-Seg.	10	400	4.0	0.25	5.5	0.84	4 QW
Mon.	Passive Two-Seg.	5.5	550	3.0	0.53	11	0.84	4 QW
Mon.	Hybrid Three-Seg.	2.2	500	1.1	0.03	21	1.58	4 QW
Mon.	Passive Two-Seg.	1.3	600	0.78	0.02	41	1.58	4 QW
Mon.	Q-Switch Two-Seg.	15	2400	36	4	1	0.825	Bulk
Mon.	Gain-Switch Two-Seg.	13	4000	52	3.4	1	0.822	Bulk

4.1.1 Monolithic cavity devices

a. Hybrid mode-locking produced the shortest pulsewidths followed by passive and then active mode-locking.

b. Low repetition rate monolithic cavity devices produced wider pulsewidths than higher repetition rate monolithic cavity devices. As an example, a 3.5 mm passive mode-locked laser (11 GHz repetition rate) produced a 5 ps pulse whereas a 7 mm long laser (5.5 GHz repetition rate) from the same wafer with the same saturable absorber length produced a 5.5 ps pulse.

As a further example, a two-section 20 GHz passive mode-locked laser produce a 2.5 ps pulse whereas a 36 GHz passively mode-locked laser from the same wafer produced a 1.7 ps pulses. The saturable absorber length was 40 μm in both cases.

4.1.2 External cavity devices

a. As in the monolithic cavity case, hybrid mode-locking gave the shortest pulsewidth followed by passive, and then active mode-locking.

b. Devices with a shorter gain section length in general produced narrower pulsewidths. As an example, a 1.3 mm long (80 μm long absorber) passive mode-locked quantum well device in an external cavity with a repetition rate of 5 GHz produced a 3.5 ps pulsewidth. A 0.5 mm long device (80 μm long absorber) from the same wafer produced a 2.5 ps pulse. From the analysis of section 2.4, this trend does not continue for very short gain lengths (150 μm).

4.1.3 Monolithic versus external cavity

a. Over the repetition rates where there is overlap between the external and monolithic cavities, external cavity devices showed shorter pulsewidths. As an example, an external cavity passive mode-locked device (500 μm long gain, 80

μm absorber, four quantum well) produced a 2.5 ps pulse whereas a passive mode-locked monolithic cavity device (7 mm long gain, 80 μm long absorber) from the same wafer produced 10 ps pulses. The difference between the two cases is that the external cavity device has predominantly air waveguide and the monolithic cavity device has predominantly all-active semiconductor waveguide. Air waveguide has much more ideal pulse propagation characteristics than all-active waveguide. The effective bandwidth of the gain medium becomes much narrower for the monolithic cavity device since very large overall gains are required to overcome the internal loss of the active waveguide. Active waveguide is also much more dispersive than passive waveguide. It is thought that the differences between external and monolithic cavities can be minimized if long sections of low-loss passive waveguide can be incorporated into the structure.

b. It is in general easier to get short optical pulses using hybrid and passive mode-locking techniques for both monolithic and external cavity devices than using active mode-locking. The saturable absorber is primarily responsible for pulse narrowing with the active modulation providing amplitude and phase stabilization. Monolithic cavity mode-locked semiconductor lasers showed better performance as the repetition rates increase into the millimeter wave frequencies.

4.2 Spectral width

The experimental results of Table 4.1 show that for designs in which bandwidth control filter elements are not placed in the cavity, the optical pulses exhibit excess optical bandwidth beyond the Fourier transform limit. The principle cause of this extra bandwidth is self-phase modulation of the optical pulses induced by gain saturation, absorption saturation, and active gain modulation. Figure 4.2 illustrates the concepts of self-phase modulation. The

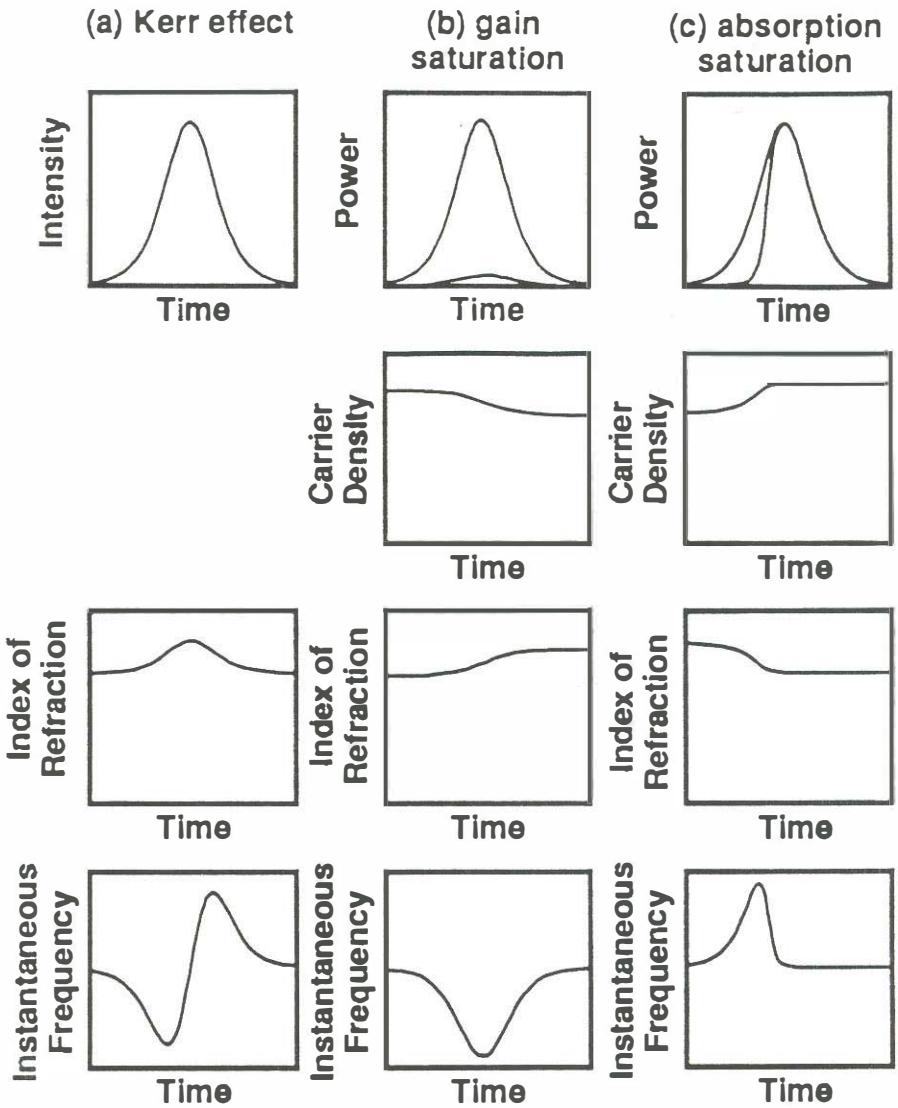

Figure 4.2 Self-phase modulation effects in mode-locked semiconductor lasers. (a) Kerr effect self phase modulation (this is **not** dominant in semiconductor lasers). Self-phase modulation due to (a) gain saturation and (b) absorption saturation.

first self-phase modulation shown is that caused by the optical Kerr effect (Figure 4.2a) in which the index of refraction is intensity dependent. **Kerr effect self phase modulation is *not* the dominant effect in multi-section mode-locked lasers. The dominant self-phase modulation effect is that caused by gain and absorption saturation** (Figures 4.2b and 4.2c). When a semiconductor amplifier amplifies an optical pulse with an input energy approaching the saturation energy of the amplifier, the gain of the amplifier and thus the carrier density is reduced. Index of refraction changes are coupled to gain changes through the linewidth enhancement factor, α. The drop in carrier density causes an increase in the index of refraction which in turn phase modulates the optical pulse. In a semiconductor laser amplifier, gain saturation causes a drop in the instantaneous frequency over the duration of the pulse. When a pulse propagates through a saturable absorber, the carrier density increase results in an instantaneous frequency rise in the leading edge of the optical pulse. The chirp induced by self-phase modulation builds up with every pass of the optical pulse around the laser cavity until the gain bandwidth of the optical amplifier limits the frequency excursions. The effects of self-phase modulation can in general be reduced by decreasing the pulse energy and therefore the amount of self-phase modulation in the device. Note that the chirp that occurs in mode-locked semiconductor lasers is in general not linear over the central portion of the pulse. Linear chirp is important because pulses that are linearly chirped lend themselves well to pulse compression techniques. It has been found experimentally that the chirp from both active, passive, and hybrid mode-locked external-cavity lasers in certain circumstances has been linear enough to accomplish pulse compression. Figure 4.3 illustrates the types of pulse compressors which have been used in pulse compression of semiconductor lasers and also shows the sign of the group velocity dispersion available from each compressor. Helkey et al. [9] have accomplished pulse

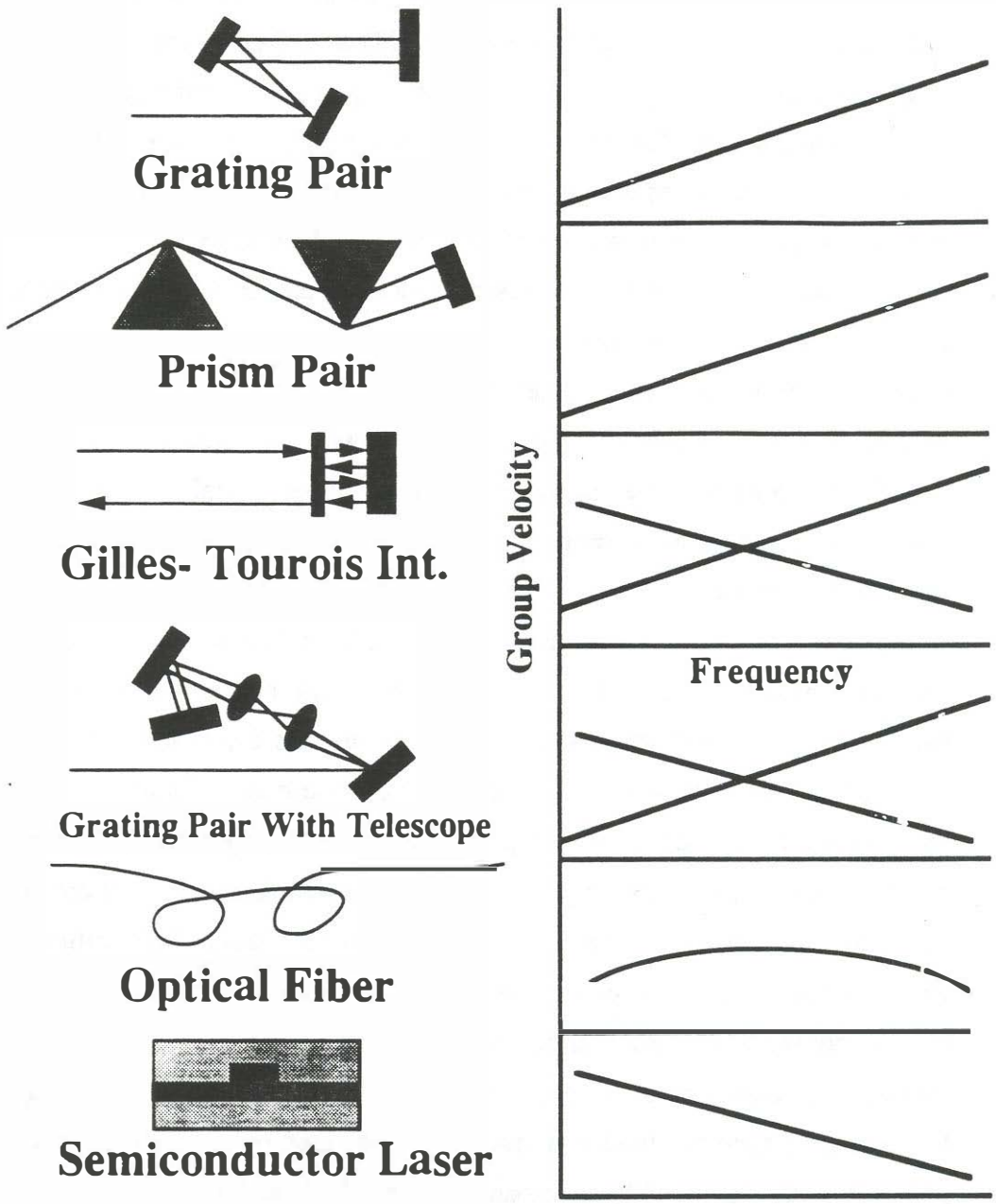

Figure 4.3 The types of pulse compressors which are useful for mode-locked semiconductor lasers. The sign of their group velocity dispersion is also given.

compression of the two-section passive mode-locked lasers (the external cavity design of Figure 2.28 with 16 μm long saturable absorber, 500 μm long gain section, and bulk active region of Figure 2.27) described in this dissertation with a modified grating pair compressor resulting in a pulsewidth compression from 3.5 ps to 0.5 ps. The frequency chirp from the passive mode-locked laser rises from the leading edge to the trailing edge of the pulse. Other researchers have accomplished pulse compression down to widths of 0.25 ps [60].

In external-cavity lasers, it is possible to achieve closer to transform-limited pulses by adding a bandwidth-limiting element such as a diffraction grating, etalon, or birefringent tuning filter into the external cavity. The bandwidth-limiting element filters out the excess bandwidth created by self-phase modulation on each pass at the expense of a wider optical pulsewidth. Figure 4.4 shows the experimental set-up used to introduce an extra bandwidth limiting element into the external cavity. The experiment was done for both a collimated 2 mm diameter beam and for a cat's eye configuration where the beam is focussed on the grating. The collimated feedback case gives a narrower bandwidth optical reflection since more grating lines are illuminated. The grating was gold coated with 1200 grooves per millimeter. Figure 4.4 shows the pulsewidth and time-bandwidth product for the passively mode-locked laser as a function of the center frequency. The pulsewidth increased and the time bandwidth decreased for the case of collimated feedback. The collimated feedback pulses have a lower time-bandwidth product than for mirror feedback but still are far from transform limited. The tuning range endpoints represent the limits of passive mode-locking operation with respect to center wavelength. In general the time bandwidth product can be lowered by reducing the output power from the device. The time-bandwidth product can be lower for actively mode-locked devices with grating feedback since the devices typically operate at a lower pulse energy and lower current bias producing smaller levels of self-

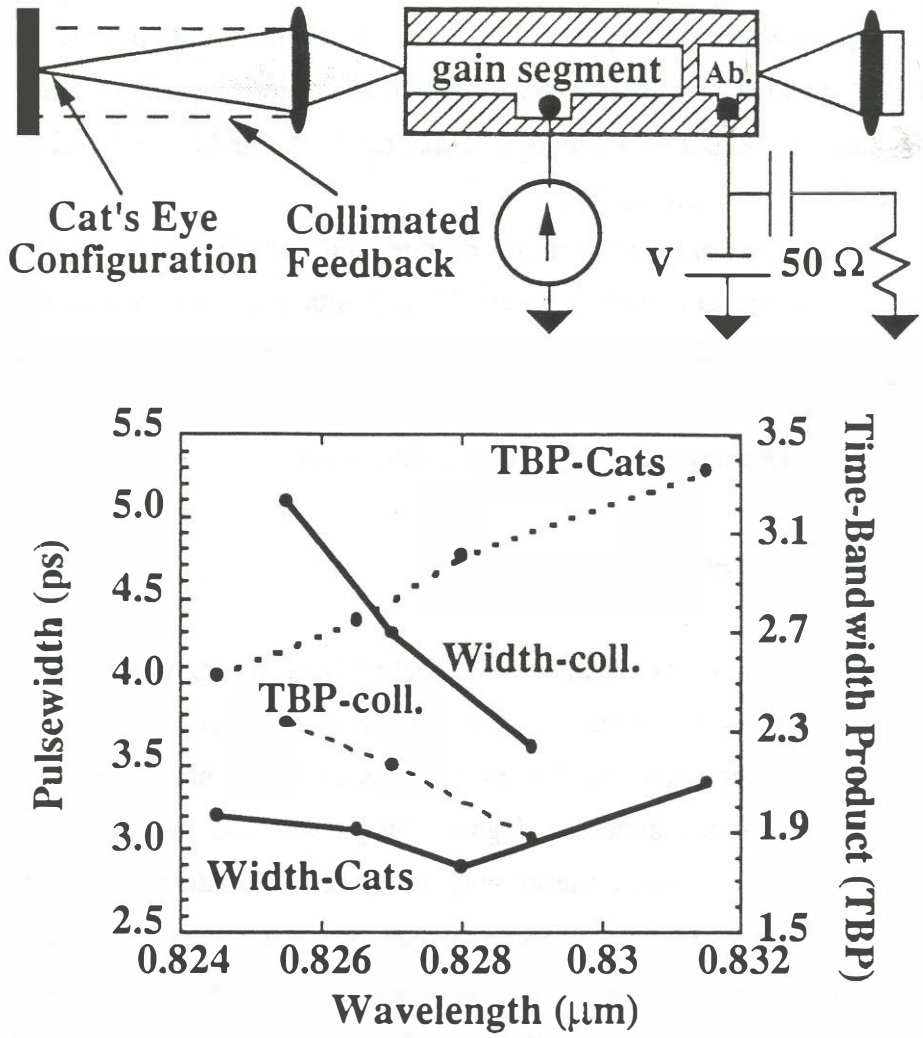

Figure 4.4 Performance of a grating feedback passive mode-locked semiconductor laser. The pulsewidth and time-bandwidth product versus wavelength is shown. The end points of the detuning are the ranges over which passive mode-locking could be obtained for the structure. The device is a 500 μm long bulk active region device (see Figure 2.27) with a 16 μm long saturable absorber. The experiment was done both for collimated feedback onto the grating (2 mm beam diameter) and for a focussed beam onto the grating. The repetition rate for the experiment is 5 GHz. The collimated feedback shows a wider pulsewidth and lower time-bandwidth product as can be expected for the narrower bandwidth of the feedback from the diffraction grating. The diffraction grating has 1200 grooves per millimeter.

phase modulation. The pulsewidth from the device increased from 2.5 ps to 4 ps on going from focussed to collimated grating feedback. The cat's eye configuration feedback produces similar pulsewidths and spectral widths as mirror feedback but still allows tuning of the center frequency. Since only a few lines of the grating are hit in focussed feedback, the frequency selectivity of the cat's eye feedback is small.

Bragg reflectors have been incorporated into monolithic cavity devices in a similar manner to reduce the optical bandwidth and obtain nearly transform limited pulses [56]. The origin and implications of the large time-bandwidth pulses that are typically achieved in multi-section mode-locked semiconductor lasers are more thoroughly discussed in Chapter 5.

4.3 Pulse energy

The available energy from a mode-locked laser is limited by the saturation energy of the gain region. As was described in Section 2.4, the saturation energy is proportional to the mode cross-sectional energy and inversely proportional to the differential gain. In passive and hybrid mode-locked devices, the output pulse energy is typically near the saturation energy of the gain segment for optimal mode-locking conditions. Large saturation energies in a semiconductor optical amplifier can obtained from a device with a large cross sectional mode area and for a very low differential gain versus carrier density value. The saturation energy for semiconductor laser amplifiers may range from 1 pJ in a tightly confined index-guided laser up to 20 pJ for lightly-confined gain guided edge emitting structures. Single quantum well devices should offer the lowest differential gain when operated at very high carrier densities. Operation of amplifiers at very high carrier densities also leads to a lower noise figure amplifier [61]. In active mode-locking, the mode-locked laser is typically operated at a slightly lower pulse energy so that the active gain

modulation effect remains strong.

Figure 4.5 shows autocorrelation traces versus output power for a two-section passively mode-locked semiconductor laser (bulk active region device of Figure 2.28 with 16 μm long saturable absorber and bulk active region composition of Figure 2.27). The estimated amplifier saturation energy of this structure is 2 pJ. The pulsewidth increases from 4.2 to 5.1 ps as the output power is increased. The level of the secondary pulse spaced at the round-trip time of the laser diode also increases. The higher current levels associated with higher output powers produce faster gain recover for the secondary pulses. It would be desirable to have a larger saturable absorber length to increase the loss for the secondary pulse in the higher output power cases. The measured pulse energy for the highest power case is 1.2 pJ. When accounting for the output coupling loss and 70 % facet transmission, this would correspond to approximately 3 pJ of energy inside the semiconductor laser amplifier, in good agreement with the estimated saturation energy of 2 pJ. The optical spectrum associated with the autocorrelations of Figure 4.5 is shown in Figure 4.6. The trend is increased time-bandwidth product with increased output power.

The pulse energy from mode-locked semiconductor lasers can be further increased with external semiconductor laser amplifiers or erbium-doped fiber amplifiers. Erbium doped fiber amplifiers, with large mode-cross sectional areas and lower differential gain, can produce output pulses with energies of over 100 pJ. Although other types of fiber lasers are being developed for wavelengths other than 1.53 μm, semiconductor laser amplifiers offer the only presently available amplifier for other wavelengths.

Figure 4.7 shows an experiment that was done in semiconductor laser amplification of the output of a passive mode-locked laser. The passive mode-locked two-section laser was a bulk active region device (500 μm long gain section with 16 μm long saturable absorber and bulk active region of Figure

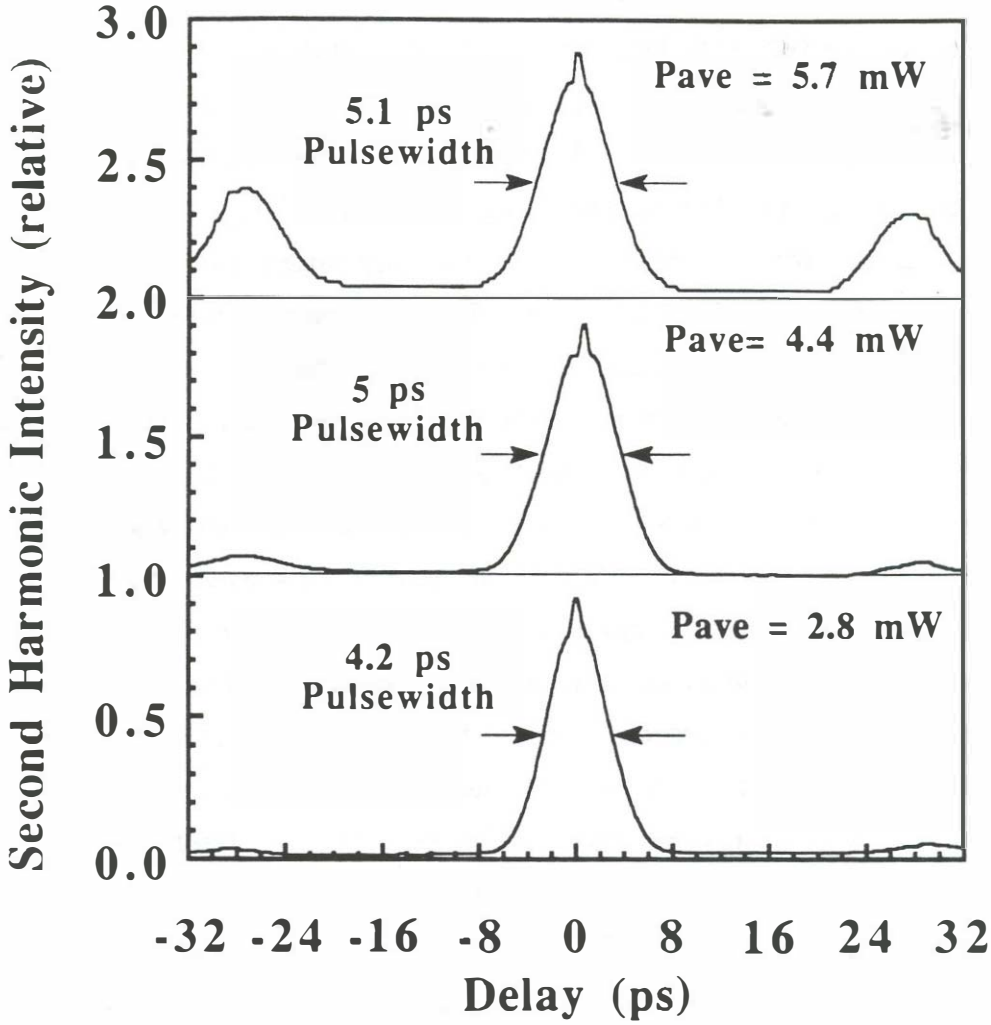

Figure 4.5 Autocorrelation traces as a function of the output power for a two-section passively mode-locked laser. The active region is that of Figure 2.27 with a 500 μm length and a 16 μm long saturable absorber. As the output power is increased, the pulsewidth broadens and the amplitude of the secondary pulse spaced at the round trip time of the laser diode also increases.

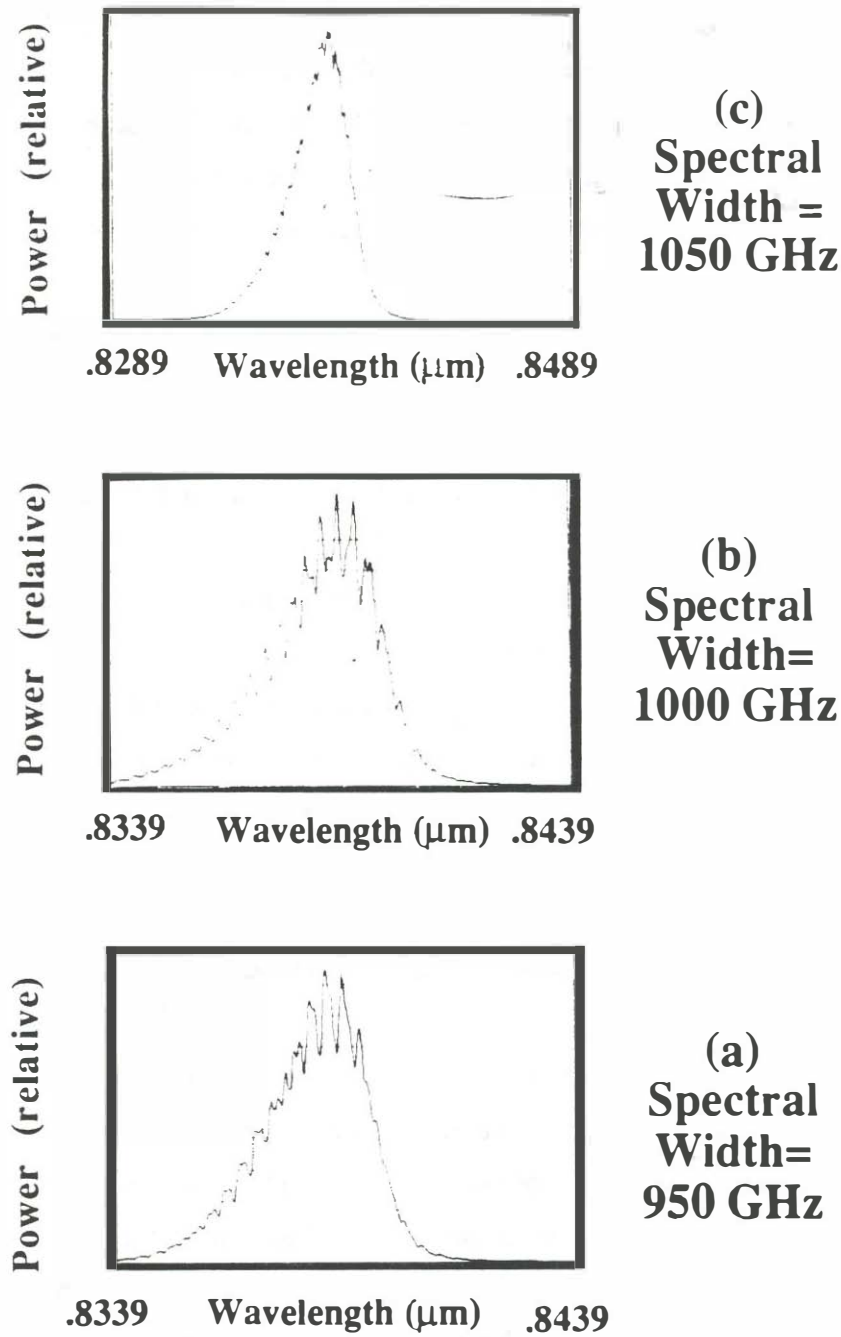

Figure 4.6 The optical spectrum for the three cases of Figure 4.5. The optical spectral width increases with output power due to increased self-phase modulation levels caused by gain and saturable absorber saturation.

2.27) operating at a repetition rate of 0.8 GHz. The amplifier is 500 μm long and came from the same wafer as the mode-locked laser. The amplifier is anti-reflection coated on both facets. The amplifier is unique in that it incorporates two 8 μm saturable absorbers, one at the center and one at the output. The saturable absorbers enhance the amplifiers operation for pulse input signals in several ways.

a. The saturable absorbers can recover their absorption very quickly after the passage of the optical pulse through the saturable absorber (around 15 ps recovery time as demonstrated in Section 2.4). This absorption recovery allows a reduction in the spontaneous emission output from the amplifier between optical pulses.

b. The saturable absorbers help in suppression of lasing so that larger gains can can be achieved.

Figure 4.8 shows the autocorrelation trace and optical spectrum from the amplified mode-locked laser experiment of Figure 4.7. The output pulse energy is 1.9 pJ. The pulsewidth output from the amplifier is very similar in width to the input pulsewidth. The saturable absorbers were very necessary to this experiment in that if the saturable absorbers are connected to the gain region, the amplifier lases on its own. One thing to note in this amplifier experiment is that only a very small net gain is achieved (about 3 dB). There are several things that contribute to the small net gain. Since the amplifier and the mode-locked laser are from the same wafer, the gain maximum wavelength of the amplifier is not centered at the mode-locked laser center wavelength thereby reducing the achievable gain. The coupling transmission from the laser to the amplifier is estimated to be 35%. Most importantly, the amplifier is operated in the highly saturated regime since the mode-locked laser puts out a pulse energy very near the saturation energy of the amplifier.

Vertical-cavity surface-emitting laser structures, which have much higher

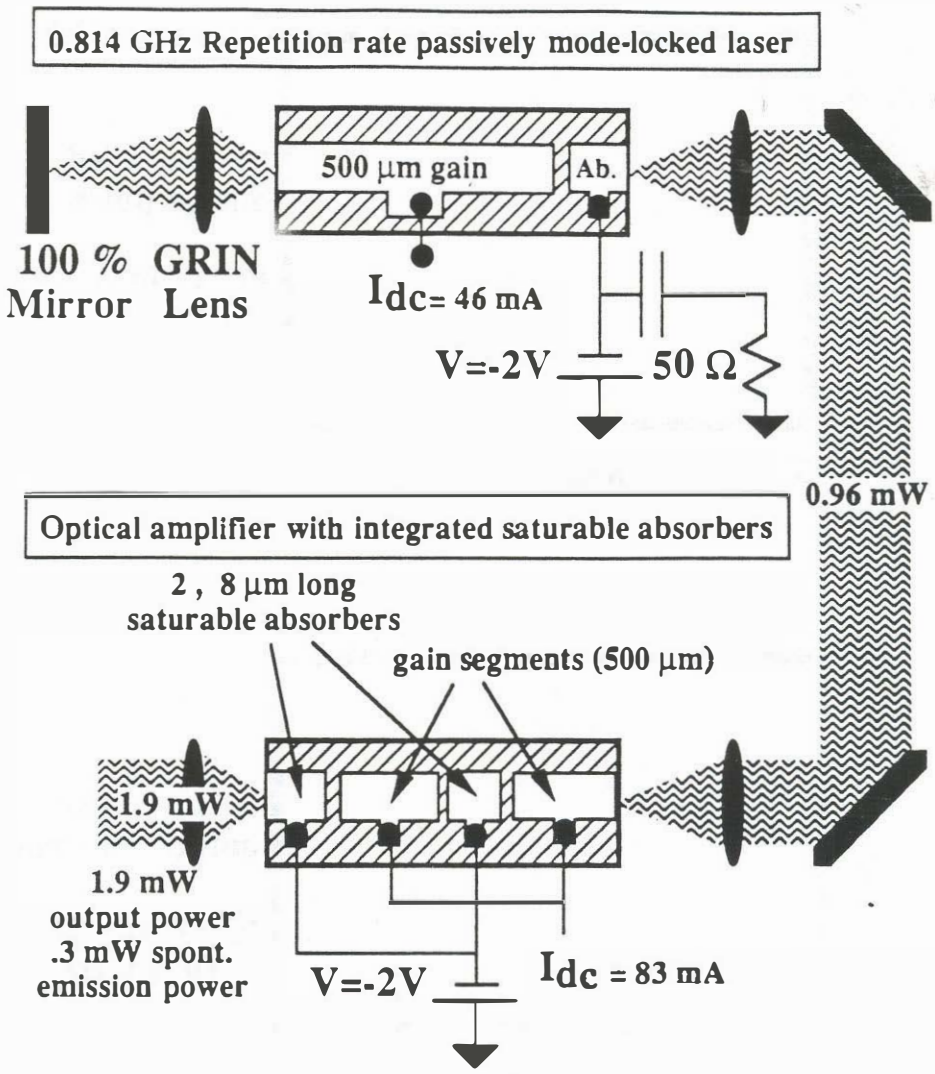

Figure 4.7 This is the experimental set-up used to amplify the output of a two-section passive mode-locked laser. The amplifier is a double anti-reflection coated laser of the same material as that of the mode-locked laser diode. The amplifier has two integrated saturable absorbers that give better amplification properties when used in a pulse amplifier. Since the saturable absorbers can recovery its absorption very quickly (about 15 ps recovery time see chapter 2.4), the spontaneous emission output between optical pulses can be suppressed. The saturable absorbers also help suppress lasing in the amplifier due to the finite reflectivity of the antireflection coatings. Without the saturable absorbers being reverse-biased in this experiment, the amplifier began lasing.

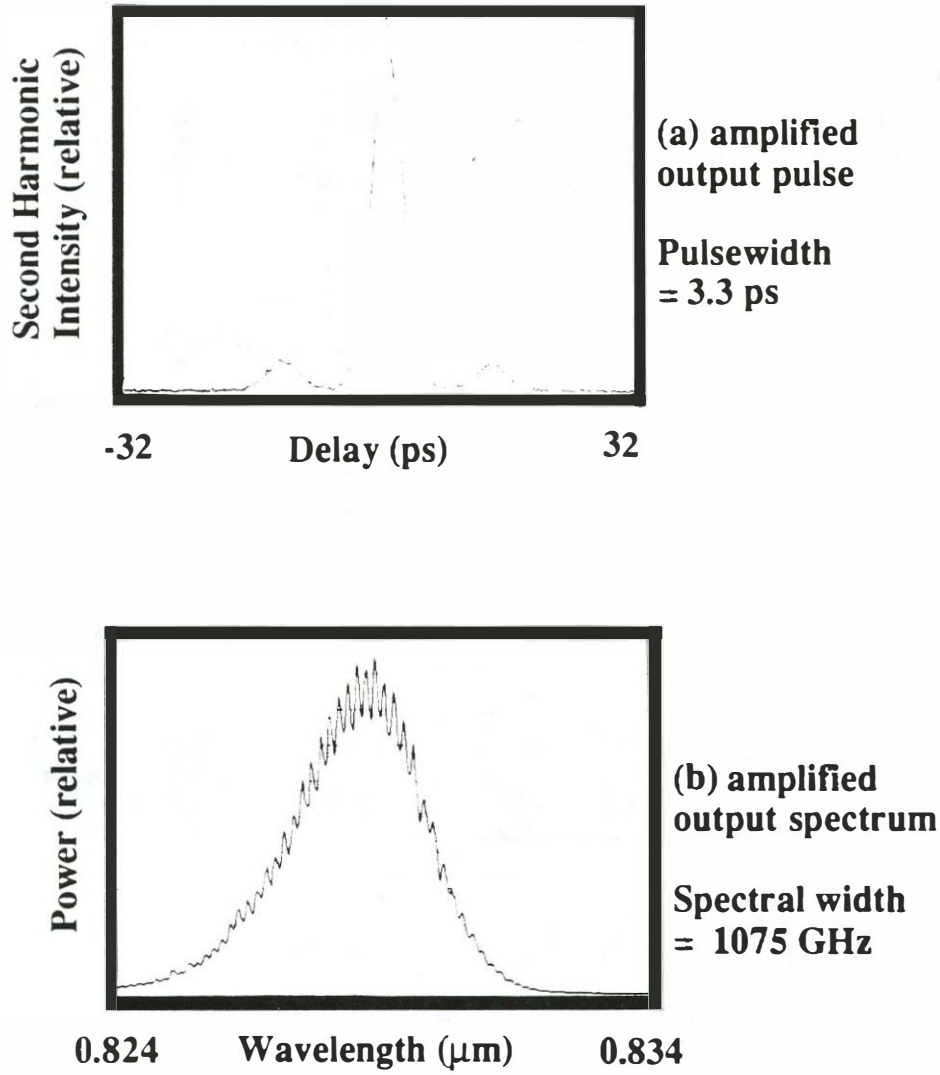

Figure 4.8 The (a) autocorrelation and (b) optical spectrum obtained from the amplifier output in the experiment of Figure 4.7. The optical pulsewidth is 3.3 ps with an energy of 1.9 pJ. The optical spectral width is 1075 GHz.

saturation energies due to their large mode cross-sectional areas, have been shown to give pulse energies as large as 300 pJ [62,63]. Techniques which are used for high power semiconductor arrays should be applicable to mode-locked semiconductor lasers. These techniques included MOPA [64], talbot plane [65], ARROW [66], unstable resonator [67], and anti-guide power combining techniques.

4.4 Repetition rate

For repetition rates below a few MHz, gain-switched and Q-switched devices work well. For repetition rates in the hundreds of MHz to 20 GHz range, external-cavity mode-locked lasers work well. The upper limit on the repetition rate of external cavity lasers is imposed by the finite length of the external cavity optical elements. The lower repetition rate of external cavity lasers is limited by several factors. The most fundamental problem is efficient optical feedback from the external cavity back to the laser diode. In a bulk optics external cavity approach, the light from a laser diode facet is not well collimated due to astigmatic effects and an elliptical beam shape. This could be solved with a compensating optics design. As the external cavity length increases, the coupling loss to the external cavity increases. The largest external cavity length that this author has obtained with reasonable coupling efficiency was a 2 meter cavity using the bulk optics approach. The problem can be circumvented with the use of a fiber external cavity [68]. There still seems to be a problem with long external cavities in fiber. A 10 MHz external cavity active mode-locked laser with fiber external cavity worked very poorly when operated at 10 MHz, but worked very well when operated at a several hundred MHz harmonic.

Passive mode-locked lasers do not work well at very low repetition rates (<500 MHz). Figure 4.9 shows the performance versus repetition rate of a passive mode-locked two-section external cavity laser. Since passive mode-

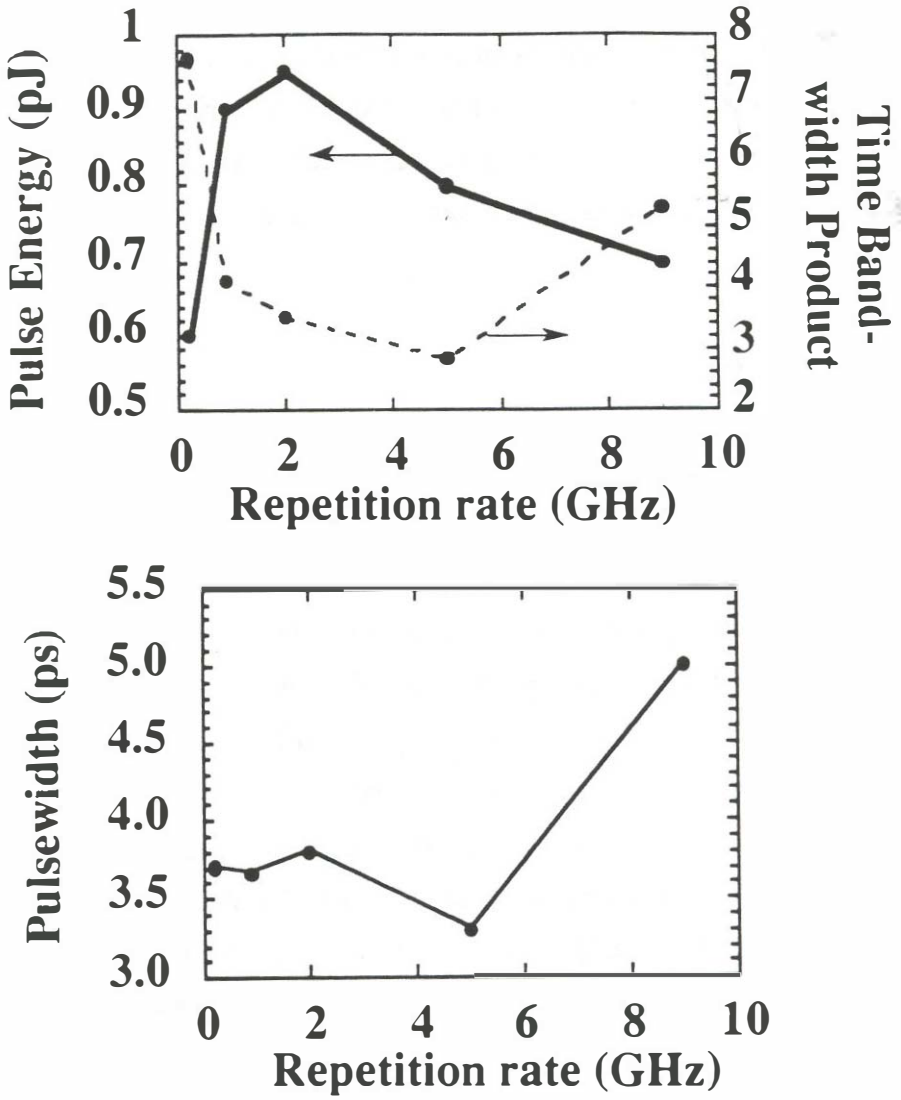

Figure 4.9 Time-bandwidth product, pulse energy, and pulsewidth versus repetition rate of a passively mode-locked laser. The structure is that of the bulk active device of Figure 1.27 with a 500 μm gain length and 16 μm saturable absorber. The point of this figure is to show that with passive mode-locking, it is possible to get short pulses over a wide range of repetition rates without requiring a short electrical modulation pulse as would be needed for active mode-locking. The device does have limitations on repetition rate though. At low repetition rates, the devices have a narrow range of bias conditions over which they will operate at the cavity fundamental repetition rate. Passive mode-locked lasers prefer to operate at harmonics of the cavity frequency below 1 GHz. For high repetition rates, The current required to replenish the gain on each round trip becomes very high and it is more difficult to get passive mode-locked operation.

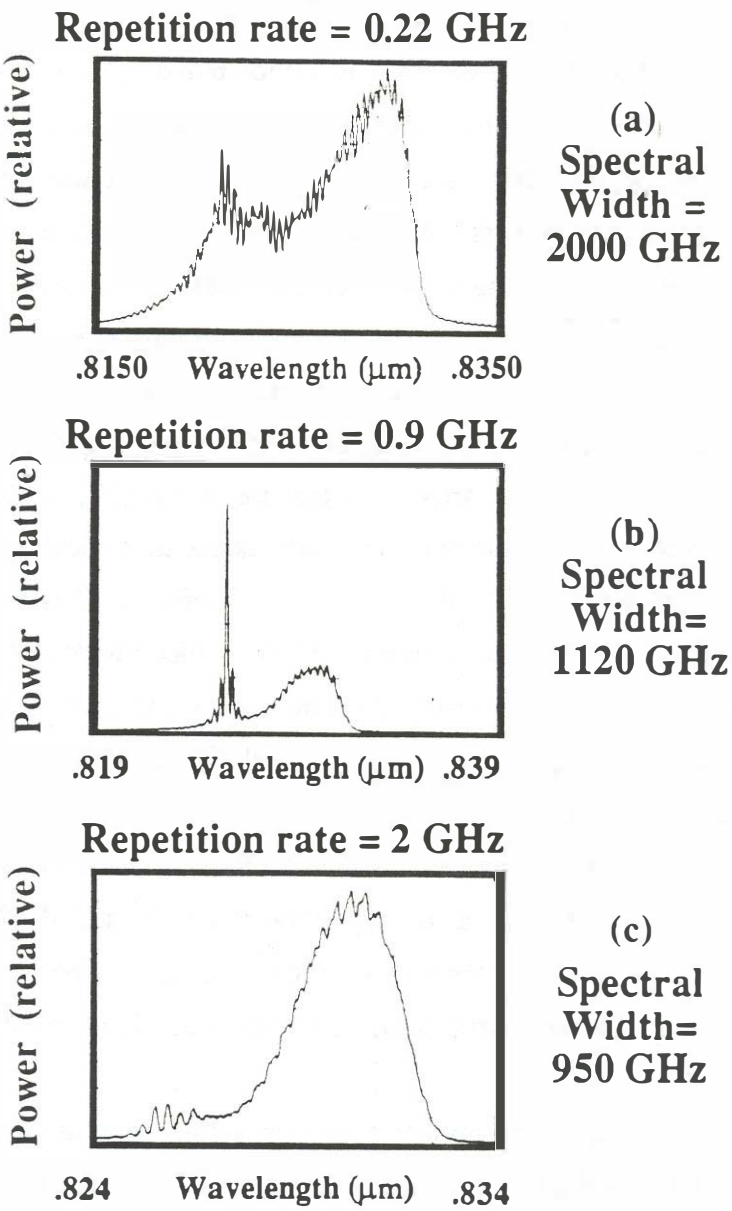

Figure 4.10 Optical spectrum for several repetition rates: (a) 0.22 GHz, (b) 0.9 GHz, and (c) 2 GHz. This figure shows an unusual shape of the optical spectrum with a two lobe maxima. The two lobe maxima are due to self-phase modulation effects caused by gain saturation. Referring to Figure 4.2 on self-phase modulation, it can be seen that the instantaneous frequency goes down and then back up. There are several points in time that show the same instantaneous frequency. These frequencies components add in and out of phase to produce the spectrum shown above.

locked lasers operate in a very specific pulse energy range , the average power of the laser must decrease as the pulse repetition rate decreases. As the average power decreases, the relative spontaneous emission power to stimulated emission power ratio increases and eventually the device will not operate for low average optical powers. The relatively constant pulse energy versus repetition rate shown in Figure 4.9 demonstrates that passive mode-locked lasers work best at a specific energy near the saturation energy of the laser amplifier. The pumping current range for operation at low repetition rates is also very small. For too large of bias currents, the passive mode-locked laser wants to operate at a higher harmonic of the laser cavity [27]. At low repetition rates, it is often impossible to reach the fundamental mode-locking frequencies by slowly increasing the current due to hysteresis effects. This bias point must be accessed by going higher in current to induce mode-locking (typically at a cavity harmonic) and then reducing the current to achieve a lower repetition rate. Hybrid mode-locking partially solves the instability problems at low repetition rates since the active gain modulation forces the laser to have the desired repetition rate. Commercially available step recovery diode modules typically have pulsewidths that widen as the repetition rate is decreased. Step recovery diode circuits do not fundamentally have to be slower at lower repetition rates but the designs for such circuits are not readily available from commercial market sources.

Figure 4.10 shows the optical spectrum versus repetition rate that was found for the experiment of Figure 4.9. The figure shows an unusual two-lobed maximum for the device as the repetition rate is lowered. The two-lobed maxima are due to self-phase modulation effects caused by gain saturation. Referring to Figure 4.2 on self-phase modulation, it can be seen that the instantaneous frequency goes down and then back up. There are several points in time that show the same instantaneous frequency. These frequencies

components add in and out of phase to produce the spectrum shown in Figure 4.2.

Monolithic cavity devices have been shown to operate at repetition rates between 5 GHz [49] and 350 GHz[30]. The lower repetition rate is limited by fabrication technology limits for monolithic devices approaching 1 cm in length. The upper repetition rate limit is reached with passive mode-locking techniques and is limited by the saturable absorber recovery time constant. The saturable absorber recovery time constant as measured in Section 2.4 was approximately 10 ps showing that 100 GHz mode-locking results are reasonable to expect based on saturable absorber recovery arguments. At a rate of 350 GHz, one would also think that the very fast amplifier recovery dynamics such as dynamic carrier heating [69] would play an important roll in device operation also, but theses connections are not well developed yet.

In mode-locked lasers, the repetition period is limited to be near the round trip time in the device. For a fixed cavity length, mode-locked lasers can be slightly tuned from this resonance with minimal degradation in device performance. The pulsewidth performance versus repetition rate of actively and hybrid mode-locked monolithic and external cavity lasers is compared in Figure 4.11. The monolithic device is a 2.75 mm long bulk GaAs active region device [50] operating at 13 GHz (see Figure 2.27). The external-cavity device is 500 μm long, operates at a 6.5 GHz repetition rate, and comes from the same wafer as the monolithic cavity device. The plotted tuning range limits represent the points at which the mode-locked lasers exhibit significant phase or amplitude instabilities as measured in an electrical spectrum analyzer with a photodiode input. **Monolithic cavity devices show a greater tunability that external cavity devices.** This is partially due to the lower cold cavity Q of the monolithic cavity device with all-active waveguide. It may also be due to the fact that the carrier density and thus the index of refraction can self-adjust to

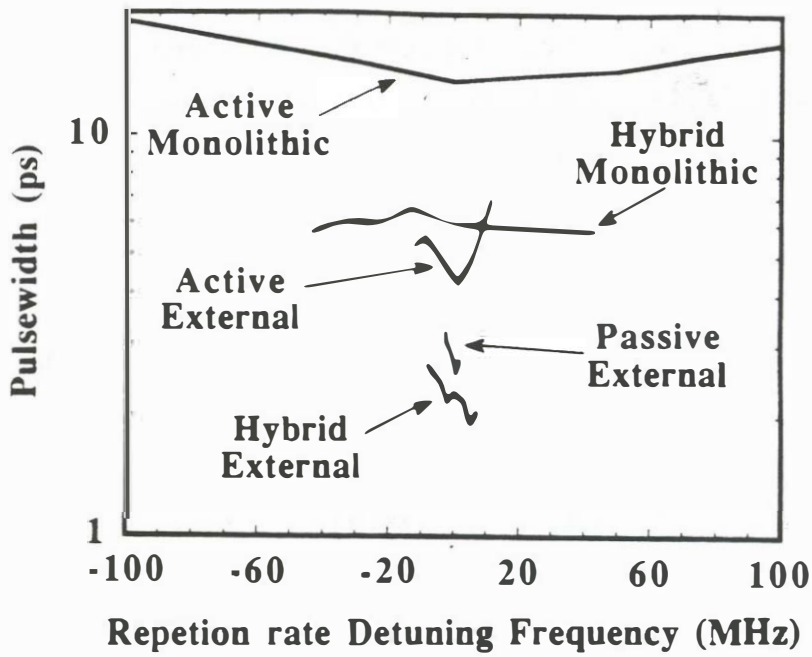

Figure 4.11. Pulsewidth versus detuning of the repetition rate for monolithic and external cavity devices using active, passive, and hybrid mode-locking techniques. The structure for both devices is the bulk active of Figure 1.27. The monolithic cavity device has a center repetition rate of 13 GHz (2.75 mm long device with 16 μm long modulation segment and 16 μm absorber segment) and the external cavity device has a center repetition rate of 6.1 GHz (500 μm long device, 16 μm long modulation segment, and 16 μm absorber segment).

bring the laser back into resonance with the modulation signal. One would expect that the cold cavity Q for a very long monolithic cavity device with active waveguide would be smaller than for an external cavity device which has large sections of air in the external cavity. The extra loss in the monolithic cavity case comes from the waveguide loss (typically 5-10 cm^{-1} for quantum well devices). The effects of the cold-cavity Q on tunability are explored in the small signal modulation frequency detuning curves of Figure 4.12. Because the modulation signals are very small, changes in the carrier density are small when the modulation frequency is changed. Index of refraction self-adjustment is thus eliminated in this experiment. The monolithic cavity device shows a much larger detuning bandwidth than the higher cold-cavity Q external cavity case. This evidence shows that the cold-cavity Q effect may be stronger than the index of refraction adjustment effect. **For a given cavity configuration, active mode-locking showed the widest tunability followed by hybrid and passive mode-locking techniques.**

Mode-locked lasers which incorporate distributed Bragg reflectors in the cavity have shown a larger modulation frequency tuning range due to the frequency dependence of the effective reflection point [70]. Recently, chirped reflection gratings have produced tuning ranges that approach an octave. Passive mode-locked semiconductor lasers can be tuned electronically with the incorporation of a repetition rate tuning element as is shown in Figure 4.13. The external cavity device showed a tuning range of 8 MHz for a 7 mA bias current change into a 16 μm long tuning segment. Longer tuning segments will provide a wider repetition rate tuning range. These repetition rate tuning sections work by changing the carrier density. The carrier density changes modify the repetition rate through a gain to repetition rate conversion mechanism that is described in Chapter 6. This electronic tuning of the repetition rate is important because it provides a convenient way of phase locking the device to a lower frequency standard in order to reduce the timing

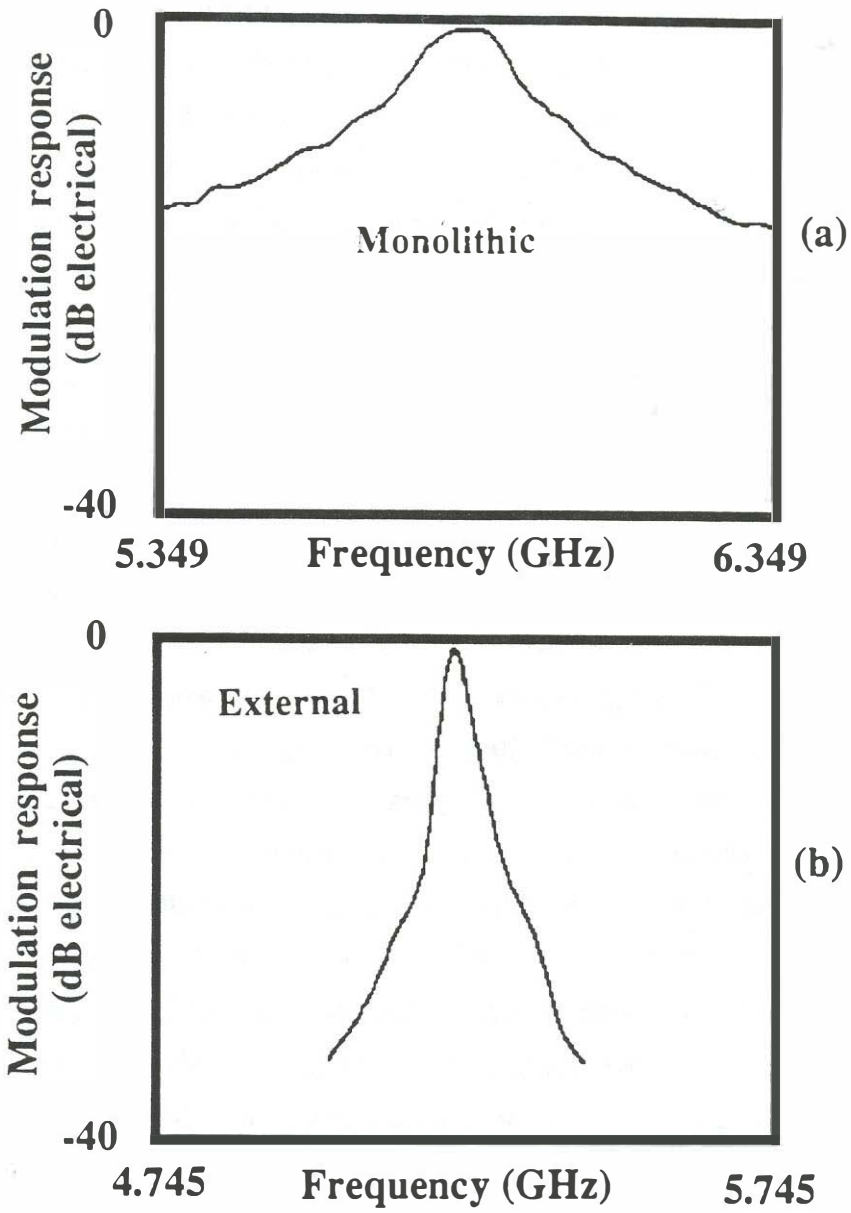

Figure 4.12 Small signal modulation experiment with a two section monolithic and external cavity device. The devices are the same as that of Figure 4.11. This figure shows that the large difference in modulation frequency detuning between monolithic and external cavity devices is largely due to the difference in the cold-cavity Q (or the difference in photon lifetime since $\omega \tau_p$ is the cold cavity Q). The other mechanism that can allow a larger modulation frequency detuning is the fact that the index of refraction changes with carrier density with the connection found in the linewidth enhancement factor. This small signal modulation experiment indicates that the effects of the linewidth enhancement on detuning are smaller than the cavity Q effects.

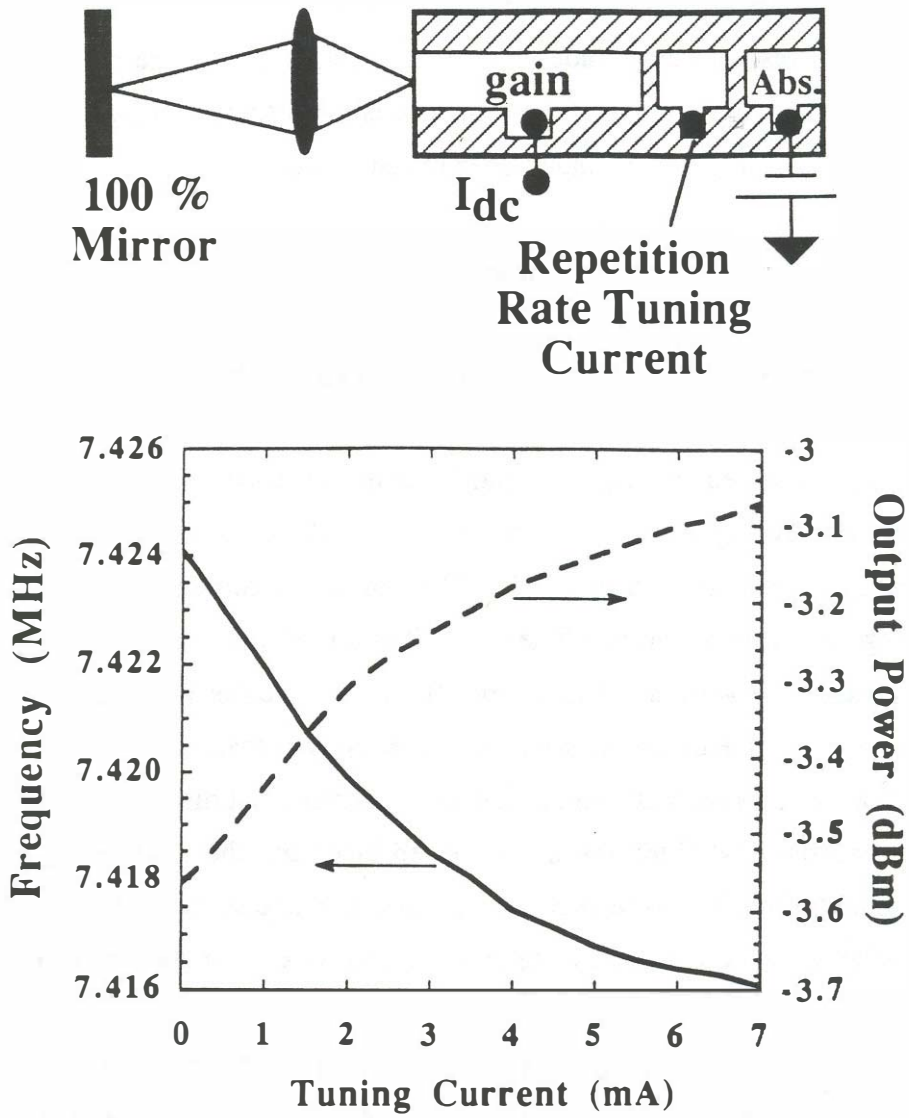

Figure 4.13 This figure demonstrates repetition rate detuning in passive mode-locking using electrical adjustment. By varying the tuning current in a short segment and therefore the gain, the repetition rate can be slightly varied in passive mode-locked lasers. This adjustment can be useful for phase-locking a passively mode-locked laser repetition rate to that of a microwave reference oscillator. The saturable absorber can serve as the electrical output signal from the mode-locked laser in these phase-locking schemes. The figure also shows the undesirable amplitude changes that come along with the frequency changes.

jitter [71]. The photocurrent from the saturable absorber also provides a convenient electrical input for the phase-locking circuitry. Figure 4.13 also shows the residual amplitude change that occurs during the repetition rate tuning. This amplitude modulation is undesirable since it represents a phase modulation to amplitude modulation conversion process.

4.5 Timing jitter and amplitude noise

4.5.1 Timing jitter in mode-locked lasers and why it is important

While optical pulses as short as 1.9 ps with 250 mW peak powers [72] have been demonstrated in Chapters 2 and 3, the usefulness of these short pulses for many time averaged measurements is influenced by the pulse to pulse timing stability. Previous works [73,74,75] show measurements of the absolute timing jitter due to the combined contributions of the electrical modulating source together with the contributions from the mode-locked laser. This work examines absolute timing jitter with higher sensitivity than earlier measurements and introduces a residual timing jitter measurement that distinguishes between the contributions of the the mode-locked laser and the modulating source. Residual timing jitter is important in situations where several lasers are driven from the same modulation source and is useful for examining the nature of the laser timing fluctuations.

The concept of absolute and residual timing jitter is illustrated in Figure 4.14. Three mode-locked lasers are actively mode-locked from the same electronic modulation source, and produce three separate pulse streams which should be coordinated together in time. Let's first examine the output of a single mode-locked laser. The dashed lines represent the expected arrival times of the mode-locked pulses based on the modulation frequency of the electronic source. Timing jitter on the pulse streams cause some of the pulses to arrive

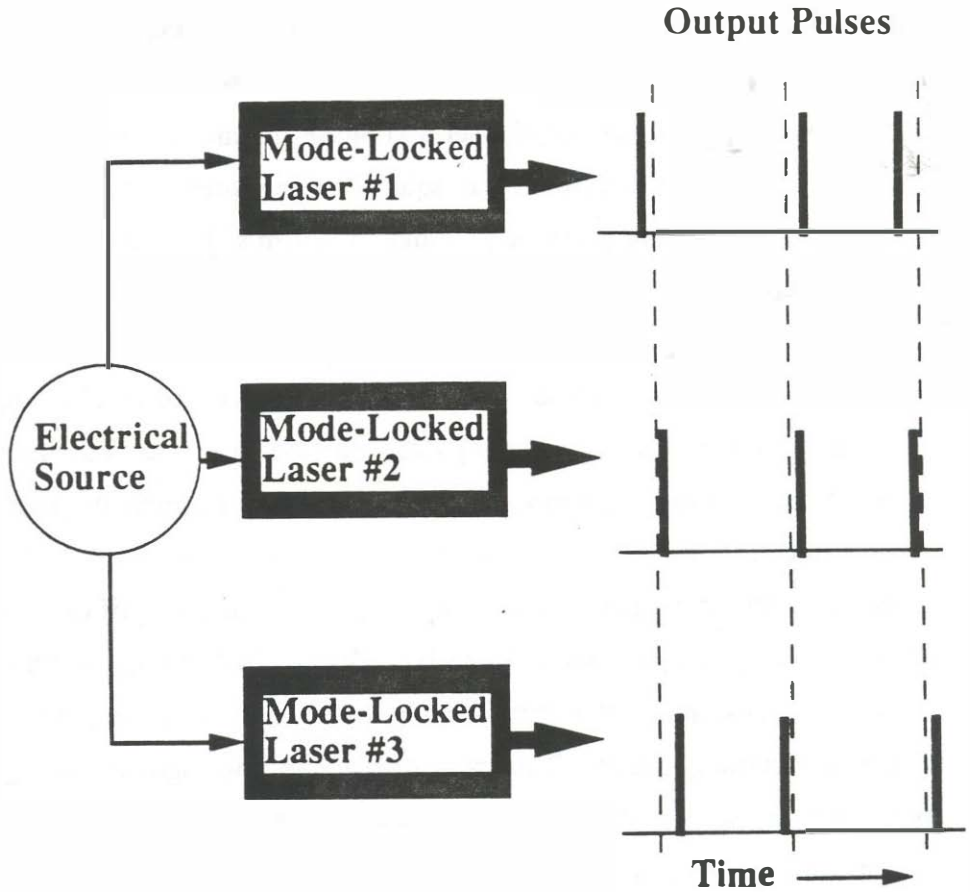

Figure 4.14 This figure demonstrates the concepts of residual and absolute timing jitter. Imagine three actively mode-locked lasers all driven from the same electrical modulation source. The optical outputs from the three lasers should all occur at regular intervals along the dashed lines. For any one laser output, the amount of deviation from the expected time of arrival of a pulse is measured by the absolute timing jitter. Absolute timing jitter is often measured as an r.m.s (root mean square) deviation from the expected time. Absolute timing jitter includes contributions from the electrical modulation source and from the mode-locked laser. Residual timing jitter is a measurement of how the optical pulses from the three mode-locked lasers deviate in time with respect to each other. The contribution of the electrical modulation source to residual timing jitter is zero. Residual timing jitter is a measure of the jitter added by the mode-locked laser alone.

earlier and some of the pulses to arrive later than the expected time. Absolute timing jitter is a measure of the time difference between the expected arrival time and the actual arrival time. The timing jitter can be cause by both phase fluctuations in the mode-locked laser and phase fluctuations in the electrical driving source. The r.m.s (root mean square) timing jitter is used as the figure of merit for the timing jitter magnitude. The r.m.s. jitter is similar to the statistical standard deviation of the pulse location from the expected location for a wide sense stationary process.

Residual timing jitter is also illustrated in Figure 4.14. Residual timing jitter measures the relative position of the pulses from the 3 mode-locked lasers with respect to each other. If the mode-locked lasers did not contribute jitter to the system, the pulses from the mode-locked lasers would deviate from the expected locations but they would all deviate in the same way (if mode locked pulse were early, they all would be early). The residual timing jitter therefore measures the amount of jitter contributed by the mode-locked laser, independent of the modulation source. This type of jitter is important in pump-probe measurements with multiple optical frequency sources or for time division multiplexed optical communication systems. Residual timing jitter would also be important in situations where only the timing jitter difference between the source and mode-locked laser are important.

4.5.2 Timing jitter measurement

Figure 4.15 shows the experimental configuration used to measure residual and absolute timing jitter. The absolute timing jitter is measured with a frequency domain technique [76] using a high-speed photodetector, preamplifier, and microwave spectrum analyzer with the switch in Figure 4.15 connected to point "A". The spectrum analyzer can not directly distinguish between amplitude and phase noise, but the nature of the noise can be

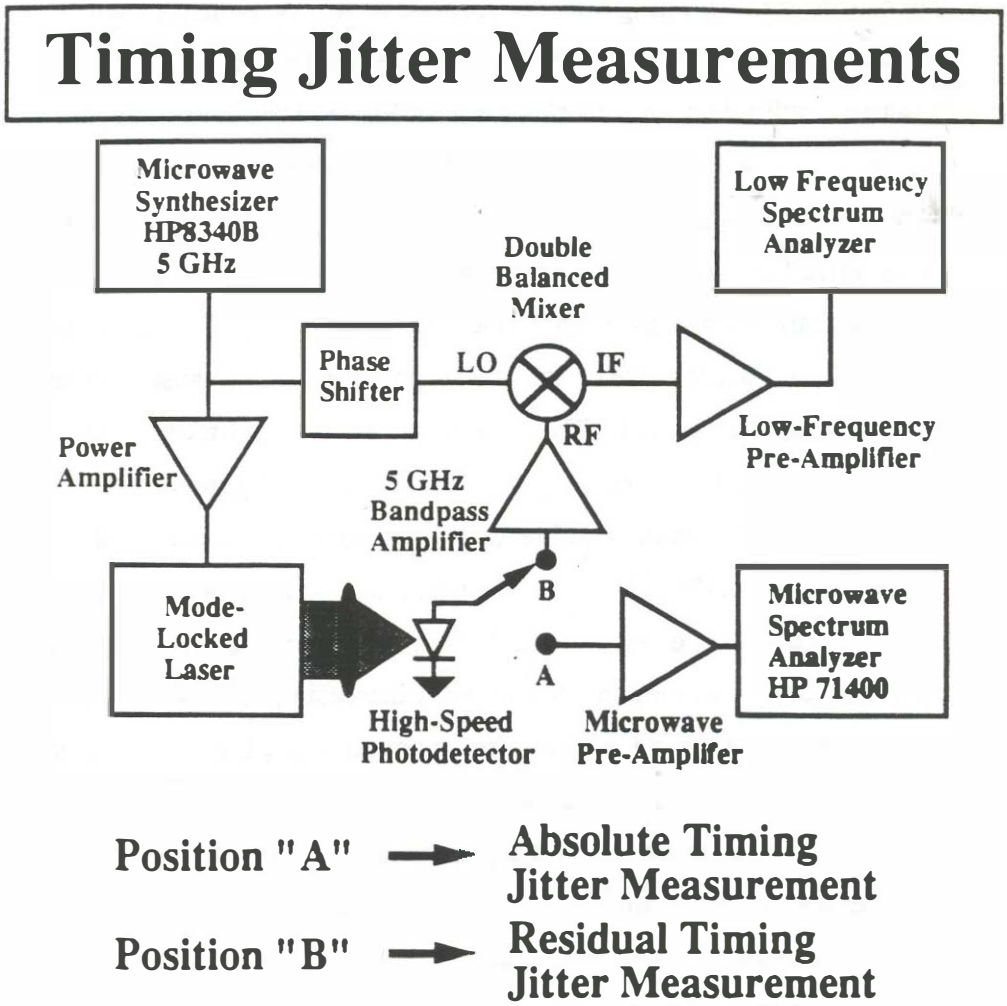

Figure 4.15 The experimental configuration used to measure absolute and residual timing jitter. When the switch is to position "A", absolute timing jitter is measured. The mode-locked laser is driven by the modulation source and the optical output pulses are detected and applied to a pre-amplified spectrum analyzer. The limitation on phase noise in this measurement is the phase noise of the modulation source and of the local oscillator in the spectrum analyzer. When the switch is in the "B" position, residual timing jitter is measured. The detected output from the mode-locked laser is applied to the RF port of a double balanced mixer and the output from the modulation source is applied to the LO port of the mixer. When the phase difference between the LO and the RF signals is adjusted to 90°, the mixer acts as a phase detector. If the mode-locked laser adds no extra jitter to that of the modulation source, there is no output from the IF to the low frequency spectrum analyzer. If the mode-locked laser adds jitter of its own, this residual jitter is measured. The measurement floor can be calibrated by bypassing the mode-locked laser.

determined by examining how the relative noise level changes with harmonic number. Figures 4.16 and 4.17 illustrates the method that is used to distinguish between amplitude noise and phase noise. Figure 4.16 shows a repetitive pulse stream with a period, T_{rt}, in the time domain. The frequency domain picture shows spectral harmonic components spaced at $1/T_{rt}$ Hz. Amplitude noise is characterized by a randomly varying pulse amplitude and phase noise (or timing jitter) is characterized by a randomness in the temporal position of the pulses. Amplitude and phase noise on the optical power envelope cause a broadening of the individual harmonics. The relative level for amplitude noise sidebands remains constant for increasing harmonic number (Figure 4.16), whereas for phase noise sidebands the relative level increases as the square of the harmonic number (Figure 4.17) [77]. Thus relative phase noise sidebands increase by 6 dB and 9.5 dB for the second and third harmonics respectively and amplitude noise sidebands will remain constant with increasing harmonic number. Since the measurements are done in the frequency domain, it is desirable to use the frequency domain phase noise information to calculate the time domain jitter. The root mean square (r.m.s.) timing jitter can be calculated by integrating the noise versus offset frequency at a harmonic where the noise is dominated by phase fluctuations. The formula used to convert phase noise information to frequency domain information is

$$\sigma_{rms} = \frac{1}{2\pi n f_{mod}} \sqrt{2 \int_{f_{low}}^{f_{high}} \mathfrak{L}(f)\, df} \tag{4.1}$$

where σ_{rms} is the root mean square timing jitter, n is the harmonic number at which the measurement data is taken, f_{mod} is the fundamental repetition rate frequency, f_{low} is the lower offset frequency from the repetition rate harmonic carrier frequency, f_{high} is the upper offset frequency from the carrier, and L(f)

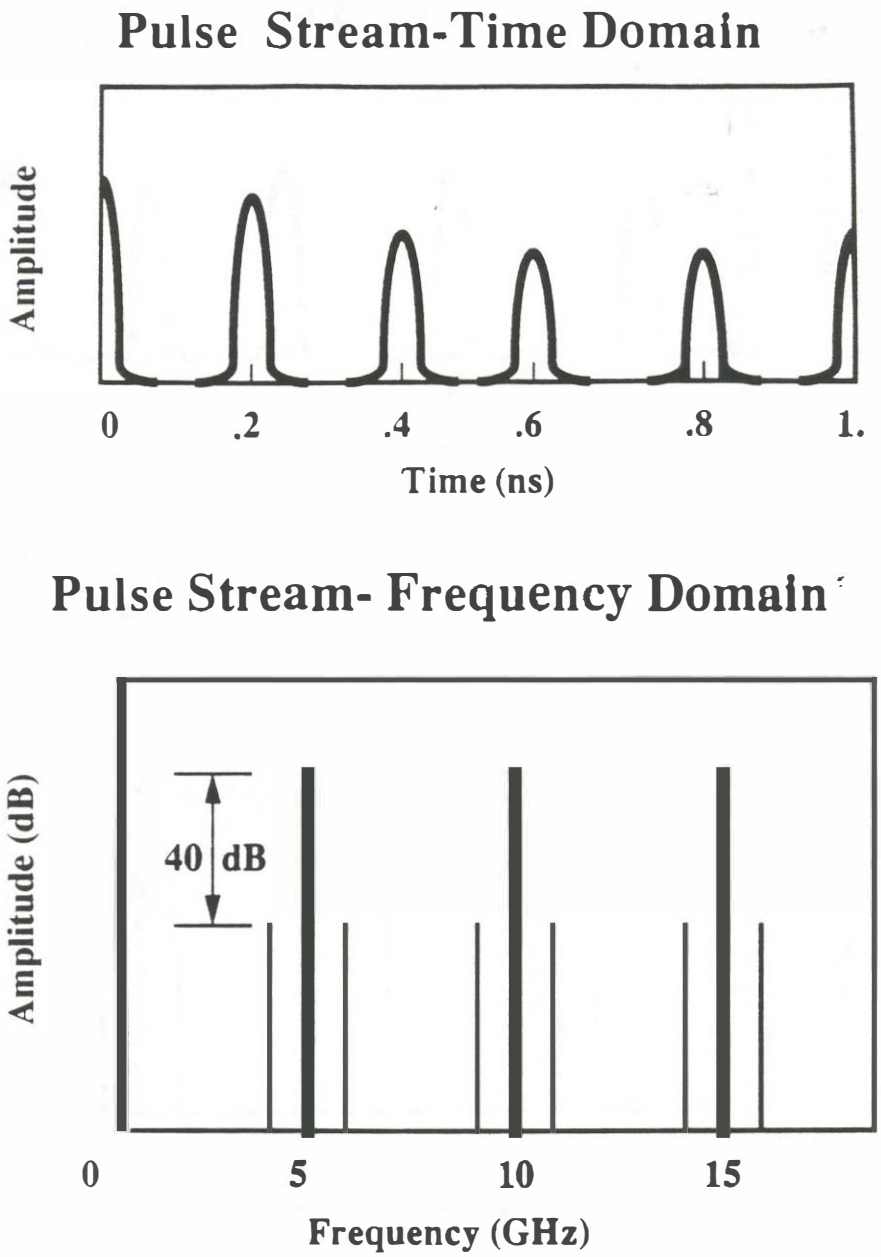

Figure 4.16 (a) The time domain picture of an amplitude modulated pulse stream. (b) The frequency domain picture of an amplitude modulated pulse stream. A comb of frequencies is spaced by the repetition rate of the mode-locked laser. Each harmonic has a modulation sideband caused by the amplitude modulation. For amplitude modulation, the relative magnitude of each sideband remains constant as the harmonic number is increased.

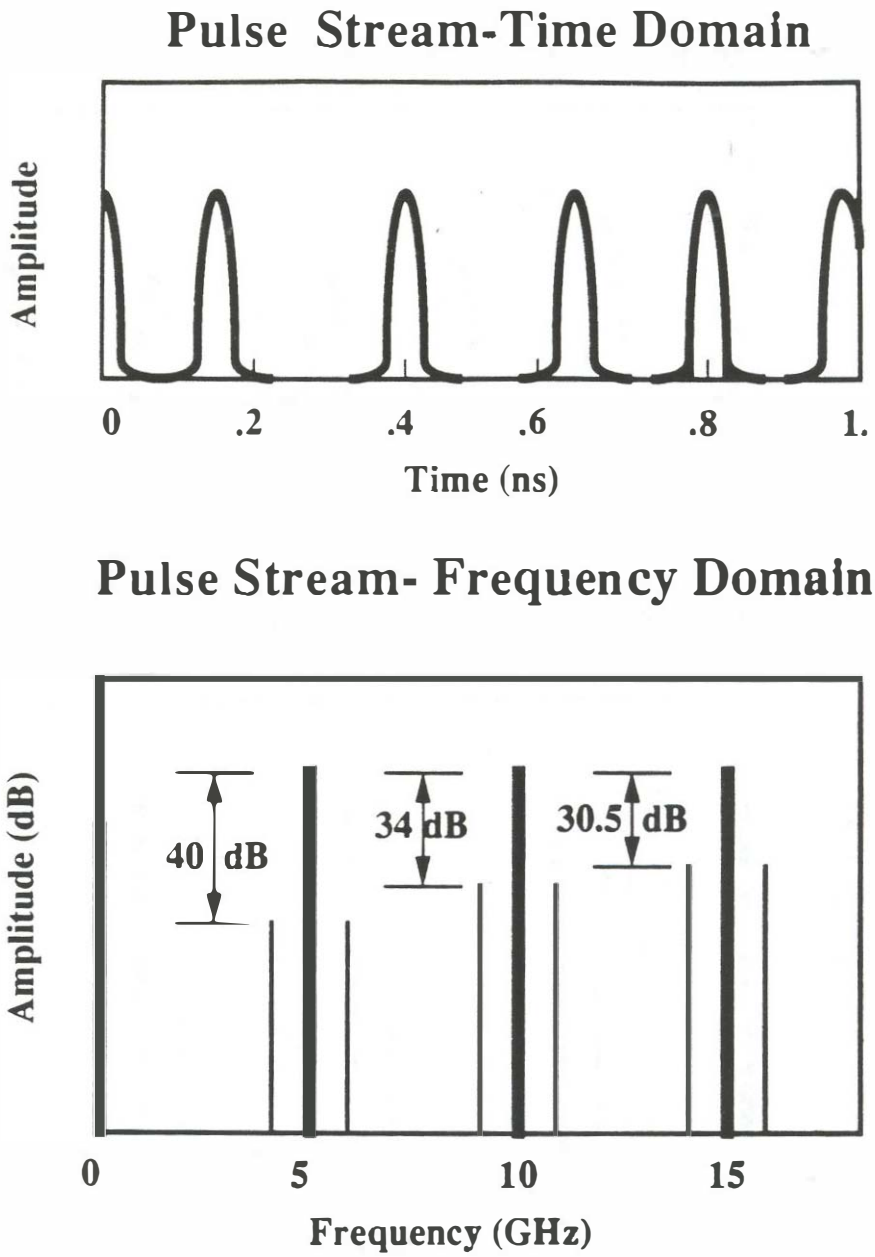

Figure 4.17 (a) The time domain picture of a phase modulated pulse stream. (b) The frequency domain picture of a phase modulated pulse stream. A comb of frequencies is spaced by the repetition rate of the mode-locked laser. Each harmonic has a modulation sideband caused by the phase modulation. For phase modulation, the relative magnitude of each sideband increases as the harmonic number squared for small modulation indexes. Thus the second and third harmonic level should be 6dB and 9.5 dB higher than the fundamental sideband level for pure phase modulation.

is the single sideband phase noise relative the the carrier and normalized to a 1 Hz bandwidth.

An important point to note is that if L(f) drops with a 1/f frequency response, each decade of noise will contribute equally to the r.m.s. timing jitter. Equation 4.1 shows that when you quote a r.m.s. timing jitter value from frequency domain phase noise information, you must always specify the limits of integration since the timing jitter value depends on the limits of integration. It is also important to understand the measurement application in timing jitter calculations since different measurements applications are more susceptible to fluctuations in certain frequency ranges. As an example, an electrooptic measurement system with a measurement averaging time of 1 ms will not be concerned with phase noise at offsets which are very much lower than 1 kHz. L(f) data is obtained directly from the spectrum analyzer by measuring the relative noise level with respect to the carrier. The raw data must then be normalized to a 1 Hz bandwidth by taking into account the measurement bandwidth used during the measurement. Things are a little more complicated though because the noise bandwidth is specified for a perfect rectangular shaped filter. The logarithmic amplifier in the optical spectrum analyzer also tends to give lower amplitude noise fluctuations more gain than large amplitude noise fluctuations. Fortunately most modern spectrum analyzers take this into account when using the noise marker function instead of the displayed noise marker function. The difference between the displayed average noise level and the true noise level when normalized to a square filter is about 2 dB (the actual relative noise is level is higher than the displayed value by 2 dB). An electronic pre-amplifier is required in most measurement systems because the noise figure of the spectrum analyzer is typically very poor (> 20 dB). The noise figure of the pre-amplifier should be as low as possible and the gain of the preamplifier should be chosen such that the gain plus noise figure of the amplifier is greater

than the noise figure of the spectrum analyzer.

The residual timing jitter contribution from the mode-locked laser is measured using the homodyne technique shown in Figure 4.15 with the switch in the "B" position. In this measurement, the driving source is applied to both the actively mode-locked laser and to the local oscillator port of a double balanced mixer. The output of the mode-locked laser is detected and the 5 GHz component of the detected signal is applied to the RF port of the double balanced mixer and is mixed to a center frequency of 0 Hz (DC). The double balanced mixer is used as a phase detector with 20 dB AM noise rejection by adjusting the average phase difference between the RF and LO ports to 90°. If the phase fluctuations of the driving source are identical to the phase fluctuations of the detected mode-locked laser output, the IF port will have no output. If the mode-locked laser contributes additional phase fluctuations to that of the modulation source, an IF output will occur. The IF output shows the noise associated with the additional phase fluctuations contributed by the mode-locked laser independent of the electrical modulation source. The calibration of the residual noise measurement level is also an important point for discussion. The calibration is started by replacing the device under test by an electronic attenuator which has the same overall loss as the mode-locked laser (the loss referred to here is the loss from input electrical modulation signal to the detected electrical signal level). One method of calibration is to plot the voltage at the IF port versus the delay in the delay line for at least a 180 degree phase difference while the actual signals are in the measurement system. The plotted peak to peak voltage is then the reference level voltage for residual noise levels. An alternate method is to place another electronic synthesizer of the correct amplitude to the RF port of the mixer and offset its frequency from that of the reference electrical oscillator. The beat frequency signal will show up on the low frequency spectrum analyzer and the measured signal level is the reference. The actual measurement may require an additional attenuator at the output of the

beat frequency oscillator to reduce signal levels and eliminate amplifier saturation in the system. The attenuator value can be added back later when establishing the reference level. The residual phase noise measurement technique can also be applied to residual amplitude noise measurements by adjusting the relative phase difference between the LO ports and IF ports to 0°. In this case, one can achieve over 20 dB rejection of phase noise.

4.5.3 Single-segment active mode-locked laser timing jitter

The active mode-locked single section external cavity laser of Figure 4.1a consists of a 1.3 μm semi-insulating buried crescent laser [41] that has an antireflection coating on one facet. The laser is coupled with a graded index lens into an external 200 ps round trip time linear cavity. The external cavity laser has a threshold current of 14 mA and an output facet differential quantum efficiency of 10 %. The laser was biased at 18 mA in this experiment and adjusted for a minimum pulsewidth of 12 ps. The laser is modulated by a 24 dBm, 5 GHz signal from a low phase noise HP8340B microwave synthesizer and HP 8349A power amplifier. An optical isolator at the laser output is included to reduce external reflections and their effect on noise measurements.

The mode-locked pulse stream produces signals at harmonics of the 5 GHz mode-locking frequency. Figure 4.18a shows absolute L(f), the single sideband relative noise level normalized to a 1 Hz bandwidth, for the first 3 harmonics of 5 GHz. This measurement is made for an optimally tuned cavity in which the cavity length is adjusted for the shortest stable pulses. The absolute measurement floor shown in Figure 4.18a is obtained by connecting the amplifier and synthesizer directly to the microwave spectrum analyzer. The measurements show that the noise at offset frequencies below 100 kHz is phase noise in nature and is dominated by the driving source. Beyond 100 kHz the laser makes a contribution to the noise and the small difference between the 5

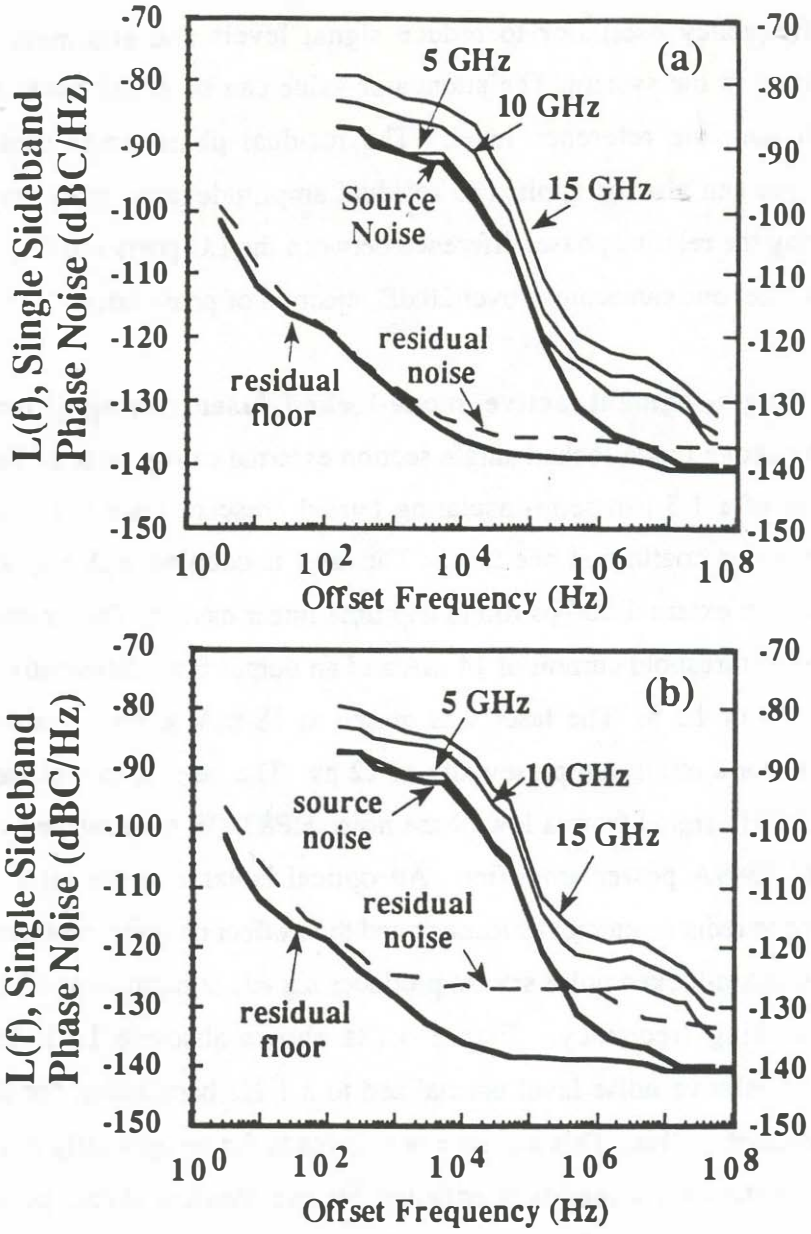

Figure 4.18 (a) Absolute and residual phase noise for a single-section actively mode-locked laser with an optimally tuned repetition rate for minimum phase noise. The laser is a 1.3 μm SIPBH laser with a 250 μm length, driven by a 24 dBm sinusoid at at nominal repetition rate of 5 GHz. (b) Absolute and residual phase noise for the laser of (a) with the optical cavity 150 μm longer than that of (a). The device in this figure had an external cavity threshold of 20 mA.

GHz and 10 GHz offset noise levels indicates it is mostly amplitude noise in nature. The absolute r.m.s. timing jitter of the source and laser combined over the 150 Hz to 50 MHz offset range from 5 GHz is 170 fs. This timing jitter value is dominated by the driving source. The question then arises about the fundamental timing jitter limits if a lower phase noise driving source were to be used. This question is addressed by residual timing jitter measurements.

Figure 4.18a also shows the residual L(f) measurement for the optimally tuned cavity. The residual r.m.s. timing jitter calculated from Figure 4.18a is 50 fs over the 10 Hz to 50 MHz offset frequency range. The residual measurement floor in Figure 4.18a is obtained by bypassing the mode-locked laser. The phase noise contribution from the laser has a low baseline contribution that rises with a 1/f noise slope below 10 kHz.

The noise levels of Figure 4.18a could be obtained over a cavity length range of plus or minus 50 μm. Significantly higher noise levels are obtained in mode-locked lasers if the optical cavity length is increased so that the electrical pulses start arriving in the laser before the optical pulses. Figure 4.18b shows the absolute and residual L(f) for the case of a cavity 170 μm longer than that of Figure 4.18a. The residual L(f) shows a much larger base-line phase noise contribution which is indicated by the increased spacing versus harmonic number at frequency offsets greater than 100 kHz. The longer cavity length introduces pulse instability (see Chapter 6) that results in amplitude and associated phase jitter in the mode-locked laser. When the electrical modulation pulse arrives early with respect to the optical pulse, the gain builds up prematurely with respect to the optical pulse. This premature gain build up causes an unstable period in time for the pulse location and increased timing and amplitude jitter. The instability is often seen experimentally as large, noisy amplitude and phase noise noise sidebands in the optical spectrum analyzer.

Figure 4.19 shows the detected electrical spectrum for the case of a large timing instability when the electrical modulation pulse arrives early with respect

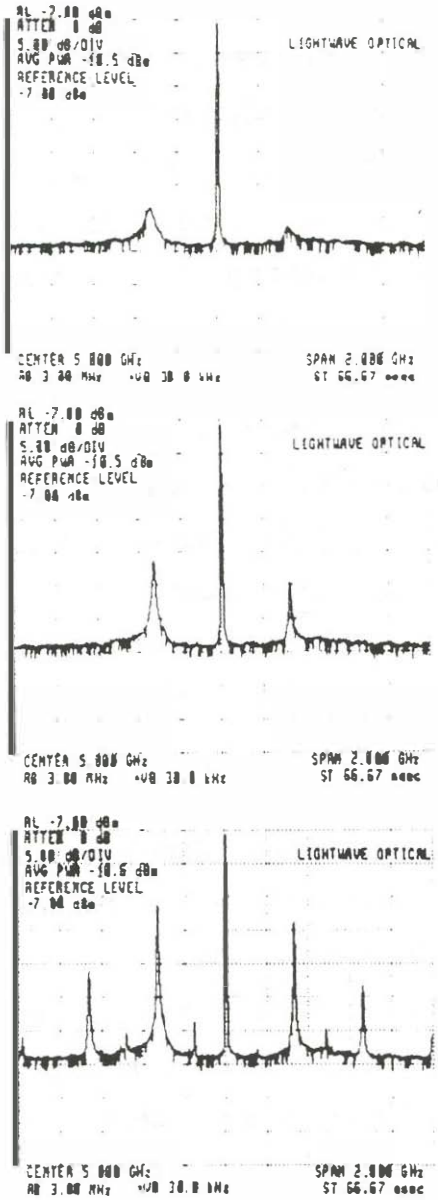

Instability versus Cavity Length

Reference Length

+60 μm

+120 μm

Figure 4.19 A frequency domain illustration of the instability that results as the length of the optical cavity is increased from the reference length (A longer optical cavity corresponds to a lowering of the cavity resonance frequency). The reference length corresponds to the phase noise measurement of Figure 4.18a. The phase and amplitude noise are correlated as can be seen from the asymmetry of the modulation sidebands.

to the optical pulse. The asymmetry of the noise sidebands indicate the presence of correlated amplitude and phase noise. The case of the electrical pulse arriving late with respect to the optical pulse is stable because the optical pulse does not have a large window in time of positive gain to choose from. The pulse narrowing process is weak in this case (see Chapter 5.4) and results in a much wider pulsewidth.

Figure 4.20 shows the absolute noise level from the active mode-locked single section laser as a function of the optical cavity length. The offset frequency from the carrier where the mode-locked laser noise dominates in this measurement is 300 kHz . Figure 4.20 demonstrates the importance of modulation frequency on phase noise performance. If one is simply adjusting the laser for least roll off in the detected spectrum, it is easy to miss the instability unless one looks very close in frequency offset to each harmonic component.

Higher jitter levels are also seen in high threshold lasers or lasers with poor coupling to the external cavity. Figure 4.21 shows the residual and absolute L(f) for a buried crescent structure with an external cavity threshold of 45 mA (compared to 12 mA for the case of Figure 4.18a). The absolute noise levels are much larger than that of Figure 4.18a. There is a large baseline residual phase noise contribution from the mode-locked laser and the 1/f noise rise is clearly lifted from the measurement noise floor. The large residual noise level is explained by an amplitude to phase noise conversion process in the laser. Spontaneous emission causes random carrier density fluctuations and associated gain and index of refraction variations in the laser. The absolute and residual r.m.s. timing jitter levels for the case of Figure 4.21 are 230 fs and 330 fs respectively over the 150 Hz to 50 MHz offset frequency range.

The absolute timing jitter of an active mode-locked single-section ring cavity laser was also measured. The cavity geometry for the experiment is shown in

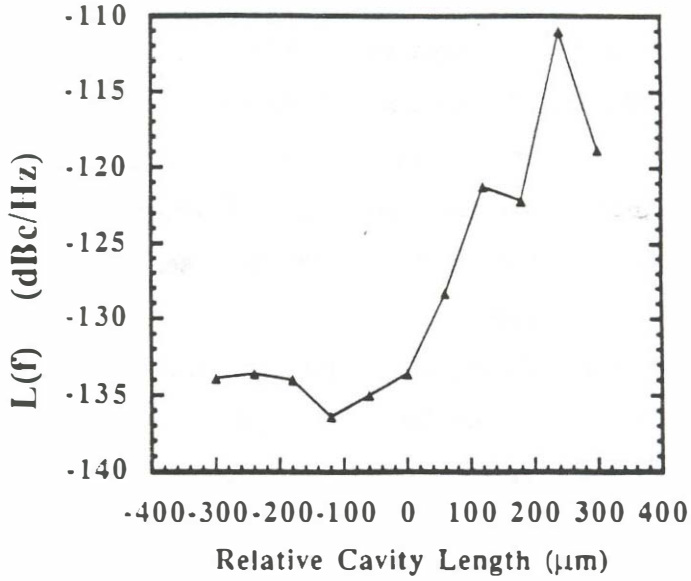

Figure 4.20 Absolute phase noise versus adjustment of the optical cavity length for the single section active mode-locked laser of Figure 4.18. The zero relative length point represents the measurement of Figure 4.18a. Increasing cavity length corresponds to a lowering of the optical cavity frequency.

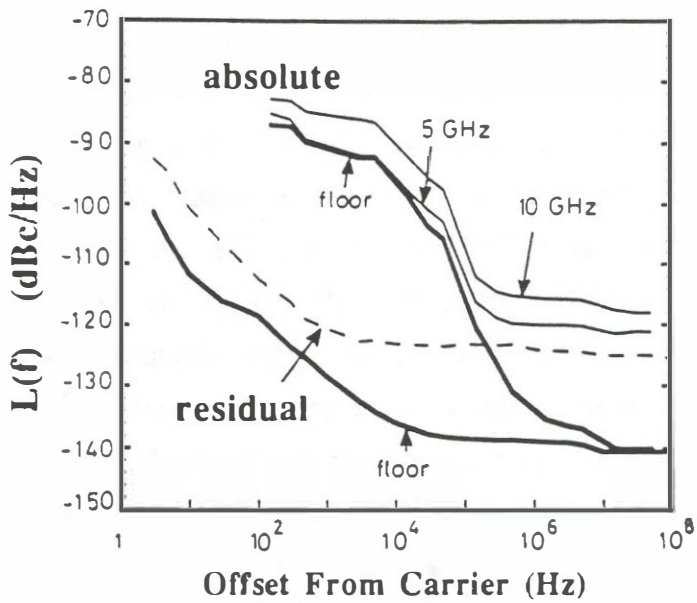

Figure 4.21 Residual and absolute phase noise for an actively mode-locked single section laser with a higher threshold than that of Figure 4.18. The external cavity threshold for this device is 45 mA compared to the threshold current of 20 mA in Figure 4.18. The higher threshold laser shows a larger phase noise contribution level from the mode-locked laser.

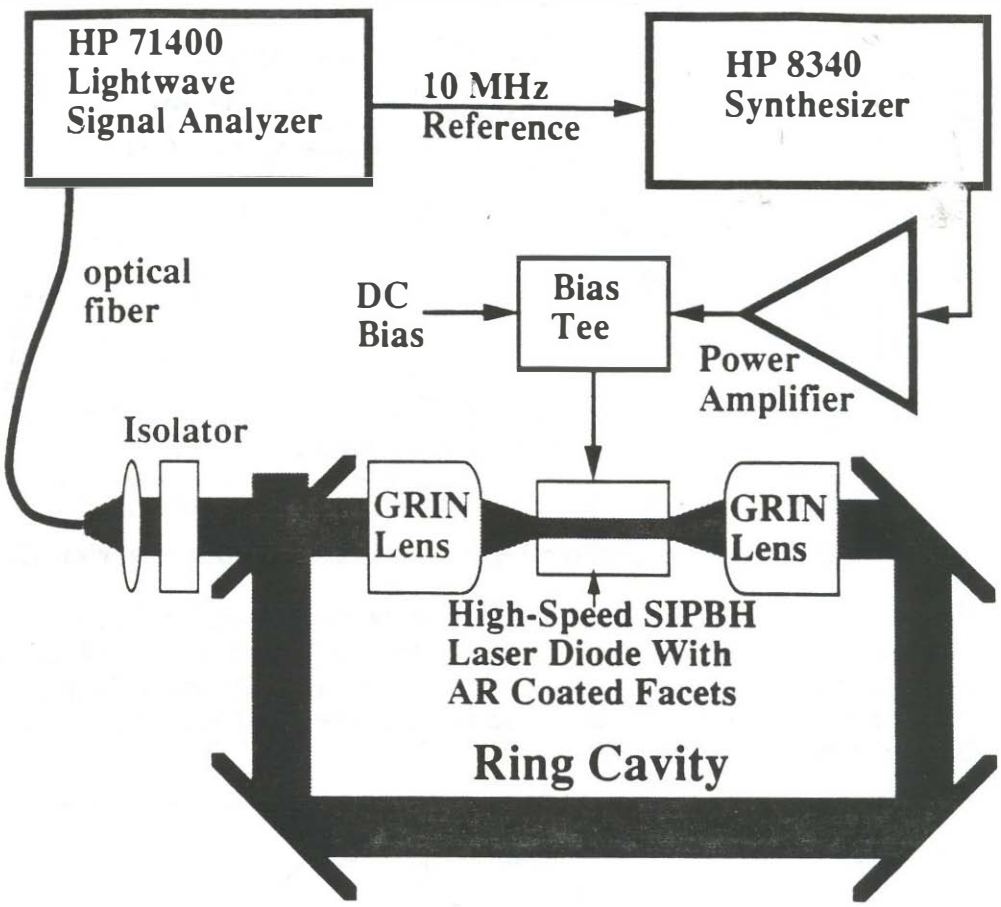

Figure 4.22 A single section ring cavity actively mode-locked single section laser and the experimental set-up used to measure absolute phase noise. An isolator has been used at the output since the phase noise of the ring laser is affected by external cavity reflections. The output coupling mirror is 50%. The laser threshold is 50 mA in the external cavity. The device is actively mode-locked at 5 GHz, the tenth harmonic of the fundamental cavity frequency. The device is driven by a 24 dBm, 5 GHz sinusoidal signal.

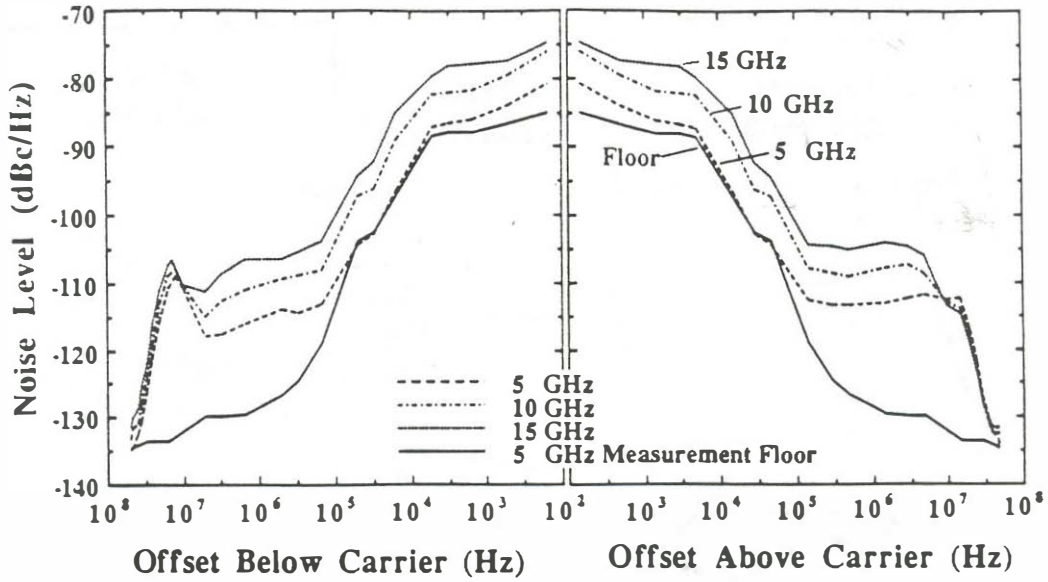

Figure 4.23 Absolute noise, above and below the modulation frequency of 5 GHz for the single section mode-locked ring cavity laser of Figure 4.22. The fundamental frequency of the ring cavity is 0.5 GHz. The mode-locked laser starts to contribute significant phase noise at offsets of 100 kHz above and below the modulation frequency.

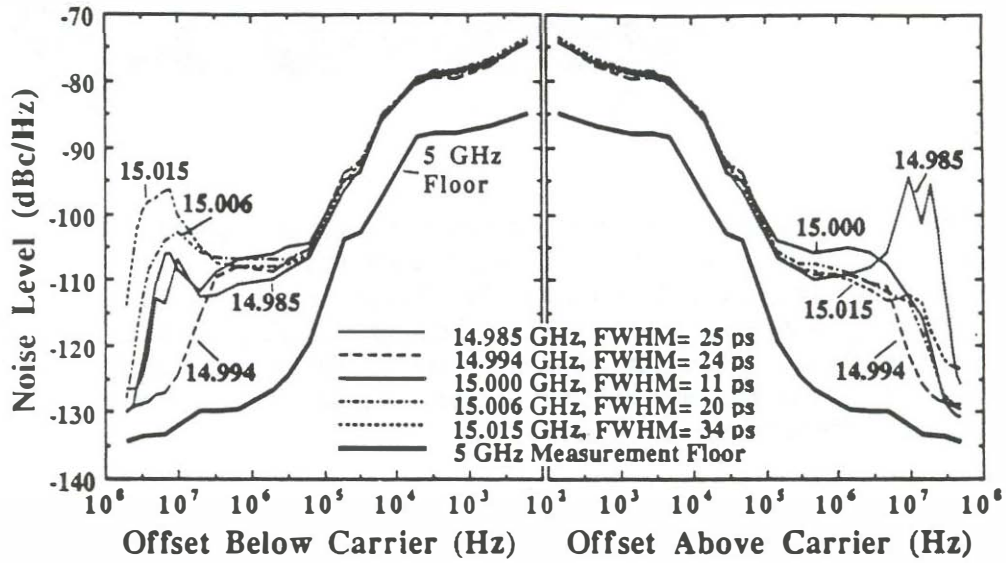

Figure 4.24 The absolute noise above and below the third harmonic of the 5 GHz repetition rate for the actively mode-locked ring cavity laser of Figure 4.22. The modulation frequency is detuned in this measurement and the third harmomic level is given.

Figure 4.22. The laser diode is a 1.3 μm SIPBH structure [41] that is antireflection coated on both facets and driven by at 24 dBm sinusoid at 5 GHz. The fundamental resonance frequency of the mode-locked laser is 0.5 GHz. The absolute phase noise above and below the repetition rate frequency of 5 GHz is shown in Figure 4.23. The mode-locked laser shows clear phase noise contributions above an offset frequency of 300 kHz. Figure 4.24 shows the level of the third harmonic noise as a function of the modulation frequency detuning from the 5 GHz center frequency. The plot again shows that there is an optimal modulation frequency which gives the best stable mode-locked laser performance. Mode-locked lasers that are operated at a cavity harmonic are also more sensitive to timing jitter.

4.5.4 Comparison of timing jitter in multi-segment structures

A comprehensive timing jitter comparison is made for mode-locked semiconductor lasers using active, passive, and hybrid mode-locking techniques in both external and monolithic cavity configurations. Active mode locking of single-segment lasers will be shown to give the lowest residual r.m.s. timing jitter of 65 fs (150Hz- 50 MHz), followed by two-section active, hybrid, and passive mode-locking techniques. It is found that monolithic cavity devices with all-active waveguides have higher timing jitter levels than the comparable external cavity case (for the same material and repetition rate).

It should be pointed out that there is a wide range of timing jitter levels in the passive, hybrid, and active mode-locking cases. For the hybrid and active mode-locking cases, the timing jitter found in semiconductor lasers is consistently lower than that found in other competing mode-locked laser types. Figure 4.25 shows a comparison of the phase noise performance found in a state-of-the-art compressed pulse YAG laser with and without timing stabilizer to that of any of the active or hybrid mode-locked lasers studied in this chapter

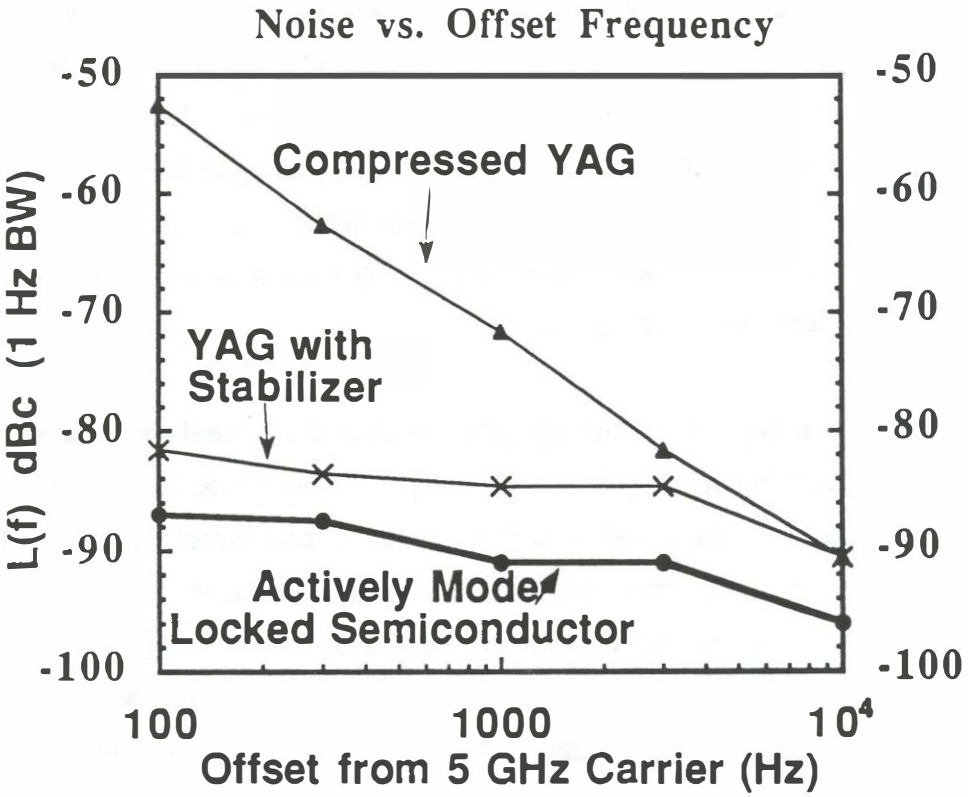

Figure 4.25 A comparison of the phase noise performance of an actively mode-locked single section semiconductor with a compressed YAG laser. The YAG phase noise data has been corrected by 20 Log(harmonic number) to make a fair comparison. The YAG laser data has been taken from reference 76.

showing the superior performance of semiconductor lasers mode-locked lasers.

The discussion on multi-section structures will start with a comparison of the absolute timing jitter levels found in *external* cavity lasers. The external cavity configurations of Figure 4.1 a, b, c, and d corresponding to single-section active, two-section active, two-section passive, and three-section hybrid mode-locking are directly compared. The device material in all cases is the bulk active region structure discussed in Figure 2.27 with 500 μm gain section lengths. The gain modulation segment length and saturable absorber segment lengths are 16 μm. The absolute timing jitter measurements for these cases are shown in Figure 4.26. The repetition rate in all cases is 5 GHz and the active modulation drive power was 24 dBm. The gain section bias conditions for cases 4.25a, b, c,and d are 20 mA, 30 mA, 50mA and 50 mA respectively. The measured timing jitter level for each case is also shown in Figure 4.26.

Active single-section mode-locking displayed the lowest level of timing jitter of 174 fs (150Hz-50 MHz) . The single-section active mode-locked laser works at a bias level nearly equal to the threshold current of the external cavity laser. The two-section, active mode-locked laser produces a significantly shorter pulsewidth (6 ps compared to 12 ps), but the timing jitter level increases to 300 fs (150 Hz-50 MHz). The three-section hybrid mode-locked laser gives the shortest optical pulsewidth (1.9 ps) but also has an increased level of timing jitter of 1250 fs (150 Hz-50 MHz). The passively mode-locked two-section laser shows the largest level of timing jitter of 12 ps (50 kHz-50 MHz). For the cases that include active gain modulation, the evidence indicates that there could be a correlation between pumping level to the laser and the measured value of the timing jitter. The passive mode-locked laser is a special case since it is a free-running optical oscillator without electronic envelope stabilization.

A comparison of the timing jitter levels found in external cavity devices to that found in monolithic cavity devices was also done. The compared devices are those of Figure 4.1 a, c, and d (external designs) to those of Figure 4.1 e, f,

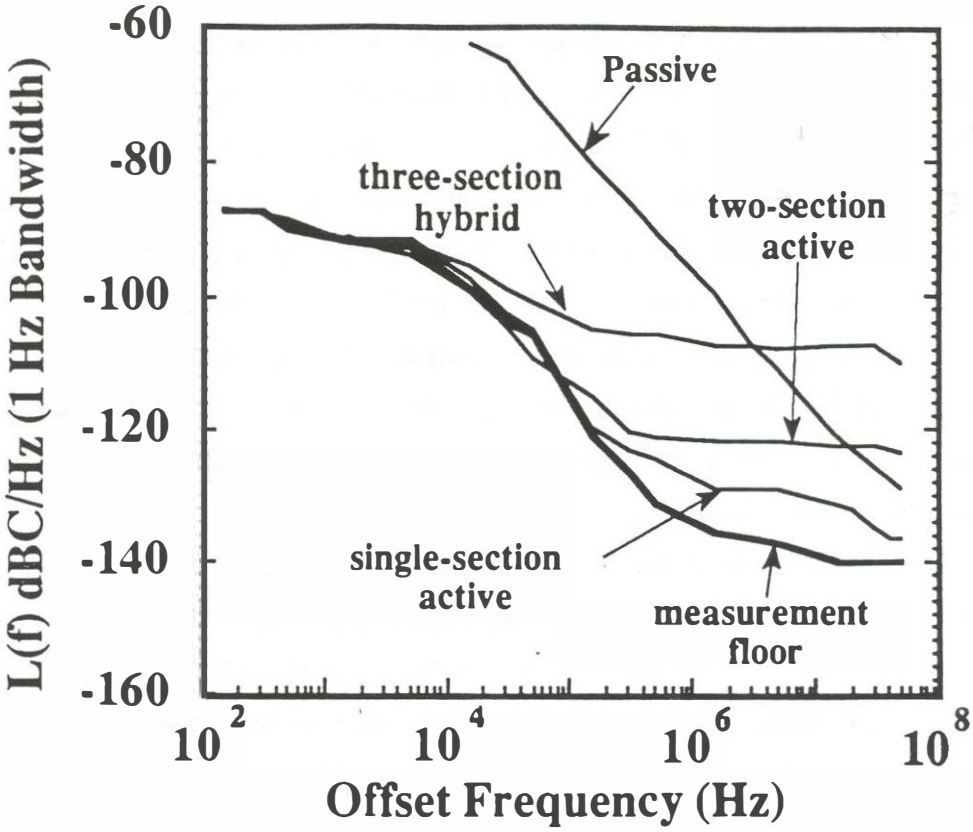

Case	r.m.s. jitter (150 Hz-50 MHz)
single section active	174 fs
two-section active	300 fs
three-section hybrid	1250 fs
two-section passive	5000 fs (15 kHz-50 MHz)

Figure 4.26 A comparison of the absolute phase noise from a (a) single-section active mode-locking (b) two-section active mode-locking (c) three-section active mode-locking and (d) two-section active mode-locking. The repetition rate for all of the experiments is 5 GHz. The material is the bulk active of Figure 2.27. The gain section length is 500 μm, the saturable absorber and gain modulation segment lengths are 16 μm. The electrical modulation signal is a 24 dBm sinusoid. The active gain modulation segment was not DC biased.

and g (monolithic cavity designs). These experiments include active, passive, and hybrid mode-locking experiments for both cavity types. The active region for all of the devices consists of 4 GaAs quantum wells (see Figure 2.27) with the lateral index guide formed by impurity induced disordering [50]. The monolithic cavity structure is 6.1 mm long with the top electrode divided into two short end segments and a long center section (see Figure 3.2). With all sections connected together, the device has a threshold of 115 mA and a single facet differential quantum efficiency of 4%. An 80 μm end segment is reverse biased for use as a saturable absorber, terminated in 50 Ω, and high-reflection coated. The 400 μm end segments in the monolithic cavity devices were modulated with a 24.5 dBm, 5.5 GHz sinusoid. The external cavity devices were cleaved from one of the monolithic devices. The single section external cavity laser has a threshold current of 13 mA with an output facet differential quantum efficiency of 10%. The saturable absorber length for the external cavity devices is also 80 μm.

Table 4.2 gives a summary of the bias conditions and the performance results for active, passive, and hybrid mode-locking of the monolithic and external cavity configurations. The average output power is held at 1 mW in all cases and the mode-locking frequency is nominally 5.5 GHz. The modulation frequency in the active and hybrid mode-locking cases is adjusted to give the shortest optical pulsewidths compatible with low amplitude noise and timing jitter. It is found that modulation frequencies slightly lower than those for minimum pulsewidth give the most stable results with higher modulation frequencies producing amplitude and timing instabilities [78]. In all cases the pulses have a large time-bandwidth product and frequency chirp. The excess bandwidth is due to self phase modulation of the pulses as the carrier density and index of refraction change during the pulse propagation [53] (also see Figure 4.19). Hybrid mode-locking produces the shortest pulsewidths of 6.5

ps and 2.5 ps, in the monolithic and external cavity cases respectively, due to the combined action of saturable absorption, saturable gain, and active gain modulation. The performance of the 7 mm long monolithic cavity device is degraded by the large amount of gain that is required to overcome the total loss of the device. For a waveguide loss of 7.5 cm^{-1}, a 7 mm long device must have a gain of 36,000 to over come the total loss of the device. For shorter devices, the waveguide loss is much smaller. The gain per unit length in these long monolithic cavity devices is also lower so that the ratio in differential gains between the saturable absorber and the gain region is smaller resulting in a smaller pulse shortening per pass (see section 5.3) and therefore a wider pulsewidth.

Figure 4.27 shows absolute L(f) for the active external and active monolithic cavity mode-locked lasers for the first three harmonics of the 5.5 GHz mode-locking frequency. Amplitude noise can be distinguished from phase noise by noting how the relative noise level changes with harmonic number for a constant offset frequency. The relative phase noise level will increase by 6 dB and 9.5 dB respectively for the second and third harmonic, whereas the relative amplitude noise level will remain constant with harmonic number. The floor curve shows the limitation of the measurement system due to the spectral purity of the modulation source and the local oscillator in the spectrum analyzer. The noise at offsets below 100 kHz is phase noise in nature and is dominated by the modulating source. Beyond 100 kHz, the noise from the monolithic cavity device becomes dominant and is phase noise in nature as is shown by the rising noise level with harmonic number. The absolute timing jitter for this case is 600 fs (150 Hz-50 MHz), with the dominant source of the jitter being the mode-locked laser. By drawing curves of decreasing proportionality to 1/f and noting which offset frequency ranges are intersected first it can be seen that the offset frequencies above 3 MHz dominate the timing

Table 4.2 Bias and performance comparison

Mode-Locking Technique	Saturable Absorber Bias Ia or V	Center Section Bias Ic(mA)	End Section Bias Ie, Prf	Pulse Width (ps)	Spectral Width (GHz)	Time/ Band-width Product
Active Monolithic	2.0 mA	126	12 mA 24.5 dBm	13	330	4.3
Passive Monolithic	-1 V	170	10 mA	10	400	4.0
Hybrid Monolithic	-1 V	160	10 mA 24.5 dBm	6.5	540	3.5
Active External	2.0 mA	——	18 mA 24.5 dBm	9	320	2.9
Passive External	-1 V	——	80 mA	2.5	720	1.8
Hybrid External	-IV	——	80 mA 24.5 dBm	2.7	800	2.2

Table 4.3 Comparison of timing jitter and intensity noise levels

Mode-Locking Technique	Absolute r.m.s timing jitter 150 Hz- 50 MHz	Residual r.m.s. timing jitter 150 Hz- 50 MHz	Relative Intensity Noise @ 100 MHz
Active Monolithic	600 fs	530 fs	-122 dB/Hz
Passive Monolithic	12.5 ps (150 kHz-50 MHz)	12.5 ps (150 kHz-50 MHz)	-116 dB/Hz
Hybrid Monolithic	1200 fs	1130 fs	-109 dB/Hz
Active External	240 fs	65 fs	<-126 dB/Hz
Passive External	12.2 ps (1.5 kHz- 50 MHz)	12.2 ps (1.5 kHz- 50 MHz)	-103 dB/Hz
Hybrid External	1060 fs	980 fs	-105 dB/Hz

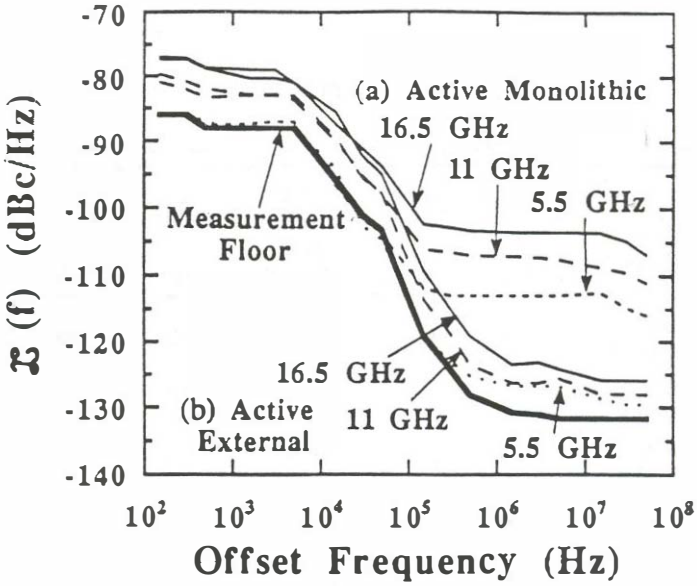

Figure 4.27 A comparison of the absolute phase noise of a single section actively mode-locked laser and a two-section monolithic cavity mode-locked laser. The repetition rate for both devices is 5.5 GHz. The noise added by the monolithic cavity device at offsets greater than 100 kHz is phase noise in nature. The noise added by the actively mode-locked external cavity device is mostly amplitude noise.

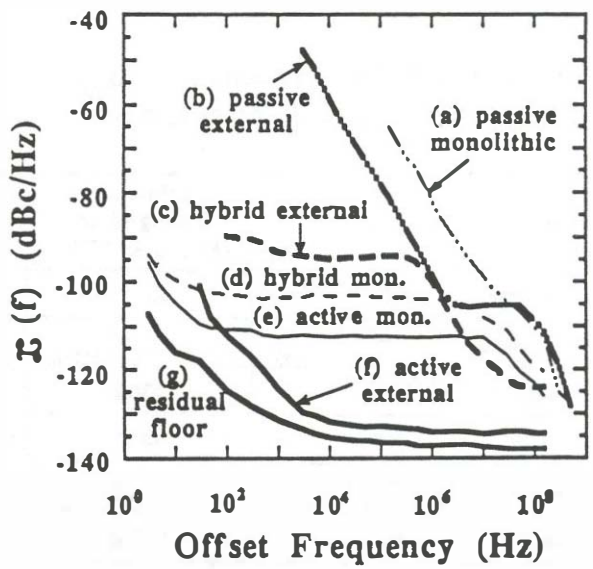

Figure 4.28 A comparison of the residual phase noise levels for (a) passive monolithic, (b) passive external, (c) hybrid external, (d) hybrid monolithic (e) active monolithic, (f) active external and (g) the measurement noise floor. The bias conditions are described in Table 4.2 and the calculated timing jitter levels are shown in Table 4.3. The residual floor level is established by bypassing the mode-locked laser.

jitter fluctuations in the monolithic cavity case. Figure 4.27 shows that the active mode-locked external cavity laser starts to add noise at offsets larger than 300 kHz. This contribution is amplitude noise because its relative level remains constant with harmonic number. The absolute timing jitter in the single section external cavity case is less than 240 fs and is dominated by the modulation source. Figure 4.27 illustrates that monolithic cavity mode-locked lasers with all-active waveguides have significantly higher jitter than their external cavity counterparts. Timing jitter introduced by active and hybrid mode-locked lasers is a result of a gain jitter to timing jitter conversion process (see Chapter 6).

Figure 4.28 compares the residual phase noise of the hybrid and active mode-locked devices and the absolute noise of the passive mode-locked devices. This plot compares the noise contribution of the laser only, independent of modulation sources. Table 4.3 lists the timing jitter results and intensity noise levels for the six experiments.

The active mode-locked monolithic and external cavity devices differ in the length and carrier density of the active waveguide in the cavity. Carrier density fluctuations modulate the round trip delay time for the optical pulses (see Chapter 6). The delay variations for the monolithic cavity device are larger because of the longer active waveguide length in the cavity. Noise with 1/f slope is observed in the output of the mode-locked lasers at low offset frequencies and the noise contribution from the laser falls off above the relaxation resonance frequencies.

Passive mode-locked lasers have the highest timing jitter levels due to the absence of a high stability driving source. The jitter in passive mode-locked lasers is causes by a gain to repetition rate conversion process (see Chapter 6). Because of the 20 dB/decade L(f) roll-off, the timing jitter will be dominated by the phase noise at low offset frequencies.

For either the monolithic or external cavity case, Figure 4.28 shows that hybrid mode-locking gives a higher noise level than active mode-locking. The

residual timing jitter of the hybrid mode-locked external and monolithic cavity devices is 980 fs and 1100 fs respectively, and is laser dominated. When the absorber section is reverse-biased, the gain segment carrier density level must be substantially increased to overcome the loss of the saturable absorber. This carrier density rise is especially high in the external cavity case where all of the extra gain must be made up in a relatively short gain length. For the external case, the pumping current was increased from 18 mA to 80 mA. The higher carrier density level and decreased carrier recombination lifetimes cause increased spontaneous emission levels in the external cavity devices but the shorter active waveguide length reduces the contribution to phase noise and timing jitter. The larger carrier density level in the gain region helps the saturable absorption process by lowering the differential gain but at the price of higher timing jitter levels. Short optical pulses are more susceptible to timing jitter fluctuations than wide optical pulsewidths. Short optical pulses have a wider optical spectrum and more spontaneous emission noise coupled into the lasing longitudinal modes. Short optical pulses are also less efficiently confined in time by the active gain modulation.

The noise output from a gain-switched laser does not have the cavity filtering effects which the mode-locked semiconductor lasers have. Gain-switched and Q-switched lasers produce intensity and phase noise which spans from DC to the relaxation resonance frequency of the laser (e.g. 10 GHz). In mode-locked lasers, the intensity and phase noise is filtered by the optical cavity between the harmonics of the mode-locking frequencies. The mode-locked devices that give the lowest values of timing jitter give the lowest value of intensity noise. This is reasonable since the spontaneous emission noise levels in the cavity are the fundamental causes for both amplitude and phase noise.

In summary, it is shown that the monolithic cavity devices with active waveguides have larger timing jitter compared to external cavity devices of the

same repetition rate. For either monolithic or external cavity devices, active mode-locking gives the lowest jitter level, followed by hybrid and passive mode-locking. This larger timing jitter in monolithic cavity devices is partially due to index of refraction and gain variations occurring along the entire cavity length compared to a small fraction of the cavity length in the external cavity case. Hybrid mode-locked devices have higher timing jitter levels than active mode-locked semiconductor lasers due to the higher lasing thresholds that are associated with the added losses of the saturable absorber. Mode-locked lasers with short optical pulsewidths produce higher timing jitter levels than lasers with wide optical pulsewidths. Passive mode-locked lasers have the largest timing jitter levels due to the fact that they are free running oscillators with relatively low device Q.

4.6 Self-pulsation effects

Mode-locked lasers are also susceptible to large amplitude and timing jitter instabilities if the low frequency resonance response is not highly damped [80,81]. This instability can be seen in active mode-locked lasers when the modulation frequency is tuned to a higher frequency than the natural resonance frequency of the cavity [78] and has been illustrated in Figure 4.19 and 4.20.

Active mode-locked two section lasers with reverse-biased gain modulation segments are more susceptible than single section designs. Passive and hybrid mode-locked lasers are particularly susceptible to a pulse instability. The positive feedback of the saturable absorber reduces damping. Lasers with saturable absorbers of very high initial loss are more susceptible to self-pulsations. As an example, a monolithic SCPM cavity mode-locked lasers with 40 GHz nominal repetition rate and varying saturable absorber lengths were tested for susceptibility to self-pulsations. The SCPM device with an 80μm

long saturable absorber did not mode-lock for any bias and only exhibited self-pulsations. A device with 37 μm long saturable absorber was found to give wide regions of mode-locking operation without self pulsation effects. Figure 4.29 shows a stability map versus bias conditions for the 37 μm long saturable SCPM case of absorber case of Figure 3.8b. Figure 4.30 shows a stability map versus bias conditions for the 50 μm long saturable absorber CPM case of Figure 3.8a and 3.15. Both devices display wide regions in which the mode-locked laser operates well. The higher energy regions of the CPM device show poor mode-suppression and poor contrast ratio at high output power though (see Chapter 3.2).

For small negative saturable absorber voltages, the device tends to operate in the self-pulsation mode-of operation. The self-pulsation mode of operation is illustrated in Figure 5.13. The self-pulsation frequency is typically 1-3 GHz. The self-pulsation is most easily observed with a spectrum analyzer with a photodiode input. The self-pulsation amplitude can be very large, with a 100 % modulation depth. The harmonic content drops off very quickly showing that the self-pulsation is more sinusoidal than pulse-like. The self-pulsation is more prevalent at low saturable absorber bias voltages The self-pulsation frequency is found to increase with the drive current to the device. The instability problem is also found to increase with the repetition rate of the laser and with the length of the saturable absorber. Monolithic cavity 4 quantum well devices with 80 μm saturable absorbers were tested for several over-all device lengths. The 7 mm device (5.5 GHz rep rate) showed wide regions of mode-locking, the 3.5 mm long device produced a narrower region of mode-locked operation, and a 1.6 mm device failed to mode-lock and only produced self-pulsation conditions.

In summary, self-pulsation is an undesirable mode of operation that competes with the mode-locking condition. Self-pulsation effects are especially prevalent in devices that have a reverse-biased segment. Self pulsation effects are larger for very long saturable absorber lengths and for higher repetition

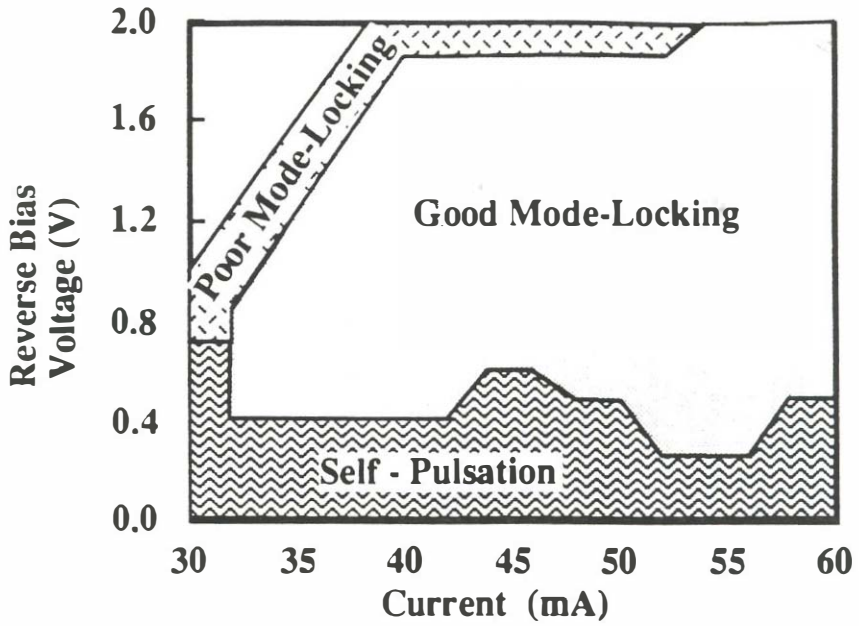

Figure 4.29 The measured stability regions for the SCPM passive mode-locked laser of Figure 2.8b. The device length is 1.2 mm (36 GHz repetition rate) with a saturable absorber length of 37 μm.

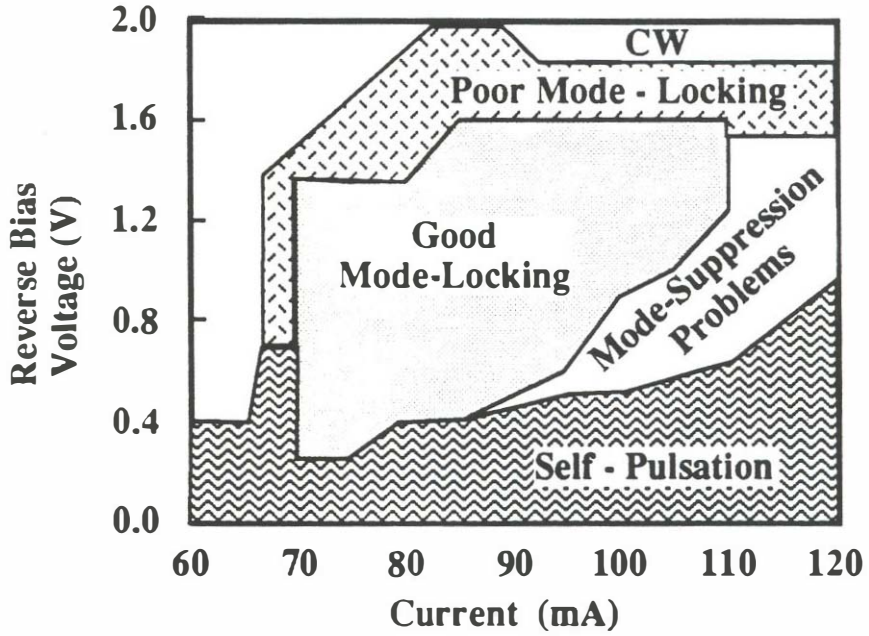

Figure 4.30 The measured stability regions for the CPM passive mode-locked laser of Figure 2.8a. The device length is 2 mm (42 GHz repetition rate) with a saturable absorber length of 50 μm.

rates.

Chapter 5
Optimization of multi-segment mode-locked semiconductor laser designs

5.1 Introduction and design variables

The multi-section lasers outlined in sections 2-4 have produced short optical pulses in a simple structure where the gain section, saturable absorber segment, modulation segment, and tuning segment can all be fabricated together in a single integrated process. In this Chapter, a theoretical analysis is performed to understand how to optimize these structures. The theoretical analysis will help explain the trends that were found in the experimental Chapters 2-4. The variables that the designer has under his control are shown in Figure 5.1 and are explained below.

5.1.1 Segment length and segment location

Figure 5.1 shows an example of the segments and functionality that are useful in mode-locked semiconductor lasers. They are the saturable absorber, gain modulation, gain, and waveguide segments. The repetition rate tuning, delay, and wavelength control segments are also shown in Figure 4.1 but are not analyzed in this chapter. This chapter focuses on the length and the position of the saturable absorber, gain modulation, and the gain segments. Wavelength control filters will be discussed only for external cavity experiments using diffraction gratings. Monolithic cavity devices with integrated Bragg reflectors were not fabricated in this work.

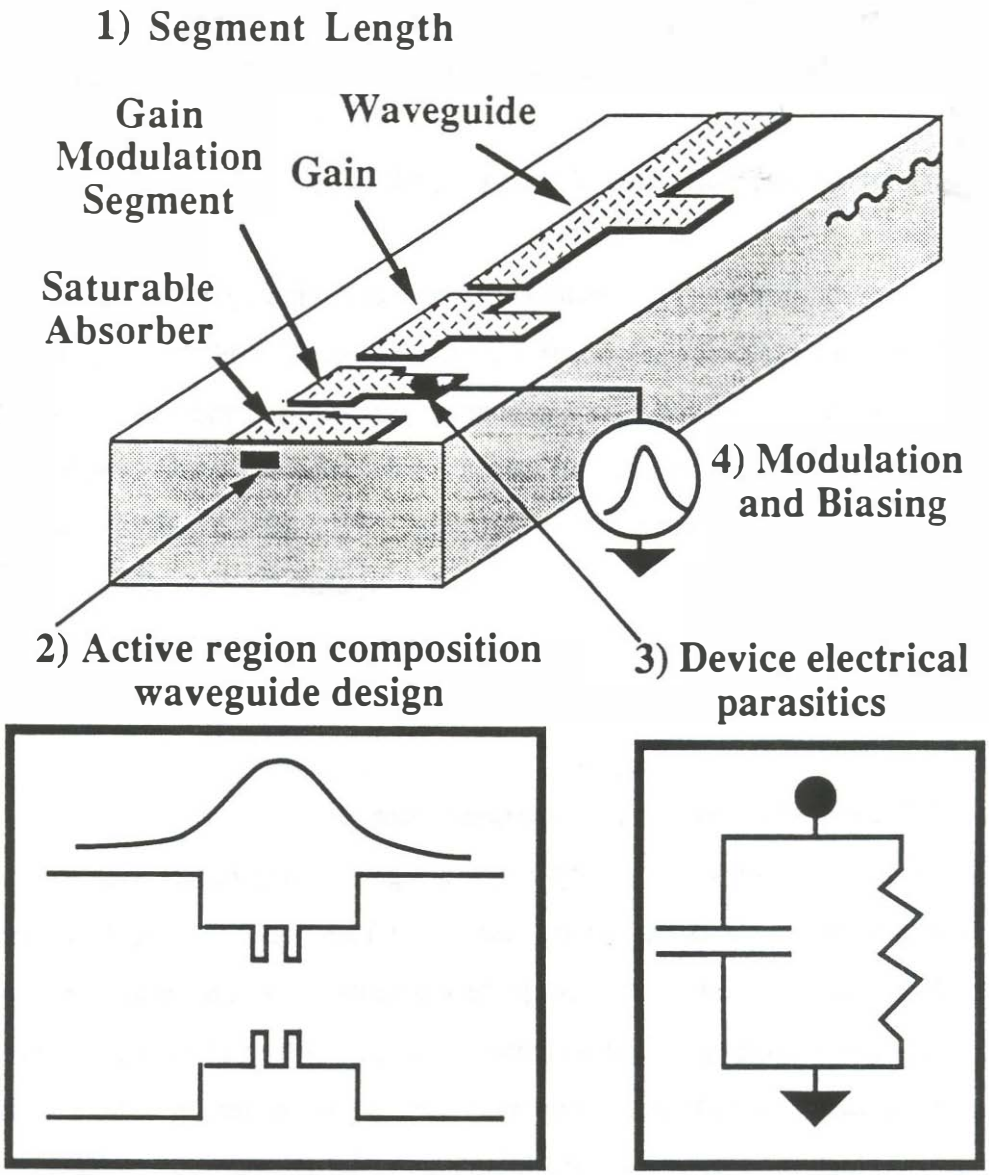

Figure 5.1 The items that an engineer has at his control when designing a multi-segment mode-locked semiconductor laser. (1) The segment length and position. (2) The active region composition and waveguide design. (3) The electrical parasitics of the structure. (4) The electrical active gain modulation signal.

5.1.2 Active region composition and waveguiding

Many choices are available for the design of the active region composition. Semiconductor laser research has focussed on optimization for high-speed or low-threshold design. Very little research has been done on optimization of a laser structure for mode-locked laser operation. The active region can consist of a bulk active region or a quantum well active region. For quantum well lasers, the number of design variables increases very rapidly since the number of quantum wells, well depth, well thickness, barrier thickness, separate confinement width, and optical confinement factor may all be varied. In addition, the quantum wells may also be lattice matched to the barriers or strained in order to induce changes in the energy band structure. In this chapter, guidelines are presented to show the directions that produce better mode-locked laser performance.

5.1.3 Device electrical parasitics

The electrical parasitics of the various segments are important in mode-locked laser design. For gain modulation segments, the parallel resistive-capacitance low pass corner frequency (see Figure 5.1) often determines how fast one can modulate the gain. There is no advantage to actively gain modulating a segment with a 20 ps electrical pulse if the segment low-pass cut-off frequency is only 2 GHz. When passive and hybrid mode-locking techniques involving a saturable absorber are used, larger parasitics can be tolerated (especially in the saturable absorber segment) while still generating short optical pulses.

5.1.4 Modulation Signals and Biasing

The width and amplitude of the electrical gain modulation pulses are important factors in determining the achievable pulsewidth and the stability of the mode-locked laser. In general, it is found that the narrower the pulsewidth and the larger the amplitude (the amplitude must not heat the segment excessively though), the better the performance. The trend is not linear though and this chapter shows that there are diminishing returns for narrowing the width and increasing the amplitude of the modulation pulse. The reverse bias on a saturable absorber also highly influences the performance of the mode-locked laser. Larger reverse biases can decrease the carrier sweep out time in the segment and also red-shift the band edge due to the Franz-Keldysh and quantum-confined Stark effects.

5.1.5 Outline of Chapter 5

With these variables as free design parameters, this chapter will outline the trade-offs involved in getting the best device performance.

The bandwidth potential of semiconductor lasers is very large. The bandwidth potential of the semiconductor laser medium is illustrated in Figure 5.2. Reverse biasing one segment of a two segment laser stops lasing action due to the formation of an optical termination at one facet. The reverse biased optical termination has a power reflection coefficient of less than 10^{-4}. The forward-biased segment amplifies the spontaneous emission and a superluminescent LED is formed. Figure 5.2 shows the spontaneous emission output from a four quantum well 1.55 μm laser for a bias current of 100 mA in a 1 mm amplifier length. If the noise figure versus frequency of the laser is

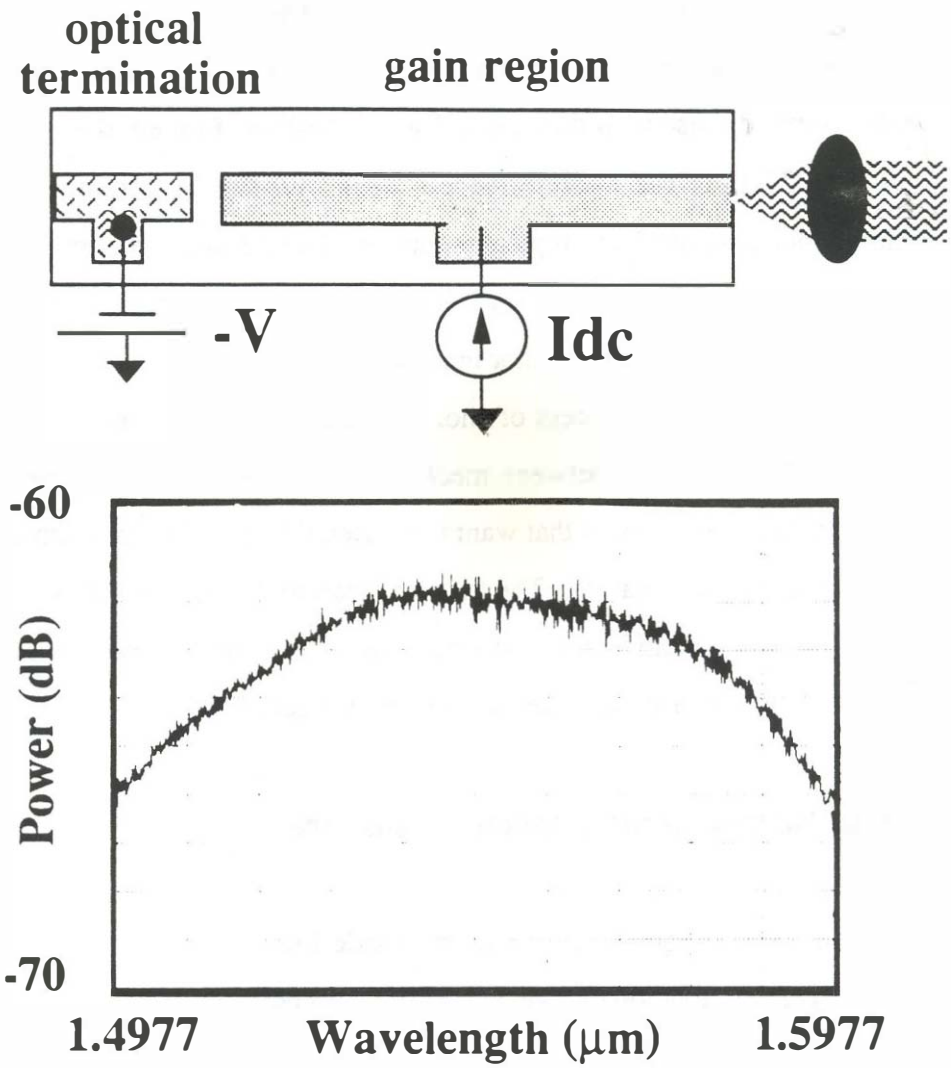

Figure 5.2 The spontaneous emission output of a superluminescent light emitting diode (SLED). The SLED is formed by breaking the pumping contact into two segments. One segment is reverse-biased to form an optical termination with a reflection coefficient below 10^{-4}. The long segment is forward biased to produce gain and amplified spontaneous emission output. If the noise figure is assumed to be constant versus frequency, the spontaneous emission output is a measure of the gain bandwidth. This figure is designed to demonstrate that very large bandwidths (in this case 80 nm) are possible in semiconductor laser amplifiers.

assumed to be constant with wavelength, the gain width for this laser would be 90 nm. This corresponds to a bandwidth of 16 THz. If a time-bandwidth product limited pulse with this spectral width could be formed, the pulsewidth would be 27 fs. In the experimental work outlined in Sections 2-4, the achieved pulse widths were typically between 1 and 3 ps for the multi-section devices. This chapter explains why it is very difficult to directly achieve a 27 fs pulse without pulse compression or intra-cavity phase filters.

In this chapter, the process of short pulse generation will be described in terms of the competition between mechanisms that want to widen the optical pulsewidth and mechanisms that want to shorten the optical pulsewidth on each pass through the laser cavity. The final solution to the pulsewidth is achieved when the pulse widening mechanisms equilibrate with the pulse narrowing mechanisms so that a steady state pulsewidth is reached.

The pulse shortening mechanisms are:

1) Saturable absorption (passive or hybrid mode-locking).

2) Active gain modulation (active or hybrid mode-locking).

The pulse widening mechanisms are:

1) The gain response (magnitude and phase) versus frequency of the laser. Pulsewidth reduction can possibly occur for certain input pulsewidths and chirp signs.

2) Saturable gain.

3) Self-phase modulation due to saturable gain, saturable absorption, and active

gain modulation.

4) Dispersion in the cavity. This can be glass in the optical components or waveguide dispersion.

5) Intentionally added wavelength filters such as etalons, diffraction gratings, prisms, birefringent tuning filters, or Gires-Tournois interferometers.

6) Spontaneous emission noise.

The goal of mode-locking is to be limited only by the gain response of the laser. The most important pulse narrowing mechanism will be shown to be saturable absorption. The most important pulse broadening mechanisms will be shown to be the gain response versus frequency combined with self-phase modulation.

Chapter 5 starts out with a discussion of the model that is used to analyze mode-locked semiconductor laser characteristics. The discussion then concentrates on the pulse narrowing mechanisms of passive gain modulation and active gain modulation in Sections 5.3 and 5.4. Section 5.5 discusses the effects that cause frequency chirp in mode-locked lasers by self-phase modulation. The pulse broadening effects in semiconductor laser amplifiers are then discussed in Section 5.6. Section 5.7 concentrates on the active region design. Section 5.8 discusses the limitations on the achievable pulsewidth in mode-locked semiconductor lasers. Section 5.8 combines the information presented in Sections 5.1-5.7 and discusses the strengths of the various pulse shortening and widening mechanisms and how they interact to limit the achievable pulsewidth from multi-section mode-locked semiconductor lasers.

5.2 Simplified model for multi-section mode-locked lasers

The rate equations similar to those formulated by Agrawal and Olsson [53] are used to analyze the mode-locked laser structures of Chapters 2-4. This rate equation formulation is as follows:

$$\frac{\partial A}{\partial z} + \frac{1}{v_g}\frac{\partial A}{\partial t} = \frac{-i\beta_2}{2}\frac{\partial^2 A}{\partial t^2} - \frac{\alpha_{int} A}{2} + \frac{(1-i\alpha) g_p A}{2} + \frac{g_p t_2^2}{2}\frac{\partial^2 A}{\partial t^2} \tag{5.1}$$

$$\frac{\partial g_p}{\partial t} = \frac{g_{goal} - g_p}{\tau_c} - \frac{g_p |A|^2}{E_{sat}} \tag{5.2}$$

$$g_p = \Gamma_t a (n - n_{tr}) \tag{5.3}$$

$$E_{sat} = \frac{h \omega_o w_a h_a}{a \Gamma_t} \tag{5.4}$$

$$g_{goal} = \Gamma_t a n_{tr} \left(I/I_0 - 1 \right) \tag{5.5}$$

$$I_o = \frac{q V n_{tr}}{\tau_c} \tag{5.6}$$

where A is the complex electric field normalized so that the magnitude squared

is optical power, z is the distance coordinate, v_g is the group velocity in the material, t is the time coordinate, β_2 is the material dispersion coefficient of the medium, α_{int} is the internal loss of the waveguide, α is the linewidth enhancement factor, g_p is the peak gain of the laser medium, t_2 is the optical bandwidth parameter of the laser medium (typically 0.1 ps), g_{goal} is the maximum gain that is achievable for a given pump rate, E_{sat} is the saturation energy of a semiconductor laser (typically 1-20 pJ), τ_c is the carrier lifetime in the material, Γ_t is the transverse optical confinement factor (typically 0.02 (single quantum well) to 0.3 (bulk active)), a is the differential gain with respect to carrier density (at a particular wavelength), n_{tr} is the carrier density at transparency, I is the injected current value, I_0 is the current injection value necessary for transparency, w_a is the width of the active region (typically 1-4 μm), h_a is the height of the active region (typically 0.1-0.15 μm for bulk active region lasers), h is Planck's constant, and ω is the optical frequency.

Equation 5.1 is the equation that keeps track of the field value and the interactions with the carriers. The material dispersion term (the term containing β_2) will not be ignored in this analysis (as has been done by many authors) because it is found to have a significant effect on determining the achievable pulsewidth. Equation 5.2 keeps track of the gain level and carrier density level in the laser and its interaction with the electric field.

The saturation energy, E_{sat}, is a very important parameter in a semiconductor laser. It is a measure of the energy that it takes to saturate the gain medium or the energy it takes to saturate the saturable absorber. Figure 5.3 illustrates the parameters that go into making up the saturation energy of a laser. The saturation energy is directly proportional to the mode-cross sectional area of the laser. This would imply that devices with weak confinement and

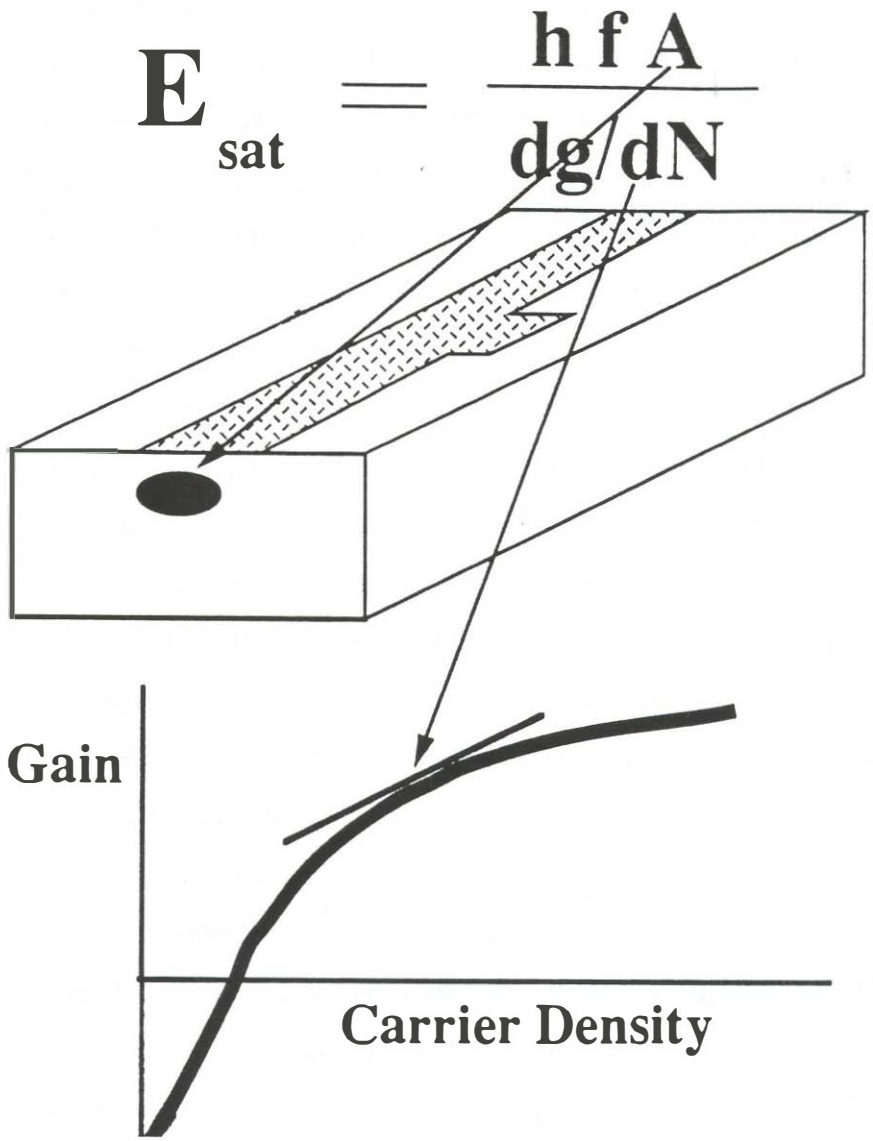

Figure 5.3 This is a graphic illustration of the saturation energy of a semiconductor laser amplifier or saturable absorber. The saturation energy is directly proportional to the area of the optical mode. Thus lightly confined modes or gain-guided structures should have larger saturation energies. The saturation energy is inversely proportional to the differential gain. Semiconductor lasers show a decreasing differential gain with increasing carrier density. The sublinear slope is of critical importance in passive mode-locking.

wide active region widths should deliver higher energy pulses. The saturation energy is inversely proportional to the slope of the gain with respect to carrier density. Carriers must be removed from the active region in order to achieve amplification. The gain drop due to the removal of a fixed number of carriers will be much larger for high differential gain amplifiers compared with low differential gain amplifiers. Thus low differential gain leads to a higher saturation energy. The differential gain is carrier density dependent. The saturation energy for low carrier density levels is much smaller than that for high carrier density levels due to the sublinear slope of the gain versus carrier density curve. Since a saturable absorber always operates below transparency carrier density level, it will have a lower saturation energy than an optical amplifier.

Equation 5.1 takes into account the finite gain bandwidth of the laser via the t_2 parameter with the frequency domain expression for the magnitude response of the gain as follows:

$$\tilde{g}(\omega) = g_p\left[1-t_2^2(\omega-\omega_0)^2\right] \tag{5.7}$$

where ω_o is the center frequency of the gain peak. Normally the peak gain frequency moves with carrier density, but this fact is ignored in the model.

Coupled Equations 5.1 - 5.2 could be solved numerically using Runge-Kutta solution methods as was done in Reference 82. This procedure is not followed in this chapter because it is desired to separately look at the individual pulse broadening and pulse narrowing mechanisms that are contained within these equations. The Runge-Kutta solution method was also found to require very small step size (10 fs) and considerable computer time to achieve a

consistent answer [82].

The solution method in this chapter follows in spirit that of Roger Helkey's partial integration method [43] but instead uses the rate equation solutions found in Agrawal and Olsson [53]. Agrawal and Olsson present an analytic solution to Equation 5.1 and 5.2 under the condition that $t_2=0$ (infinite gain bandwidth), that noise terms are neglected (notice that noise terms are not even given in 5.1-5.6), amplification is unidirectional, and that the pulsewidth is much shorter than the carrier lifetime, τ_c. The input-output relationships for a semiconductor laser amplifier under these conditions can then be analytically solved to give the following solution:

$$P_{out}(\tau) = \frac{P_{in}(\tau)}{1-\left(1-{}^{1}\!/_{G_o}\right)\exp\left({}^{-U_{in}(\tau)}\!/_{E_{sat}}\right)} \tag{5.8}$$

$$\phi_{out}(\tau) = \phi_{in}(\tau) + \frac{\alpha}{2}\ln\left[1-\left(\frac{1}{G_o}\right)\exp\left(\frac{-U_{in}(\tau)}{E_{sat}}\right)\right] \tag{5.9}$$

$$U_{in}(\tau) = \int_{-\infty}^{\tau} P_{in}(\tau')\,d\tau' \tag{5.10}$$

$$G_0 = e^{h_{eff}} \tag{5.11}$$

$$h_{eff}(\tau) = \int_0^L g_p(z,\tau)\,dz \tag{5.12}$$

where G_0 is the gain found in the laser amplifier just before the propagation of the input pulse, h is the total gain integrated along the length of the laser, U_{in} is the fraction of the pulse energy contained in the leading part of the pulse to τ, $P_{in}(\tau)$ is the input power with respect to time, $P_{out}(\tau)$ is the output power with respect to time, $\phi_{in}(\tau)$ is the input phase with respect to time, $\phi_{out}(\tau)$ is the output phase with respect to time, τ is the time measured with respect to the center of the pulse in a coordinate system that travels at the group velocity of the laser pulse, and L is the device length.

Rate equation 5.1 can also be solved under a different set of approximations in which the assumptions are that g_p does not change during the propagation of the pulse (in other words, it does not include gain saturation effects). This approximation does include the effects of a finite gain bandwidth ($t_2>0$) in the laser which were not included in the previous approximations (Equations 5.8-5.12). The solution is obtained by Fourier transform methods and is given by:

$$A_{out}(\tau) = F^{-1}\left[\tilde{A}_{in}(\omega)\exp\left(\frac{-\omega^2 t_2^2 g' L}{2}\right)\exp\left(\frac{i\beta_2 L\omega^2}{2}\right)\right] \tag{5.13}$$

where $A_{out}(\tau)$ is the normalized output electric field with respect to time, $A_{in}(\tau)$ is the normalized input electric field with respect to time. (square root of power), $A_{in}(\omega)$ is the Fourier transform of the input pulse, and F^{-1} is the inverse Fourier transform.

Equation 5.13 illustrates the filtering qualities of the gain medium. The magnitude and phase effects are separated out in this expression. β_2 is the group velocity dispersion parameter. For a symmetrical lorentian lineshape, β_2

would be zero at the gain maximum and maximum at the 3 dB down points of the filter. Actual semiconductor line-shapes have an asymmetrical gain shape and display a group velocity dispersion at the gain maximum. A typical value for β_2 at gain maximum for a semiconductor laser is given as $\beta_2 = g_p t_2^2$.

Much like the an electrical bandpass filter has a gain and phase response, so does a semiconductor laser. In filter theory, the input waveform can be convolved with the impulse response of the circuit to obtain the output waveform. In the frequency domain, the Fourier transform of the input pulse can be multiplied by the magnitude and phase response of the filter to obtain the output in the Frequency domain. The output in the time domain is that found by inverse Fourier transforms. Equation 5.13 represents the same type of filter analysis where the filter in this case is the semiconductor laser amplifier. The gain and phase response of a semiconductor laser amplifier with Lorentzian gain shape are illustrated in Figure 5.4.

The actual shape of the gain versus frequency curve may deviate substantially from a Lorentzian shape in actual semiconductor laser amplifiers. The deviation can be especially large for the high frequency side of the gain peak in quantum well lasers. The model fits better for bulk active region devices. A more complicated gain shape model can be incorporated by including higher order terms in the expression for the gain versus frequency function (Equation 5.13). Equations similar to 5.13 can still be found analytically using Fourier solution techniques. Only parabolic gain shapes and Lorentzian gain shapes have been used in the modelling of Chapter 5.

A very important parameter to notice in Equation 5.1 is the linewidth enhancement factor. The linewidth enhancement factor is a number that controls the coupling between changes in gain to changes in the index of

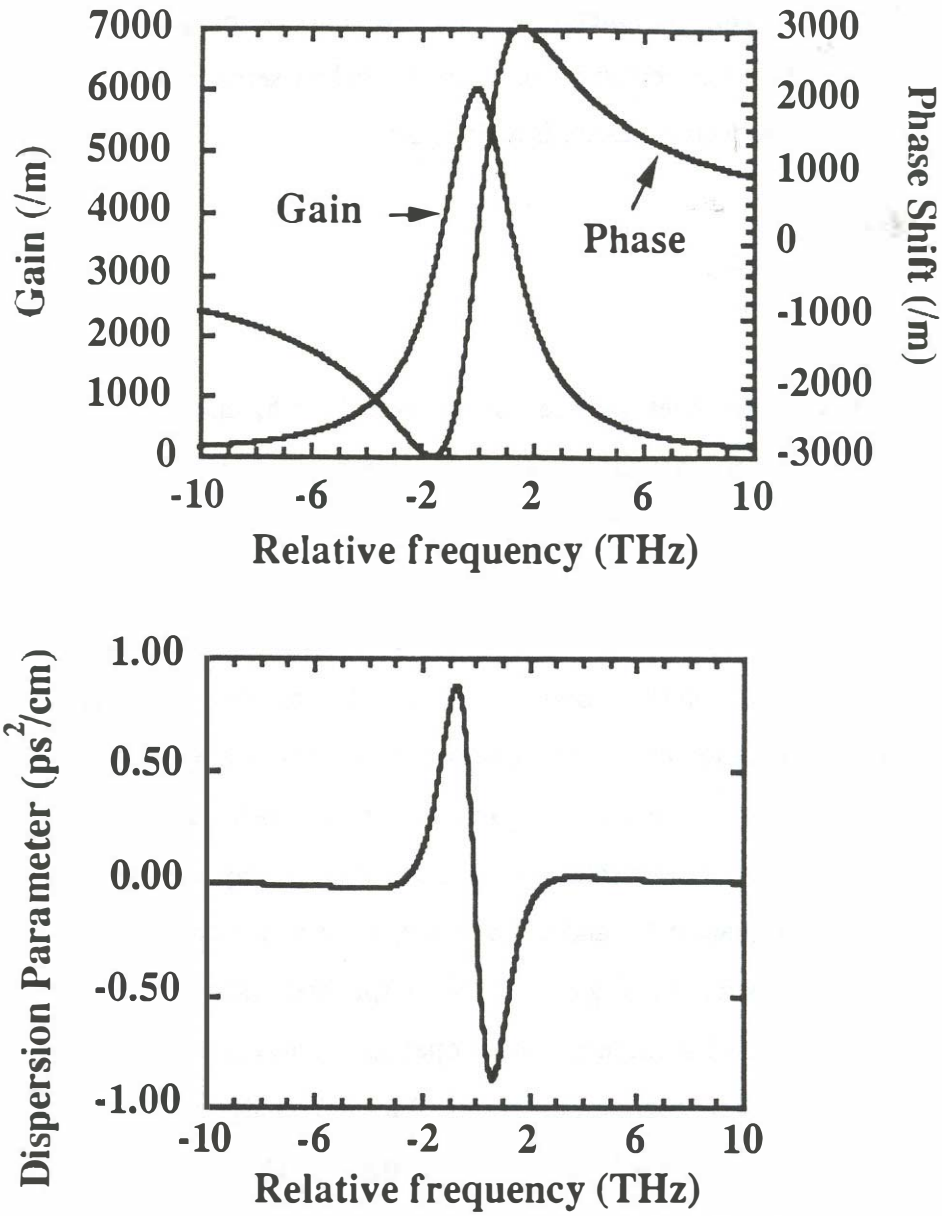

Figure 5.4 A Lorentzian lineshape model showing the magnitude and phase response versus frequency separately. Also included is the group velocity dispersion parameter which is the second derivative of the phase with respect to frequency. The Lorentzian model has zero dispersion at the gain maximum. This is not really the case for semiconductor laser amplifiers since the gain is not symmetrical around the gain peak. An alternative model which is also used in this chapter is to model the dispersion parameter as a frequency independent parameter (this implies a parabolic phase response).

refraction. This parameter will be found to be of great importance in understanding the performance of mode-locked semiconductor lasers. The linewidth enhancement factor is defined as:

$$\alpha = 2\, k_0 \frac{dn_{in}/dn}{dg/dn} \tag{5.14}$$

where k_o is 2π over the free space wavelength, and n_{in} is the index of refraction. Note that in this work the sign of α is chosen to be positive in semiconductor lasers following the convention of Agrawal (this is not a common usage).

The first analytic solutions handled the cases of infinite laser bandwidth with gain saturation (Equations 5.8-5.12) and therefore includes all of the non-linear amplification effects in the semiconductor laser amplifier. The case of a finite gain bandwidth without gain saturation non-linearities is included in Equation 5.13. The two solutions can be used iteratively to approximate the full solution of Equation 5.1 and 5.2 by the split-step method [83]. The split-step method is illustrated in Figure 5.5. In the split step method, the laser amplifier is split into small segments. The propagation through each small segment is then done in two separate operations. First the analytic solution to the non-linearity (Equations 5.8-5.12) is used to model the gain saturation that occurs in semiconductor laser amplifiers and saturable absorbers. Next, the effects of the finite gain bandwidth are included. The magnitude response filters the pulse and the phase response provides group velocity dispersion. Since both solutions (Equations 5.8-5.12 and 5.13) are analytic under their given assumptions, larger segment lengths are possible than what would be used for

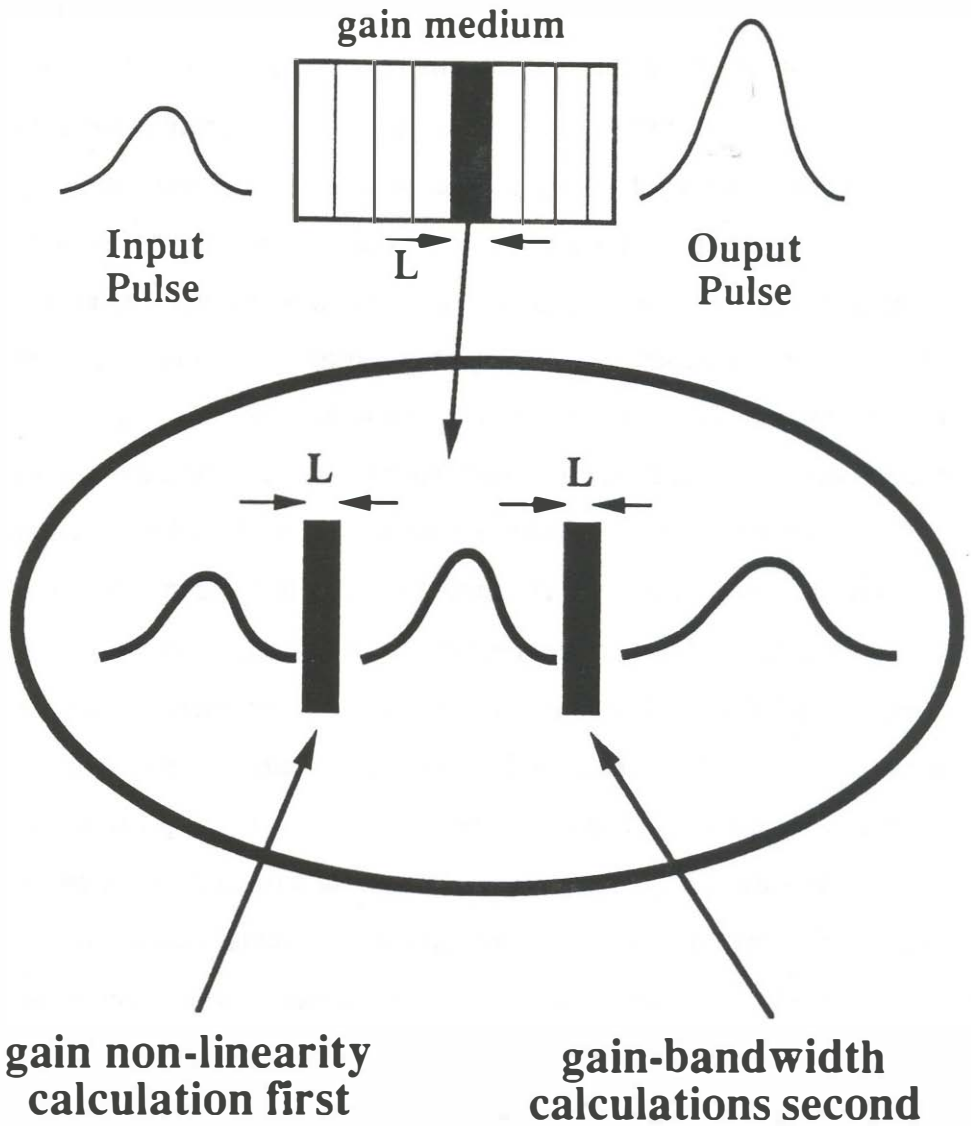

Figure 5.5 The two-step analysis model used for analysis. The laser is first broken up into small segments. Then each small segment is operated on twice. First the gain non-linearities are calculated on the first pass. On the second pass, the effects of the gain bandwidth are included. In the actual situation the gain-nonlinearity and the gain-bandwidth are occurring simultaneously. If the segment length is small enough, the separation of the two functions becomes a good approximation.

direct solution of Equations 5.1 and 5.2 by Runge-Kutta techniques. Equation 5.1 simultaneously treats the effects of the non-linearity and bandwidth effects. The segment lengths should be kept small, especially in situations when the pulse energy approaches that of the saturation energy. There is some question as to the correct value of gain to choose for the gain in expression of Equation 5.13 since the gain is constantly changing versus time during the pulse propagation through the small segment. The chosen value is the gain that the peak of the pulse experiences during propagation through the small segment. This represents an average value of the gain with the leading edge of the pulse experiencing higher and the trailing edge of the pulse experiencing lower gain.

The device model used to analyze multi-section mode-locked semiconductor lasers is shown in Figure 5.6 The model shows a three-section laser in which the first segment is the gain section, the second section is the gain modulation segment, and the third segment is the saturable absorber. In the two-step method, each of these functional segments are in turn broken up into smaller segments for analysis. The model assumes unidirectional pulse propagation through the small analysis segments. The use of a unidirectional propagation model in the small segments does not represent the actual situation of the linear cavity mode-locked laser devices studied in chapters 2-4 in which pulses may be travelling in both directions in the analysis segments. For short optical pulses, this problem arises only near the laser facets where the pulses collide with their reflections off of the output facets. For most of the experiments performed in chapters 2-4, cleaved facets were used representing a 30% power reflection coefficient. This small value of reflection coating makes one wave direction dominate the depletion of gain and makes the unidirectional assumption more accurate. Internal waveguide losses are accounted for in the

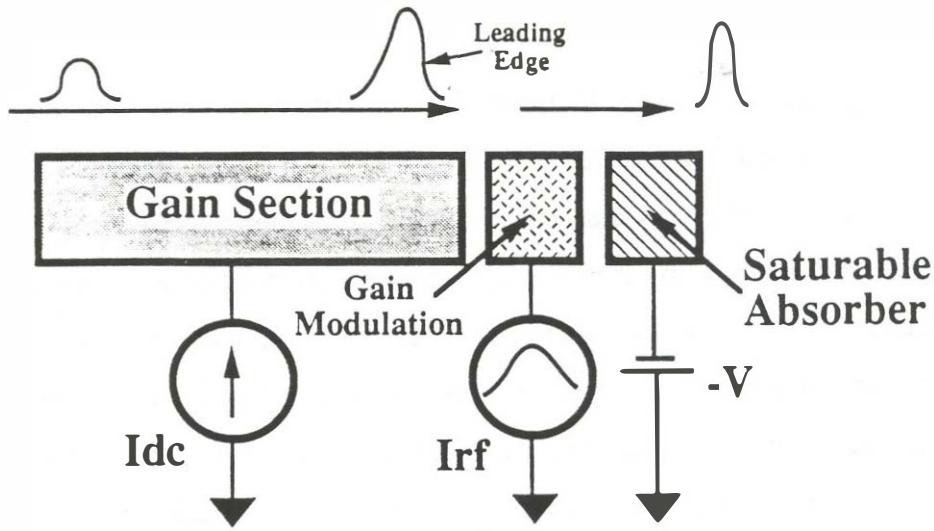

Figure 5.6 The three-section model used for analyzing multi-section mode-locked semiconductor lasers. The three segments are the gain segment, the gain modulation segment, and the saturable absorber.

model by discrete losses at the end of every analysis segment.

5.3 Pulse shortening in waveguide saturable absorbers

E_{sat} was introduced in Chapter 5.2 as a parameter that measures the amount of energy it takes to saturate an optical amplifier. E_{sat} also represents a measure of the amount of energy that it takes to saturate a saturable absorber. Figure 5.7 illustrates more clearly the saturation energy effects for optical amplifiers and saturable absorbers. The energy gain versus the input energy divided by the saturation energy of the segment is shown. The calculations are done using a gaussian input pulse shape and using Equation 5.8 to calculate the input-output pulse relationships. For an optical amplifier, the gain starts to drop from its unsaturated value when the output energy from the amplifier approaches the saturation energy. For the saturable absorber, the input energy necessary to bleach the saturable absorber is on the order of 3 to 20 times the saturation energy of the segment depending on the segment length. For good passive mode-locking, it is important to have a larger saturation energy in the amplifier than in the saturable absorber [18]. This requirement of saturation energies can be understood intuitively. It takes 3-20 times the saturation energy of the absorber to cause bleaching. The amplifier output power can only provide energies near its saturation energy. For an amplifier to bleaching the saturable absorber, its saturation energy must be several times larger than that of the saturable absorber. This ratio of saturation energies between the gain and saturable absorber segments is a parameter that the designer can control. Figure 5.8 shows a calculated gain versus carrier density plot for a 0.83 μm GaAs quantum well laser with a 10 nm well width and $Al_{.4}Ga_{.6}As$ barriers (the plot

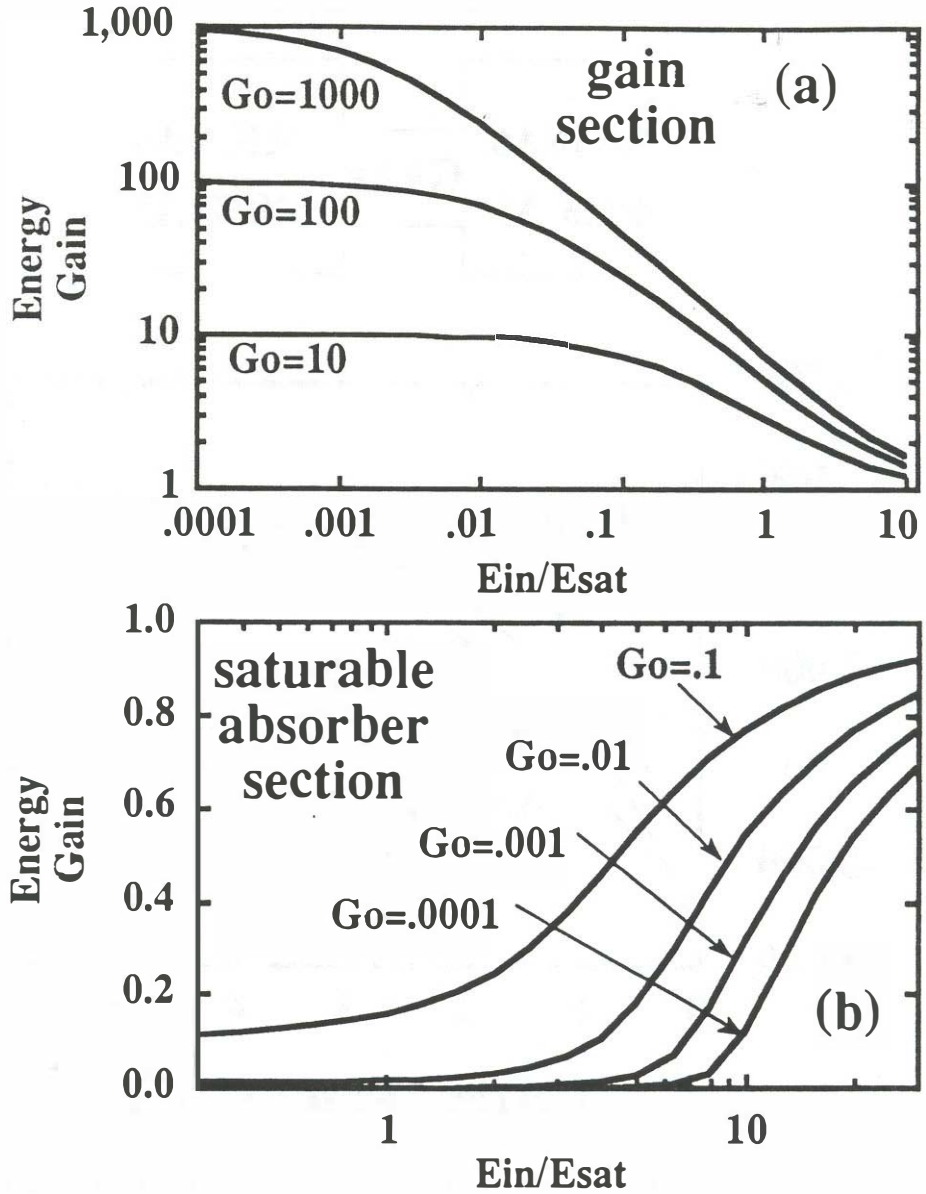

Figure 5.7 The importance of the saturation energy is illustrated in this figure. (a) The energy gain versus input energy divided by the saturation energy for a gain segment with three values of the unsaturated gain. (b) The energy gain versus input energy divided by the saturation energy for a saturable absorber with several values of unsaturated absorber transmission.

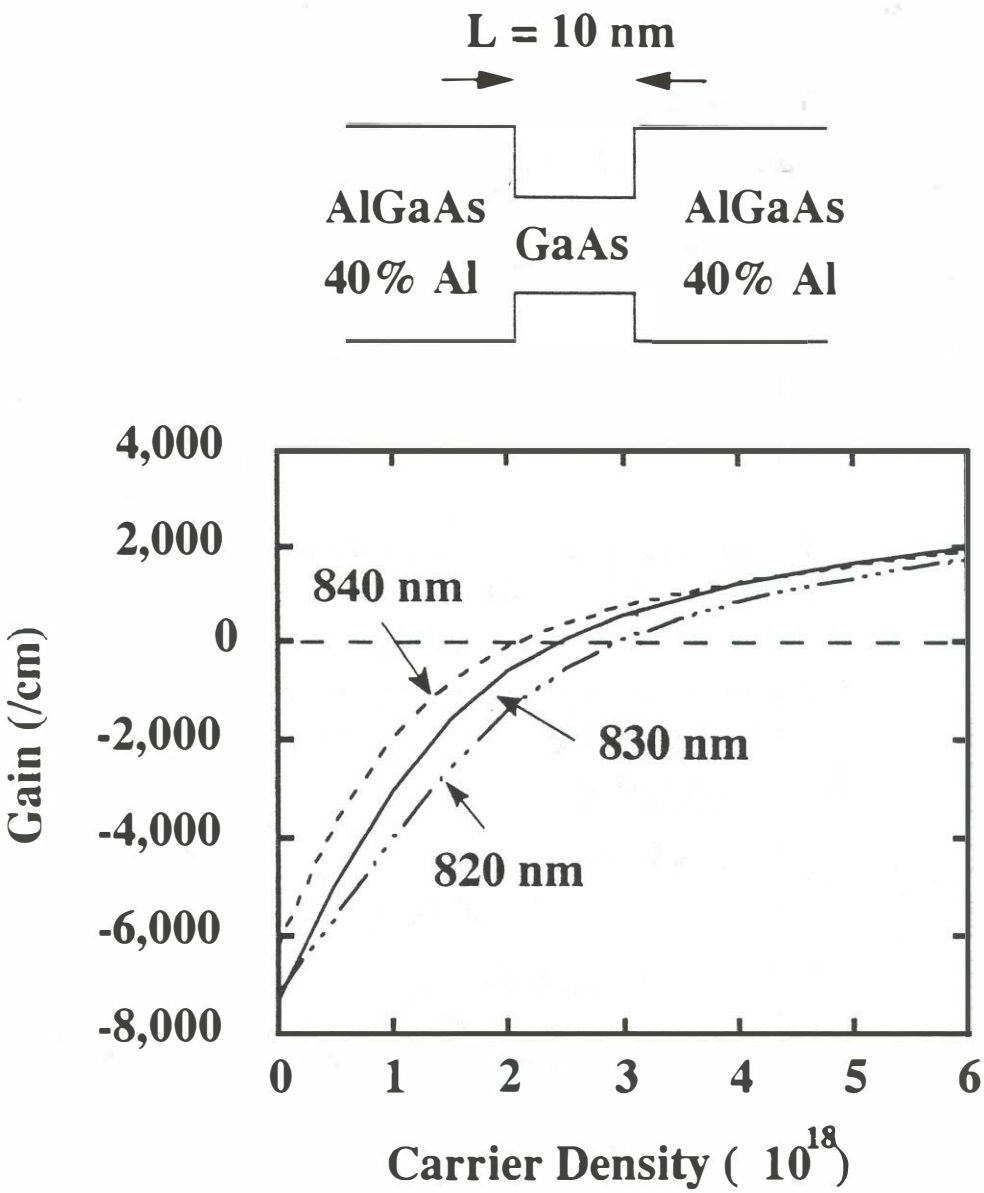

Figure 5.8 The calculated gain versus carrier density for a 10 nm wide GaAs/AlGaAs quantum well with x=.4 barriers. The gain data is taken for three different wavelengths. Scott Corzine's gain calculation program was used to produce this curve.

was calculated using a program written by Scott Corzine at UCSB). Figure 5.8 shows the gain versus carrier density for several values of wavelength. The important characteristic of this curve is the falling differential gain with increasing carrier density. A typical ratio of saturation energies between the gain and absorber segment is 3.

Let's examine the implications of Figure 5.8 on the ratio of saturation energies between the gain and saturable absorber segments. The mode-cross sectional area for multi-segment devices is identical in the gain and saturable absorber regions since they are constructed from the same optical waveguide. The important parameter in determining the saturation energy is the differential gain versus carrier density. Since saturable absorbers operate well below transparency carrier density levels and and gain regions operate well above transparency carrier density levels, we are guaranteed that the saturable absorber will have a lower saturation energy than that of the gain region. The actual ratio in saturation energies between the gain and saturable absorber sections is highly material dependent and these trade-offs will be discussed in Section 5.7. This nonlinearity in the gain versus carrier density function is larger in quantum well devices compared with bulk active region devices due to the step-like density of states for quantum well lasers compared to the square root of energy dependence for bulk active region lasers.

In the next section the ratio of saturation energies between the gain segment and the saturable absorber segment will be explored to see how important this ratio is and how large it must be for good performance in a passive mode-locked laser system using waveguide saturable absorbers.

In this discussion, results will be first be presented for the simplest model in

which the the linewidth enhancement factor is set to zero and an infinite gain bandwidth is assumed. This simplified model shows more clearly how to maximize the pulse shaping in passive mode-locked lasers. In the first simplified analysis, we shall only be concerned with the saturable gain and saturable absorber elements in the model of Figure 5.6. This section evaluates the relative strength of a two-section passive mode-locked laser in terms of how much pulse shortening occurs on each pass of an optical pulse around the laser cavity. The analysis uses repeated application of equation 5.8 which provides an analytic input-output relationship for each of the two sections.

Figures 5.9 a shows pulse shortening per pass as a function of the input energy to the amplifier over the saturation energy of the amplifier. Figure 5.9b shows the energy gain through the amplifier, through the saturable absorber, and the net gain through the gain-absorber cascade. Figure 5.9 is done for a ratio of saturation energies between the gain and absorber sections of 3. The unsaturated gain through the amplifier is 150 and the unsaturated transmission of the saturable absorber is 0.05 in this simulation. For a typical external cavity device, 1/9 of the energy is transmitted in coupling to the external cavity and back to the laser diode. The output coupler and internal losses of the waveguide cause another 1/3 transmission. The amplifier and absorber need to have a net gain of 27 to overcome the loss. The maximum net gain for these simulations is 27. The pulse shape for this simulation is gaussian and the full width at half of maximum is used for the pulsewidth.

The simulations of Figure 5.9 are representative of the passive and hybrid mode-locking experiments found in Sections 2.4 and 2.5 of this dissertation. At low input energies, the amplifier can not saturate the absorber leading to a small net gain through the gain-absorber cascade equal to the product of the

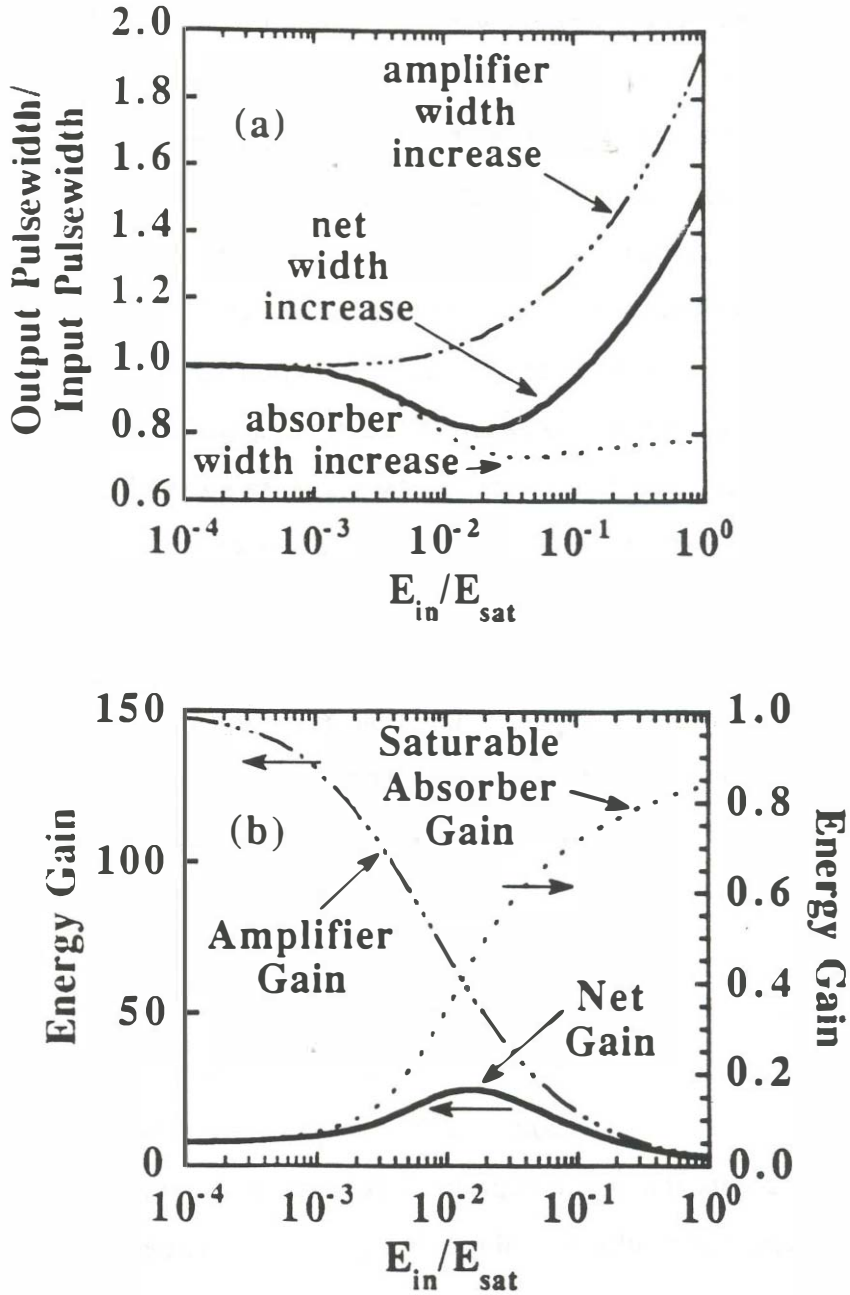

Figure 5.9 (a) Pulse shortening per pass and (b) net energy gain for one pass through the laser model of Figure 5.6 (no gain modulation segment). The maximum net gain through the device is 27. The unsaturated gain of the amplifier is 150 and the unsaturated transmission of the absorber is 0.05. The ratio of saturation energies between the gain section and the saturable absorber segment is 3.

unsaturated gain of the gain section and the unsaturated gain of the absorber section. As the input power is increased, the pulse energy from the amplifier becomes large enough to cause absorption saturation and the pulsewidth becomes narrowed in time. As the amplifier gain becomes increasingly saturated with increasing input energy, the amplifier widens the input pulse. This widening of the input pulse in the amplifier from gain saturation decreases the effectiveness of the passive mode-locked laser. The amount of pulse broadening in the amplifier can be minimized by maximizing the ratio of saturation energies between the gain and absorber segments. The saturable absorber starts to saturate and causes pulse shortening with increased input energy. Eventually the pulse shortening factor from the saturable absorber goes back to one as the input energy becomes extremely large with respect to the absorber saturation energy.

Figure 5.10a shows the input pulse and the amplified output pulse from a semiconductor laser amplifier under the conditions of significant gain saturation for various values of the input energy. The amplifier selectively amplifies the leading edge of the pulse as compared to the trailing edge of the pulse, and the resulting output pulse is widened. Figure 5.10b demonstrates the leading edge shaping that occurs in a saturable absorber. Figure 5.9a shows that there exists an input power at which the system experiences the largest pulse shaping per pass, in this case about a 20% pulsewidth shortening. This input power represents the best compromise between pulse shortening in the saturable absorber and pulse widening in the gain region. The energy of maximum pulse shortening per pass occurs at a similar energy to that of the maximum net gain.

Figure 5.9 represents a simulation for a specific choice of gain section and saturable absorber section parameters. It is plotted for values typical of those

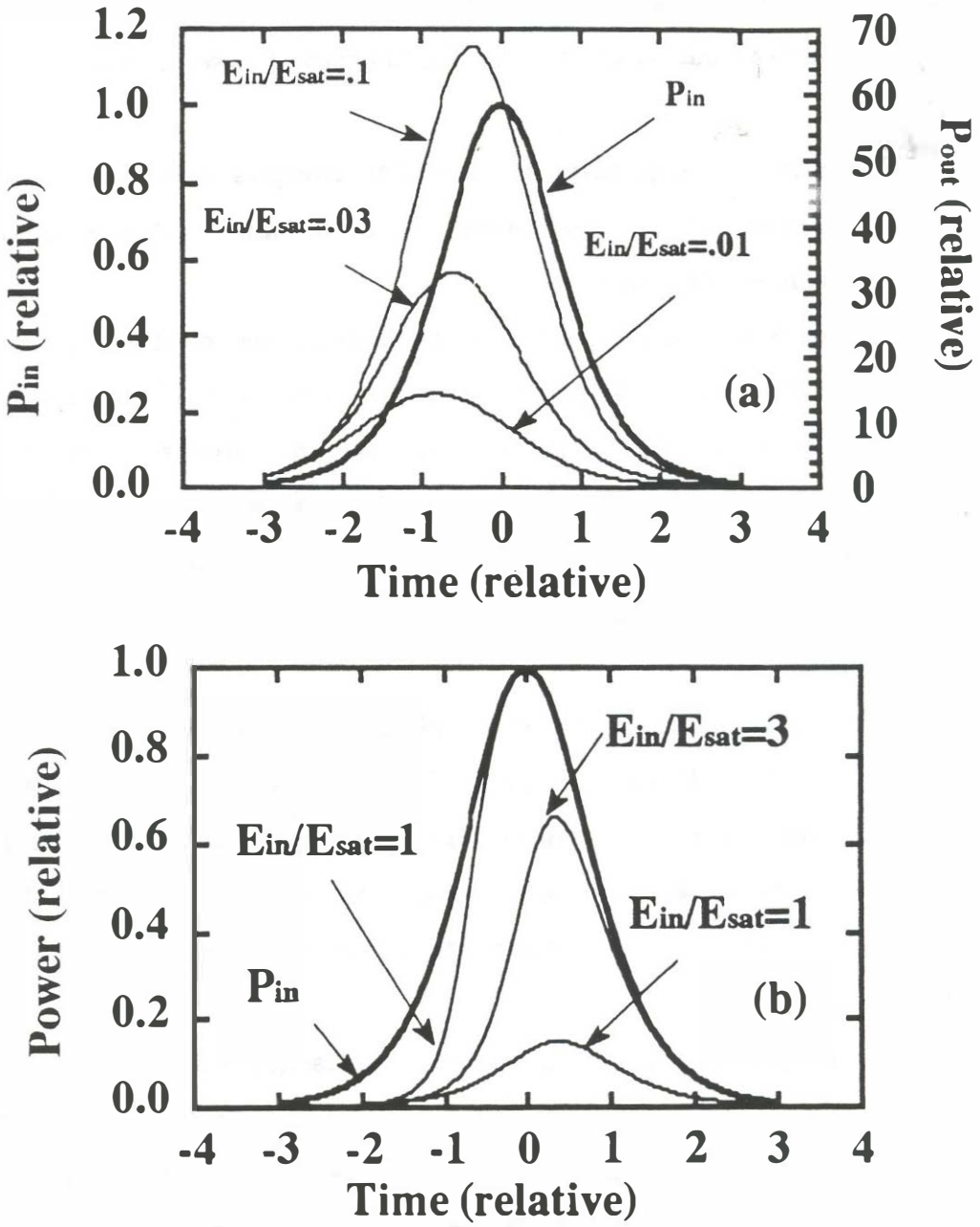

Figure 5.10 (a) The pulse broadening effects caused by gain saturation as a function of the input energy to the laser amplifier. The unsaturated gain through the amplifier is 150. (b) The pulse narrowing effects caused by absorption saturation as a function of the input energy to the saturable absorber. The unsaturated transmission of the saturable absorber is 0.05.

found in the passive mode-locked external cavity experiments of Sections 1.5 and 1.6. Figure 5.9 was used to identify the trends which are necessary to get the best passive mode-locking results. The summary of these trends are:

1) One wants a large ratio of saturation energies between the gain and absorber section, but there are diminishing returns as the ratio becomes very large.

2) The mode-locked laser will operate best at the input energy that provides the maximum pulse shortening per pass. This optimal energy decreases with an increasing ratio of saturation energies. The input energy for maximum pulse shortening per pass is found to be near the input energy for maximum net gain through the device. Therefore this input energy will be a stable operating point.

3) Gain saturation in optical amplifiers causes widening of the optical pulse. Gain saturation is also necessary for passive mode-locking because it causes pulse shaping in the trailing edge of the optical pulse. The best situation is to have some amount of gain saturation but not enough to cause substantial pulsewidth broadening.

As a designer of mode-locked semiconductor lasers, it is important to know how to choose the optimal length of the saturable absorber and gain regions based on input parameters such as the saturation energy of each segment and the required gain on each pass. Actually, the length of the absorber segment is the most critical parameter in a passive mode-locked laser design so this parameter will be focussed on. Figure 5.11a and b show the pulse shortening per pass

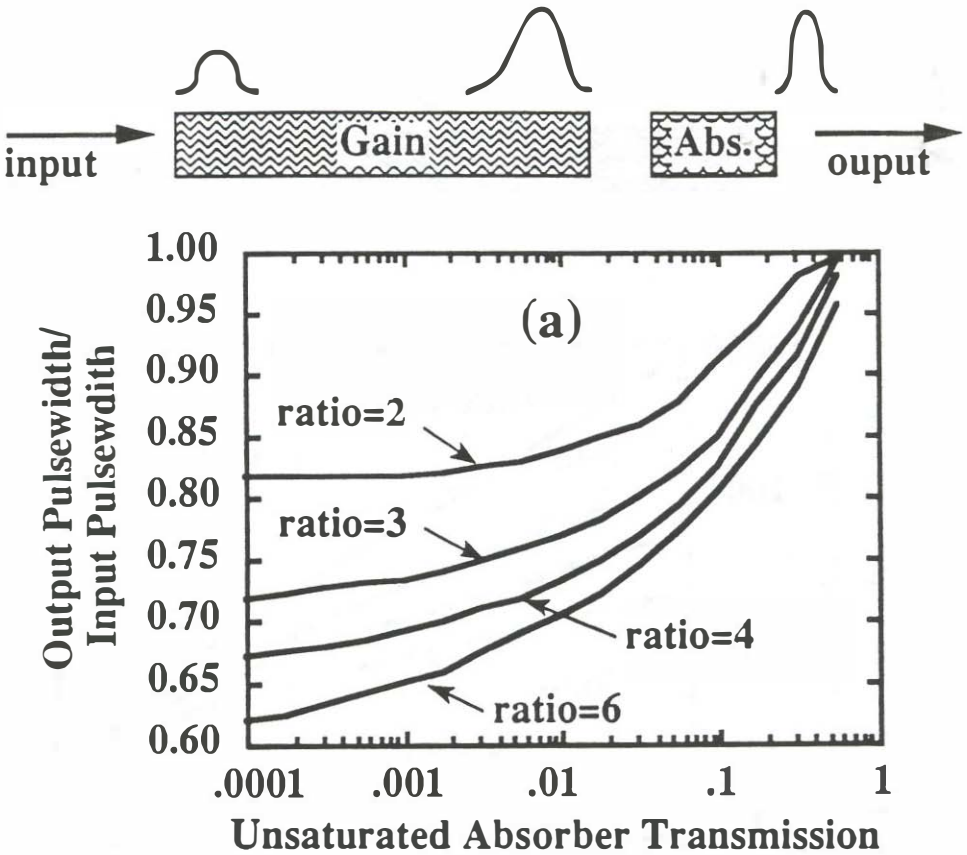

Figure 5.11a The pulse shortening per pass as a function of the unsaturated transmission through the saturable absorber. This simulation is for a gain absorber cascade with a net gain of 27 in all cases. The unsaturated gain of the amplifier is 150 and the unsaturated transmission of the absorber is 0.05. The plot is done for four values of the ratio in saturation energies between the gain and absorber segment. The indicated pulse shortening per pass is the maximum value in each case as is seen in Figure 5.9. This plot is intended to be a design guideline for the design of saturable absorber lengths.

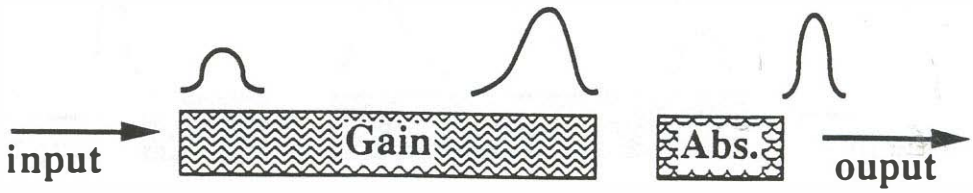

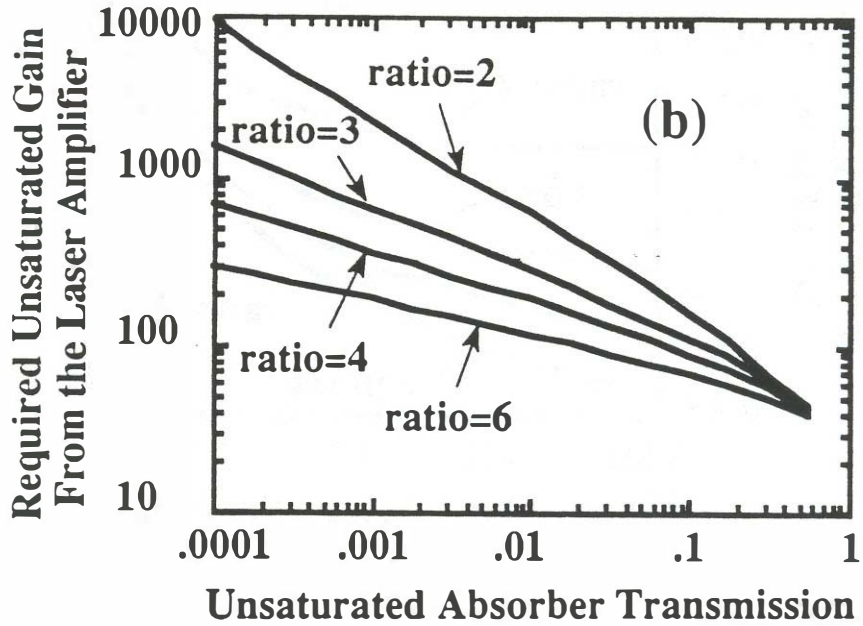

Figure 5.11b The required gain from the laser amplifier to achieve a gain absorber cascade with a net gain of 27 for the cases of Figure 5.11a. The unsaturated gain of the amplifier is 150 and the unsaturated transmission of the absorber is 0.05. The plot is done for four values of the ratio in saturation energies between the gain and absorber segment. This plot is intended to be a guideline for the design of gain segment lengths.

and unsaturated gain required from the amplifier as a function of the unsaturated transmission through the saturable absorber segment. The plots are done for several values of the ratio of saturation energies and are chosen to cover a large range of situations that may be encountered in practical designs. The x-axis in the plots is related to the actual absorber length using the relationship:

$$L_{seg} = \frac{\ln (T_{oab})}{g'} \tag{5.15}$$

where L_{seg} is the length of the saturable absorber segment, T_{oab} is the unsaturated transmission through the segment, g' is the gain coefficient through the absorber (g' will be negative for an absorber and g' includes the transverse confinement factor) The identifiable trends shown in Figure 5.11a and b are:

1) The longer the saturable absorber, the better the pulse shortening per pass strength.

2) The longer the saturable absorber, the larger the gain required from the optical amplifier.

3) The larger the ratio in saturation energies, the stronger the pulse shortening per pass.

4) For larger ratios in saturation energies, longer saturable absorber section lengths can be used without demanding too large of gain from the amplifier.

These design curves show that the best passively mode-locked laser has a large ratio in saturation energies and the longest possible saturable absorber lengths.

While these trends are correct, there are several other points that must be c nsidered before rushing off to make the design mask.

The first important limitation of the design curves of Figure 5.11 is that we can not arbitrarily make the saturable absorber extremely long. Extremely long saturable absorbers are not practical because the crequired values of unsaturated gain from the amplifiers becomes unachievable. The most fundamental reason for having a maximum achievable gain in semiconductor laser amplifier is amplified spontaneous emission. If the gain in the amplifier is too large, the amplified spontaneous emission level will become large enough to cause saturation of the gain. The effective input noise for a semiconductor laser amplifier is given by [84]:

$$P_{in\ eff} = h\nu\ \eta_{sp}\ K\ B_o \tag{5.16}$$

where $P_{in\ eff}$ is the effective spontaneous emission input power to the amplifier, h is Planck's constant, ν is the optical frequency, η_{sp} is the inversion factor (typically 1.5-5.), and B_o is the optical bandwidth. K is the Peterman K factor that describes how much of the spontaneous emission couples into the optical waveguide. K has a value of 1 for an index guided laser and increases for gain guided lasers or lasers that do not have a tightly confined mode.

$P_{in\ eff}$ is typically 1-10 μW. The gain of an amplifier starts to be saturated when the amplified spontaneous emission level at the output of the amplifier approaches the saturation power of the amplifier. The saturation power of an optical amplifier is $P_{sat} = E_{sat}/\tau_c$. The saturation power is important rather than the saturation energy because here we are dealing with a CW input noise signal. The saturation energy is important in pulse amplification were there is no

significant gain recovery due to pumping during the pulse amplification. Figure 5.12 illustrates the limitations on achievable gain in semiconductor laser amplifiers due to amplified spontaneous emission. For the index guided lasers used in these experiments, gains of about 30 dB are achievable. For gain-guided structures, the achievable gain is much smaller, although the saturation energy from these lasers may be much larger than for index guided lasers.

The other factor that limits the length of the saturable absorber is a self-pulsation phenomena that can occur in passive mode-locked lasers. Experimentally, passive mode-locked semiconductor lasers can exhibit a mode of operation in which the laser pulsates at a relatively low frequency (typically around $1/\tau_c$). The pulsations are usually more sinusoidal than pulse-like. Figure 5.13 shows the detected spectral characteristics and optical spectrum found during a self-pulsation mode-of operation. The self pulsation is at 2 GHz. If the current drive to the laser is increased, the self-pulsation frequency will increase. The experimentally observed bias conditions for lack of self-pulsation were shown for a monolithic cavity device in Figure 4.30. It has been found experimentally that passive mode-locked lasers with very long saturable absorbers are more susceptible to the self-pulsation phenomena. For example, a 40 GHz repetition rate SCPM monolithic cavity device from Chapter 3 with an 80 μm saturable absorber would not mode-lock and would only exhibit a self-pulsation mode-of operation. A 40 GHz repetition rate device with a 40 μm saturable absorber exhibited large bias regions of mode locking without self-pulsation. The self-pulsation phenomena becomes more pronounced as the repetition rate increases. As an example, a 7 mm long monolithic cavity device with an 80 μm saturable absorber passively mode-locked over a wide range of bias conditions. The same device when cleaved down to 2.5 mm with an 80

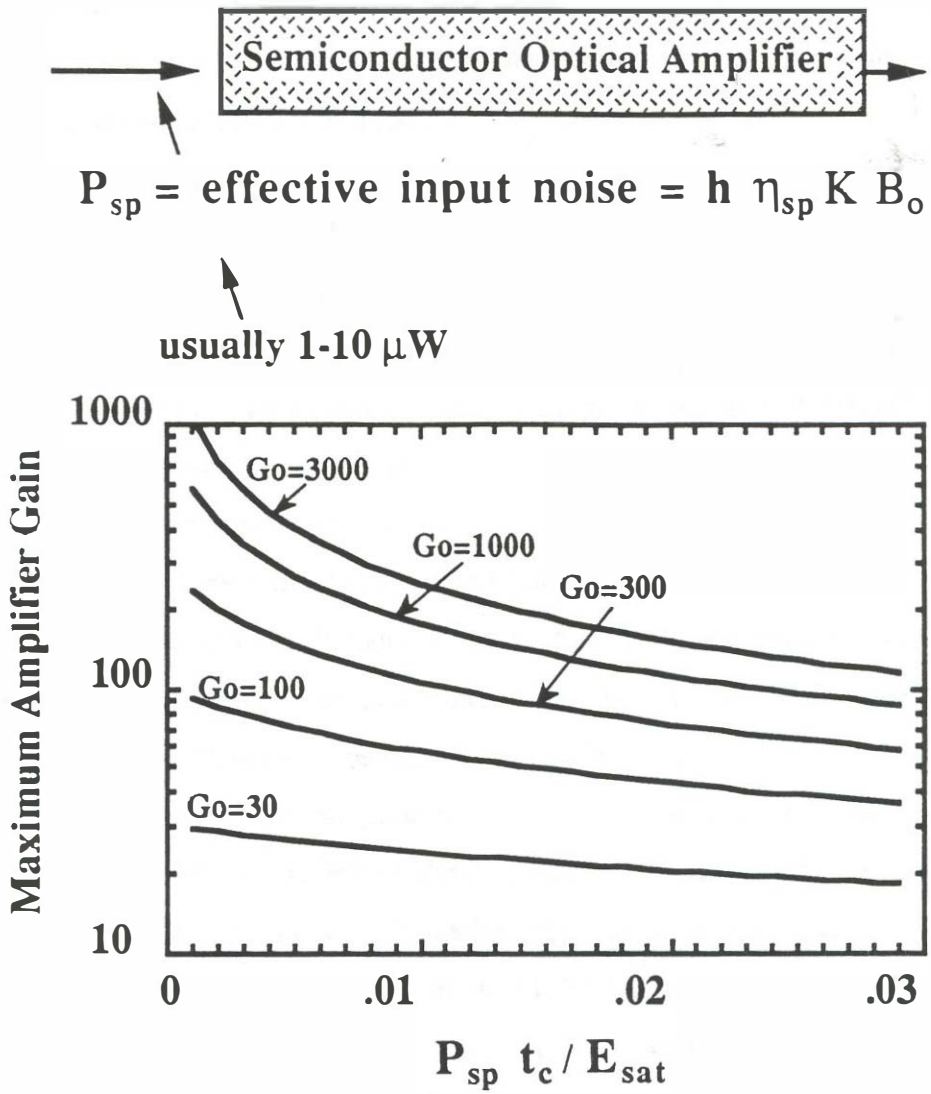

Figure 5.12 The small signal amplifier gain from a semiconductor laser as a function of the effective input noise of the amplifier. P_{sp} is the spontaneous emission power from the equation listed above. t_c is the spontaneous emission lifetime, η_{sp} in the inversion factor, G_o is the unsaturated amplifier gain, and K is the Peterman factor. The plot is done for several values of unsaturated gain. Amplified spontaneous emission saturates the gain and reduces the achievable gain in the amplifier. It is hard to achieve over 30 dB of gain from a semiconductor laser amplifier.

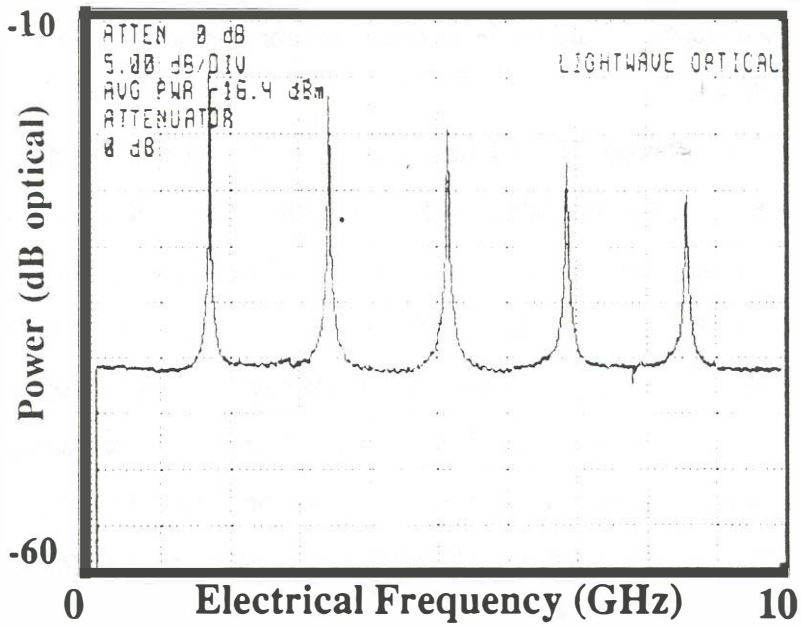

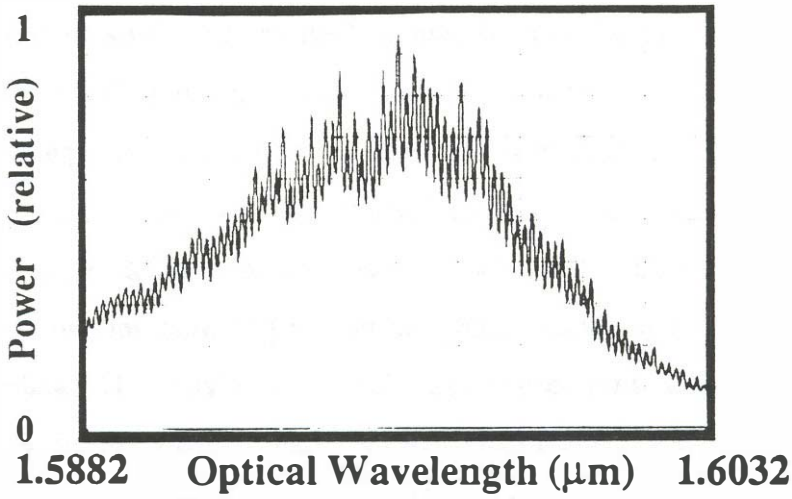

Figure 5.13 An experimental presentation on the effects of the self-pulsation mode of operation in multi-segment structures. (a) The detected electrical spectrum. (b) The optical spectrum. The laser is a two segment design with a 40 μm saturable absorber and 1 mm gain segment. The saturable absorber bias is -0.5 volt and the gain section current is 70 mA. The laser is self-pulsating at a repetition rate of 1.7 GHz. The self-pulsation envelope is approximately sinusoidal as can be seen from the relationship between the average power and the first modulation harmonic.

μm absorber would only exhibit self-pulsations. The origin of the competition between self-pulsation and mode-locked operation has been explored by several authors [80,81].

The best compromise for choice of saturable absorber lengths is then to choose the maximum saturable absorber length that does not cause a problem with self-pulsations or that does not require too large of unsaturated gain from the saturable absorber. As stated earlier, longer saturable absorbers give more pulse shortening per pass. On closer examination of the design curves of Figure 5.11a, the pulse shortening rapidly increases for increasing absorber length at first and then it flattens out. A good compromise saturable absorber length is to choose a saturable absorber length where the slope of the pulse shaping versus absorber length changes abruptly as is shown in Figure 5.14. Figure 5.14 is an example chosen to simulate the external cavity passive mode-locked laser experiment shown in Section 2.4. **The optimal absorber unsaturated transmission value for this case is in the range of 0.05 to 0.3.** This corresponds well to the experimental pulsewidth versus absorber length range used in Sections 2.4 and 2.5. Calculations similar to those of Figure 5.11 were done for a net gain of 10 and a net gain of 75 through the device. The pulse-shaping per pass levels were very similar to those of Figure 5.11a and the required gain function of Figure 5.11b scaled by the ratio of the net gains. This implies that the experimental results of Figure 5.11 are applicable to a wider range of mode-locking experiments.

The calculations done for Figures 5.9 and 5.11 were done for the unidirectional model of Figure 5.6. The question then arises as to how to make a correspondence between these results and those for the self-colliding pulse bi-

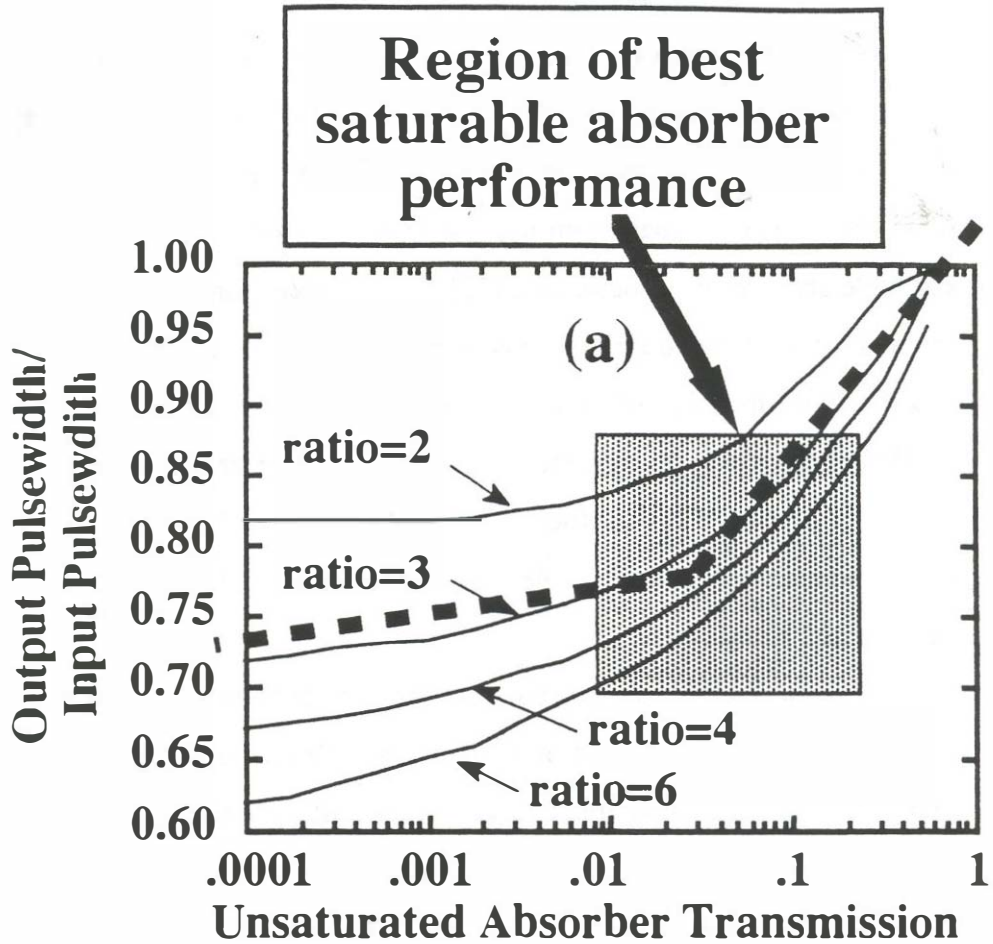

Figure 5.14 The shaded region in the plot indicates the best compromise in the choice of saturable absorber length. The plot contains the same data as Figure 5.11a. Too long of saturable absorber requires an unachievable gain from the laser amplifier. Long saturable absorbers are also susceptible to a self-pulsation mode of operation. Too short of saturable absorber gives a small pulse shortening per pass. The best compromise is to choose an unsaturated saturable absorber transmission between 0.01 and 0.3.

directional saturable absorbers which where used in Chapters 2-4. For low values of saturable absorber facet reflectivity (for example, a 30% reflectivity cleaved facet), the results from the unidirectional analysis can be directly applied to the same length bi-directional saturable absorber. For a 100 % reflectivity facet, the energy for maximum pulse shaping is reduced in the bi-directional saturable absorber by a factor of 2 [72]. The unidirectional simulation results can then be used to choose the one-way transmission through the bi-directional absorber with the ratio of saturation energies chosen to be twice that of the unidirectional value. Bi-directional saturable absorbers also have reduced saturation energies due to colliding pulse effects [72]. The effects of standing waves in semiconductor saturable absorbers have been studied extensively by Helkey et al. [9,72].

The first part of this section on saturable absorber analysis concentrated on the saturation characteristics of the gain and absorption media. It is also required that the absorber must saturate very quickly after the passage of the optical pulse through the saturable absorber. The experimentally measured recovery of waveguide saturable absorbers was presented in Section 2.4.

5.4 Pulse shortening by active gain modulation

Section 5.3 studied pulse shortening by passive gain modulation with a saturable absorber. In this section the other pulse shortening mechanism, active gain modulation, is studied. The physical model used to analyze active gain modulation is shown in Figure 5.6 with the saturable absorber section omitted. The rate equations used to analyze active gain modulation are equations 5.1 and 5.2 using Runge-Kutta solution techniques and a short segment length. The bandwidth and dispersion effects are not included in these simulations (t_2=0 and β_2=0). The approximate analytic solution of equation 5.8 can not be used in this analysis because of the time varying pumping condition of active gain modulation.

The first point to be made in this discussion is a comparison of the relative pulse-narrowing strengths of passive versus active gain modulation. To do this simulation, the pulse shortening per pass is compared for active and passive gain modulation. As was seen in section 5.3, the pulse-shortening per pass is independent of pulsewidth for a constant input energy pulse in passive mode-locking. How does the pulse shaping per pass in active gain modulation depend on the input pulse width for a constant input energy ? From first intuition, it would seem that the pulse shaping strength for active gain modulation would get less and less effective as the duration of the optical pulse becomes short compared to the duration of the electrical pumping pulse. The gain changes induced by the electrical pumping will become nearly zero for very short optical pulses. This intuitive guess turns out to be correct.

Figure 5.15 shows a comparison of the pulse shortening per pass for active and passive modulation examples. The passive example was that studied in

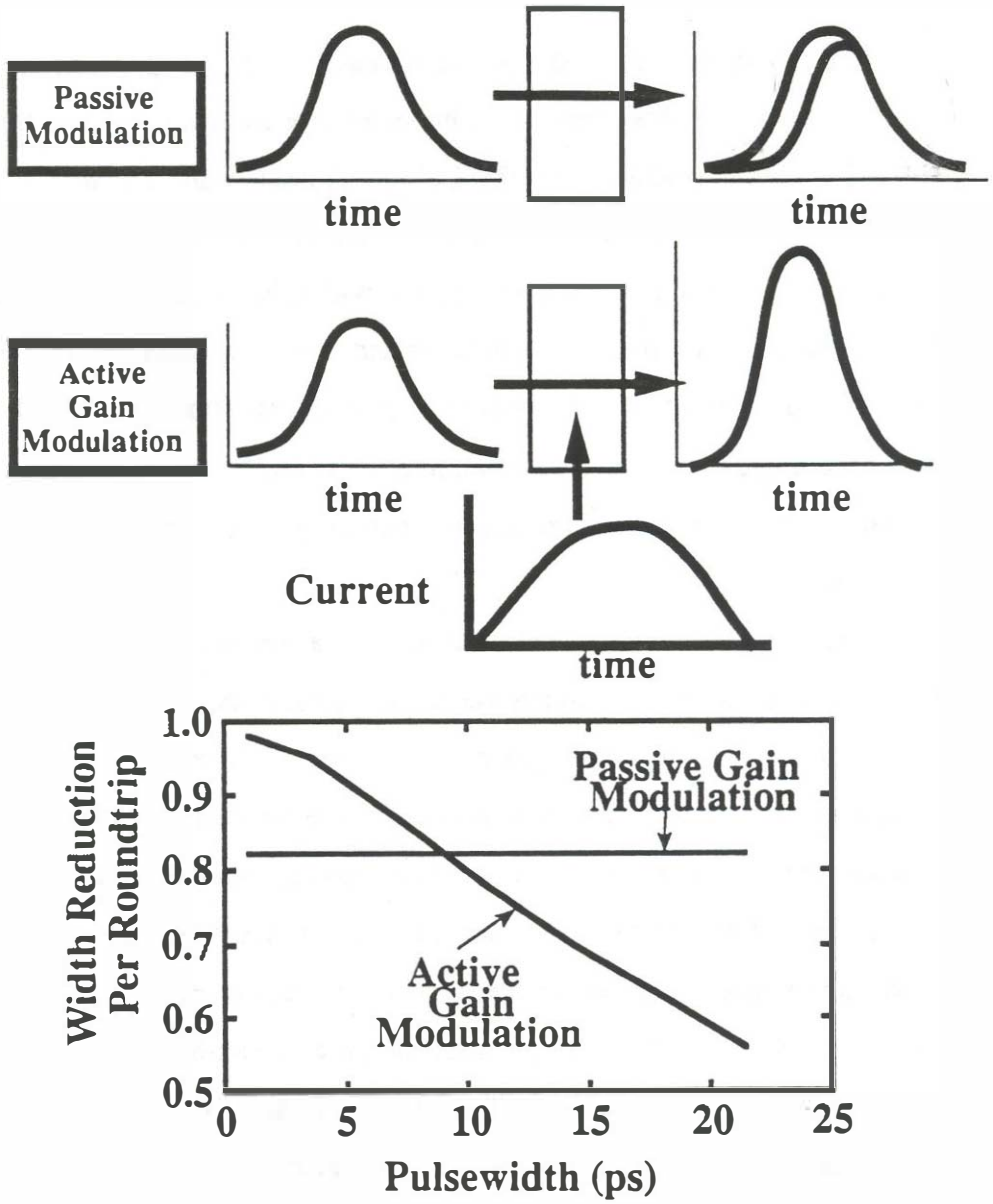

Figure 5.15 A comparison of the strength of passive gain modulation and active gain modulation. For a constant input energy pulse, the pulse shortening per pass is constant, in this case a 20% shortening as was shown in Figure 5.9a. Active gain modulation is very effective for wide input pulses but the narrowing strength weakens as the optical pulsewidth becomes small compared to the electrical pulsewidth. The modulation segment length is 100 μm, the modulation pulsewidth is 20 ps, and the peak modulation current is 100 times the transparency value.

Section 5.3. The pulse shortening per pass is independent of pulsewidth and has a value of 0.83. For the active modulation case, the input driving pulse was a 20 ps gaussian current pulse. The gain modulation segment is 50 μm long with a peak current 100 times the transparency current (Equation 5.6). The curve shows that active gain modulation is stronger than passive gain modulation in reducing the pulsewidth for very wide input pulses. The pulsewidth narrowing becomes increasingly weak as the optical pulsewidth narrows. The function seems to show a nearly linear relationship with input pulsewidth. Although this example is done for a specific example, the trend will hold true for any width electrical modulation pulse. As the electrical modulation pulsewidth narrows, active gain modulation becomes more effective for narrow width optical pulses. Because passive gain modulation is the stronger pulse shortening mechanisms for narrow width pulses, this will be the only pulse narrowing function that will be used when examining the limits on achievable pulsewidth in Section 5.8. This is not to say that active gain modulation is not important. It was found in Section 4 that active gain modulation is very effective in stabilizing the amplitude and temporal stability of the optical pulse stream.

Active gain modulation is actually similar to passive gain modulation in several ways. Both active and passive modulation rely on pulse shortening at the leading edge of the input optical pulse. In passive gain modulation, the leading edge of the optical pulse receives more attenuation than the trailing edge of the pulse. In active gain modulation, the leading edge of the optical pulse receives less amplification than the later portions of the pulse. In both cases, gain saturation in the optical amplifier is required to suppress the trailing edge of the optical pulse. Figure 5.16 illustrates the pulse-shortening mechanism of

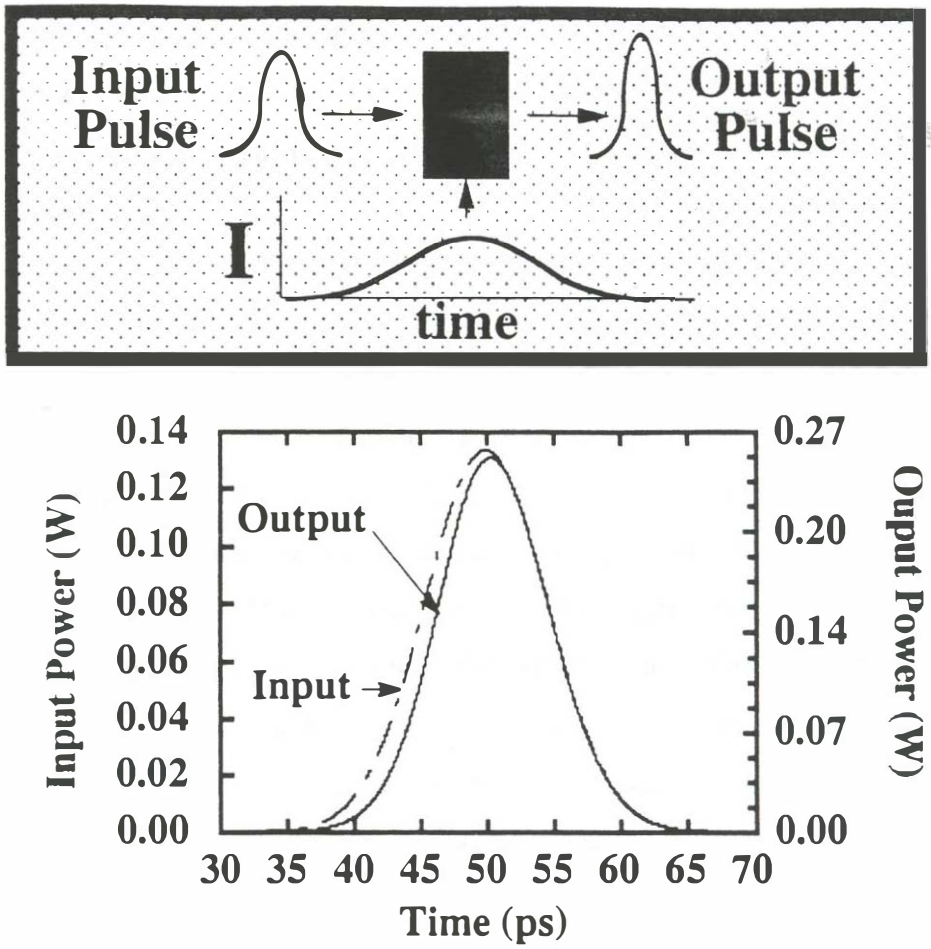

Figure 5.16 This figure illustrates pulse narrowing by active gain modulation. The electrical gain modulation signal is a 20 ps gaussian pulse with an amplitude 100 times the current for transparency in a 100 μm long gain modulation segment. The saturation energy of the segment is 2 pJ. The graph is done for a 5 ps delay between the optical and electrical pulse (the electrical pulse arrives earlier) which gives the maximum pulse shortening per pass. Note that the pulse shortening in active gain modulation is a leading edge phenomena just as is the case for passive gain modulation. Instead of having a time dependent loss, here we have a time dependent gain. Both active and passive gain modulation depend on gain saturation for trailing edge suppression.

active gain modulation. There are several more variables in evaluating the maximum pulse-shortening per pass for active gain modulation as compared to passive gain modulation. To study the trends in active gain modulation, the parameters of electrical input pulsewidth, optical input pulsewidth, optical input pulse energy, and timing delay between the electrical and optical pulse waveforms will be varied. The method used to evaluate the strength of active gain modulation will again be the pulse shaping per pass.

Figure 5.17a shows the pulse shortening per pass as a function of delay between the input and output electrical pulses (positive delay means the the center of the electrical pulse arrives at the gain segment earlier in time than the center of the optical pulse). The plot is done for three values of input optical pulsewidth (5, 10, and 20ps) and for a gaussian current pulse with a 20 ps FWHM. The peak value of the electrical current pulse is 100 times the transparency current (Equation 5.6) for all three optical pulsewidths. The optical confinement factor is 0.25 for all of the simulations in this section. The results for 7 values of the input energy with respect to the saturation energy are given in Figure 5.17. Figure 5.17b shows the energy gain through the modulation segment as a function of delay through the segment. It is seen that the delay for maximum pulse shortening is not the delay for maximum gain. Figure 5.17 shows that slight positive delays produce the maximum pulse shortening ratios for all of the input optical pulsewidths. This makes sense intuitively since active gain modulation is a leading edge pulse shortening mechanism. Fast electrical pulses with respect to the optical pulsewidth allow the difference in gain between the leading edge and the central portion of the pulse to be maximized.

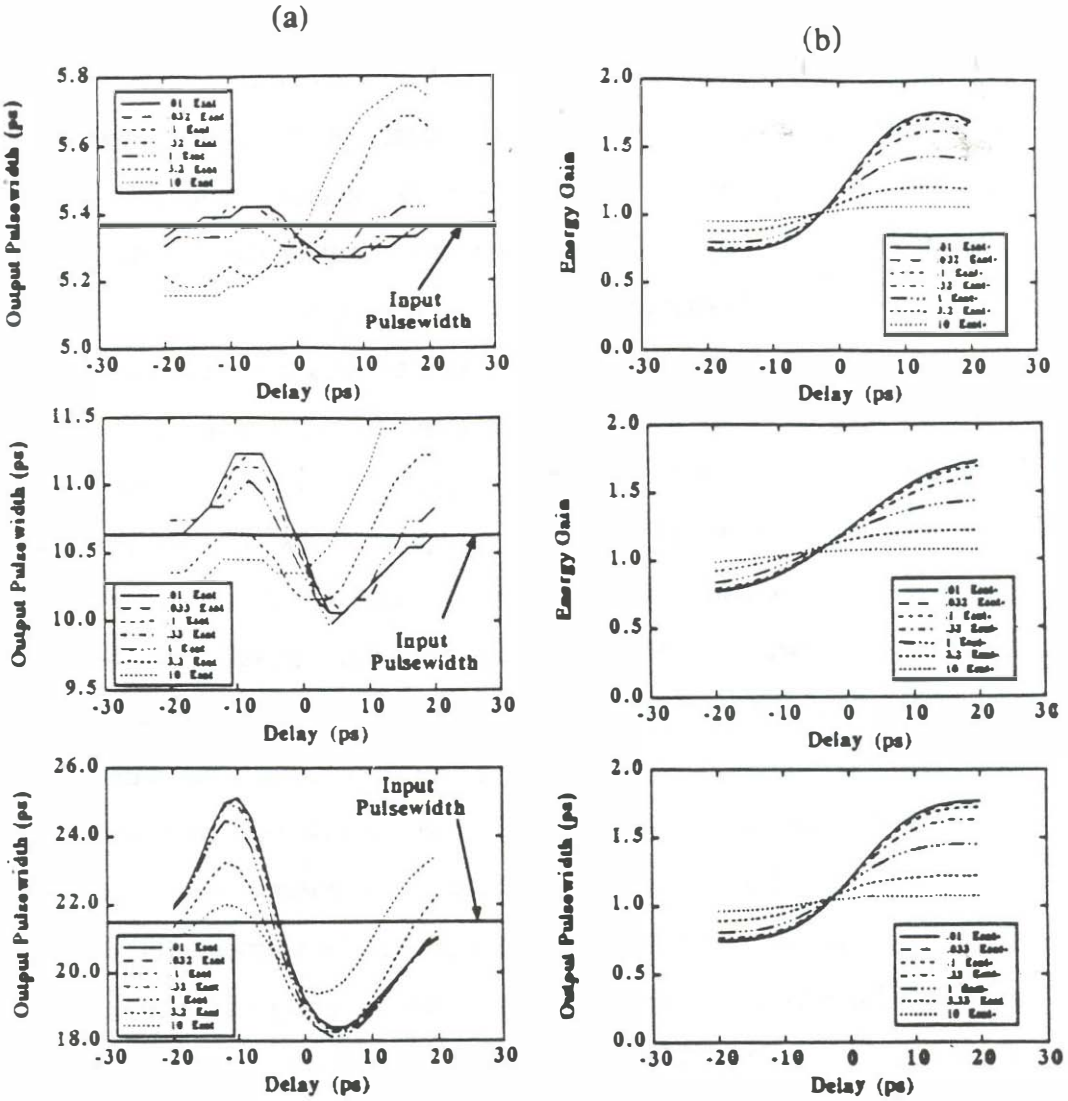

Figure 5.17 Pulse shaping by active gain modulation. The length of the modulation segment is 100 μm and the width of the electrical modulation is 20 ps in this simulation. The optical pulsewidth is varied from 5 to 10 to 20 ps. The peak modulation current was 100 times the current required for transparency. Positive delay means that the electrical pulse arrives earlier to the gain modulation segment. (a) The pulsewidth reduction and (b) the energy gain through the segment. The input energy is also a variable for each plot.

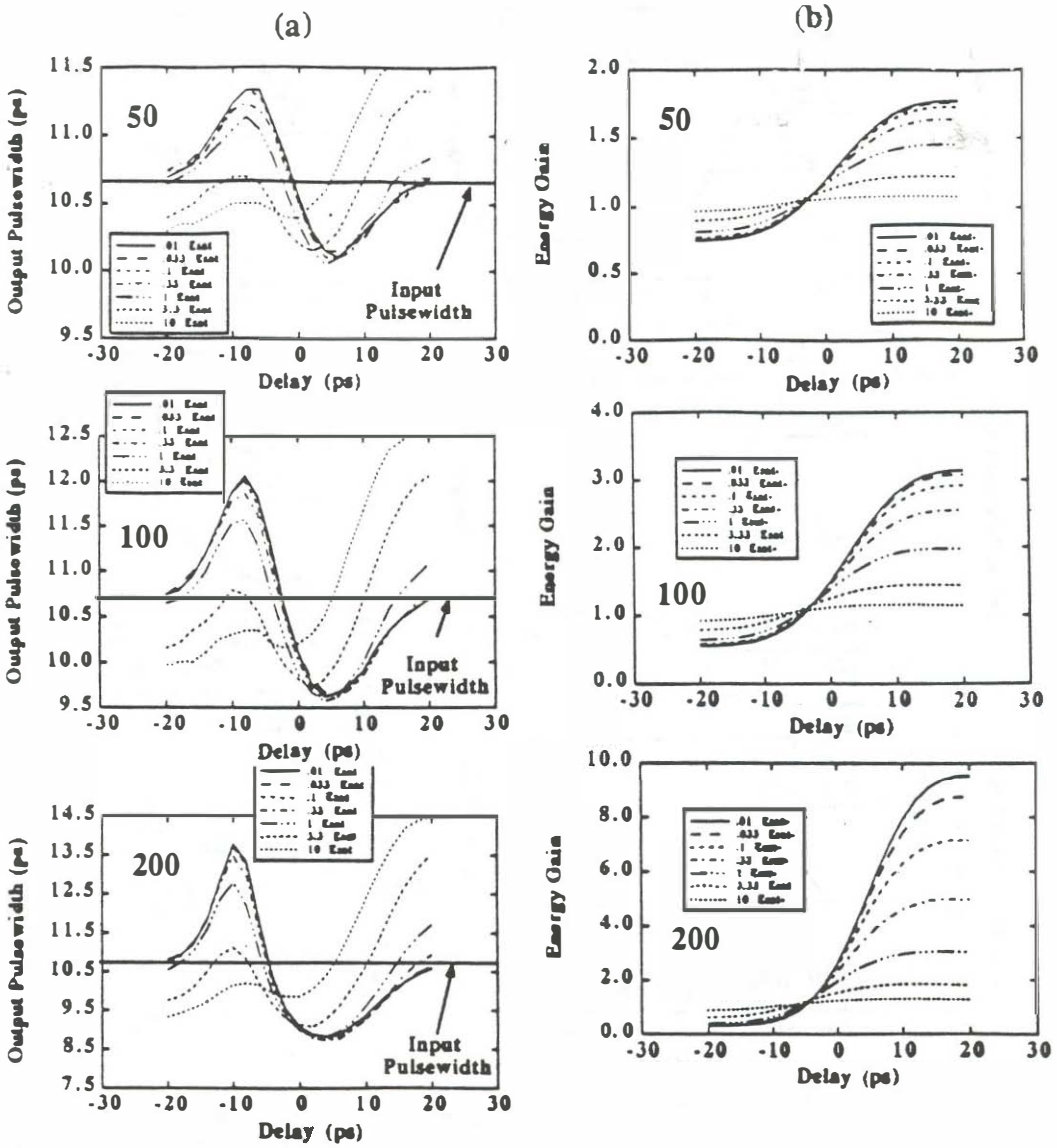

Figure 5.18 Pulse shaping by active gain modulation. The length of the modulation segment is 100 μm and the width of the electrical modulation is 20 ps in this simulation. The optical pulsewidth is held constant a 10 ps. The peak value of the modulation current is varied from 50 to 100 to 200 times the transparency current value. Positive delay means that the electrical pulse arrives earlier to the gain modulation segment. (a) The pulsewidth reduction and (b) the energy gain through the segment. The input energy is also a variable for each plot.

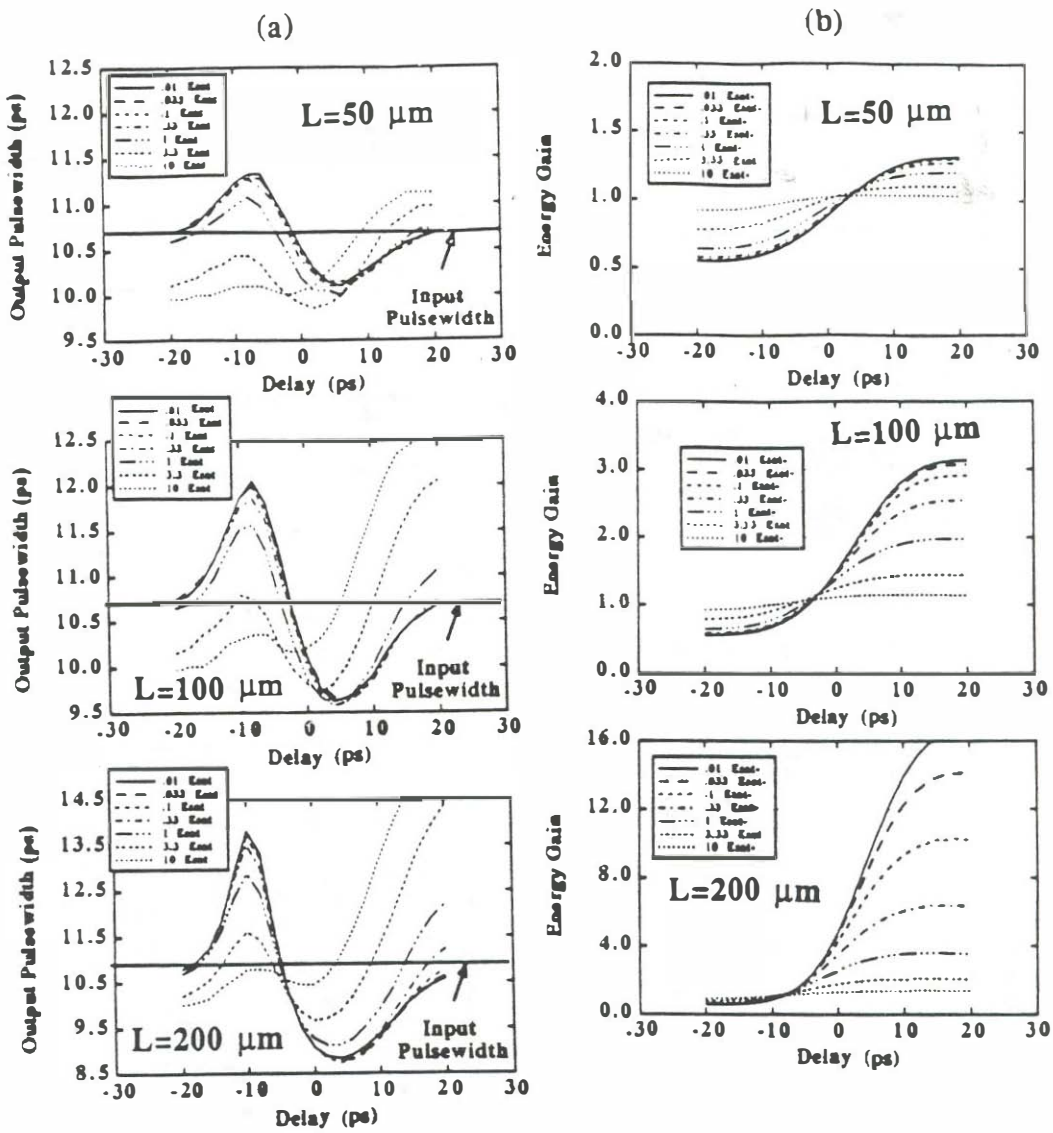

Figure 5.19 Pulse shaping by active gain modulation. The length of the modulation segment is varied from 50 to 100 μm to 200 μm. The width of the electrical modulation is 20 ps in this simulation. The optical pulsewidth is held constant a 10 ps. The peak value of the modulation current is held at 100 times the transparency current value. The peak current thus scales with segment length in this simulation. Positive delay means that the electrical pulse arrives earlier to the gain modulation segment. (a) The pulsewidth reduction and (b) the energy gain through the segment. The input energy is also a variable for each plot.

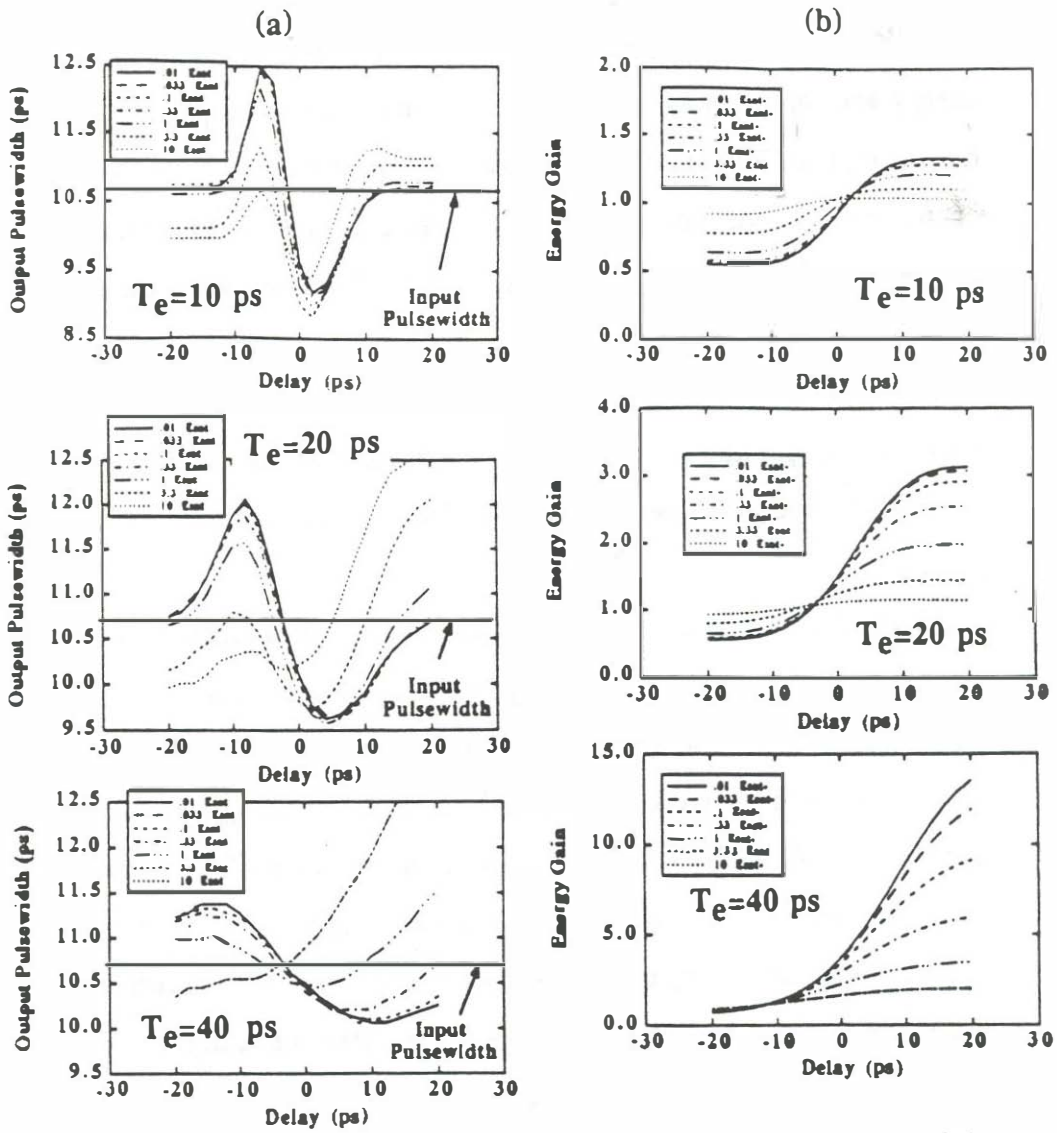

Figure 5.20 Pulse shaping by active gain modulation. The length of the modulation segment is held at 100 μm. The width of the electrical modulation is varied form 10 to 20 to 40ps in this simulation. The optical pulsewidth is held constant a 10 ps. The peak value of the modulation current is held at 100 times the transparency current value. Positive delay means that the electrical pulse arrives earlier to the gain modulation segment. (a) The pulsewidth reduction and (b) the energy gain through the segment. The input energy is also a variable for each plot.

Figure 5.18 shows pulse shortening per pass and energy gain per pass through a 50 μm modulation segment as a function of the gain modulation pulse energy and input optical pulse energy. The input optical pulsewidth for the simulation is 10.7 ps and the gain modulation pulsewidth is 20 ps FWHM. The maximum gain modulation current is increased from 50 times the transparency current to 200 times the transparency current. The minimum pulse shortening ratio decreases from 0.95 to 0.8 over this range of current increase. Large electrical modulation currents (while holding the modulation pulsewidth constant) strongly improve the pulse shortening strength by increasing the range of gain differences between the leading edge and central portions of the optical pulse.

Figure 5.19 shows the pulse shortening per pass as a function of the length of the modulation segment for a 20 ps electrical modulation pulse. The three segment lengths are chosen to be 50, 100, and 200 μm. The gain modulation peak current is held constant as a ratio of peak current to the transparency current (I/I_0=100). Since the transparency current scales directly with length, the peak current is changing with segment length. This is a reasonable assumption in that heating effects most often limit the maximum current that can be applied to a gain modulation segment. The maximum current that does not introduce heating effects will scale with the length of the gain modulation segment. The maximum pulse shortening ratio increases as the segment length increases. The length of the modulation segment can not be increased indefinitely because the available modulation current from short modulation pulse sources is limited. Step recovery diodes are the most readily available gain modulation pulse source. The peak current available from commercially available step recovery diodes varies with pulsewidth and repetition rate. At

100 MHz, 100 mA of peak current with 110 ps FWHM is available (into 50Ω load). At 1 GHz, 140 mA of peak current with 60 ps FWHM is available. At 3 GHz, 120 mA of peak current with 30 ps FWHM is available. (This data is taken from measurements on HP step recovery diode modules). Above 3 GHz, sinusoidal gain modulation becomes more practical since the effective pulsewidth of the sinusoid is quite short. For sinusoidal signals, power levels up to 1 Watt (peak current of 2 amps into a 50Ω load) are possible with decreasing pulsewidth as the frequency is raised.

Figure 5.20 shows the pulse shortening per pass versus the gain modulation pulsewidth for a fixed peak current (I/I_0=100). The electrical modulation pulsewidth is varied from 10 to 20 to 40ps. The length of the modulation segment is 100 μm in all cases. The trend again shows that the ratio of the optical pulsewidth to the modulation signal pulsewidth is the important factor in pulse shaping per pass. What are the limits on how short of gain modulation pulses are available? The shortest commercially available pulsewidths from step recovery diodes is 30 ps as was mentioned in the laser paragraph. The effective pulsewidth can be reduced by reverse biasing the gain modulation segment so that only the peak part of the modulation signal actually causes carrier injection into the diode. In this way it is possible to get 20 ps electrical modulation pulses. In all cases, the effective modulation pulsewidth into the active region is widened by the electrical parasitics of the gain modulation segment. The low-pass cut-off frequency of a state of the art laser diode is approximately 20 GHz. This means that it does not pay to try and produce a gain modulation pulse of less than about 20 ps duration.

The basic trends identified in the analysis of active gain modulation are

summarized as:

a. Active gain modulation is not as strong as passive gain modulation for narrow input optical pulsewidths (e.g.<5 ps).

b. There exists a band of input energies over which the maximum pulse-shortening per pass occurs. This energy is typically 0.1-0.8 times the saturation energy of the amplifier.

c. Shorter electrical pulsewidth produce shorter optical pulse widths. Gain modulation pulses narrower than about 20 ps do not add substantial performance improvement for a typical low parasitic laser structure. Reverse biased modulation segments allow shorter effective pumping intervals.

d. The larger the input electrical driving current, the larger the pulse shortening. The limit on the electrical modulation current is segment heating.

e. The longer the modulation segment (as long as the current drive to pulse the segment to many times the transparency current is available) the larger the pulse shortening.

These conclusions show that the optimal gain modulation segment would be long, the modulation current would be large, and the current modulation pulsewidth would be as narrow as possible. Obviously there are some upper limits to these trends which must be addressed. The upper current modulation level is limited by heating effects in the segment. This heating can be severe for very short segments. I have found out very clearly that power levels of 20 dBm are more than sufficient to damage short (16 μm) modulation segments if the positive portion of the drive signal is allowed to forward bias the diode

significantly. The obtainable electrical pulsewidth is also a very important issue. Sinusoids work very well at high frequencies (e.g. >10 GHz). For lower repetition rates, step recovery diodes [31] or non-linear transmission lines [32] work well to drive the laser.

5.5 Self phase-modulation effects in semiconductor laser amplifiers, saturable absorbers, and gain modulation segments

Self-phase modulation results when the optical pulse induces changes in the index of refraction in the material it is propagating through. This is a well known effect in optical fibers where the optical Kerr effect produces an intensity dependent index of refraction.

$$n_{in}(t) = n_0 + n_2 I \tag{5.17}$$

where n_{in} is the index of refraction, n_o is the low-intensity index of refraction, n_2 is the nonlinear index coefficient (m^2/W), and I is the intensity (W/m^2).

Figure 4.2a demonstrates self-phase modulation due to the Kerr effect. The Kerr effect self-phase modulation is well known in the non-linear fiber optics field. The index of refraction in the material rises nearly instantaneously with the input intensity. The resulting instantaneous frequency (proportional to the negative time derivative of the index of refraction with respect to time) results in a frequency chirping of the optical pulse with a nearly linear instantaneous frequency rise over the central portion of the optical pulse.

The dominant self-phase modulation effect in semiconductor lasers is of a different origin that that of the optical Kerr effect. Self-phase modulation in semiconductor lasers is a result of the coupling between the index of refraction and the carrier density in the device. Figure 4.2b shows the self-phase modulation that results from gain saturation in semiconductor laser amplifiers. As a pulse is amplified in a semiconductor laser

amplifier, the carrier density drops. A drop in the carrier density causes a rise in the associated index of refraction. The instantaneous frequency shows a dip at the central portion of the pulse. Figure 4.2c shows the self-phase modulation that results from absorption saturation in a saturable absorber. As the leading edge of the pulse is absorbed, the carrier density level rises. The rising carrier density causes a drop in the index of refraction. The resulting instantaneous frequency shows a rise at the leading edge of the pulse. Note that in general that the frequency chirp is not linear over the central portion of the pulse. This important in that linear chirp can be compensated for by grating compressors [9,85]. Non-linear chirp compensation requires a much more complicated hardware implementation. Also notice that the chirp found from gain saturation is an integrating non-linearity in that the index of refraction change is proportional to the integral of the input pulse instead of directly proportional to the input pulse as is found in the optical Kerr effect.

Active gain modulation also produces a frequency chirp on the optical pulse. Figure 5.21 shows an example of the type of self-phase modulation effect that can be found in gain modulation segments. Figure 5.21a shows the input optical pulse shape and Figure 5.21b shows the gain modulation current waveform which is aligned with the optical pulse to give the maximum pulse shortening effect (see Section 5.4). The gain modulation causes an increase in the carrier density in the first part of the pulse and gain saturation causes a decrease in the trailing edge of the pulse. The over-all chirp is first an upswing and then a down-swing in frequency.

The index of refraction changes in a semiconductor laser due to a pulse propagation through an amplifier are described by (derived from Agrawal and Olsson's equations [53]):

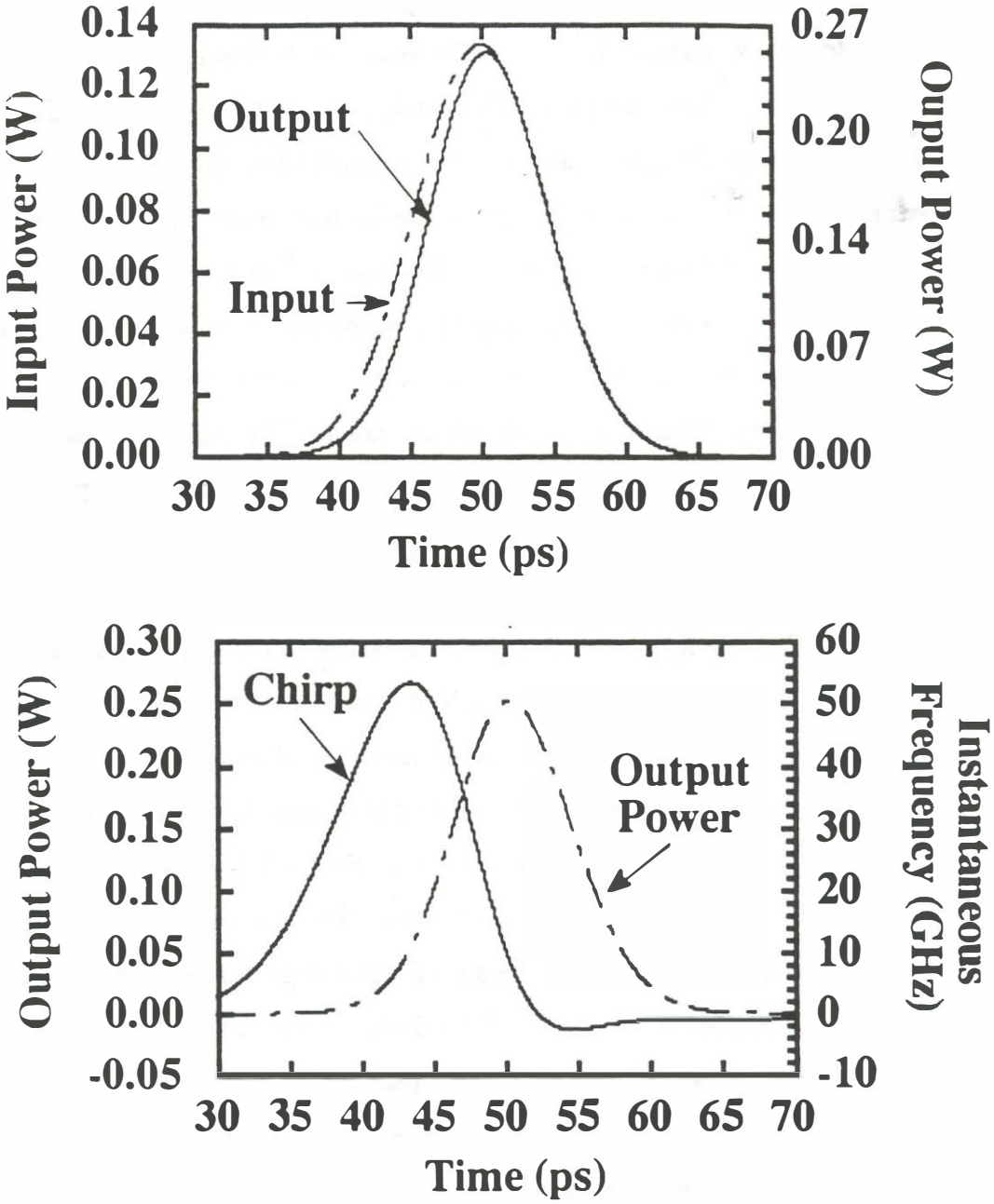

Figure 5.21. Self-phase modulation due to active gain modulation. The carrier density rise during active gain modulation causes a rise in the instantaneous frequency during the leading edge of the pulse.

$$n_{in}(t)=n_o - \frac{dn_{in}}{dn}\left((n-n_{tr}) - \frac{1}{aL}\ln\left[\frac{1}{1-\frac{1}{G_o}e^{\left(\frac{U_{in}(t)}{E_{sat}}\right)}}\right]\right) \tag{5.18}$$

where

$$U_{in}(t) = \int_{-\infty}^{t} P_{in}(t')\,dt' \tag{5.19}$$

dn_{in}/dn is the change in the index of refraction with respect to carrier density, $P_{in}(t)$ is the optical power versus time of the input pulse pulse, n_0 is the initial index of refraction before the passage of the optical pulse, n_{tr} the carrier density at transparency, a the differential gain coefficient, G_o the initial unsaturated gain value, L the device length, and t the time with respect to the center of the input optical pulse.

The carrier density drops approximately as the integral of the input pulse energy versus time. The linewidth enhancement factor controls the magnitude of the chirp and is a very important parameter in mode-locked lasers. The α parameter has often been measured in the forward biased condition [87,88] of the laser with values typically between 2 and 6. Quantum well devices generally have a smaller value of α. The linewidth enhancement factor for reverse biased saturable absorbers has not been extensively studied or measured but is very important to understand the magnitude of chirp in saturable absorbers. For saturable absorbers we need to know the value of alpha in the reverse biased case, with carrier densities between zero and transparency. A new method for measurement of α was developed to measure α in reverse-biased segments. The method involves the use of a two section laser as shown in Figure 5.22. The long segment is forward biased to act as an amplifier in

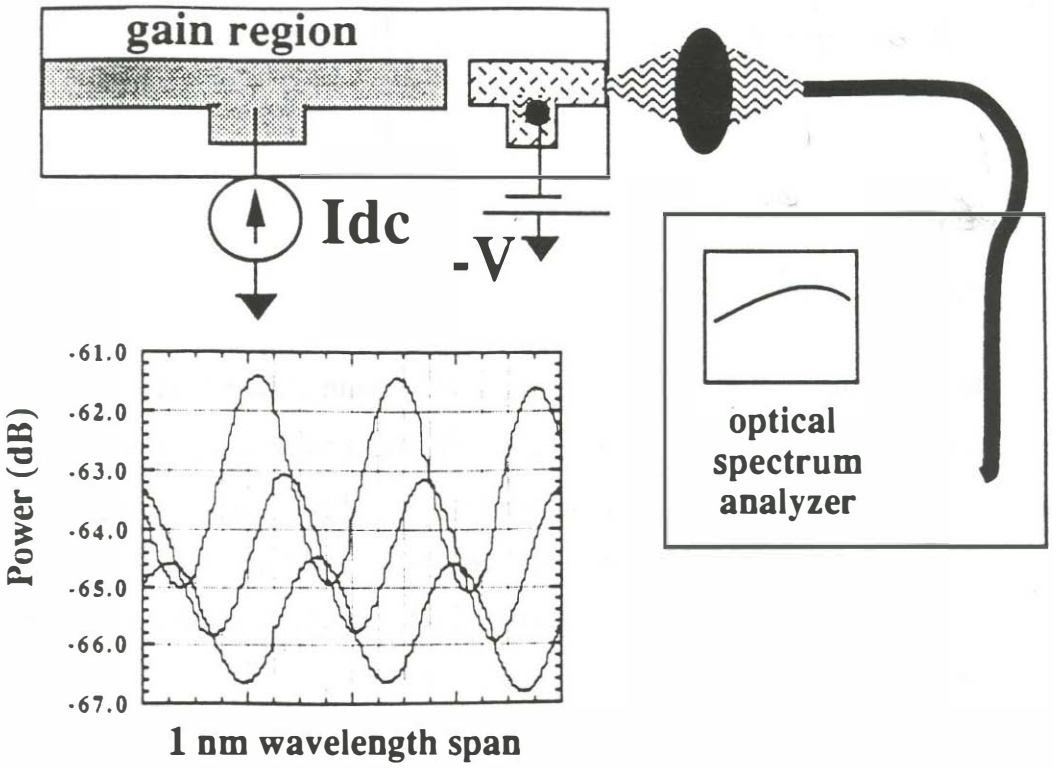

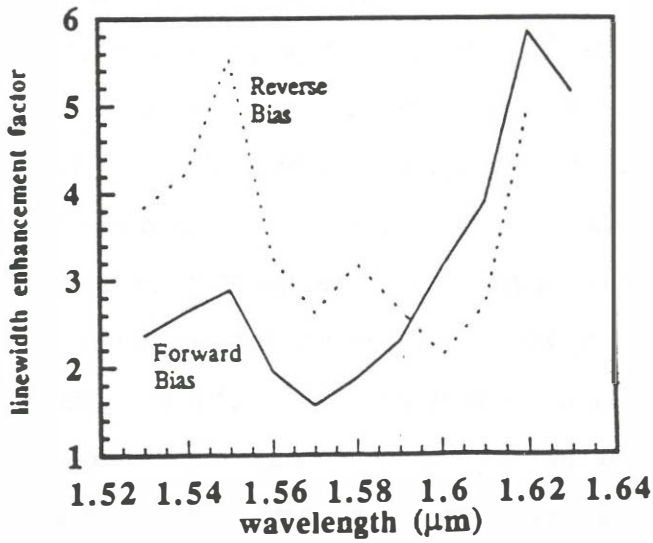

Figure 5.22 A technique to measure the linewidth enhancement factor in forward and reverse biased segments. The long segment of a two segment laser acts as a spontaneous emission source for the short segment under test. The shift in longitudinal modal frequency and gain through the section with bias voltage or current is used to calculate α. Measurements of α versus wavelength are given for forward and reverse biases in a 4 InGaAs quantum well structure (1.55 μm with 1.3 μm Q barriers).

order to produce a broadband amplified spontaneous emission output for the test signal to the right hand segment. The right hand segment is the saturable absorber segment under test. The amplified spontaneous emission from the middle section acts as a "white" noise segment to look at the gain and phase shift through the segment under test. The amplifier current is made large enough to provide substantial noise output but the gain is small enough that lasing can not occur. Lasing is also prevented due to the extra loss of the unsaturated absorber segment. To measure α, the change in phase delay through the segment must be connected with the change in gain through the segment. The variable of change is the voltage bias or current of the segment. The change in gain with respect to reverse bias is measured by noting the change in the output level to an optical spectrum analyzer. The spontaneous emission output level is then noted for several values of reverse bias voltages. There is enough gain in the cavity so that there are peaks and valleys in the spontaneous emission output due to Fabry-Perot longitudinal mode effects. The change in the mode location and the change in transmission through the absorber with respect to voltage level are noted and the information can be used to directly calculate the linewidth enhancement factor in the reverse biased segment using the formula:

$$\alpha = \frac{-2\, k_o\, \Delta\lambda\, L_{tot}}{\Delta g\, \lambda\, L_{seg}} \tag{5.21}$$

where k_o is 2π/(free space wavelength), $\Delta\lambda$ is the change in wavelength for a change in short segment bias, Δg is the change in the gain coefficient for a change in the short segment bias, L_{tot} is the total device length, and L_{seg} is the

length of the segment under test.

The forward biased α of the short segment can also be measured by taking the derivatives with respect to bias current of the segment instead of with respect to bias voltage. For the forward bias case on the short segment, the current in the main section must be reduced so that the device does not lase.

Figure 5.22 shows the measurement results for α in the forward and reverse biases for a 1.55 μm 4 quantum well laser structure [50] (see Figure 3.9). The quantum well structure tested here is from the same wafer that most of the high frequency mode-locking results were obtained in Section 3. Figure 5.22a shows a measured α of 3 near the gain peak of the structure with α increasing away from the gain peak for the forward biased case. The reverse biased segment shows similar behavior with slightly higher α values.

The single pass chirp through the gain-absorber cascade model of Figure 5.6 is shown in Figure 5.23. Equation 5.8 and 5.9 are used in the analysis. The leading edge of the pulse shows an up-chirp due to saturable absorption and the trailing edge shows a down-chirp due to gain saturation. The magnitude of the frequency chirp is very large and increases as the input pulse becomes narrower. In the mode-locking case, the chirp from each pass adds to that of the previous passes. The chirp would build up indefinitely on each pass through the laser if it weren't for the gain and phase response of the laser which ultimately limits these frequency excursions and therefore the achievable pulse width. Frequency chirp caused by gain and absorber saturation, and active gain modulation is the dominant mechanism for excess bandwidth production (beyond the Fourier transform limit) in mode-locked semiconductor lasers.

The gain and phase response of the amplifier actually causes a chirp of its

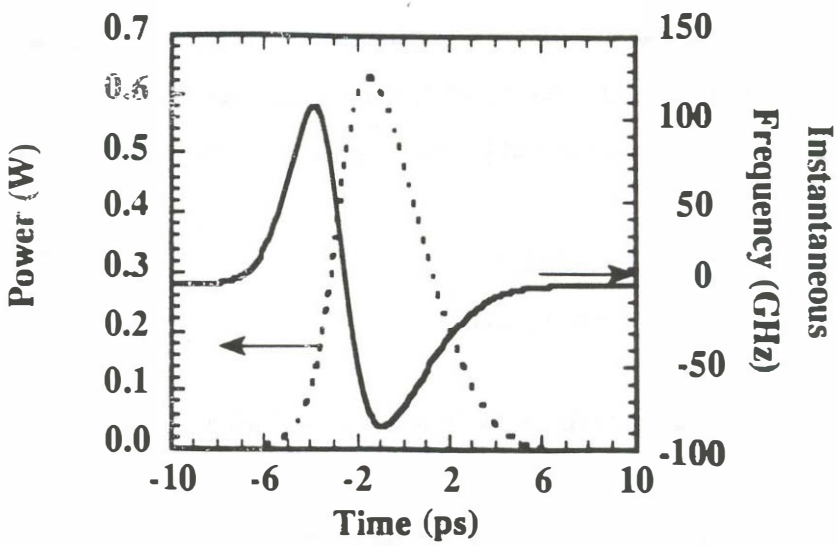

Figure 5.23 Chirp produced in a gain-absorber cascade. The unsaturated gain of the amplifier is 150 and the unsaturated transmission through the absorber is 0.05. The ratio of saturation energies is 3 and the linewidth enhancement factor is 3. The input pulse in a gaussian pulse with 5% of the saturation energy of the amplifier segment. The pulse is up-chirped on the leading edge due to absorption saturation and down chirped at the trailing edge due to gain saturation.

own, independent of gain saturation. The chirp is caused by gain dispersion due to the magnitude and phase response of the gain medium as is shown in Figure 5.4. For the case of no gain saturation the input-output relationship was represented analytically by Equation 5.13. Agrawal has presented an analytical solution for the pulse chirp of a gaussian input pulse to an unsaturated amplifier. The formula from Agrawal is shown for $\alpha=1$ which models well the group velocity dispersion found in semiconductor lasers at the gain maximum:

$$\delta\nu(t) = \frac{(d^2 g_{goal} L)t/(2\pi T_o)}{(1+ d^2 g_{goal} L)^2 + (d^2 g_{goal} L)^2} \qquad (5.21)$$

where $\delta\nu(t)$ is the instantaneous frequency deviation, T_0 is the optical pulse width, and d is t_2/T_0.

The linear frequency chirp induced on an initially unchirped pulse by group velocity dispersion is shown in Figure 5.24. The chirp sign is such that the instantaneous frequency rises with time. It should also be noted that gain bandwidth widens the input pulsewidth since the spectral components away from the gain peak receive attenuation.

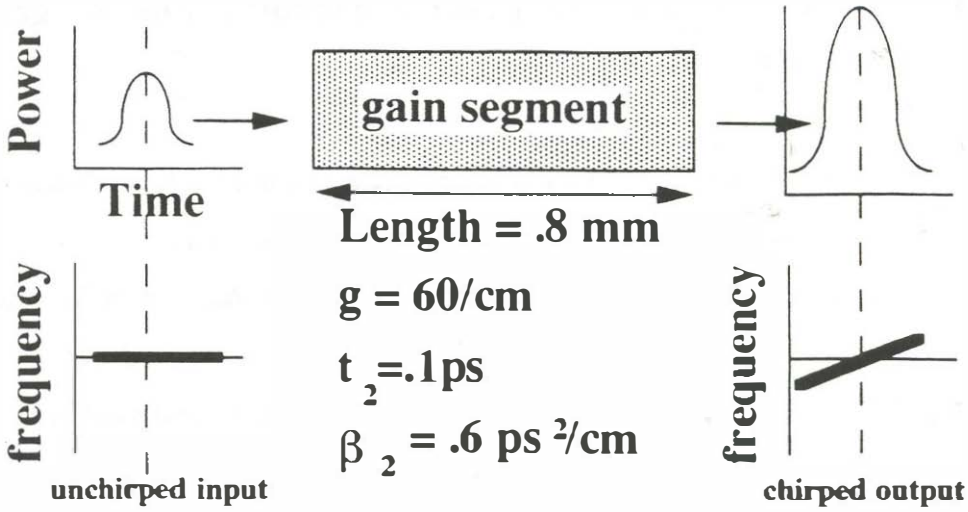

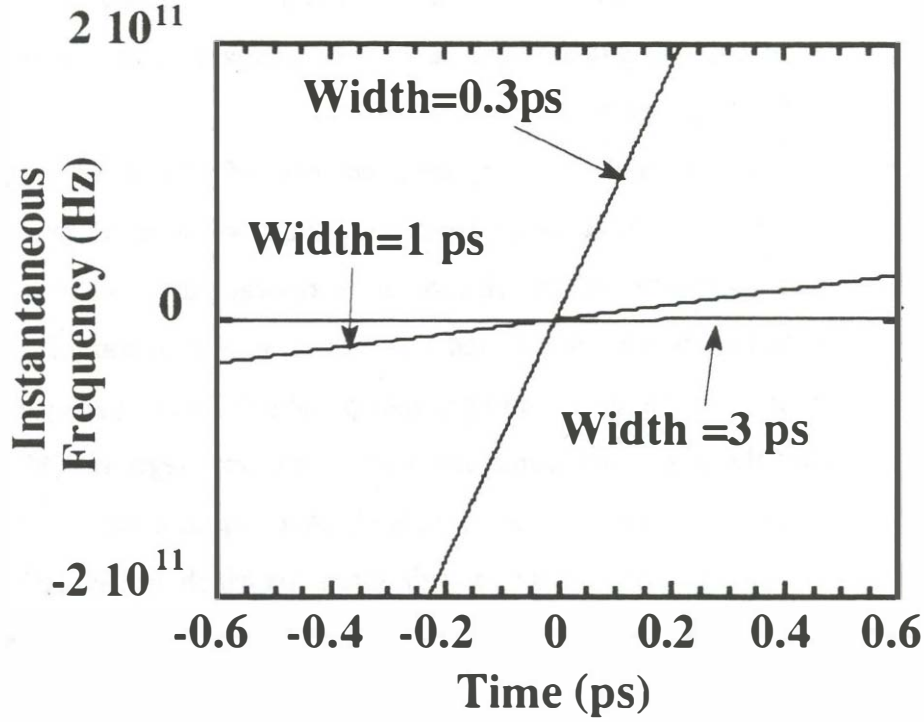

Figure 5.24 The finite gain bandwidth of a laser amplifier imparts a chirp onto a initially unchirped input signal. The simulation parameters are listed above the graph. The calculation has been done for 0.3, 1, and 3 ps gaussian input pulses. Gain saturation effects are not included in this calculation.

5.6 Amplifier induced pulse broadening due to gain-bandwidth effects

In Section 5.3 the phenomena of pulse broadening in optical amplifiers due to gain saturation was studied in conjunction with the analysis of saturable absorption. In this section, another pulse broadening mechanism in optical amplifiers is studied. This pulse broadening mechanism is produced by the amplifier's gain bandwidth. The phenomena of gain bandwidth can be compared to the performance an electrical bandpass filter. As an electrical signal passes through a bandpass filter the magnitude and phase of the spectral components of the input are modified. If the input happens to be a pulse, both the magnitude and the phase response of the bandpass filter can lead to broadening of the input pulse.

Since we have separately discussed the phenomena of pulse broadening due to gain saturation, this section concentrates on the situation where the gain in the amplifier does not change on amplification of the optical pulse. When g is not time dependent Equation 5.1 was solved analytically, with Equation 5.13 being the result. In this section, the widening of the optical pulse will be analyzed for as single pass through a semiconductor laser amplifier. Agrawal [89] has developed analytic expressions for the pulse broadening in a semiconductor laser amplifier under the condition of no gain saturation which is repeated below for convenience for the typical dispersion level found in semiconductor lasers.

$$f_b = \left[\frac{(1+d^2 g_{goal} L(1+C))^2 + (d^2 g_{goal} L)^2 (1-C)^2}{1+d^2 g_{goal} L(1+C) - d^2 g_{goal} LC(1-C)} \right]^{0.5} \tag{5.22}$$

where f_b is the broadening factor (the output pulsewidth/input pulsewidth for one pass), d is t_2/(input pulsewidth), C is the linear chirp parameter for a gaussian input pulse defined by:

$$A(t) = \exp\left[-(1-iC)t^2/2\right] \qquad (5.23)$$

Equation 5.23 represents the results for a linearly chirped gaussian pulse with the instantaneous frequency deviation being zero at the pulse center. C is defined in such a way that if C is positive, the instantaneous frequency increases with time. It is very common to have a chirped input pulse to an optical amplifier because of self-phase modulation effects as was discussed in Section 5.5.

Equation 5.22 is plotted out in Figure 5.25. The plots show the pulse broadening factor versus input pulsewidth for one pass through a laser amplifier segment. A t_2 value of 0.1 ps is used for all calculations in this section. Figure 5.25 is done for the unsaturated gain level of 150 typically found in the passive mode-locked lasers of Section 2.4.

Lets first examine the case of zero input chirp. An important broadening level to look for is the input pulse width at which the pulse broadening level reaches 20%. At this input pulsewidth, the pulsewidth broadening function is equal in magnitude to the pulsewidth narrowing function found in semiconductor waveguide saturable absorbers (see section 5.3). The 20% broadening level represents a fundamental limit to the achievable pulsewidth in these multi-segment structure designs. For the gain = 150 case, a 0.5 ps pulsewidth should be achievable.

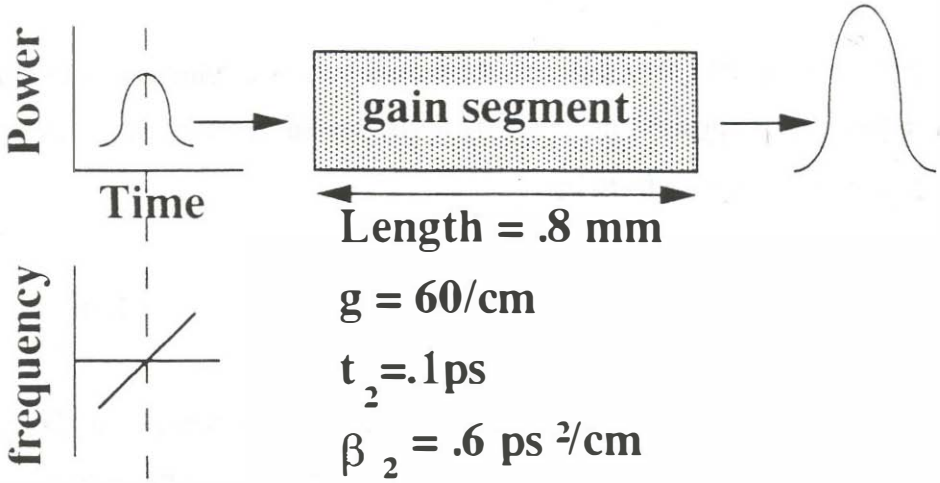

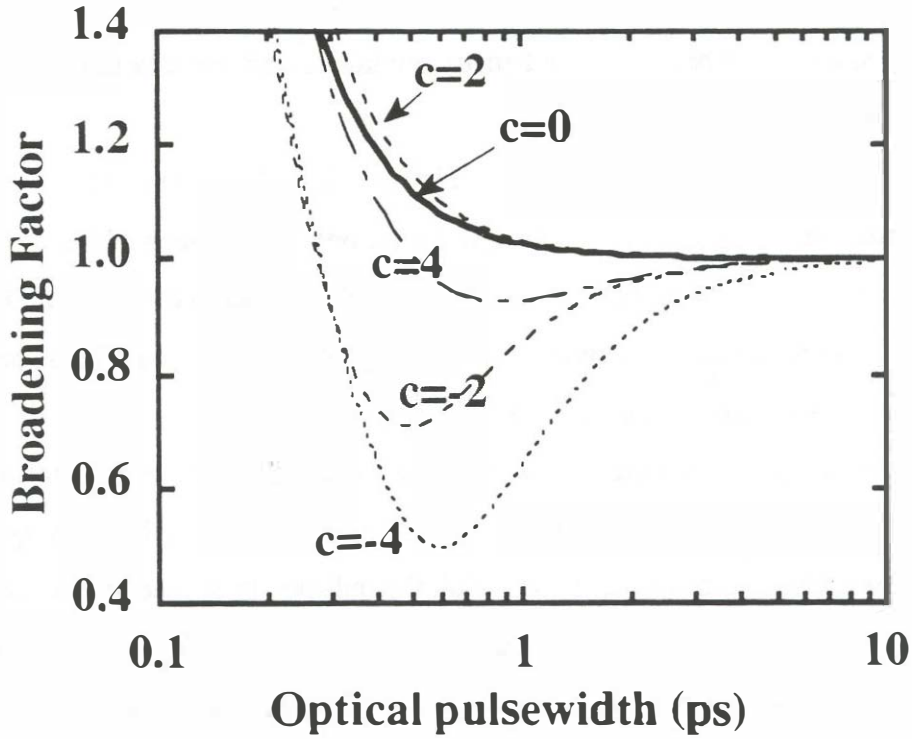

Figure 5.25 Pulse broadening factor (output pulsewidth / input pulsewidth) for a semiconductor laser amplifier not including gain saturation effects. The input pulse is a chirped gaussian pulse with chirp parameter, C. The chirp is linear with the frequency deviation zero at the center of the optical pulse. Note that this type of chirp is not typically found in mode-locked semiconductor lasers. This plot is meant to be informative and lead up to the information in Figure 5.30.

For the case of C>0 (an upward chirping input in time), the pulsewidth broadening function becomes even stronger. This can be understood from the sense of the group velocity dispersion. Semiconductor laser amplifiers have a group velocity dispersion such that the group velocity decreases with increasing optical frequency. If the chirp is upward in time, the leading edge of the pulse will travel faster than the trailing edge of the pulse leading to pulse broadening.

For the case of C<0 (a downward chirping input in time), the pulsewidth actually can become narrowed for certain input pulsewidth ranges. As the instantaneous frequency swings from negative to positive instantaneous frequency deviations, the center portion of the pulse receives more gain than the edges of the pulse.

As the pulsewidth changes due to gain dispersion, so does the energy gain of the semiconductor laser amplifier. The energy gain in the laser amplifier for the case of no gain saturation is given as [89]:

$$G_e = \frac{G_o}{(1+d^2 g_{goal} \; L)^{0.5}} \qquad (5.24)$$

where G_e is the energy gain through the amplifier, and G_o is $\exp(g_{goal}L)$.

Figure 5.26 shows the energy gain as a function of the optical pulsewidth for several values of the unsaturated gain through the device. As the pulse broadening effects increase for short input pulsewidths, the energy gain in the device also drops.

Since we are concerned with the operation of a mode-locked laser, dispersion can build up over many round-trips and the pulse effectively sees an infinite length of the gain medium. Agrawal [89] defines a dispersion length

For the case of C>0 (an upward chirping input in time), the pulsewidth broadening function becomes even stronger. This can be understood from the sense of the group velocity dispersion. Semiconductor laser amplifiers have a group velocity dispersion such that the group velocity decreases with increasing optical frequency. If the chirp is upward in time, the leading edge of the pulse will travel faster than the trailing edge of the pulse leading to pulse broadening.

For the case of C<0 (a downward chirping input in time), the pulsewidth actually can become narrowed for certain input pulsewidth ranges. As the instantaneous frequency swings from negative to positive instantaneous frequency deviations, the center portion of the pulse receives more gain than the edges of the pulse.

As the pulsewidth changes due to gain dispersion, so does the energy gain of the semiconductor laser amplifier. The energy gain in the laser amplifier for the case of no gain saturation is given as [89]:

$$G_e = \frac{G_o}{(1+d^2 g_{goal} \; L)^{0.5}} \qquad (5.24)$$

where G_e is the energy gain through the amplifier, and G_o is $\exp(g_{goal}L)$.

Figure 5.26 shows the energy gain as a function of the optical pulsewidth for several values of the unsaturated gain through the device. As the pulse broadening effects increase for short input pulsewidths, the energy gain in the device also drops.

Since we are concerned with the operation of a mode-locked laser, dispersion can build up over many round-trips and the pulse effectively sees an infinite length of the gain medium. Agrawal [89] defines a dispersion length

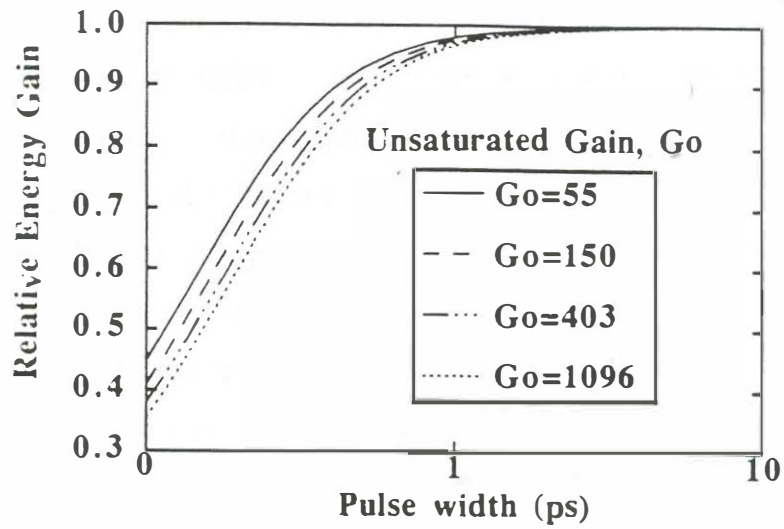

Figure 5.26 Relative energy gain versus input pulsewidth for several values of the unsaturated amplifier gain. The optical bandwidth is reduced with increasing gain. The t_2 value in this simulation is 0.1ps.

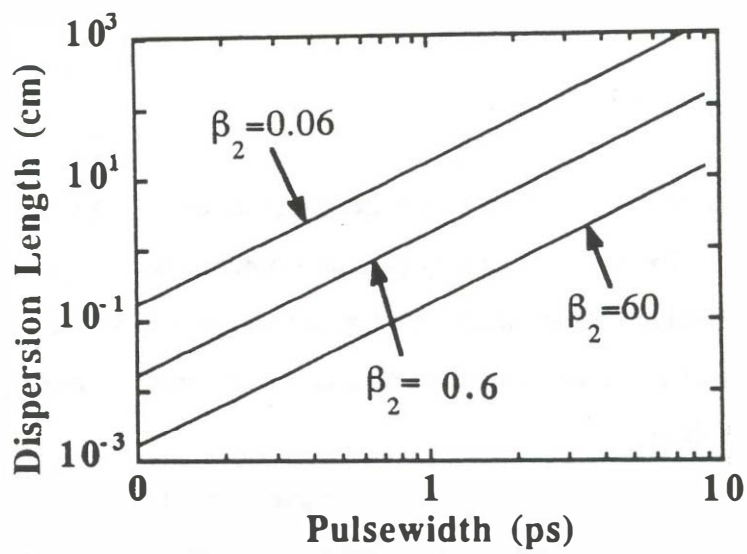

Figure 5.27 Dispersion length as a function of the input optical pulsewidth. The plot is done for several group velocity dispersion values. The gain for the calculation is 60/cm and the bandwidth parameter, t_2 is 0.1ps.

parameter that estimates the distance that the pulse must travel in order for gain dispersion effects to become significant. The dispersion length, L_d, was defined as:

$$L_d = \frac{1}{\beta_{eff}} \tag{5.25}$$

Figure 5.27 shows the dispersion length versus input pulsewidth for several values of the group velocity dispersion coefficient, β_{eff}. For the typical group velocity dispersion value of 0.6 ps^2/cm, and an optical pulsewidth of 2 ps, the dispersion length would be 1 cm which represents 10 round trips around the external cavity mode-locked laser lengths of section 1.5. This shows that dispersion is an important factor in mode-locked semiconductor lasers.

For the case of a down-chirped signal ($C>0$, the leading edge of the pulse is higher in frequency than the trailing edge of the pulse) it is clear that there is certain range of input pulsewidths there can be pulse compression as is shown in Figure 5.25. This compression of the pulsewidth can not continue indefinitely. The pulse will compress until the chirp on the pulse reverses and the chirp becomes wider on each pass. Figure 5.28 illustrates the pulse evolution versus round trip number for an input pulse that is initially down-chirped such that the pulse is initially compressed. The pulse widens and then expands showing that in a mode-locked laser where the pulse makes many round trips around the laser, that the pulse compression condition of Figure 5.25 can not continue over many passes.

The chirped input pulses that are produced in the laser amplifier from self-phase modulation do not show the perfectly linear chirps which have been

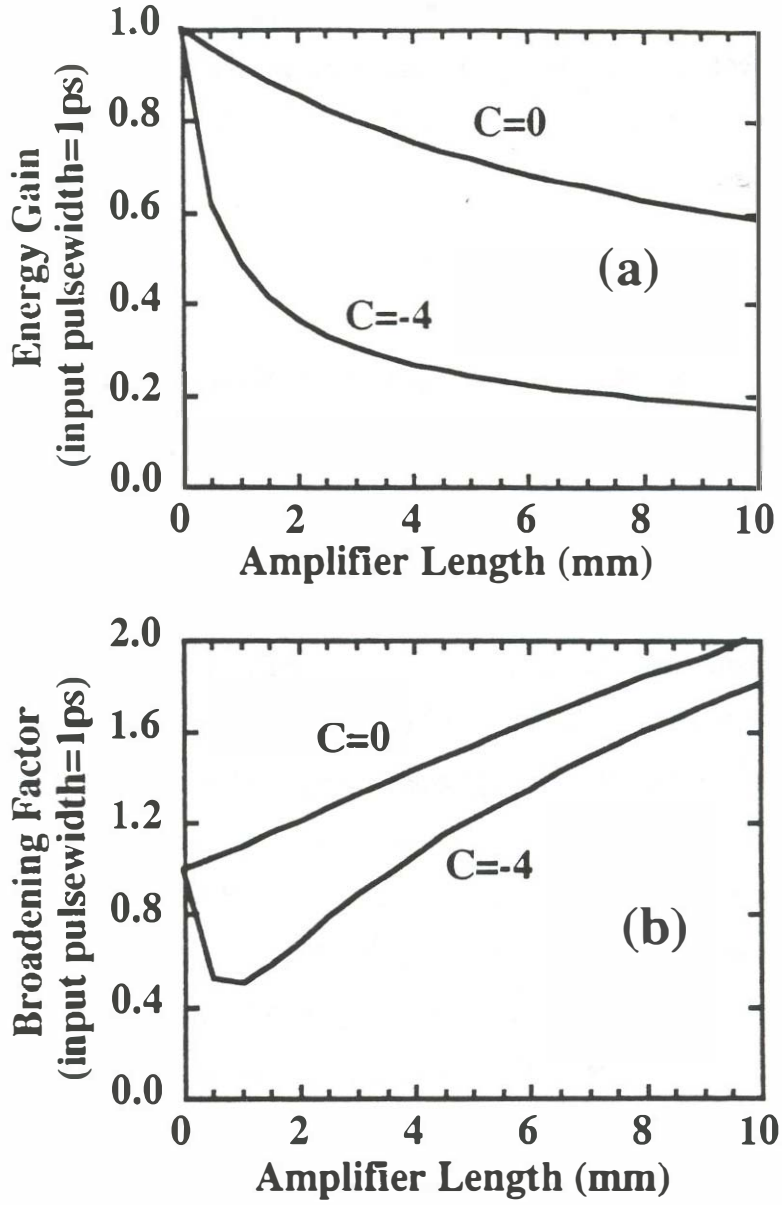

Figure 5.28 The relative energy gain (a) and pulsewidth evolution (b) for different lengths of an optical amplifier and signs of input chirp. The gain coefficient is 60 /cm, the bandwidth parameter is 0.1 ps, the group velocity dispersion is 0.6 ps*ps/cm and the input pulsewidth is 1 ps. This plot shows that pulses with a sign of chirp that causes initial compression will eventually become broadened. The energy gain is also much smaller for the pulse which is initially compressed.

studied in this section so far. Figure 4.2b shows that the chirp caused by gain saturation causes a down shift in the instantaneous frequency in the center portion of the optical pulse. Figure 5.29 graphically shows the implications of this type of chirp on the pulse broadening due to gain bandwidth effects. The wings of the pulse obtain large amplification because the instantaneous frequency is more centered near the peak of the gain. The center part of the pulse experiences less gain because the instantaneous frequency is away from the gain maximum in frequency. Thus this type of chirp sees a much large pulse broadening effect than the linear chirps found in Figure 5.25. Figure 5.30 shows the effects of having a chirped input pulse caused by self-phase modulation together with the gain-bandwidth effects of the laser. The chirped input pulse is created using equations 5.8-5.12 and with an unchirped input pulse, unsaturated gain of 150, t_2 value of 0.1ps, and α=0,3, and 6. The output pulse energy is chosen to be at E_{sat}. The pulse broadening function shows that the pulsewidth is much more strongly broadened than the results of Figure 5.25. For a saturable absorber broadening factor of 0.8 and a typical linewidth enhancement factor of 3, the achievable pulsewidths is in the 2 ps region. This plot gives the most clear evidence so far in the chapter as to why sub-picosecond pulsewidths are not achieved in multi-segment mode-locked lasers. Figure 5.30b also shows the decreased energy gain in the segment when the pulse-width narrows. Since the chirp actually builds up with each pass through the laser Figure 5.30 would over-estimate the achievable pulsewidth. The curves will scale with the required power from the amplifier and the limitations on pulsewidth will be smaller if less energy is extracted from the amplifier due to reduced self-phase modulation levels.

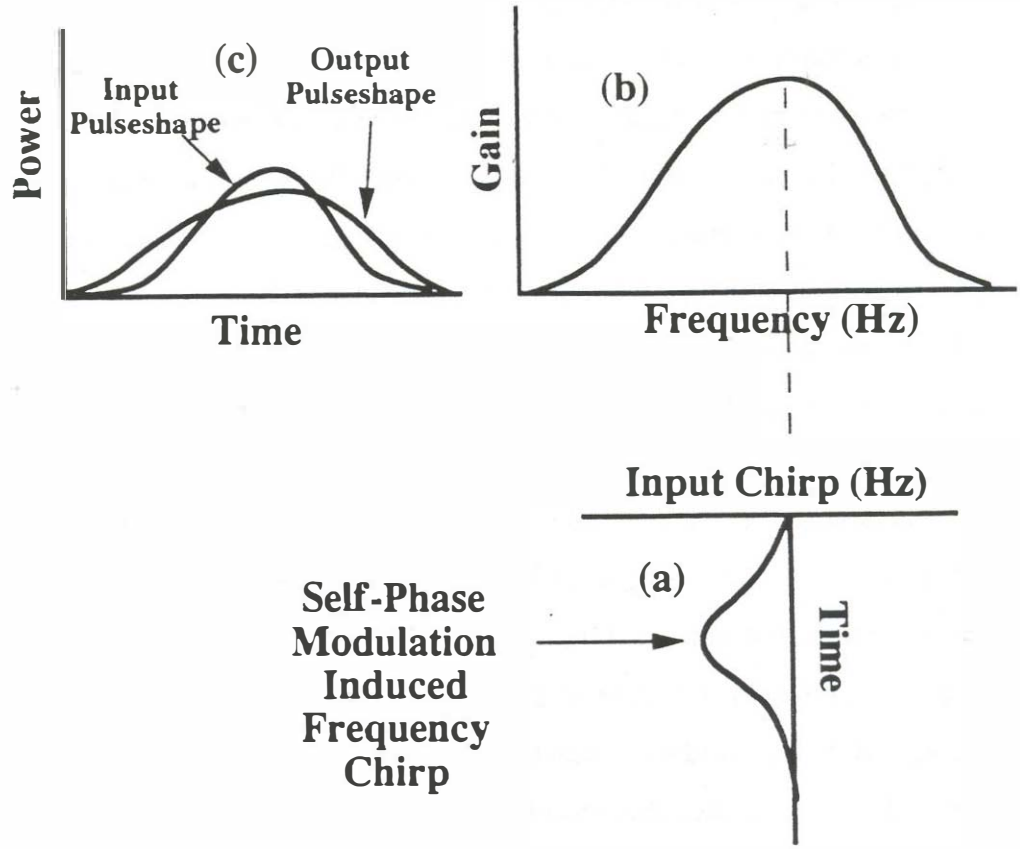

Figure 5.29 Pulse broadening in an optical amplifier for the type of input chirp caused by gain saturation. (a) The chirped input pulse that is caused by gain saturation (see Figure 4.2b) (b) The gain-bandwidth function of a Lorentzian shape (c) The approximate input and output pulse shapes are given. Note that this type of input chirp is very effective in broadening the input pulse. The wings of the pulse receive more gain that the peak of the pulse.

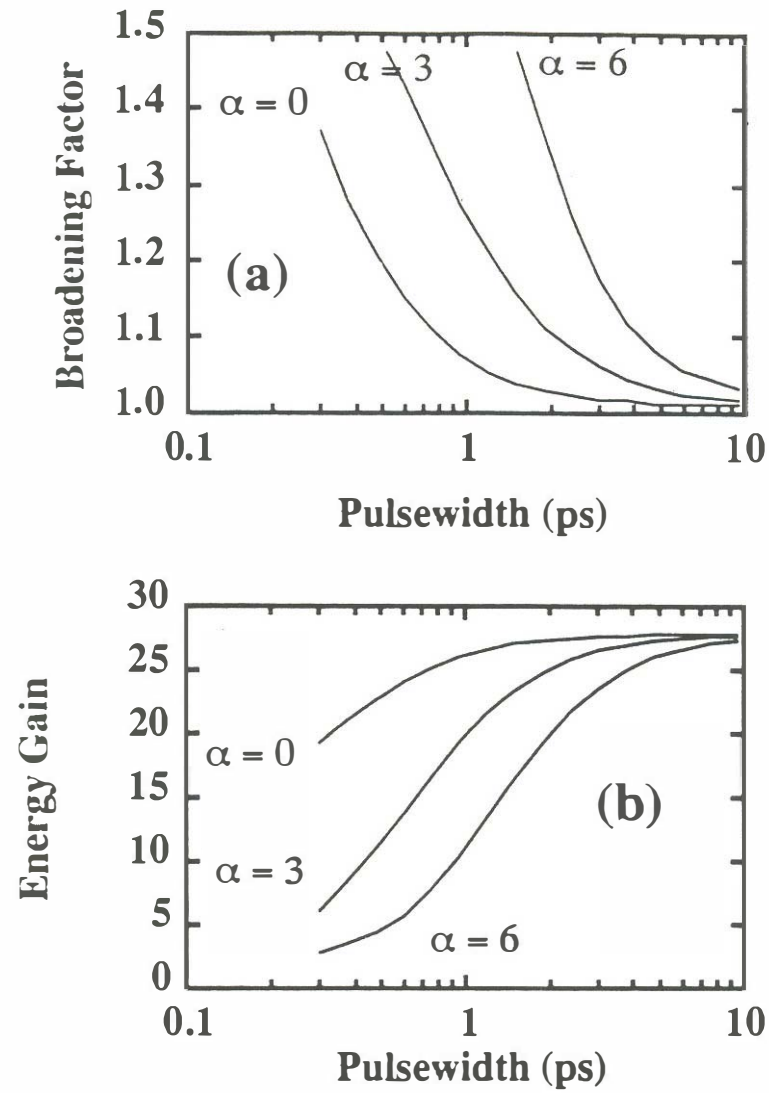

Figure 5.30 Pulsewidth broadening of the type illustrated in Figure 5.29. (a) The pulsewidth broadening factor for an input chirp caused by gain saturation. The chirped input pulse is formed by passing an input pulse into a laser amplifier and saturating it. The output energy is chosen to be equal to the saturation energy of the amplifier. This provides the chirped input pulse to an amplifier which only has the gain bandwidth effects included and gain saturation effects are omitted. The gain coefficient for the simulation is 60/cm and the amplifier length is 800 μm. The bandwidth parameter is 0.1ps. (b) The energy gain for the corresponding cases of (a). All simulations are done for three values of the linewidth enhancement factor. The simulations show clearly the effects of α on limiting the optical pulsewidth.

5.7 Laser structure design

The previous sections in chapter 5 analyzed the pulse narrowing and pulse broadening effects that occurred for a given set of parameters. Many of those parameters were structure dependent and this section discusses how these structure parameters can be optimized for best mode-locked laser performance. From the previous sections, the following structure parameters are under the designers control:

a. The gain bandwidth of the laser. (One wants to maximize the bandwidth)

b. The ratio of saturation energies between the gain and saturable absorber segments. (One wants to maximize the ratio)

c. The linewidth enhancement factor.(One wants to minimize α)

d. Device parasitics. (One wants a large cut-off frequency)

e. Waveguiding parameters

Each of these points will be addressed separately and suggestions will be made for best mode-locked laser performance.

5.7.1 Gain bandwidth

Quantum well lasers can be designed to have a larger gain bandwidth than bulk active region semiconductor lasers. An approximate expression (see reference 90 for a more accurate formulation including k selection rules) for the gain in a semiconductor laser amlifier is given as [19]:

$$\alpha(E) = \frac{c1}{E} \int_{-\infty}^{+\infty} \rho_c(E') \rho_v(E'') \left|M_{if}\right|^2 (1-f_v(E'')-f_c(E')) \, dE' \tag{5.26}$$

where α is the loss or gain coefficient, c1 is a proportionality constant, E is the photon energy that you want to calculate the gain for, E' is the dummy variable of integration with E"=E'-E, ρ_c is the conduction band density of states, ρ_v is the valence band density of states, f_c is the fermi function for the conduction band, f_v is the fermi function for the valence band with increasing energy measured in the opposite direction as that for the conduction band, and M_{if} is the momentum matrix element between state i and f.

Because of the step-like density of states in a quantum well semiconductor lasers, the gain versus carrier density curve will be flatter at high carrier densities. Also, quantum well lasers usually operate at much higher carrier density level than bulk active region lasers. This higher carrier density level means that the Fermi level is higher in energy and there is gain over a much wider range of energies. It is also possible to space the quantized energy sub-band levels in quantum well lasers so that there is a flat versus gain versus energy well into the second quantized energy level. Figure 5.31a shows calculated gain versus wavelength curves for various widths of a quantum well structure. These calculations are for a single quantum well. To get the actual gain for a device you must multiple by the optical confinement factor. The calculations are done for the InGaAs/InP system which is used for long wavelength (1.3-1.5 μm) quantum well lasers (these calculations were done using the gain calculation program from Scott Corzine's Ph.D dissertation). Similar calculations are done for a GaAs/AlGaAs quantum well laser example in Figure 5.31b. Amplifier bandwidths of over 10 THz are shown in both of these calculations.

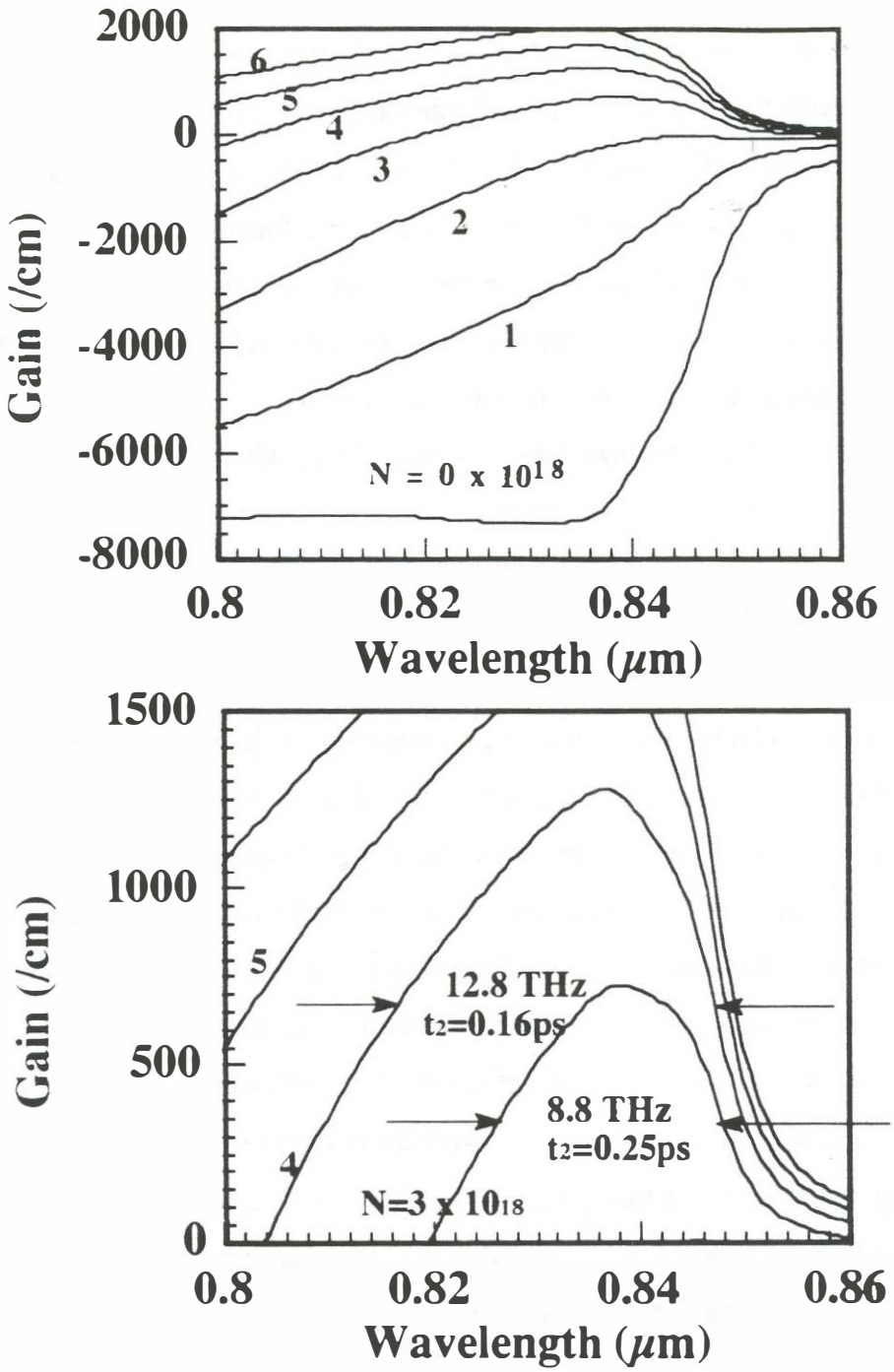

Figure 5.31a Gain versus wavelength for a 10 nm GaAs quantum well with AlGaAs (40% Al) barriers. The bottom curve shows a blow-up of the gain region with two example measurements of the bandwidth parameter, t_2. A bandwidth parameter of 0.1ps was used for most of the calculations in this chapter.

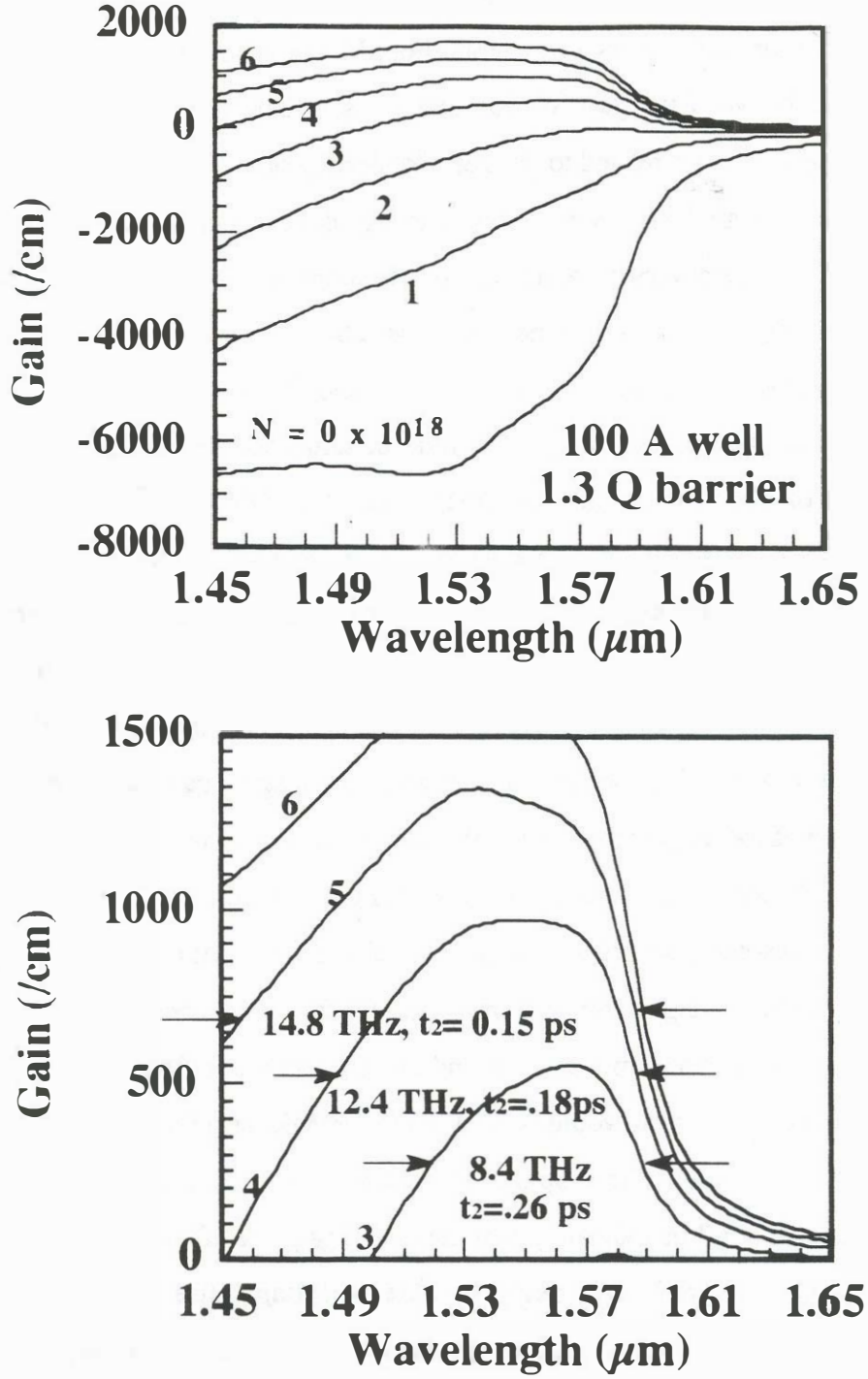

Figure 5.31b Gain versus wavelength for a 10 nm InGaAs quantum well with a lattice matched InGaAsP barrier (1.3μm Quaternary composition). The bottom curve shows a blow-up of the curve with example calculations of the bandwidth parameter, t_2.

5.7.2 Ratio in saturation energies

Quantum well lasers in general should have a larger ratio in saturation energies between the gain section and the saturable absorber section. This phenomena is again related to the step-like density of states function in quantum wells as compared to the square root of energy dependence in bulk active region lasers. The gain versus carrier density function at a specific wavelength is shown in Figure 5.8. The trend is that the ratio of saturation energies is found to be largest for the narrow quantum wells and for operation at near the gain maximum. The actual value of the ratio of saturation energy depends on the number of wells chosen and the actual carrier density used in device operation but values in the range of 2-5 are achievable. It would seem that the largest ratio in saturation energies would be for single quantum well devices since they tend to operate at the highest carrier density levels. Single quantum well devices also require larger saturable absorber lengths since the confinement factor is so low. The longer saturable absorber lengths can lead to decreased saturable absorber performance if the propagation time through the saturable absorber becomes comparable to the optical pulse width. In the case of a long saturable absorber, the self-colliding pulse effects would be diminished, leading to a higher bleaching energy and wider pulsewidth. For a confinement factor of 0.03 in a single quantum well laser and an absorption coefficient of 8000 cm^{-1} and the absorber length would be 120 μm (SCPM design) for a 2% unsaturated transmission value. The propagation time across a 120 μm long segment is approximately 3.2 ps indicating that the colliding pulse effect is not as large in single quantum-well laser designs. The colliding pulse argument favors designs with large optical confinement factors such as bulk active region lasers or multi-quantum well lasers. Limited experimental evidence shows that large

optical confinement factor designs perform better.

The gain characteristics of quantum well lasers can also be substantially altered with the incorporation of strain into the quantum well. By growing lattice mismatched layers with thickness smaller than the critical thickness, the bandstructure of the device can be substantially altered. This may lead to the possibility of a higher differential gain ratio between the gain and saturable absorber segment.

5.7.3 Linewidth enhancement factor

The theoretical analysis of Section 5.5 and 5.6 clearly show that large α factors are detrimental to mode-locked laser performance. Experimentally α factor values as low as 1 and as high as 30 have been measured [93]. The values of α are reported to be lower for quantum well lasers as compared to bulk active region lasers. This is presumable due to the flatter magnitude response that is achievable for quantum well lasers that was observed earlier in this section. Strain has been shown to substantially affect the α factor [94]. Recent theoretical research has shown that it may be possible to achieve $\alpha=0$ by the simultaneous use of strain, p-doping in the active region, and detuning the operation wavelength to a wavelength slightly shorter than that for maximum gain. In any case, one is best to operate at the gain maximum or slightly shorter wavelength for the smallest α. Often times the operating wavelength in passive mode-locked laser is longer than the gain maximum. The tendency to move to longer wavelengths is important because the α factor increases away from the gain peak and large α factors result in larger pulse broadening effects.

5.7.4 Device parasitics

In general the smaller the device parasitics, the better the mode-locked laser performance. The need for small electrical parasitics is especially true for active gain modulation. For passive and hybrid gain modulation, the laser parasitics are of less importance because saturable absorption is the dominant pulse shortening mechanism. The general guidelines for achieving a low capacitance structure are:

1) Raise the bondpads off the semiconductor surface to reduce capacitance[95].

2) Optimize the to p-contact for lowest contact resistance.[96,97]

3) Avoid the formation of large parasitic diode layers parallel to the lasing region (even if they have a larger turn-on voltage as they will contribute to device capacitance)

Inter-contact resistance is another device parameter that is important for multi-section mode-locked laser designs. Since the gain section typically will be biased at approximately 1.5 volts positively and the saturable absorber may have a negative 2 volts applied, there is a possibility of a large inter-contact current if the inter-contact resistance is not large enough. The drawing of current between contacts represents no particular disadvantage in terms of mode-locked laser performance unless it contributes substantially to heating of the device. In the 1.55 μm monolithic cavity devices of Chapter 3, 0.5-1.5 kΩ of resistance was sufficient. A 10 μm gap was used between segments and the low bandgap contact layer was etched away. Proton bombardment in GaAs material is an effective way to increase the inter-contact resistance. Proton bombardment does not work well in the long wavelength system. Larger gap widths can also increase the inter-contact resistance, but these unpumped segments must be easily bleached. Long unpumped regions contribute to

higher device operating currents and are not effective as saturable absorber segments due to their long recombination lifetime (>0.5 ns).

5.7.5 Waveguiding parameters

As was discussed in the saturation energy ratio part of section 5.7, large confinement factors tend to produce better results. In high-speed laser design, it is important to have a tightly confined optical mode in order to get a high photon density. High photon densities are important because the resonance frequency of a high speed laser is proportional to the square root of the photon density. In mode-locked lasers, the design goals are different. In most cases we are searching for higher energy pulses and the goal is therefore to achieve a higher saturation energy. The saturation energy can be increased by decreasing the differential gain as was discussed earlier in the chapter. Alternately, the modal cross section area can be increased. Single lateral and transverse mode operation is desired for mode-locked operation in most cases. The modal cross sectional area can be increased by increasing the waveguide width and height toward the limits of single mode operation.

5.8 Limits on the achievable pulsewidth

Section 5.1-5.7 discussed the various pulse widening and pulse narrowing mechanisms separately to understand their functional dependencies. The limits on the final achievable pulsewidth are reached when the gain broadening mechanisms balance with the gain narrowing mechanisms. In this section, all of the pulse shaping mechanisms will be included to determine the achievable pulsewidth limits in passive mode-locked semiconductor lasers. It is found that all of the shaping mechanisms are not equal contributors. The goal of the section is to identify the strongest pulse shaping mechanisms and how they influence the final pulsewidth.

The analysis done in this section will use the split-step method described in Section 5.2 in which the non-linearity is first calculated and then gain bandwidth effects are calculated. The equations to calculate the non-linearity are 5.8-5.12 (under the assumption of no bandwidth effects). These equations show the input-output relationship of a semiconductor laser amplifier or saturable absorber segment. The equation used to model the bandwidth effects (under the assumption of no gain saturation) is 5.13.

There are several pulse widening mechanisms that will not be considered in this section:

1) The effects of spontaneous emission noise are not included.

2) External bandwidth limiting elements are not included. Although these elements could be included in the analysis, they were not since they tend to further limit the achievable pulsewidth. This omission does not imply that the bandwidth limiting or tuning filters are not important. They are useful and may be very important if Fourier transform limited optical pulses are desired.

To explore the limits of the achievable pulsewidth, an external cavity laser example will be studied. Since passive gain modulation is the strongest pulse shortening mechanism, it will be the only shortening mechanism considered here. The example that will be studied is one that is intended to simulate the 5 GHz passive mode-locked laser experiment found in Section 2.4. In this experiment, 2.5 ps pulses with 0.7 pJ of energy were produced. The estimated saturation energy of the device was 2 pJ, the external cavity loss factor was 27, and the estimated unsaturated absorber transmission level is 0.05. The ratio of saturation energies between the gain and saturable absorber sections is 3. From Figure 5.11 the maximum pulse shortening per pass for this design is about 20%. The assumed α for the gain section is 3 and the assumed α for the saturable absorber section is 1. The smaller α in the saturable absorber section is based on measurements of this material using the method presented in Figure 5.22. The unsaturated gain in the gain section is 150 in order to obtain a saturated net gain of 27 in the gain absorber cascade model of Figure 5.6. The input energy in the model for each pass is assumed to be the input energy for maximum pulse shortening per pass (this is in the spirit of this section since the goal is to explore the minimum achievable pulsewidth). The simulations are not concerned with start-up issues. The simulation assumes an initial gaussian input pulsewidth of 10 ps and then analyzes the pulsewidth change on each pass until a steady state solution is reached in which the pulse reproduces itself on each pass around the laser.

Figure 5.32 shows the pulsewidth versus pass for the two-section passive mode-locked laser described in the last paragraph. The laser gain region is divided into 8 - 100 μm gain segments and 1 - 50 μm saturable absorber

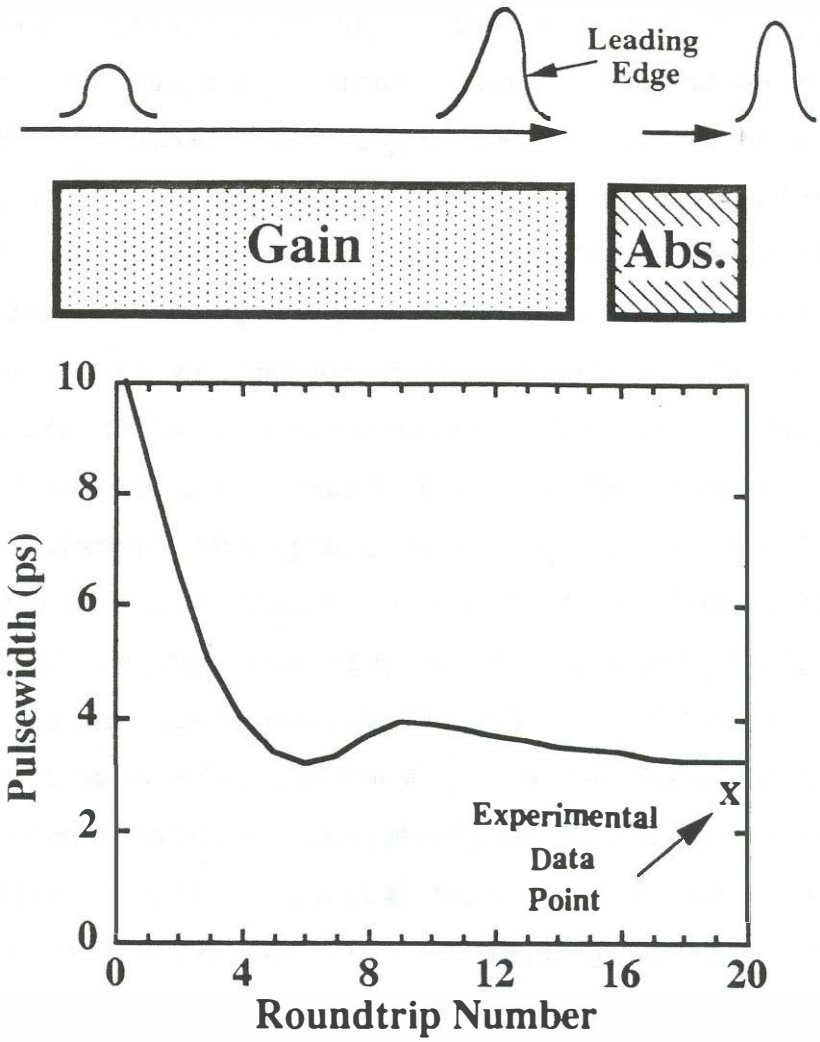

Figure 5.32 The pulsewidth evolution versus roundtrip number around a two section gain-absorber cascade model. Bandwidth effects, self-phase modulation effects, gain and absorber saturation effects are all included in the model. The unsaturated amplifier gain is 150, the unsaturated absorber transmission is 0.05, t_2 is 0.1 ps, and the ratio of saturation energies between the gain and absorber segments is 3. The initial input pulse is an unchirped 10 ps gaussian pulse. The linewidth enhancement factor is 4 in this simulation. The pulsewidth at 20 roundtrips represents the final pulsewidth in which the pulse broadening mechanisms have equilibrated with the pulse narrowing mechanisms.

segment. The starting input pulse for the simulation is a 10 ps gaussian pulse that is unchirped. The pulsewidth narrows on each pass initially at a rate slightly greater than the 20% per pass shown in Figure 5.5. After several round trips, the pulsewidth reaches a minimum steady state pulsewidth of about 3 ps. This simulated pulsewidth is typical of the 2-3 ps pulsewidths found in the two-section passive mode-locking experiments of Section 2.4.

At this point in the discussion it is instructive to try and sort out which of the listed mechanisms from Section 5.1 are most important. This will be addressed by re-doing the simulation of Figure 5.32 and eliminating widening mechanisms in order to find out which ones were the most important. Figure 5.33 shows the same analysis as that of Figure 5.32 with the linewidth enhancement factor varied from 0 to 4.. When α=0, self-phase modulation effects are not included in the simulation. The pulsewidth easily achieves half picosecond pulsewidths in this case. When the linewidth enhancement factor is increased to 4, the pulsewidth is dramatically increased to slightly over 3ps. This simulation shows the dramatic effects of the linewidth enhancement factor on the achievable optical pulsewidth.

Figure 5.34 shows the calculated optical spectrum for the steady state solution for the case of α=0 (no self-phase modulation) and α=4 (significant self-phase modulation). The time bandwidth product for the α=4 simulation is 1.9, which is far above the Fourier transform limit of 0.314 for a hyperbolic secant squared optical pulse shape. For the case of α=0, the pulses produced by the mode-locked laser are always transform limited and centered at the gain maximum. Self-phase modulation in which gain saturation dominates, causes a down-shift in frequency (see Figure 4.2b). The down shift in frequency is stopped by the decreased amplification as the spectrum moves away from the

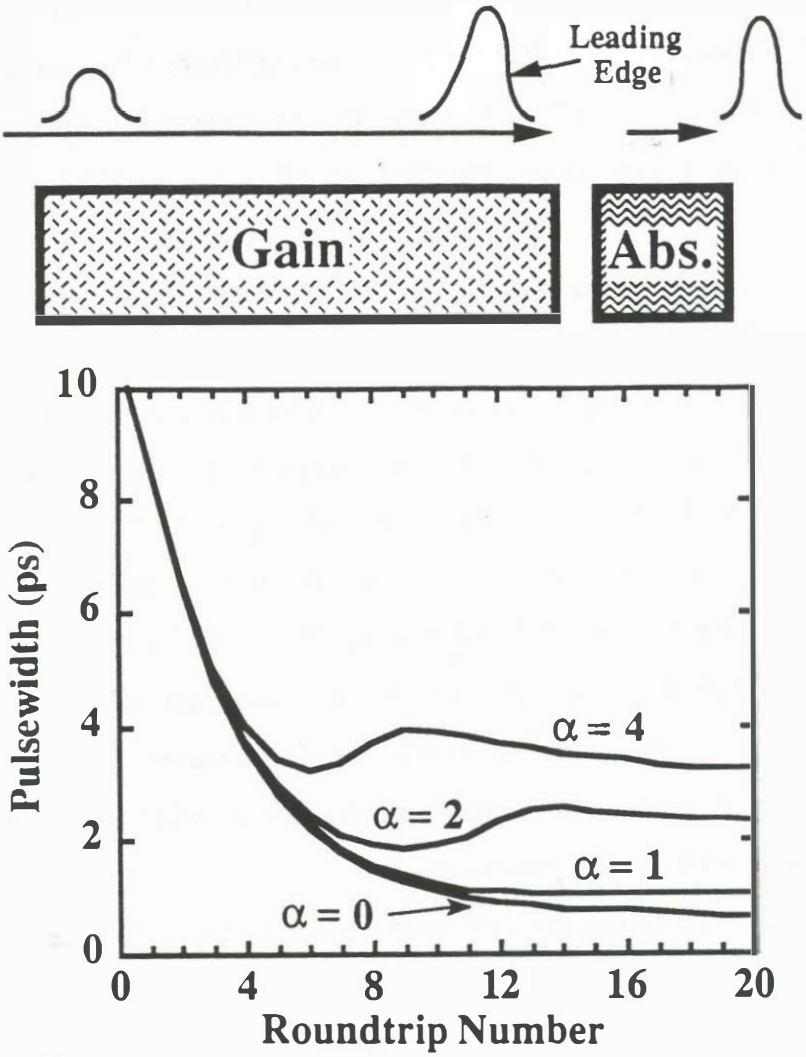

Figure 5.33 The same simulation as that of Figure 5.32 with the linewidth enhancement factor varied from 0 to 4. This simulation shows the large effect the linewidth enhancement factor has on the achievable pulsewidth in multi-section mode-locked semiconductor lasers.

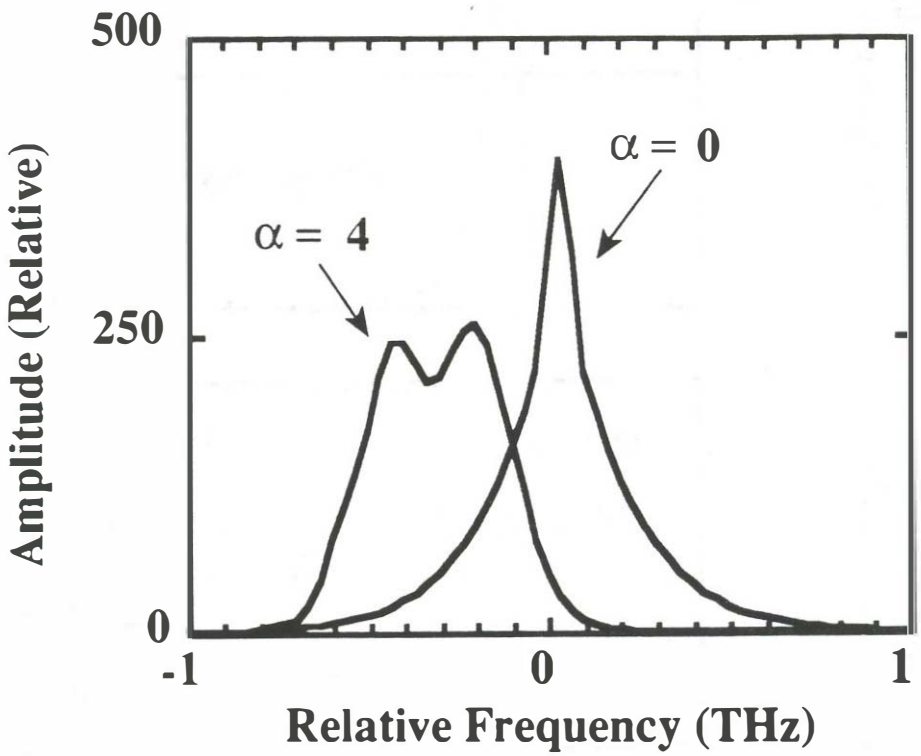

Figure 5.34 The optical spectrum after 20 round trips for the simulation of Figure 5.33 for the cases of α=0 and α=4. The optical spectrum for α=0 is Fourier transform limited since self-phase modulation is not present. The optical spectral width for α=4 is much larger even though the optical pulsewidth is much wider. The excess bandwidth is caused by self-phase modulation, which also lowers the frequency due to the fact that gain saturation dominates and causes a lowering of the optical frequency (see Figure 4.2).

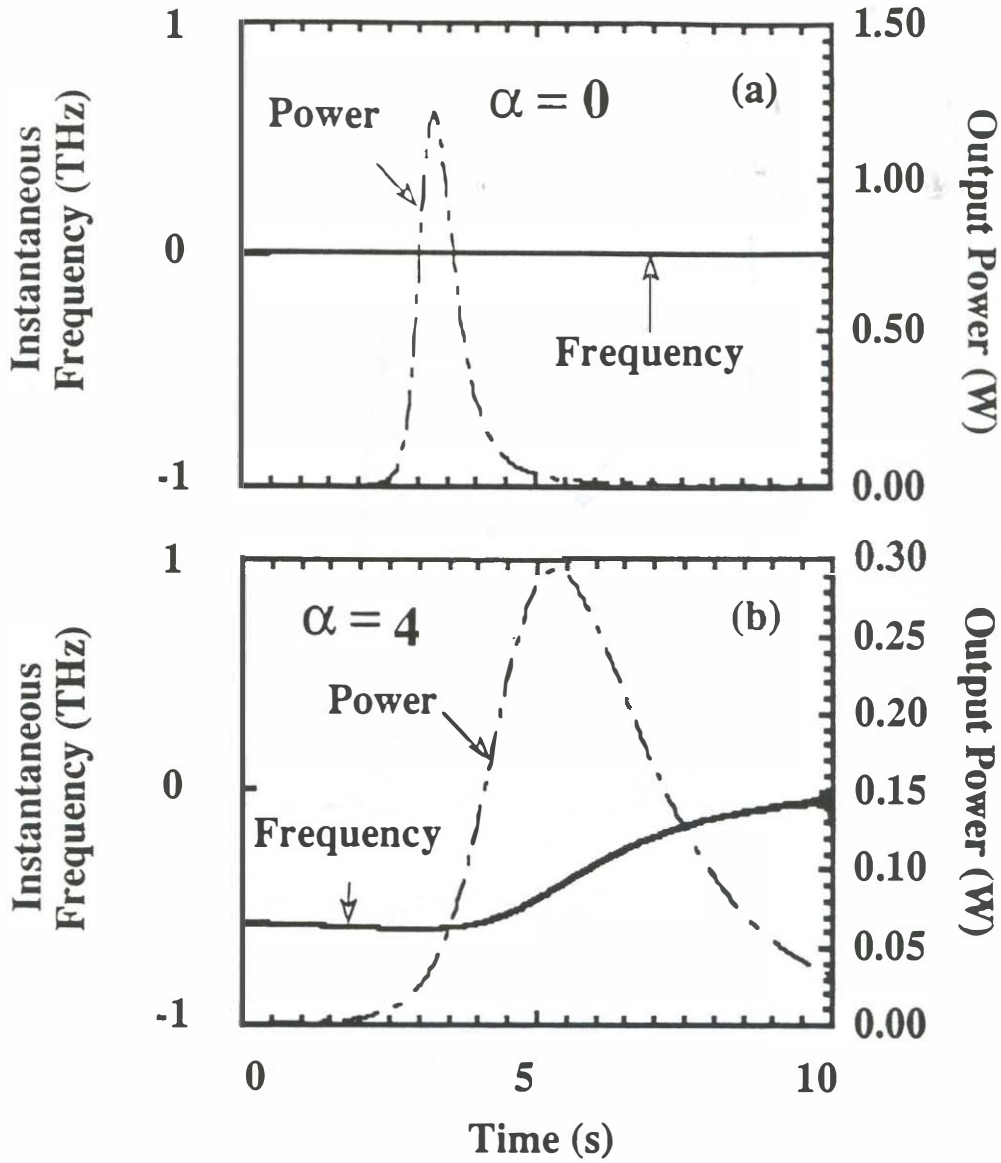

Figure 5.35 Instantaneous frequency versus time after 20 round trips for the simulation of Figure 5.33 with α=0 and α=4. The α=0 shows no frequency chirp due to the lack of self-phase modulation effects. The α=4 cases shows a rising frequency shift cause by the effects of gain saturation building up over many round-trips.

gain maximum.

Figure 5.35 shows the calculated instantaneous frequency versus time for the case of α=4 and α=0. The chirp is zero for the case of no self-phase modulation. The chirp is upward sloping for the α=4 case, but the up-chirp is such that it recovers to the gain maximum frequency only at the trailing edge of the pulse. The sign of frequency chirp has been measured by Helkey et al.[9] using a grating pair compressor. Grating pair compressors can only compress upwardly chirped signals. The 3 ps pulses were compressed to 0.5 ps in Helkey's experiment. The measured sign of chirp therefore agrees with the sense of chirp found in these calculations.

From this analysis, several important conclusions can be made.

a. *Both* the magnitude and phase response of the laser amplifier contribute to pulse broadening, but their magnitudes alone do not explain the relatively broad pulses which are observed experimentally in the passive mode-locked experiments of Section 2.4 (approximately 3 ps pulsewidth).

b. The linewidth enhancement factor, α, slows the pulse narrowing process by widening the optical spectrum and introducing a chirp that produces less gain at the peak of the optical pulse (see Figure 5.30).

The ultimate limit on achievable pulsewidth for this external cavity experiment and for these multi-segment mode-locked laser structures in general can be described as follows: **As the pulsewidth narrows, self-phase modulation creates extra bandwidth in the optical pulses. The excess bandwidth induced by self-phase modulation makes the gain bandwidth broadening mechanism much more effective.**

In summary, the optimal design of multi-section passively mode-locked semiconductor lasers has been studied. It is important to maximize the ratio of

saturation energies between the saturable absorber and gain sections. For a given ratio of saturation energies there is an optimum saturable absorber length that produces the maximum pulse shortening per pass without requiring too high of gain from the gain section. The effects of self-phase modulation and gain bandwidth were then included to establish the minimum obtainable pulse widths from these structures. For reasonably available gain-bandwidths, saturation energy ratios, and linewidth enhancement factors, it is hard to achieve pulsewidths much less than 1 ps.

Chapter 6
Analysis of timing jitter in monolithic and external cavity mode-locked semiconductor lasers

6.1 Introduction

Chapter 4 contains a section in which the pulse-to-pulse timing jitter was measured and compared for monolithic and external cavity configurations using active, passive, and hybrid mode-locking techniques. The various experiments showed a wide range of timing jitter values from 0.2 ps to over 12 ps. The experimental conclusions from Chapter 4 are listed below.

1) Passive mode-locking produces the largest timing jitter and phase noise level.
2) Monolithic cavity devices in general demonstrated higher timing jitter levels than their external cavity counterparts using the same repetition rates and mode-locking techniques.
2) Single-section external cavity active mode-locking with relatively wide (10 ps) pulsewidths produced the lowest timing jitter levels. The absolute timing jitter is dominated by the electrical modulation source.
3) Two-section external cavity active mode-locked lasers with 5 ps pulsewidths produced higher timing jitter levels than single-section external cavity active mode-locked lasers.
4) Two and three-section hybrid mode-locked lasers produced higher timing jitter levels than two-section external cavity active mode-locked lasers.

The purpose of this chapter is to understand the origin and magnitude of the differences in timing jitter measurements seen in

the experimental results of Chapter 4. Figure 6.1 illustrates the structures that are studied in this Chapter and introduces notation which will be used for describing the laser parameters incorporated in the analysis of mode-locked laser jitter. For modelling convenience, the external cavity device is considered to be similar to the monolithic cavity device except that an ideal passive waveguide is substituted for the air external cavity. An ideal passive waveguide is lossless, has an infinite bandwidth and has the same index of refraction as the gain region. The current driving pulses used in the analysis are assumed to be Gaussian shaped pulses.

The dominant cause of timing jitter in mode-locked semiconductor lasers is spontaneous emission noise. Figure 6.2 illustrates the paths that connect spontaneous emission to timing jitter. Spontaneous emission noise causes carrier density fluctuations, index of refraction fluctuations, and photon density fluctuations. Each of these fluctuation types has the potential to induce timing jitter on the optical pulse stream. Carrier density fluctuations cause gain fluctuations which are converted to laser pulse location fluctuations when the laser amplifier is operating in a highly gain saturated condition. Carrier density fluctuations couple to index of refraction variations that in turn modulate the round trip time of the mode-locked laser cavity. Photon density fluctuations, which are correlated to gain fluctuations, also lead to timing fluctuations in the highly gain saturated condition through AM to PM conversion.

In Section 6.2, the magnitude of the carrier density, index of refraction, and photon density fluctuations will be analyzed using rate equations with spontaneous emission noise sources included. The rate equations are linearized around the laser operating point taking into account the effects of the external cavity. The linearization around a steady state operating point is clearly an approximation since the photon density and carrier density values are changing

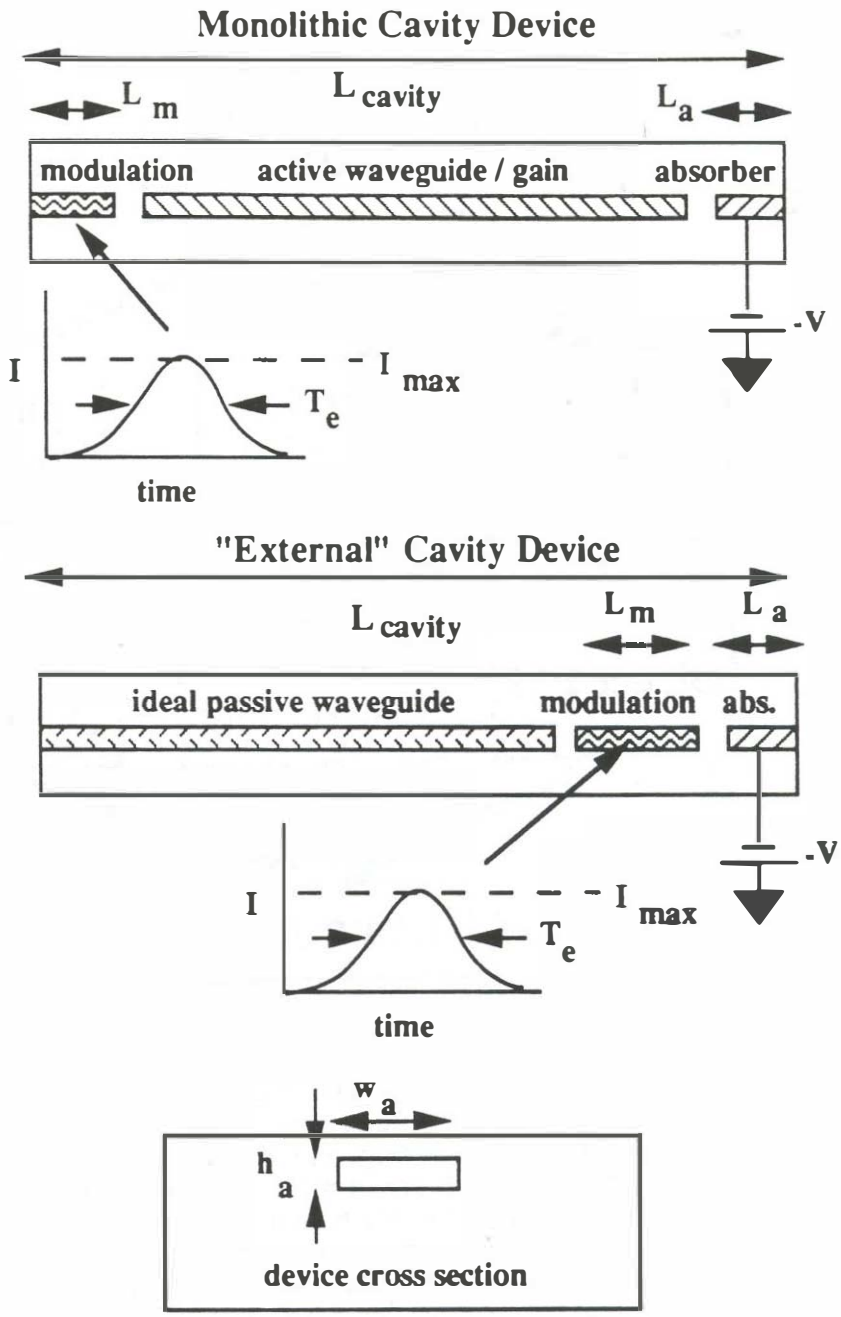

Figure 6.1. The monolithic and external cavity geometries used in analysis of timing jitter in external and monolithic cavity mode-locked lasers. Active, passive, and hybrid mode-locking techniques are used for both types.

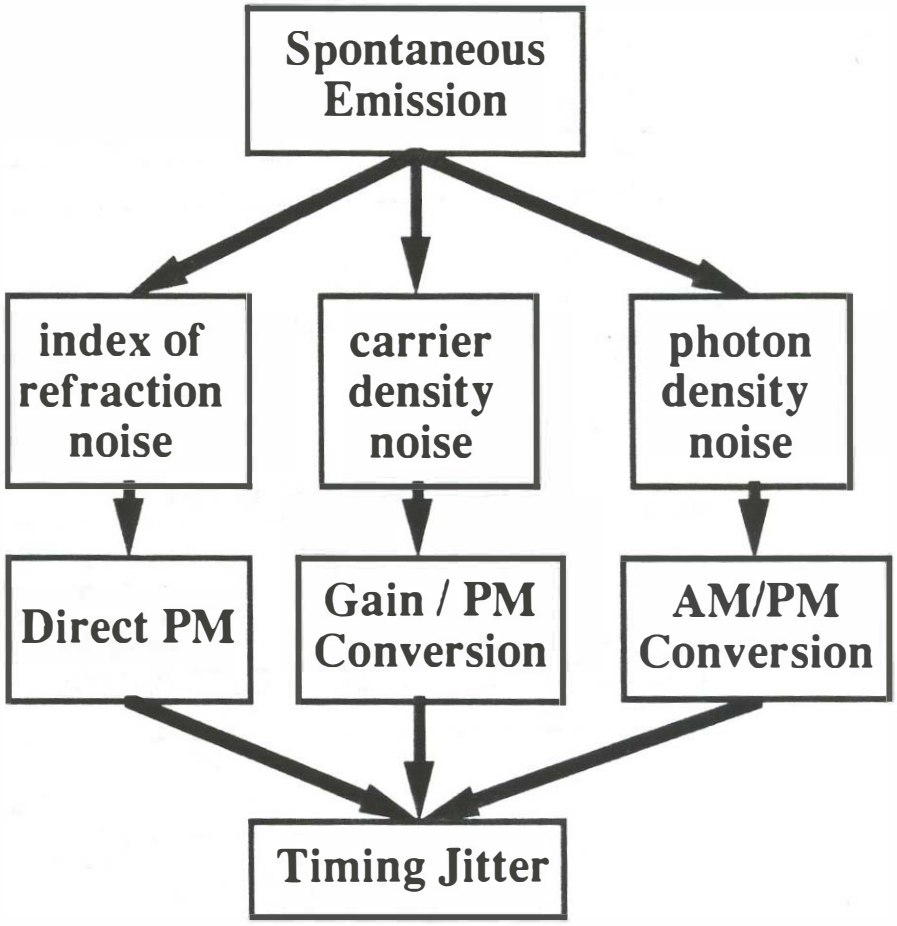

Figure 6.2 Spontaneous emission can take several paths to induce timing jitter in mode-locked lasers. A spontaneous emission event causes a carrier density drop, an index of refraction rise, and a photon density rise. Index of refraction variations directly lead to a modulation of the round trip time in the laser. Carrier density fluctuations can lead to pulse position fluctuations through a gain to phase modulation conversion process. Photon density noise can couple into timing jitter through an amplitude to phase noise conversion process.

with time in a mode-locked laser. In actual fact, the spontaneous emission rate is highly time dependent. It is assumed that a time averaged value of the carrier density and photon density can be used to get a reasonable approximation to the magnitude of the noise sources since in this analysis the noise sources of interest are at a much lower frequency than the repetition rate of the mode-locked laser. Thus the details of the time dependence of the spontaneous emission rate are not as important as its time averaged value. This simplified analysis technique may produce errors in the absolute value of the noise sources but should produce a reasonable framework for a comparison of the relative values of the noise sources involved. Since we are trying to compare the results of different mode-locked laser types, it is this comparison of noise levels which will be most important point in this analysis.

In Section 6.3, the sensitivity of laser pulse temporal position to the three different noise excitation types (carrier density, photon density, and index of refraction) is illustrated. This sensitivity analysis is done with a large signal simulation. The sensitivity to noise perturbations are calculated numerically for the various mode-locking cases under study.

Section 6.4 combines the small signal noise strength analysis of Section 6.2 with the large signal sensitivity to noise analysis of Section 6.3 to find the resulting timing jitter for the cases under consideration.

6.2 The noise sources responsible for timing jitter

In this section, a rate equation analysis will be used to model the strength of the noise sources that are responsible for introducing timing jitter into mode-locked lasers. The analysis starts from the rate equations including noise for the photon number, carrier number, and phase similar to those given by Agrawal

and Dutta [19]. The rate equations have been modified for external cavities in which the gain region does not occupy the entire cavity length.

$$\frac{\partial P}{\partial t} = \Gamma_2 GP - \gamma P + R_{sp}' + F_p(t) \tag{6.1}$$

$$\frac{\partial N}{\partial t} = -\Gamma_1 GP - \gamma_e N + \frac{I}{q} + F_n(t) \tag{6.2}$$

$$\frac{\partial \phi}{\partial t} = \frac{\alpha}{2} G + F_\phi(t) \tag{6.3}$$

$$\Gamma_1 = \frac{L_{gain}}{L_{cavity}} \tag{6.4}$$

$$\Gamma_2 = \Gamma_1 \Gamma_t \tag{6.5}$$

$$n = \frac{N}{w_a h_a L_{gain}} \tag{6.6}$$

$$G = v_g g \tag{6.7}$$

$$R_{sp}' = \Gamma_1 M \beta_{sp} \gamma_e N \tag{6.8}$$

where P is the photon number, N is the carrier number, ϕ is the optical phase, G is the gain coefficient, γ is one over the photon lifetime, γ_e is one over the carrier lifetime, R_{sp}' is the spontaneous emission rate, α is the linewidth enhancement factor, Γ_1 is the occupancy fraction of the gain in the laser cavity, Γ_t is the transverse optical mode confinement factor, w_a is the width of the

active region, h_a is the height of the active region, β_{sp} is the fraction of the spontaneous emission power coupled into the lasing mode, and M is the number of lasing longitudinal modes.

The noise driving terms in the rate equations are described by the variables $F_p(t)$, $F_n(t)$, and $F_\phi(t)$ which describe the random fluctuations in the photon number, carrier number, and the optical phase. Lets examine the nature of these noise source terms. The statistical correlation and cross-correlation properties of the noise are taken from Agrawal and Dutta [19] as:

$$R_{pp}(t-t') = 2\, R'_{sp}\, P\, \delta(t-t') \tag{6-9}$$

$$R_{NN}(t-t') = 2\, (R'_{sp}\, P + \gamma_e N)\, \delta(t-t') \tag{6-10}$$

$$R_{\phi\phi}(t-t') = R'_{sp}/(2\, P)\, \delta(t-t') \tag{6-11}$$

$$R_{PN}(t-t') = -2\, R'_{sp}\, P\, \delta(t-t') \tag{6-12}$$

$$R_{P\phi} = 0 \tag{6-13}$$

$$R_{N\phi} = 0 \tag{6-14}$$

Since the autocorrelation functions are delta functions, the noise power spectral density is white (constant with respect to frequency) with spectral density value given by:

$$S_{pp}(\omega) = 2\, R'_{sp}\, P \tag{6-15}$$

$$S_{NN}(\omega) = 2\, (R'_{sp}\, P + \gamma_e N) \tag{6-16}$$

$$S_{\phi\phi}(\omega) = R'_{sp}/(4\, P) \tag{6-17}$$

$$S_{PN}(\omega) = -2\, R'_{sp}\, P \tag{6-18}$$

In order to find the resulting noise spectral densities in the laser, the rate equations are linearized around a quiescent operating point by assuming the

following forms for the terms in the rate equations.

$$P \Rightarrow P + \delta P\, e^{i\omega t} \tag{6.19}$$

$$N \Rightarrow N + \delta N\, e^{i\omega t} \tag{6.20}$$

$$\phi \Rightarrow \phi + \delta\phi\, e^{i\omega t} \tag{6.21}$$

$$F_p \Rightarrow \delta F_p\, e^{i\omega t} \tag{6.22}$$

$$F_N \Rightarrow \delta F_N\, e^{i\omega t} \tag{6.23}$$

The variables are converted to a constant portion plus a small sinusoidal component. In the mode-locked laser case, the photon density and carrier density are actually time dependent variables. In this analysis, a time averaged value for the constant portion of the substitution will be assumed. The time interval for averaging is one round trip period in the laser cavity. When these new variables are substituted into the rate equations (6.1-6.3), terms at 2ω are ignored and the time independent variables are dropped from both sides of the equation. The resulting linearized external or monolithic cavity equations are given as:

$$\delta N(\omega) = \frac{\Gamma_1(G+G_N P)\delta F_p + (i\omega+\Gamma_p)\delta F_N}{(\Omega_R + \omega - i\Gamma_R)(\Omega_R - \omega + i\Gamma_R)} \tag{6.24}$$

$$\delta P(\omega) = \frac{(\Gamma_2 G_N P + \frac{\partial R_{sp}}{\partial N})\delta F_N + (i\omega+\Gamma_N)\delta F_P}{(\Omega_R + \omega - i\Gamma_R)(\Omega_R - \omega + i\Gamma_R)} \tag{6.25}$$

$$\Omega_R^2 = \Gamma_1(G+G_P P)(\Gamma_2 G_N P + \frac{\partial R_{sp}}{\partial N}) - \frac{(\Gamma_N - \Gamma_p)^2}{4} \tag{6.26}$$

$$\Gamma_R = (\Gamma_N + \Gamma_P)/2 \tag{6.27}$$

$$\Gamma_N = (\Gamma_1 G_N P + \gamma_e + \frac{\partial \gamma_e}{\partial N} N) \tag{6.28}$$

$$\Gamma_P = (-\Gamma_2 G_P P + \frac{R_{sp}}{P}) \tag{6.39}$$

$$G_N = v_g \frac{dg}{dn} \tag{6.30}$$

where G_N is the change in gain with respect to carrier density and G_P is the change in gain with respect to photon density. The spectral densities are obtained by taking the magnitude squared of the Equation 6.24 and 6.25, and substituting in the values for the power spectral density of the noise terms.

$$S_N(\omega) = \frac{\Gamma_1(G+G_P P)S_{PP}(\omega) + (\Gamma_p^2 + \omega^2)S_{NN}(\omega) + 2\Gamma_1\Gamma_p(G+G_P P)S_{PN}(\omega)}{(\Omega_R^2 - \omega^2)^2 + (2\omega\Gamma_R)^2} \tag{6.31}$$

$$S_p(\omega) = \frac{(\Gamma_2 G_N P + \frac{\partial R_{sp}}{\partial N})S_{NN}(\omega) + (\Gamma_N^2 + \omega^2)S_{PP}(\omega) + 2\Gamma_N(\Gamma_2 G_N P + \frac{\partial R_{sp}}{\partial N})S_{PN}(\omega)}{(\Omega_R^2 - \omega^2)^2 + (2\omega\Gamma_R)^2} \tag{6.32}$$

Table 6.1 lists typical parameter values for monolithic cavity mode-locked lasers operating in active, passive, and hybrid mode-locking conditions. Table 6.2 lists typical parameter values for external cavity mode-locked lasers operating in active, passive, and hybrid mode-locking conditions. The conditions are

Table 6.1 Monolithic cavity parameters

Parameter	units	Active	Hybrid	Passive
Average output power, P_{out}	mW	1	1	1
Cavity length, L_{cavity}	mm	7	7	7
Gain length, L_{gain}	mm	7	7	7
Saturable absorber length, L_a	μm	N.A.	70	70
Modulation segment length, L_m	μm	200	200	N.A.
Peak modulation current, I_{mod}	mA	200	200	N.A.
Modulation pulse width, T_e	ps	25	25	N.A.
Confinement factor, Γ_t	unitless	0.2	0.2	0.2
Active region width, w_A	μm	2	2	2
Active region height, h_A	μm	0.1	0.1	0.1
Alpha factor, α	unitless	4	4	4
Group index, n_g	unitless	4	4	4
Average photon number, P	photons	1.5×10^5	1.5×10^5	1.5×10^5
Average electron number, N	electrons	3.1×10^9	3.5×10^9	3.6×10^9
Fraction to lasing mode, β_{sp}	unitless	1×10^{-5}	1×10^{-5}	1×10^{-5}
Output facet reflectivity, R	unitless	0.3	0.3	0.3
Waveguide loss, α_{int}	cm^{-1}	7.5	7.5	7.5
Unsatuated amp. gain, $\Gamma_t g_o$	cm^{-1}	11.5	19.5	21
Differential gain, dg/dn	cm^2	2×10^{-16}	2×10^{-16}	2×10^{-16}
Carrier density at trans., n_{tr}	cm^{-3}	2×10^{18}	2×10^{18}	2×10^{18}
Nonlinear gain coeff., G_p	s^{-1}	-3.4×10^4	-3.4×10^4	-3.4×10^4
Spontaneous decay rate, γ_e	s^{-1}	2×10^9	2×10^9	2×10^9

Table 6.2 External cavity parameters

Parameter	units	Active	Hybrid	Passive
Average output power, P_{out}	mW	1	1	1
Cavity length, L_{cavity}	mm	7	7	7
Gain length, L_{gain}	mm	0.5	0.5	0.5
Saturable absorber length, L_a	µm	N.A.	70	70
Modulation segment length, L_m	µm	200	420	N.A.
Peak modulation current, I_{mod}	mA	200	200	N.A.
Modulation pulse width, T_e	ps	25	25	N.A.
Confinement factor, Γ_1	unitless	0.2	0.2	0.2
Active region width, w_A	µm	2	2	2
Active region height, h_A	µm	0.1	0.1	0.1
Alpha factor, α	unitless	4	4	4
Group index, n_g	unitless	4	4	4
Average photon number, P	photons	1.5×10^5	1.5×10^5	1.5×10^5
Average electron number, N	electrons	2.4×10^8	3×10^8	3.1×10^8
Fraction to lasing mode, β_{sp}	unitless	10^{-5}	10^{-5}	10^{-5}
Output facet reflectivity, R	unitless	0.3	0.3	0.3
Waveguide loss, α_{int}	cm^{-1}	7.5	7.5	7.5
Unsatuated amp. gain, $\Gamma_t g_o$	cm^{-1}	41	62	66
Differential gain, dg/dn	cm^2	2×10^{-16}	2×10^{-16}	2×10^{-16}
Carrier density at trans., n_{tr}	cm^{-3}	2×10^{18}	2×10^{18}	2×10^{18}
Nonlinear gain coeff., G_p	s^{-1}	-3.4×10^4	-3.4×10^4	-3.4×10^4
Spontaneous decay rate, γ_e	s^{-1}	2×10^9	2×10^9	2×10^9

chosen to simulate the experimental conditions for the experiments of Figures 4.26, 4.27, and 4.28. These experiments were done at average output powers between 1 and 3 mW. The average output power can be converted to the internal photon number using the formula:

$$P = \frac{P_{out}\, L_{cavity}\, \Gamma_t}{\frac{1-R}{1+R}\, h\, \nu\, v_g} \tag{6.33}$$

where R is the output facet reflectivity, and P_{out} is the average output power from the mode-locked laser output facet.

Figure 6.3 shows the resulting carrier number spectral density normalized to the carrier number population. The spectral density has been normalized to a 1 Hz bandwidth. Results are given for the passive mode-locked monolithic and external cavity simulation data given in Tables 6.1 and 6.2. Table 4.2 shows that much larger DC bias currents are necessary to operate in passive and hybrid mode-locking conditions. This is due to the fact that passive and hybrid mode-locked lasers operate near the saturation energy of the semiconductor laser amplifier. Active mode-locked lasers typically operate at lower output energies and require less DC pumping.

The spectral density curves of Figure 6.3 show a low frequency response value, a slight rise near the low frequency relaxation resonance and then a drop-off. The fact that the low frequency response is reasonable flat with frequency demonstrates that the frequency dependent terms in the numerator of Equations 6.31 and 6.32 are small compared to the frequency independent terms. In the analysis of timing jitter, another parameter of interest will be the spectral density for index of refraction variations. The spectral density for index of refraction fluctuations is related to the spectral density of the carrier density fluctuations

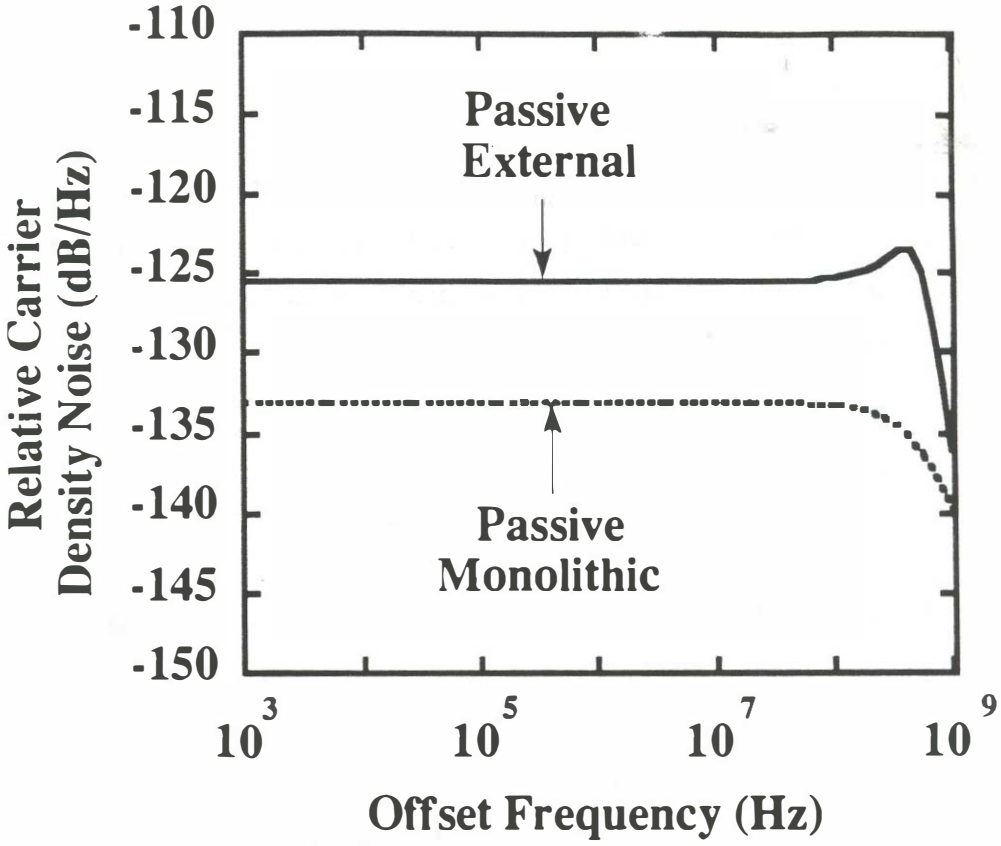

Figure 6.3 The carrier number spectral density for the passive external and passive monolithic cavity mode-locked laser cases. The spectral density is normalized to the carrier number and plotted for a 1 Hz bandwidth. The simulation parameters are given in Table 6.1 and 6.2.

as:

$$S_{in}(\omega) = \left(\frac{\partial n_{in}}{\partial n}\right)^2 \frac{S_N(\omega)}{V^2} \tag{6.34}$$

where $S_{in}(\omega)$ is the spectral density of index fluctuations. The parameter dn_{in}/dn describes the coupling of index fluctuations from carrier density fluctuations which is obtained from the linewidth enhancement factor and an estimate of the differential gain in the laser.

$$\frac{\partial n_{in}}{\partial n} = \frac{\alpha \frac{dg}{dn}}{2\, k_0} \tag{6.35}$$

The noise spectral density curves are the starting point for analyzing the timing jitter found in mode-locked semiconductor lasers. The noise spectral density data can be used in two ways to do further calculations on jitter. In the time domain it is desirable to find the standard deviation or the r.m.s. value of the carrier number or photon number fluctuation (It will be assumed that the random variables are wide-sense stationary random variables). The variance (standard deviation squared) of the process can be obtained from the spectral density of a band-limited noise process by integrating the area under the spectral density curve (see Chapter 4.5).

$$\sigma_x^2 = \frac{1}{2\pi}\int_{-\infty}^{\infty} S_{xx}(\omega)\, d\omega \tag{6.36}$$

where it is assumed that the random process is zero mean, σ_x is the standard

deviation of the random process, and S_{xx} is an unspecified spectral density function. Using Equation 6.32, the standard deviation of the carrier number, photon number, and the index of refraction can be calculated for the monolithic and external cavity cases being studied in this Chapter.

The spectral density information is useful in calculating the frequency domain description of timing jitter. The frequency domain measurement technique was the one used for the timing jitter measurements found in Chapter 4. In the frequency domain technique, the single sideband phase noise normalized to a 1 Hz bandwidth, L(f), is measured. In order to calculate L(f) in this Chapter, the noise spectral density functions of Equations 6.31 and 6.32 will be treated as a collection of sinusoidal oscillators with the noise power associated with a 1 Hz noise slice. This collection of sinusoidal oscillators will then be used to find the corresponding sinusoidal variations in pulse position (timing jitter) in the next section.

6.3 Noise source to timing jitter relationships

In section 6.2, the magnitude and frequency response of the spectral densities for the carrier number, photon number, and index of refraction were calculated. In this section, the conversion of these noise parameters to timing jitter parameters will be discussed.

6.3.1 Timing jitter in active and hybrid mode-locked lasers

Figure 6.4 illustrates the timing relationships between the optical pulse and the electrical gain modulation pulse in an active or hybrid mode-locked semiconductor laser. Under stable steady state operation, a timing relationship between the current modulation pulse and the laser pulse will be established.

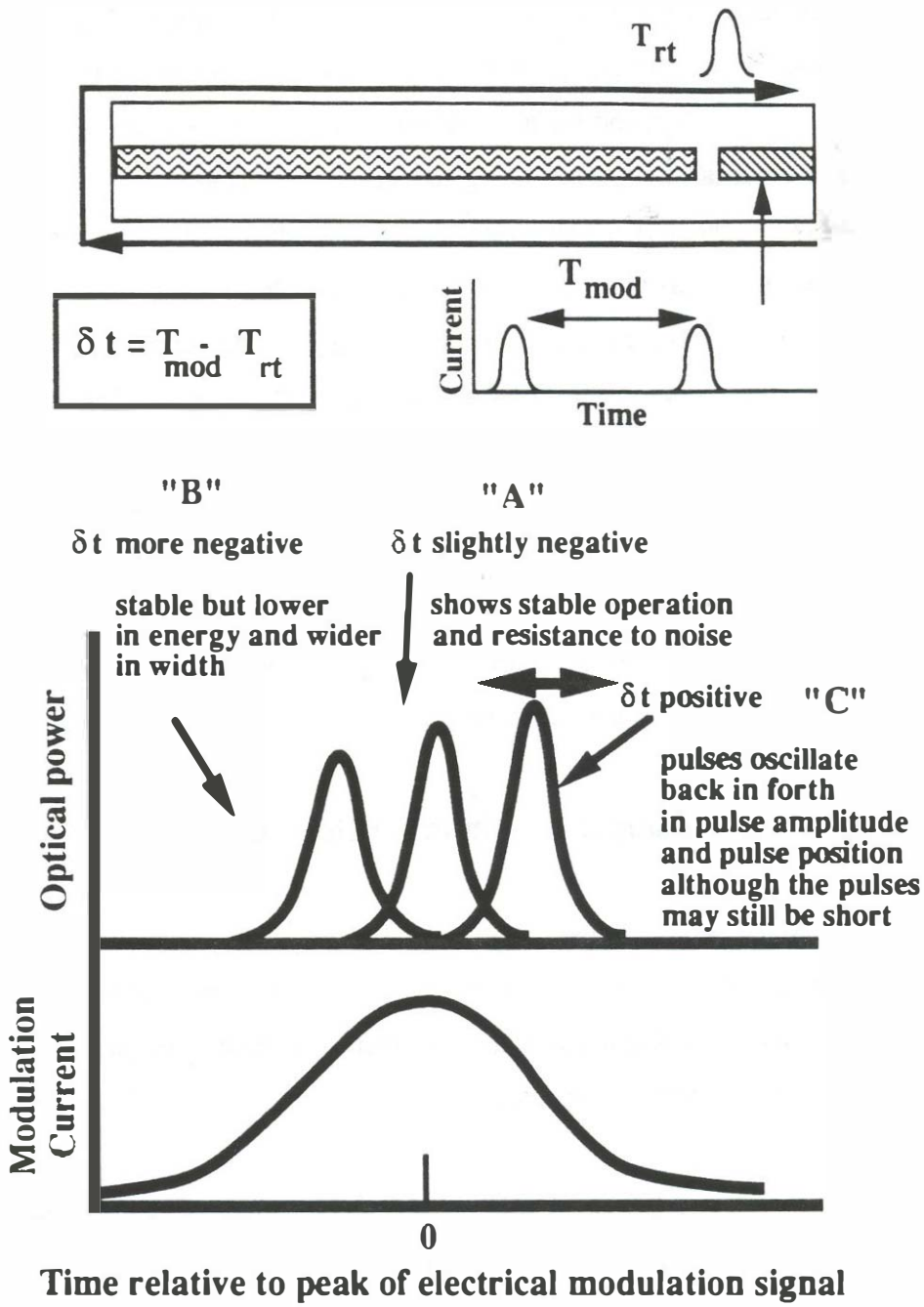

Figure 6.4 The equilibrium optical pulse position relative to the electrical modulation signal as a function of the time difference, δt. Noise in the index of refraction can cause randomness in the round trip time and pulse position jitter.

After many round trips of the laser pulse around the optical cavity, an equilibrium pulse position such as pulse position "A" in Figure 6.3 is reached. This steady-state operating point under ideal circumstances would be for the timing relationship that gives the maximum pulse shaping per pass as is discussed in Figures 5.17 to 5.20. If noise were not present in the electrical modulation pulse and in the optical amplifier medium, the timing relationship between the optical pulse and the electrical modulation pulse would remain fixed. Let's assume now that we can ignore noise in the electrical modulation pulse and concentrate on the consequences of spontaneous emission induced noise on this timing relationship.

The repetition rate of the active gain modulation defines the repetition rate of the laser pulse stream. Let us take snapshots of the timing relationship between the optical pulse and the electrical modulation pulse at time intervals corresponding to the electrical modulation pulse period. It is useful now to speak of a relative time, where relative time is the location of the optical pulse with respect to the peak of the electrical modulation pulse.

If the electrical modulation pulse period is adjusted to be slightly greater than the round trip time in the laser,T_{rt}, (this is the usual operating case or conversely the modulation frequency is slightly decreased) in the mode-locked laser cavity, the optical pulse will be forced to occur earlier in relative time with respect to the electrical modulation pulse as is illustrated by pulse "B" in Figure 6.4. On first thought, it would seem that the optical pulse would keep moving earlier in relative time on each cavity round trip until the optical pulse would occur very much earlier than the modulation pulse. The pulse does not keep moving earlier in relative time with respect to the electrical modulation pulses due to a restoring force moving it back later in relative time. This restoring force is the time dependent gain introduced by the

active gain modulation. Later portions in time of the optical pulse receive more gain than early portion of the pulse, effectively moving the pulse toward the later time section of the gain modulation waveform. This increased gain for pulses that occur later in relative time is illustrated in Figures 5.17 - 5.20. The equilibrium location for pulse "B" in which the electrical modulation period is increased is thus a balance between the repetition rate force moving the pulse earlier in relative time and the gain versus time function moving the pulse back later in relative time. If the modulation period is increased too greatly, the restoring force of the gain versus time will not be sufficiently strong to move the pulse back later in relative time. In this case of too long of modulation period, the optical pulse will walk off so that it experiences no gain in the gain modulation segment. The resulting pulse will be small in energy, wide in pulsewidth, and will not be well mode-locked.

Conversely, lets examine the case of the modulation period being slightly less than the round-trip time in the mode-locked laser cavity. In this case, the relative optical pulse location will increase with each round trip. In a system with a loss modulation element, such as an acousto-optic modulator in active mode-locked YAG laser systems, the pulse can be stabilized on both the leading edge and the trailing edge of the gain modulation waveform. In semiconductor laser active gain modulation with too short of pulse period, there is no force stopping pulse motion towards later relative times. Now both the repetition rate force and the gain versus time force are acting *together* to move the pulse later in relative time. As the pulse moves later in time (see pulse position "C"), a new pulse will form earlier in time due to seeding from spontaneous emission events. The final solution will be one where the relative position of the optical pulse is oscillating back and forth in relative time resulting in huge timing and amplitude jitter. This unstable

behavior for short electrical modulation periods has been noted by several other authors [74,78]. Figure 4.20 shows the experimentally observed phase noise behavior versus optical cavity length. The phase noise increase for a lengthened optical cavity is very dramatic.

The periodic instability in amplitude and time caused by increasing the modulation period with respect to cavity round trip time can be clearly seen in the spectrum analyzer plots of Figure 4.19. The large modulation sidebands are a result of the optical pulse moving back and forth periodically in time with respect to the electrical modulation pulse. The frequency of this pulse position instability is approximately 300 MHz, which is typical for the low frequency relaxation oscillation frequency of this long laser cavity. Note that the noise sidebands are asymmetrical. This demonstrates that the amplitude and phase noise are correlated.

6.3.2 Calculation of pulse position restoring forces

In order to calculate the timing jitter found in mode-locked lasers, it is necessary to understand the magnitude of the restoring forces that keep the pulse stabilized with respect to the electrical modulation pulses. The approach to analyze the strength of the restoring forces is to numerically establish the relative time relationships between the location of the optical pulse and the modulation pulse. Once an equilibrium operating point is established, the operating parameters of the laser are perturbed slightly and the system is allowed to find a new pulse position operating point. The types of perturbations used are those that are induced by spontaneous emission noise; a carrier number perturbation, a photon number perturbation, and an index of refraction perturbation. These noise sources are correlated, but the initial work will be to understand how strongly each of these noise sources perturb the

relative pulse location individually with no correlations assumed between the noise sources.

The numerical techniques used in Chapter 5 are used to calculate the steady state and perturbed pulse positions. For gain regions, the two-step method described in Chapter 5.2 is used including both gain saturation effects (Equations 5.8 and 5.9) and bandwidth effects (Equation 5.13). For the gain modulation segment, Equations 5.1 and 5.2 are directly solved by Runge-Kutta techniques and bandwidth effects are not included. The saturable absorber segment calculation uses Equations 5.8 and 5.9. The modulation current pulses are assumed to be Gaussian with a peak current 150 times the transparency current (see Equation 5.6) and the effective modulation pulsewidth is assumed to be 25 ps. The three different pulse position sensitivity factors will now be explained.

6.3.2a Sensitivity of pulse location to the modulation period

Let's first examine the sensitivity of the optical pulse position to the period of the electrical modulation pulses. This same detuning can be viewed as keeping the modulation period constant and slightly changing the cavity round-trip time. This perturbation is important in that the round trip time in a mode-locked laser is modified by the index of refraction fluctuation noise. An index of refraction variation will modify the round trip time in the laser cavity resulting in a movement of the laser pulse with respect to the modulation pulse (timing jitter).

Figure 6.5 shows the calculated equilibrium pulse position versus the time difference between the optical cavity round trip time and the modulation period time, δt. δt is positive for the modulation period being slightly shorter than the cavity round trip time. It is assumed that the noise perturbation is slow

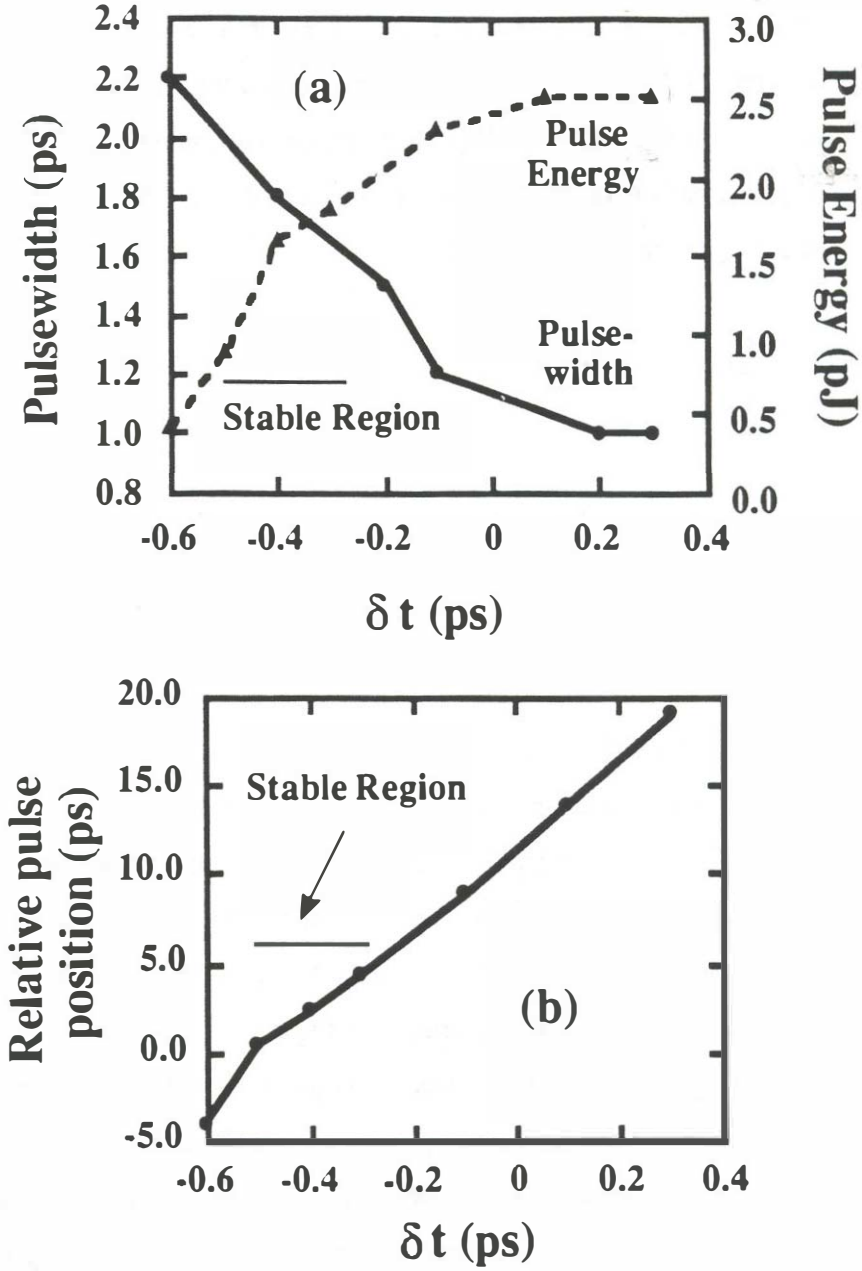

Figure 6.5. The (a) pulsewidth, pulse energy, and (b) relative pulse position as a function of the time difference, δt, between the cavity round trip time and the electrical modulation period.

compared to the repetition rate of the laser pulse stream. The calculation results of Figure 6.5 are done for the hybrid external cavity mode-locked laser parameters of Table 6.2. For calculations of the timing jitter induced by index of refraction variations, the slope of the pulse position with respect to round trip time perturbation is the important constant to take from this curve. This sensitivity parameter is defined as:

$$O_{na} = \frac{\partial P_p}{\partial \delta t} \tag{6.37}$$

where P_p is the equilibrium laser pulse position with respect to the modulation current pulse position and δt is the difference in time between the modulation period and the cavity round trip time.

6.3.2b Sensitivity of pulse position to changes in gain

Spontaneous emission causes random fluctuations in the carrier density of the laser. The random carrier density fluctuations also cause random gain fluctuations since gain is proportional to carrier density. When an amplifier is operating under gain saturation conditions, gain fluctuations lead to pulse position fluctuations as is illustrated in Figure 5.10a. When an amplifier is operating in gain saturation, the leading edge of the optical pulse receives more amplification than the trailing edge of the optical pulse. The amount of gain saturation in the optical amplifier determines the amount of pulse position shift in time. This selective amplification moves the center of gravity of the pulse earlier in relative time with respect to the modulation pulse. Notice that for small input energy pulses the output pulse tends to move earlier in relative time. For larger input energy pulses, the center of gravity of the pulse moves later in

relative time for an increase in the input pulse energy. Figure 6.6 shows the step response of a hybrid mode-locked semiconductor laser to a 1 cm^{-1} change in the net gain of the optical amplifier. The nominal net gain of the amplifier before the input pulse enters the amplifier is 60 cm^{-1}. The simulation parameters are given in Table 6.2. The pulse position changes on each round trip until after approximately 20 round trips a new equilibrium pulse position is established between the optical pulse and the electrical modulation pulse. The pulse position goes through several ringing periods on its way to the final pulse position. The period of the ringing corresponds to a relaxation resonance frequency for gain fluctuations. Fluctuations that occur at a rate much higher than the relaxation oscillation frequency will not be as effective in inducing timing jitter onto the mode-locked laser pulses.

Figure 6.7 shows the sensitivity of final equilibrium pulse location to gain changes for the hybrid mode-locked external cavity laser example of Table 6.2. For a particular gain level, the optical pulse will establish a certain relative position with respect to the modulation pulse. If the gain is slightly increased, the gain saturation level increases and the pulse moves later in time over a several round trip adjustment period (see Figure 5.10a for a large gain saturation condition) several round trips. This gain to pulse position sensitivity is quantified by the following sensitivity parameter:

$$O_g = \frac{\partial P_p}{\partial g'} \tag{6.38}$$

where g' here is the net gain including the transverse confinement factor.

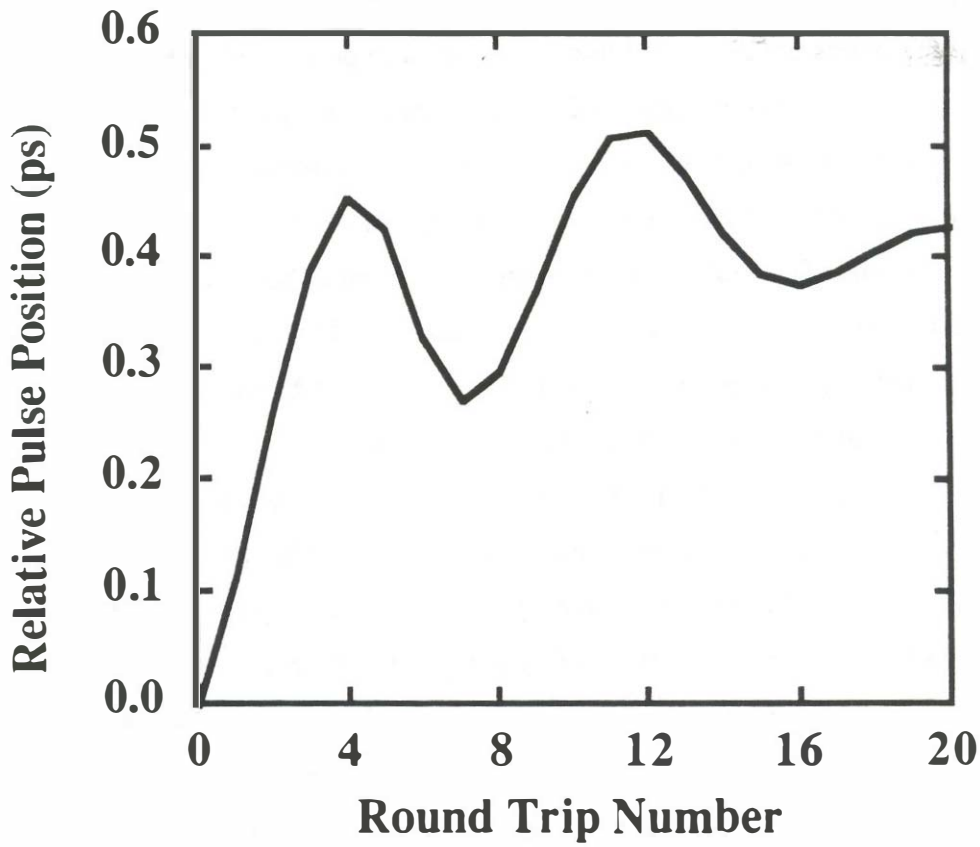

Figure 6.6 The step response to a 1/cm gain change in an external cavity hybrid mode-locked external cavity laser. The nominal unsaturated gain level in the mode-locked laser is 60/cm. After the step change of the gain in the laser amplifier, the relative optical pulse position with respect to the electrical pulse position establishes a new equilibrium value. The simulation parameters are given in Table 6.2.

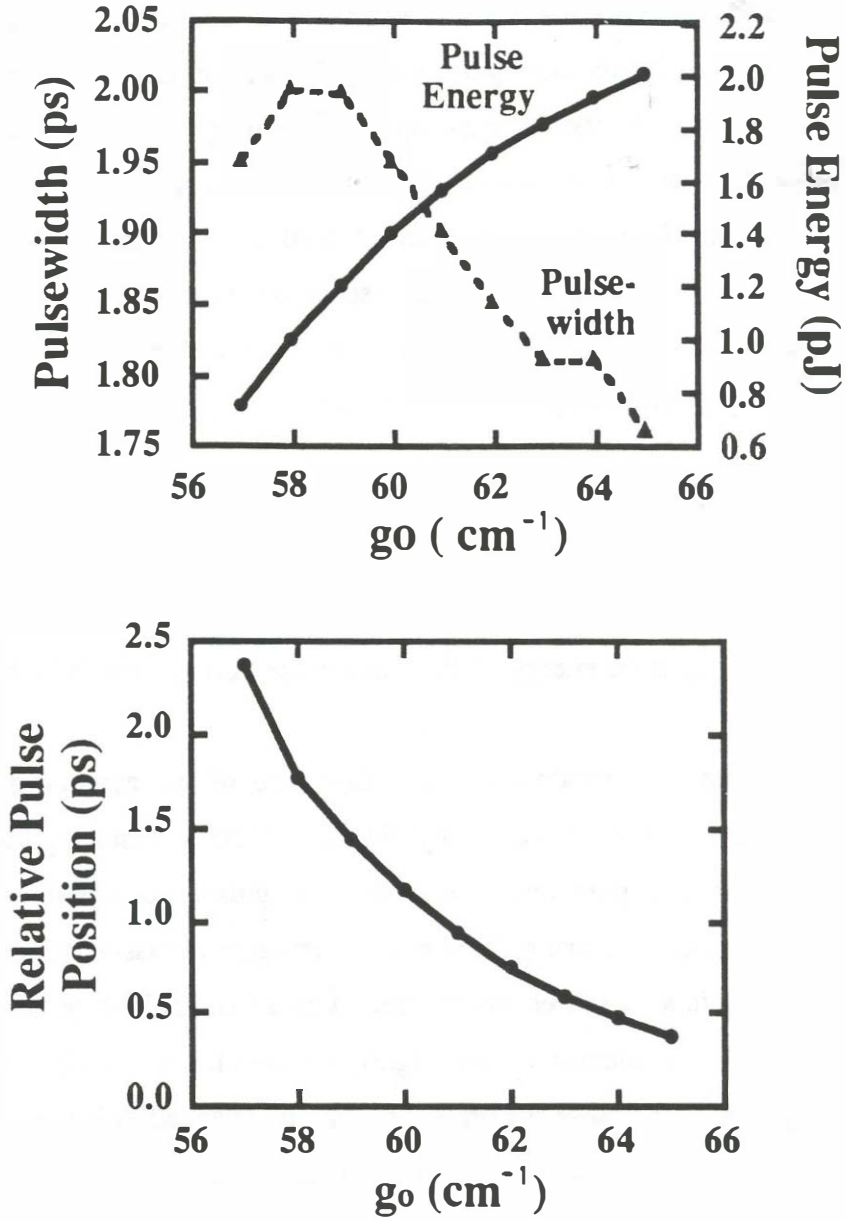

Figure 6.7. The equilibrium (a) pulsewidth, pulse energy, and (b) relative pulse position as a function of the gain in the laser amplifier (the confinement factor is included in g_o). The modelled situation is for a hybrid mode-locked external cavity laser with the parameters listed in Table 6.2.

6.3.2c Sensitivity to changes in pulse amplitude

Spontaneous emission will also cause a randomness in the pulse energy. Through gain saturation, pulse energy fluctuations can couple to pulse position fluctuations. A larger energy input pulse energy will cause the pulse to move later in time due to increased gain saturation under the typical operating conditions of a mode-locked laser. A smaller energy input pulse will cause the pulse to move earlier in time with respect to the modulation due to reduced gain saturation. The sensitivity of pulse location with respect to pulse energy is given by the following sensitivity factor:

$$O_{ea} = \frac{\partial P_p}{\partial E_{pulse}} \tag{6.39}$$

where E_{pulse} is the energy of the output pulse from the mode-locked laser.

6.3.3 Passive mode-locking - the case of no restoring forces

In the case of active and hybrid mode-locking, restoring forces helped to center the laser pulses near the modulation pulse. For a passive mode-locked laser, no such restoring force exists. Imagine a passive mode-locked laser operating in a noise free environment with a fixed pulse repetition period. If a perturbation is introduced that slightly changes the round trip time in the laser, the period of the pulse stream will be directly changed as is illustrated in Figure 6.8. The pulse position error will increase linearly with time. The lower the characteristic frequency of the perturbation, the larger the accumulated error in the position of the optical pulse. This sensitivity of maximum pulse location error to the characteristic frequency of the perturbation is well illustrated in the experimental L(f) data in Figure 4.26 and 4.28. The phase noise drops at a rate

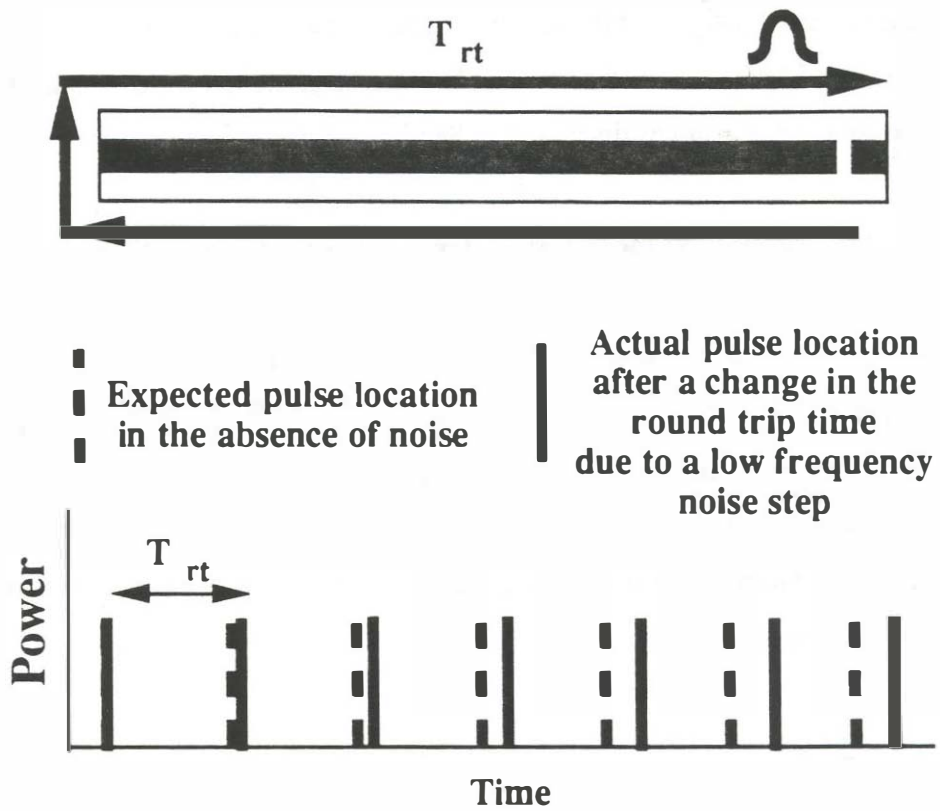

Figure 6.8 In the absence of noise, a passive mode-locked laser would expect to have the pulse positions indicated by the dashed impulses. If a step change in the cavity round trip time is applied to the laser, the pulse position error accumulates linearly with time as is shown by the solid impulses. For a sinusoidal noise modulation signal, the amount of pulse position error will be inversely proportional to the noise modulation frequency.

of 20 dB/decade of offset frequency. A 20 dB/decade drop in the phase noise of a system is a sign that the resonance frequency of the laser is being frequency modulated by a white noise source. The causes of the frequency modulation are the same noise sources discussed in Section 6.3.2.

6.3.3a Frequency modulation from index of refraction variations.

It is clear that if the index of refraction is perturbed in a mode-locked laser, the cavity round trip period is changed resulting in a shift in the cavity resonant frequency. The amount of the round trip period shift is directly dependent on the filling fraction of the gain length to the total cavity length, Γ_1. Thus monolithic and external cavity devices should behave differently. The sensitivity factor for characterizing the timing jitter caused by index of refraction variations is defined as:

$$O_{np} = \frac{\partial T_{rt}}{\partial n_{in}} \tag{6-40}$$

Previous sensitivity factors were done on a final equilibrium pulse position basis and showed the final pulse position which may take several round trips to establish. Here there are no restoring forces so every round trip will increase the pulse position error. In passive mode-locking, the pulse keeps moving away from the original equilibrium pulse locations after a noise step perturbation.

6.3.3b Frequency modulation from gain variations

As described earlier, gain changes can couple into round trip time variations. An increase in gain effectively increases the round trip time

(assuming typical mode-locked laser operating conditions) in the laser leading to a change in the repetition rate of the mode-locked laser. It is useful to look at Figure 5.10a to visualize this pulse location change for a amplifier gain change. The sensitivity factor characterizing this perturbation is defined as:

$$O_{gp} = \frac{\partial T_{rt}}{\partial g'} \tag{6.41}$$

6.3.3c Frequency modulation from pulse energy fluctuations

The sensitivity factor of the repetition period to pulse energy fluctuations is defined as:

$$O_{ep} = \frac{\partial T_{rt}}{\partial E_{pulse}} \tag{6.42}$$

This sensitivity factor is partially correlated to Equation 6.41 since gain and photon variations are related.

6.3.4 The magnitude of the sensitivity factors to noise perturbations

Section 6.3.2 described the sensitivity factors for active and hybrid mode-locked lasers and section 6.3.3 described the sensitivity factors for passive mode-locked lasers. Table 6.3 lists the numerically calculated sensitivity factors for the 6 timing jitter cases studied in Chapter 4: active, passive, and hybrid mode-locked lasers in the monolithic and external cavity configurations (see also Figure 6.1). Table 6.1 and 6.2 show the parameters used in the numerical simulation of the sensitivity factors. In general, the sensitivity factors for monolithic cavity devices are larger than those for external cavity devices. For index change perturbations, the longer active waveguide length is more effective

Table 6.3 Noise sensitivity factors

	Active noise parameters		Passive noise parameters	
	O_{na}	O_{ga}	O_{np}	O_{gp}
Units	ps/ps	ps/cm^{-1}	$ps/\delta n_{in}$	fs/cm^{-1}
Active Mon.	8	2.6		
Hybrid Mon.	8	2.6		
Passive Mon.			47	76
Active External	6.5	0.5		
Hybrid External	6.5	0.5		
Passive External			3.33	3.5

in changing the round trip time. For gain perturbations, the effect on gain saturation will be greater in monolithic cavity devices since the gain region length is so large.

6.4 Calculation of timing jitter from the noise source spectral densities and the sensitivity factors

In Section 6.2, the noise sources driving timing jitter were described by their spectral density functions. By integrating to find the total area beneath the spectral density curves, (Equation 6.36) the variance and the standard deviation of the noise processes can be obtained assuming the noise still has a zero mean. The spectral density function can be considered to be a collection of sinusoidal oscillators spaced 1 Hz apart. Each oscillator has the noise power associated with the 1 Hz bandwidth slice. When these sinusoidal noise slices are combined with the sensitivity analysis section of Section 6.3, the single sideband phase noise normalized to a 1 Hz bandwidth, L(f), can be calculated. The next section outlines how the L(f) values are calculated.

The cross correlation of the photon number and carrier density number was given in Equation 6.12. The correlation is such that if you have a burst in the spontaneous emission output you will have a corresponding drop in the carrier density. The correlation between phase noise and amplitude noise is illustrated in Figure 6.9. At offset frequencies where the relative intensity noise becomes comparable to the phase noise, the sidebands become asymmetrical. Asymmetrical modulation sidebands indicate that the amplitude and phase noise sidebands are adding coherently.

It is instructive to do a simple calculation to compare the timing jitter contributions from index of refraction fluctuations and from gain fluctuations

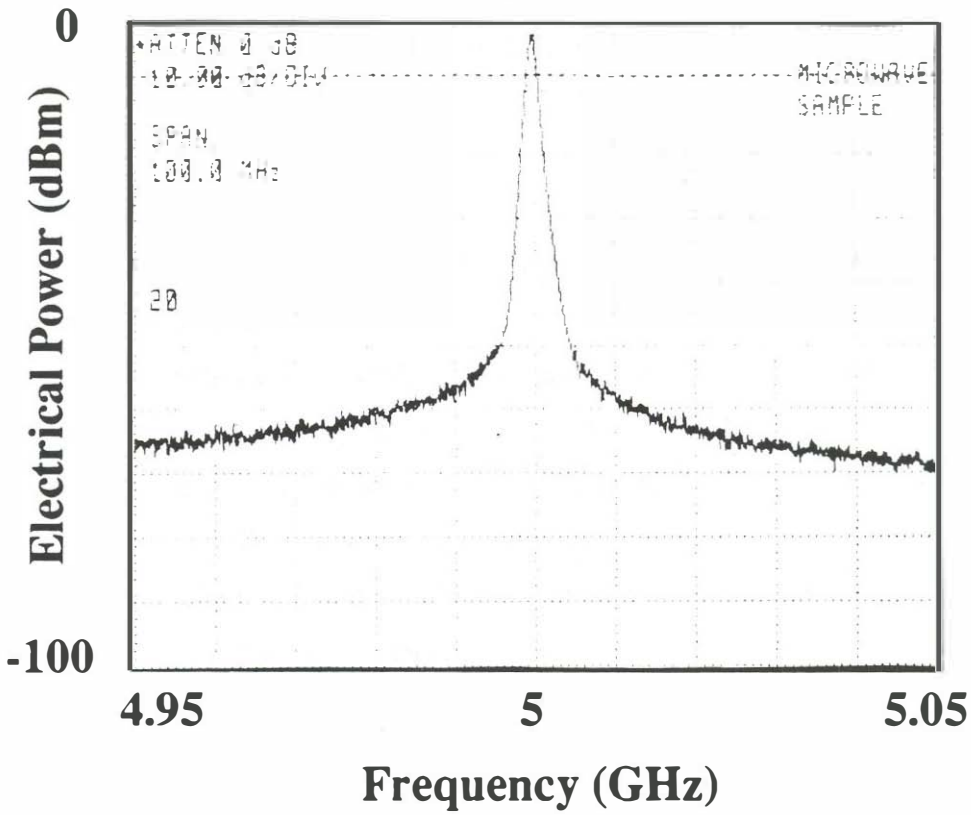

Figure 6.9 The noise measured from a 5 GHz repetition rate passive mode-locked external cavity semiconductor laser. The device has the bulk active region described in Figure 2.27. The point of this figure is to show the asymmetrical noise sidebands that are seen when the phase noise contribution to the noise is at nearly the same level as the intensity noise contribution. The asymmetrical sidebands are a sign of correlation between intensity and phase noise. The resolution bandwidth for the measurement is 1 MHz.

since they are related to the same variable, the carrier density. Changes in the gain are related to changes in the index of refraction through the linewidth enhancement factor. Let's compare the magnitude of these two noise sources in modifying the effective round trip time in a mode-locked laser cavity. The ratio of the round trip time perturbations is given as:

$$\frac{\Delta T_{rt\ gain}}{\Delta T_{rt\ index}} = \frac{O_{gp}}{O_{np}} \frac{4\pi}{\alpha \lambda_0} \tag{6.43}$$

where $\Delta T_{rt\ gain}$ is the round trip time perturbation caused by a gain change, and $\Delta T_{rt\ index}$ is the round trip time perturbation caused by a change in the index of refraction. Table 6.3 lists the sensitivity parameters for the mode-locked laser examples studied in this chapter. **Using the sensitivity values of Table 6.3 and a typical value for the linewidth enhancement factor of 4, the contribution from gain changes is found to be at least ten times larger than the index contribution for any of the cases considered. Because of the dominance of the gain to jitter conversion process over the index of refraction noise jitter process, only the former will be considered in the final timing jitter analysis simulations of Section 6.5.**

There is experimental evidence that the gain to timing jitter conversion process is dominant. The gain modulation segment in Figure 6.2 can also be used as a repetition rate tuning section in passive mode-locked lasers [71]. Figure 4.13 shows the repetition rate tuning experiment. By adjusting the current to a short segment under passive mode-locking conditions, the repetition rate of the pulse stream and the amplitude of the pulse stream is changed as is

shown in Figure 4.13. Note that the repetition rate goes down as the current drive goes up. If the current drive increases, the carrier density level in the segment should also rise. A carrier density rise leads to a drop in the index of refraction and an increase in the repetition rate of the laser. The sign of the change in repetition rate is thus inconsistent with index of refraction changes. The tuning segment length in the experiment of Figure 4.13 is only 16 μm. A 5 MHz change in the repetition rate can not be explained by any reasonable change in the index of refraction in such a short segment. From Figure 5.10, it can be seen that an increase in gain can lead to an increase in the time delay through the amplifier and thus a decrease in the passive mode-locked repetition rate. When the current to the entire gain segment was changed, the repetition rate was also found to decrease.

6.4.1 Phase noise and timing jitter calculations for the active and hybrid mode-locking cases

Lets view a 1 Hz slice of the carrier density noise spectral density as a sinusoidal noise driving function with value $\delta n(t)$ given by:

$$\delta n(t) = \frac{\sqrt{|N(\omega)|^2\, 6.28 * 1\ \text{Hz}}}{V} \sin \omega_{mod} t \qquad (6.44)$$

where ω_{mod} is the frequency of the noise slice and the "mod" subscript is to emphasize that the noise is a modulation signal at a frequency much lower than the repetition rate of the mode-locked laser.

The case of jitter caused by index of refraction noise will first be considered. The next step is to calculate the gain fluctuations that are associated with the carrier density fluctuations of Equation 6.44.

$$\delta n_{in}(t) = \frac{dn_{in}}{dn}\,\delta n(t) \tag{6.45}$$

From the index of refraction fluctuations, the maximum phase fluctuation can be calculated using:

$$\delta\phi(t) = O_{na}\,\frac{2\pi\, f_{mod}\, L_{gain}}{c}\,\delta n_{in}(t) \tag{6.46}$$

Equations 6.46 shows the phase modulation that is present due to the 1 Hz slice of carrier density noise. Using a small phase deviation approximation (much less than a radian) [79], the single sideband phase modulation sidebands that appear at modulation frequency offsets from the pulse repetition rate have the relative phase noise level given by:

$$L(f) = 20\,\mathrm{Log}_{10}(\delta\phi_{max}/2) \tag{6.47}$$

where $\delta\phi_{max}$ is the maximum phase deviation of the sinusoidal modulation.

The case of phase noise induced by gain changes will now be considered. The basic starting point is the slice of carrier density noise given by Equation 6.44. This corresponding gain fluctuations are calculated by multiplying by the differential gain.

$$\delta g(t) = \Gamma_t\,\frac{dg}{dn}\,\delta n(t) \tag{6.48}$$

The gain fluctuations are converted to phase fluctuations using the formula:

$$\delta\phi(t) = O_{ga} 2\pi\, f_{mod}\,\delta g(t) \tag{6.49}$$

Equation 6.47 can then be used to calculate the phase noise level from Equation 6.49.

6.4.2 Phase noise and timing jitter calculations for the passive mode-locking case

In the case of active and hybrid mode locking, the noise sources cause jitter in the mode-locked laser by inducing a phase modulation on the optical pulses. Active and hybrid mode locking have restoring forces to limit phase excursions. In passive mode-locking, the noise perturbations act more like frequency modulation sources. If the modulation noise frequency is slow compared to the repetition rate of the mode-locked laser, the sinusoidal signal will slowly move the repetition rate up and down at the modulation noise frequency rate. Since phase is the integral of frequency, this frequency modulation can build up considerable phase deviations, and therefore timing jitter. Lets again consider the 1 Hz slice of carrier density noise given by Equation 6.44.

We will first consider the effects of index of refraction noise. Equation 6.45 is first used to calculate the magnitude of the index of refraction fluctuations in a 1 Hz slice of noise. The phase deviation that results from this index of refraction noise is given as:

$$\delta\phi(t) = O_{np}\, 2\pi \frac{f_{rep}^{2}}{\omega_{mod}} \delta n_{in}(t) \qquad (6.50)$$

L(f) is again calculated from 6.47 under the small phase deviation assumption. This assumption of small phase deviation will be quite good for the higher noise modulation frequencies, but it will break down at low frequencies.

The phase noise caused by gain fluctuations will now be considered. Equation 6.48,which describes the gain fluctuations in a 1 Hz noise slice, is the starting point. The phase fluctuations that result from this excitation are given as:

$$\delta\phi(t) = O_{gp}\, \delta g(t)\, 2\pi \frac{f_{rep}^{2}}{\omega_{mod}} \tag{6.51}$$

L(f) can the be calculated using 6.47 for the small phase deviation approximation which may be inaccurate at low modulation frequencies.

6.5 Results of the timing jitter and phase noise calculations

Section 6.2 described the noise spectral densities of the driving noise sources. Section 6.3 described the processes that related carrier density, index of refraction, and photon density noise sources to timing jitter fluctuations. Section 6.4 connects Sections 6.2 and 6.3 by provided the formulas that are used in the timing jitter calculations. Table 6.3 contains the results of the large signal numerical simulations of the sensitivity factors which have been calculated for the configurations shown in Figure 6.1. The data for the simulations are given in Table 6.1 and Table 6.2.

Figure 6.10 shows the calculated and measured L(f) for the two passive mode-locked laser cases shown in Figure 6.1. These simulations include only the contribution of the gain fluctuation noise. The goal of these simulations is to understand the trends in the phase noise plots of Figure 4.28. The magnitude of β_{sp} has been used as an adjustable parameter in Figure 6.10 to bring the

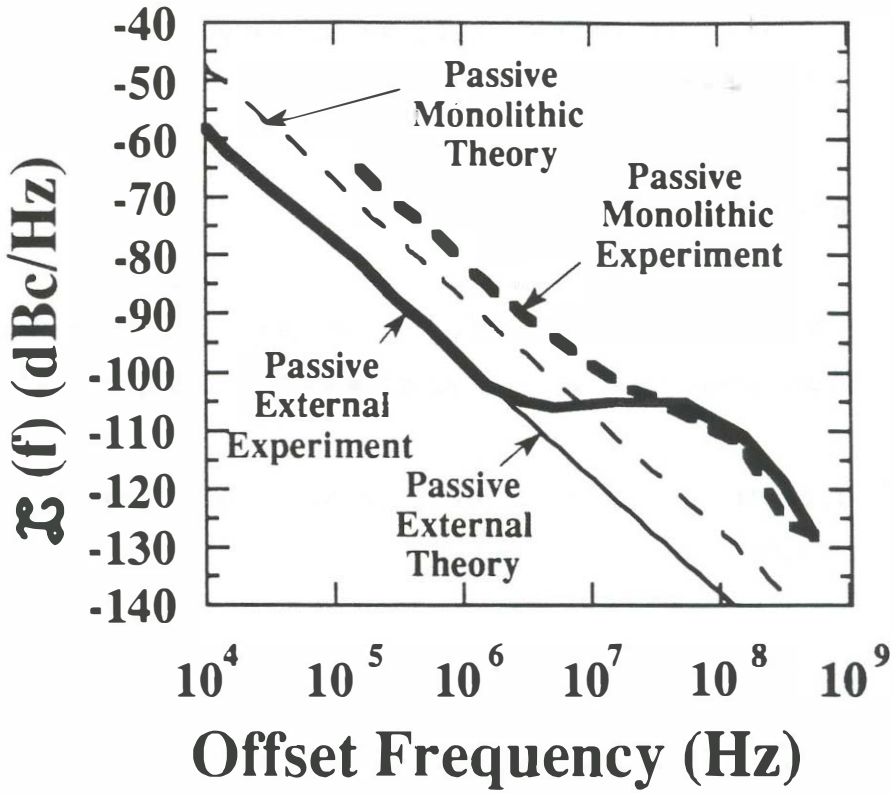

Figure 6.10 Experimental and theoretical phase noise for a two-segment passive mode-locked monolithic and external cavity mode-locked laser. The experimental data is the same as that in Figure 4.28. The theoretical simulations use the data shown in Tables 6.1 and 6.2. The experimental data departs from the 20 dB/octave phase noise slope at about 10 MHz where amplitude noise starts to dominate.

absolute levels of L(f) close to the absolute levels measured in Figure 4.28. The same value of β_{sp} (1×10^{-5}) is used for both theoretical curves in Figure 6.10. The passive mode-locked lasers simulations show a 20 dB/decade roll-off as is measured experimentally. **This means that the noise sources act to frequency modulate the mode-locked laser. The lower in frequency the disturbance is, the larger the phase deviation.** It is seen that there is a large difference in the phase noise level of the monolithic cavity case as compared to the external cavity passive mode-locked laser. The main differences between the two cases are the ratio of the sensitivity factor O_{gp} between the monolithic and external cavity case (2.6 ps cm versus 0.5 ps cm respectively), the fill fraction of the gain region in the cavity, and the required gain level in the laser amplifier. Since the monolithic cavity device has all active waveguide, a small change in gain can result in a large change in the cavity resonance frequency. The calculated difference in L(f) between the monolithic and external cavity passive mode-locking examples is about 13 dB which corresponds closely to the 17 dB difference found in the measurement.

Equation 6.51 for phase noise in passive mode-locked lasers shows that L(f) should go down as the repetition frequency squared for a constant sensitivity factor, O_{gp}. When this fact is combined with the phase noise to timing jitter Equation 4.1, it is found that timing jitter should reduce as the repetition rate is reduced. This trend has been verified experimentally by measuring the phase noise for the same laser diode when operated at two different repetition rates. Figure 6.11 shows the timing jitter for a two-section passive mode-locked laser operating at a repetition rate of 1 GHz and 5 GHz. The device is that described in Table 4.2. At small offset frequencies, both lasers show the characteristic 20 dB/octave phase noise roll-off. At higher offset frequencies, intensity noise dominates. In the purely phase noise offset

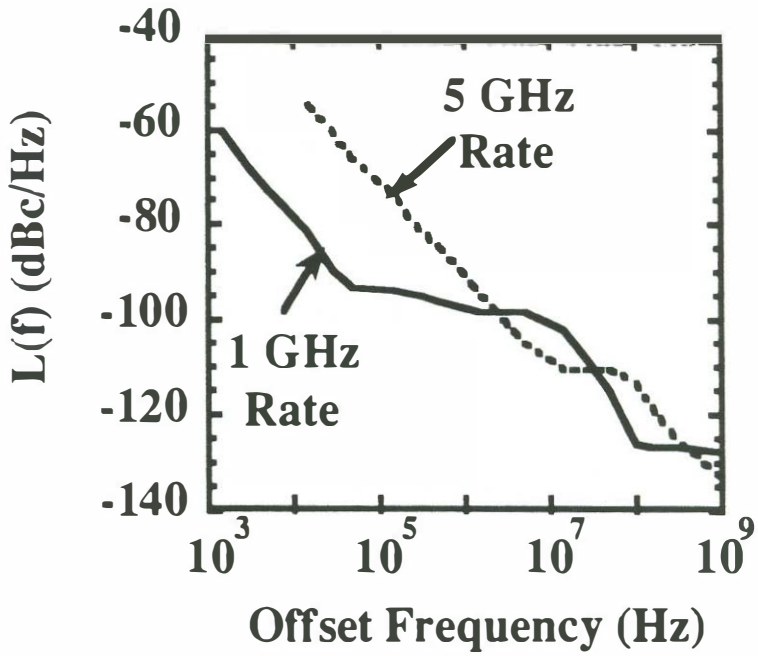

Figure 6.11 The single sideband noise level, L(f), for a two-segment external cavity passive mode-locked laser operating at repetition rates of 1 GHz and 5 GHz. The laser diode is 500 μm long with an 80 μm saturable absorber. The device structure is that of Figure 2.27 and 2.28. The integrated timing jitter is found to be lower as the repetition rate of the mode-locked laser is decreased.

frequency range, L(f) is 29 dB lower in the 1 GHz repetition rate device as compared to the 5 GHz device. This agrees well with the 28 dB difference predicted by equation 6.51. It is reasonable that O_{gp} should remain constant independent of repetition rate for the same device since passive mode-locked lasers work best at a particular pulse energy and therefore unsaturated carrier density level.

Figure 6.12 shows that active and hybrid mode-locked lasers have an L(f) that is relatively flat with frequency as is seen in the residual phase noise measurements of Figure 4.28. This is due to the fact that the modulation noise sources induce a phase modulation onto the mode-locked laser pulses. The peak phase deviation of the phase modulation is limited by the magnitude of the restoring forces in the active gain modulation segment. The phase noise response falls off above the relaxation resonance frequency of the noise response. Active mode-locking shows lower phase noise levels than hybrid mode-locking in these simulations.

A general trend is that the narrower the optical pulse, the larger the resulting timing jitter. There are several reasons for this trend. Narrower width optical pulses have a larger coupling of the spontaneous emission into the lasing mode. This is modeled by the M variable in Equation 6.8. The spontaneous emission coupling is especially high in mode-locked semiconductor lasers because the pulses are chirped with time-bandwidth products typically over 2. Narrow optical pulses are also less efficiently confined by the electrical modulation pulses as compared to wide optical pulses. This partially explains the lower timing jitter found in the active mode-locked lasers. Active mode-locked lasers also have a smaller required gain from the laser amplifier when compared to hybrid mode-locked lasers. The single-section active mode-locked laser of Figure 4.18a showed very small timing jitter since the laser was mode-locking

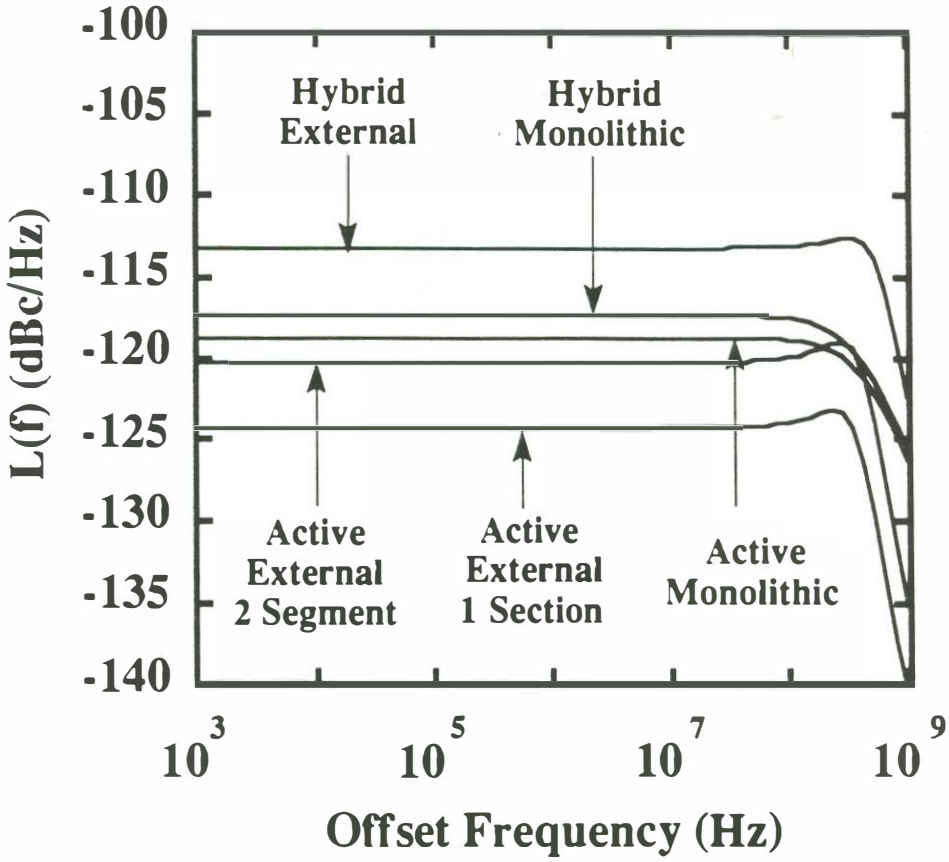

Figure 6.12 Calculated single sideband phase noise in a 1 Hz bandwidth, L(f), for active and hybrid mode-locked monolithic and external cavity mode-locked lasers. The external cavity examples should be compared with the experimental data of Figure 4.26. The monolithic cavity examples should be compared with the experimental data of Figure 4.27 and 4.28. The performance parameters for these types experiments are given in Table 4.2. The data for these simulations is given in Tables 6.1 and 6.2. Only gain to timing jitter processes were considered in this calculation. Hybrid mode-locking with shorter optical pulsewidths gave larger timing jitter than active mode-locked lasers with wider optical pulsewidths.

in a single cluster of modes (see Section 2.1), and the optical pulsewidth was relatively wide (10 ps).

The modelled levels of phase noise for the hybrid and active mode-locking cases show the proper shape but do not show as large of differences as those seen in the active and hybrid mode-locking cases in Figure 4.26-4.28. One possible explanation for the smaller differences in L(f) is that the spontaneous emission lifetime was chosen to be a constant in this analysis but in fact the lifetime decreases with increased carrier density level. The differential gains were also chosen to be identical for all cases but the differential gain is likely to be decreased in the higher carrier density situations.

In summary, the important conclusions from this chapter are:

1) The primary cause of timing jitter is from gain fluctuations (or the associated output energy fluctuations) that couple to pulse position fluctuations due to gain saturation.

2) The 20 dB/octave L(f) slope in passive mode-locked lasers is due to frequency modulation induced by the gain fluctuations.

3) The relatively flat L(f) with frequency found in active and hybrid mode-locked lasers is due to fact that the noise sources are phase modulating the carrier. The maximum phase deviation is limited by the pulse position restoring forces of active gain modulation.

4) Short pulses have a larger timing jitter due to increased spontaneous emission coupling into the lasing mode. Large optical bandwidth chirped pulses are even more efficient in coupling the spontaneous emission into the lasing mode.

Chapter 7
Future directions and conclusions

The effects of self-phase modulation at present represent the biggest obstacle in obtaining high-power, subpicosecond-pulsewidth optical pulses directly from multi-section mode-locked lasers. Researchers have initially used the excess optical bandwidth to compress the optical pulses down to subpicosecond widths. The next step is to provide the correct phase filtering inside the cavity to compensate for self-phase modulation effects and group velocity dispersion of the laser diode. There has been work in this area with the use of a Gires-Tournois interferometer in an external cavity [98]. There is promise in applying this to the multi-segment structures which produce narrower initial pulsewidths. Multi-segment mode-locked semiconductor lasers can also be combined with the more ideal gain medium in erbium-doped fiber amplifiers. The semiconductor can provide fast gain modulation and saturable absorption while the erbium amplifier provides smaller self-phase modulation levels. There are also many other structures that can be constructed that are compatible with the multi-segment configurations. The pump-probe measurements show that saturable absorbers are useful as optically controlled optical switches with less than 10 ps recovery time. This should be a useful effect for the design of all-optical de-multiplexers, optical sampling oscilloscopes, or in optical logic gates. Figure 7.1 shows an example of an all-optical sampler using a multiple-segment structure. The straight segment is a mode-locked semiconductor laser with waveguide saturable absorber. The angled waveguide is the input for the signal to be sampled. Only when the

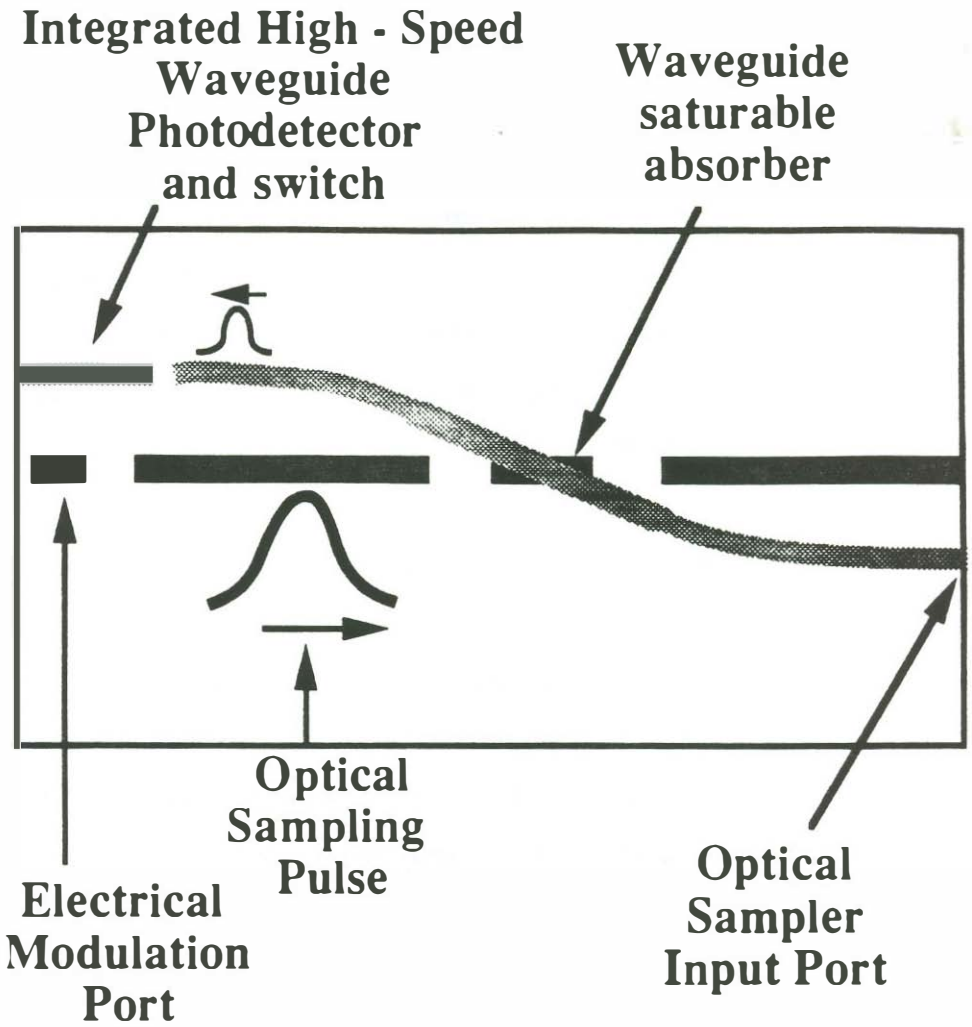

Figure 7.1 A multi-section all-optical sampler. The straight waveguide operates as a mode-locked or gain switched laser. When the optical pulse goes through the saturable absorber, a signal is allowed to pass through the curved waveguide, thereby sampling the signal level. The switch is turned off by the sweep-out of carriers in the saturable absorber segment.

mode-locked laser pulse is crossing the saturable absorber will there be significant transmission in this path.

In summary, the design and experimental characterization of multi-segment short-pulse semiconductor laser structures has been studied. Important points from each of the chapters are given.

Chapter 1 This Dissertation focuses on the characteristics of multi-segment mode-locked semiconductor lasers. The basic idea is to break up the top pumping contact in a laser process to allow for different biases along the length of the laser. With this multi-segment concept, the functions of gain, gain modulation, and saturable absorption can be accomplished on a single semiconductor chip.

Chapter 2 The problem of multiple pulsations, and mode-locking in clusters in single-segment external-cavity lasers has been suppressed with the use of two and three-segment mode-locked laser designs. Waveguide saturable absorbers can recover their absorption fast enough (measured by photodetection and pump-probe techniques) so that secondary pulses generated by the imperfect antireflection coating are absorbed. Hybrid mode-locking of a multi-section external cavity mode-locked laser was accomplished for the first time. Hybrid mode-locking combines the stability of active mode-locking with the pulse shortening ability of passive mode-locking. Pulsewidths in the 1-3 ps range are shown to be possible using passive and hybrid mode-locked external-cavity configurations. Passive and hybrid mode-locking are found to be compatible with both quantum well and bulk active region lasers.

Chapter 3 Monolithic cavity devices with record low (5.5 GHz) repetition rates were tested. These devices were fabricated using an impurity induced disordering process. The devices were mode-locked using active, passive, and

hybrid mode-locking techniques. Hybrid mode-locking provided the best results in terms of short pulsewidth (6.5 ps).

Experiments were done to show that the symmetric colliding pulse configuration (CPM) for passive and hybrid mode locking is nearly equivalent to the self-colliding pulse configuration (SCPM). The self-colliding pulse configuration is actually a more robust device, being immune to asymmetrical cleaving and performing better compared to the symmetric colliding pulse case at larger pulse energies. The SCPM configuration is also half the length and requires half the pumping current compared to the CPM configuration. The CPM device has the advantage of two optical outputs and the lack of a high reflection coating. Pulsewidths as short as 1.3 ps were generated using the colliding-pulse saturable absober devices. Repetition rates as low as 21 GHz and as high as 81 GHz were shown at 1.55 μm.

Chapter 4 Very long (several mm long) monolithic cavity devices with all active waveguides are found to perform more poorly than external cavity devices of the same repetition rate. The evidence shows that as the all-active waveguide portion of the cavity was reduced, the performance increased continually. The difference between the two configurations can be traced back to the fact that air is a better pulse propagation medium than all-active waveguide. The large internal losses associated with active waveguide cause a large amount of gain to be extracted from the amplifying medium. The larger the required gain, the narrower the bandwidth of the device. The group velocity dispersion of the laser also becomes more severe for very long devices. A possible solution to this problem for very long active waveguides is to use monolithic cavity devices with large sections of low-loss passive waveguide.

Self-phase modulation is responsible for the excess bandwidth found in

mode-locked semiconductor lasers. The self-phase modulation effects are caused by the coupling of the index of refraction to carrier density. Gain saturation, absorption saturation, and active gain modulation all contribute to self-phase modulation. It is possible to use this extra bandwidth to get optical pulse compression down to sub-picosecond levels.

Passive mode-locked lasers perform well over a wide range of repetition rates. Passive mode-locking was accomplished from 0.2 to 9 GHz from an external cavity device with nearly equal pulse energy and pulse shape independent of repetition rate. Passive mode-locking below 200 MHz became difficult due to a tendency for the system to operate at a cavity harmonic. It is hard to make an external cavity small enough in size to operate above 20 GHz.

The detuning of the modulation rate from the natural frequency of the cavity was also explored. Monolithic cavity devices with all active waveguides have a larger detuning range than external cavity devices of the same repetition rate. Active mode-locking gives the highest detuning range followed by hybrid mode-locking. A method was developed to tune the repetition rate of a passive mode-locked laser electronically using a repetition rate tuning segment.

The timing instabilities in monolithic and external cavity devices were studied. Mode-locked lasers in general perform better than other short pulse laser systems in terms of timing jitter . Active mode-locking gives the lowest level of timing jitter followed by hybrid and passive mode-locking. Active and hybrid methods can give sub-picosecond r.m.s. timing jitter levels. Passive mode-locking gives considerably higher jitter levels due to the absence of a low-phase noise driving source. Monolithic cavity devices with all active waveguides are found to give higher timing jitter levels than their external cavity counterparts at the same repetition rate. This difference can be traced back to

the non-idealities of pulse-propagation in all-active waveguides.

Self-pulsation effects can be a considerable problem in active, passive, and hybrid mode-locking techniques. Any device which has a reverse-biased segment is particularly susceptible. The design of the saturable absorber length has been found to be very important to eliminate self-pulsations. For passive and hybrid mode-locking, shorter saturable absorbers are less susceptible to self-pulsation effects. In active mode-locking, longer gain modulation segments are less susceptible to self-pulsation effects

Chapter 5 Optimization of passive and hybrid mode-locked laser structures in terms of the free design parameters of the laser was discussed. The optimization of the pulse shortening mechanisms of active and passive gain modulation was discussed. The saturable absorber performance can be maximized by using reverse biased waveguide saturable absorbers with fast absorption recovery. The optimal saturable absorber length that is not susceptible to self-pulsations and that does not require too large of gain from the optical amplifier was shown. The effects of the electrical modulation pulsewidth, pulse amplitude, and modulation segment length were analyzed.

The important pulse widening mechanisms that are largely responsible for achieving pulsewidths in the 1-3 ps range were analyzed and identified. Self-phase modulation induces chirp on the optical pulses on each pass around the laser cavity. The chirp is such that the peak of the pulse receives less gain than the sides of the pulse leading to a more effective widening of the pulse on each pass through the laser amplifier. The combined effects of self-phase modulation and the magnitude and phase response versus frequency of the laser combine to limit the achievable pulsewidth to a value much larger than would be

possible if self-phase modulation were absent.

Chapter 6 The magnitude and origin of timing jitter in multi-segment mode-locked lasers were discussed. The dominant source of timing jitter is a gain noise to pulse position noise conversion process. In mode-locked lasers, the optical amplifier is always operating in the gain saturation condition. The leading edge of the optical pulse receives more amplification than the trailing edge of the pulse. This selective amplification effectively moves the pulse position earlier or later in time depending on the amount of gain saturation. Small fluctuations in the gain of the laser will therefore lead to fluctuations in pulse position.

In active and hybrid mode-locking, the pulse position is phase modulated by the low frequency gain fluctuations in the laser. The active gain modulation tends to limit the maximum pulse position error. The resulting residual L(f) is relatively constant with offset frequency and drops off at the low frequency relaxation resonance frequency.

In passive mode-locking, there is no electrical modulation signal to limit the pulse position error. The noise sources effectively frequency modulate the laser repetition rate leading to a 20 dB/decade drop in L(f) with offset frequency.

Narrow width optical pulses are more susceptible to timing jitter than wide optical pulses. More spontaneous emission is coupled into the lasing mode for narrower width optical pulses. This is especially true for the large time-bandwidth product pulses found in hybrid and passive mode-locked lasers. The narrow width optical pulses are also less well confined by the active gain modulation.

Section 8

References

1. For a history of mode-locking see, H. A. Haus, "Mode-locking of semiconductor laser diodes," Japanese Journal of Applied Physics, **20**, pp. 1007-1020, 1981.

2. R. S. Tucker G. Eisentein, and S. K. Korotky, "Optical time-division multiplexing for very high bit-rate transmission", IEEE J. Lightwave Tech., **6**, pp. 1737-1749, 1988.

3. P. A. Andrekson, N. A. Olsson, J. R. Simpson, D. J. Digiovanni, P. A. Morton, T. Tanbun-Ek, R. A. Logan, and K. W. Wecht, "Ultra high speed demultiplexing with the non-linear optical loop mirror," 1992 Optical Fiber Conference post-deadline paper PD-8, San Jose, CA.,1992.

4 K. J. Blow N. J. Doran, B. K. Nayar, and B. P. Nelson,"Two-wavelength operation of the non-linear fiber loop mirror", Optics Lett. ,**15**, pp. 248-250, 1990.

5. P. A. Andrekson et al.,"16 Gbit/s all-optical demultiplexing using four-wave mixing" Electronics Letts., **27**, pp. 922-924, 1991.

6. H. Kataoka, and M. Ikeda, "Laser diode optical switch module," Electronics Letters, **20**, pp. 438-439, 1984.

7. A. E. Siegman, *Lasers*, Universiy Science Books, Mill Valley, CA. pp. 392-397.

8. J. M. Weisenfeld, " Electrooptic sampling of high speed devices and integrated circuits," IBM Jornal of Research and Development, **34**, pp. 141-161, 1990.

9. R. J. Helkey, D. J. Derickson, A. Mar, J.E. Bowers, and R. L. Thornton,"Colliding pulse effects in mode-locked semiconductor lasers," 1992 Conference on Lasers and Electooptics (CLEO), paper JThB2, 1992.

10. R. A. Becker et al.,"Wide-band electrooptic guided wave analog-digital converters" IEEE Proceedings, **72**, pp. 802-819, 1984.

11. W. R. Christian, M. Rosker, I. McMichael, "Picosecond pulse diode ring laser gyroscope", 1991 Optical Society of America Annual meeting, Paper TuD5, San Jose, CA., 1991.

12. P. A. Morton, J. E. Bowers, L. A. Koszi, M. Soler, J. Lopata, and D. P. Wilt, "Monolithic mode-locked laser arrays in optical computing", Digital and Optical Computing II, SPIE O/E Lase, Los Angeles, CA., 1990.

13. A. Olsson, and C. L. Tang, "Active mode-locking of a linear and ring external cavity semiconductor lasers", IEEE J. Quantum Electron., **QE-17**, pp. 1977-1978, 1981.

14 . J. P. Van Der Ziel, R. A. Logan, and R. M. Mikulyak, "Generation of subpicosecond pulses from an actively mode-locked GaAs laser in an external ring active cavity", Applied Physics Letters, **39**, pp.867-869, 1981.

15 . J. C. Goodman, and B. K. Garside, "Modulation detuning characteristics of actively mode-locked diode lasers", IEEE J. Quantum Electron., **QE-19**, pp. 1068-1073, 1983.

16. J. E. Bowers, P. A. Morton, A. Mar, and S. W. Corzine, "Actively mode-locked semiconductor lasers," IEEE J. Quantum Electron., **QE-25**, pp. 1426-1439, 1989.

17. M. Shell, A. Weber, E. Schol, and D. Bimberg, "Fundamental limits of sub-picosecond pulse generation by active mode-locking of semiconductor lasers: the spectral width and the facet reflectivities," IEEE J. Quantum Electron., **QE-27**, pp. 1661-1668, 1991.

18. H. A. Haus, "Theory of mode-locking with a slow saturable absorber," IEEE J. Quantum Electron., **QE-11**, pp. 736-746, 1975.

19. G. P. Agrawal and N. K. Dutta, Long Wavelength Semiconductor Lasers, New York, Van Nostrand Reinhold, 1986.

20. J. P. Van Der Ziel, W. T. Tsang, R. A. Logan, R. M. Mikulyak, and W. M. Augustyniak, "Subpicosecond pulses from passively mode-locked GaAs buried optical guide semiconductor lasers," Appl. Phys. Lett., **39**, pp. 525-527, 1981.

21. E. L. Portnoi and A. V. Chelnokov, "Characteristics of heterostructure lasers with a saturable absorber fabricated by deep ion implantation," Soviet Tech. Phys. Letts., **15**, pp. 432-433, 1989.

22. P. W. Smith, Y. Silverberg, D. A. B. Miller, "Mode-locking of semiconductor diode lasers using excitonic nonlinearities," J. Opt. Soc. Am. B, **2**, pp. 1228-1235, 1985.

23. C. Harder, J. S. Smith, K. L. Lau, and A. Yariv, "Passive mode-locking of buried heterostructure lasers with non-uniform current injection," Appl. Phys. Lett., vol. **42**, pp. 772-774, 1983.

24. P. A. Morton, J. E. Bowers, L. A. Koszi, M. Soler, J. Lopata, and D. P. Wilt, " Monolithic hybrid mode-locked 1.3 μm semiconductor lasers", Appl. Phys. Lett. ,**56**, pp. 111-113, 1990.

25. K. Y. Lau, "Short pulse and high frequency signal generation in semiconductor lasers", Journal of Lightwave Technology, **7**, pp 400-419, 1989.

26. K. Y. Lau, "Narrow band modulation of semiconductor lasers at millimeter wave frequencies (>100 GHz) by mode-locking", IEEE J. Quantum Electron., **QE-26**, Feb. 1990.

27. S. Sanders, A. Yariv, J. Paslaski, J. E. Ungar, H. A. Zarem, " Passive mode-locking of a 2 section multiple quantum well laser at harmonics of the cavity round trip frequency", Appl. Phys. Letts., **58**, 681-683, 1991.

28. R. S. Tucker, U. Koren, G. Raybon, C. A. Burrus, B. I. Miller, T. L. Koch, and G. Eisenstein, "40 GHz active mode-locking in a monolithic long cavity laser," Electronics Letters, **25**, 621, 1989.

29. S. Sanders, L. Eng, J. Paslaski, and A. Yariv, "108 GHz passive mode-locking of a multiple quantum well laser with an intra-cavity absorber", Appl. Phys. Lett., **56**, pp. 310-312, 1990.

30. Y. K. Chen, M. C. Wu, T. Tanbun-Ek, R. A. Logan, and M. A. Chin,"Subpicosecond monolithic colliding pulse mode-locked multiple quantum well lasers," Appl. Phys. Lett., vol. **58**, pp. 1253-1255, 1991.

31. Hewlett Packard Company , *Microwave and RF designers catalog,* Hewlett Packard Co., Palo Alto, CA., 1992

32. M. J. W. Rodwell, M. Kamegawa, R. Yu, M. Case, E. Carmen, and K. Giboney, "GaAs nonlinear transmission lines for picosecond pulse generation and millimeter wave sampling, " IEEE Transactions on Microwave Theory and Techniques, **39**, p. 1194, 1991.

33. I. W. Marshall, British Telecom Laboratories, private communication.

34. A. J. Lowrey, and I. W. Marshall, "Stabilization of mode-locked laser pulses using travelling wave semiconductor laser amplifiers", Electronics Letters, **26**, pp. 104-105, 1990.

35. A. Mar, D. J. Derickson, R. J. Helkey, and J. E. Bowers, "1.4 ps pulses directly generated using a tandem contact actively mode-locked semiconductor lasers," IEEE Lasers and Electrooptics Society 1991 Annual Meeting, San Jose, CA., paper SDL14.1, 1991.

36. J. Werner, H. Melchior, and G. Guekos, "Stable optical picosecond pulses from actively mode-locked twin-section diode lasers," Electronics Letters, **24**, pp. 140-141, 1988.

37. T. Damen and M. Duguay, "Optoelectronic regenerative pulser," Electronics Letters, **16**, pp 166, 1980.

38. K. Lau and A. Yariv, "Self-sustained picosecond pulse generation in a GaAlAs laser at an electically tunable repetition rate by optoelectronic feedback," Applied Physics Letters, **45**, pp. 124, 1984.

39. Y. G. Wey, D. L. Crawford, K. Giboney, and J. E. Bowers, M. J. Rodwell, P. Silvestre, M. J. Hafich, and G. Y. Robinson, Applied Physics Letters, **58**, pp. 2156-2158, 1991.

40. J. Orr, "A stable 2-26.5 GHz dual gate distributed MMIC amplifier," IEEE International Microwave Symposium, Paper HH-4, pp. 817-820, 1986.

41. J. Bowers, U. Koren, B. I. Miller, C. Soccolich, and W. Y. Jan, "High-speed polyimid based semi-insulating planar buried heterostructures," Electron. Letters, **23**, 1263,1987.

42. D. J. Derickson, C. M. Miller, and R.L. Van Tuyl, "A 100 kHz - 22 GHz instrumentation photoreceiver", IEEE International Microwave Symposium, Paper OO-1, pp. 1063-1066, 1988.

43. R. J. Helkey, P. A. Morton, and J. E. Bowers, "Partial integration method for analysis of mode-locked semiconductor lasers," Optics Letters, vol. **15**, pp. 112-114, 1990.

44. D. J. Derickson, R. J. Helkey, A. Mar, J. E. Bowers, and R. L. Thornton, "Suppression of multiple pulse formation in external cavity mode-locked semiconductor lasers using intra-waveguide saturable absorbers," IEEE Photonics Tech. Lett., **4**, pp. 333-335, 1992.

45. P. W. Smith, Y. Silverberg, and D. A. B. Miller, "Mode-locking of semiconductor dode lasers using excitonic nonlinearities", Journal of the Optical Society of America B, **2**, pp. 1128-1236, 1985.

46. H. A. Haus, "Theory of mode-locking of a laser diode with a multiple quantum well structure," Journal of the Optical Society of America B, **2**, pp. 1237-1243, 1985.

47. S. W. Corzine, R. S. Geels, J. W. Scott, R. H. Ran, and L. A. Coldren, "Design of fabry-perot surface emitting lasers with a periodic gain structure,", IEEE J. Quanum Electron., **QE-25**, pp. 1513-1524, 1989.

48. C. W. Chen, R. Iyer, H. Y. Lee, M. Hafich, G. Y. Robinson, and D. L. Lile, " An insulated gate multiple quantum well optical modulator on InP," Appl. Phys. Lett., **58**, 1991.

49. D. J. Derickson, P. A. Morton, J. E. Bowers and R. L.Thornton, "Comparison of timing jitter in external and monolithic cavity mode-locked semiconductor lasers", Appl. Phys. Lett., **59**, pp. 3372-3374, 1991.

50. R. L. Thornton, W. J. Mosby, T. J. Paoli,"Monolithic waveguide coupled cavity lasers and modulators fabricated by impurity induced disordering," IEEE J. Lightwave Technology, **6**, pp. 786-792, 1988.

51. Y. G. Wey, D. L. Crawform, K. Giboney, J. E. Bowers, M. J. W. Rodwell, P. Silvestre, M. J. Hafich, and G. Y. Robinson, Appl. Phys. Lett., **58**, pp. 2156-2158, 1991.

52. J. R. Karin, D. J. Derickson, R. J. Helkey, J. E. Bowers, and R. L. Thornton "Field-enhanced GaAs/AlGaAs waveguide saturable absorbers," 1992 Ultrafast Phenomena VIII conference, Antibes Juan-les-Pins, France, 1992.

53. G. P. Agrawal, N.A. Olsson," Self phase-modulation and spectral broadening of optical pulses in semiconductor laser amplifiers", IEEE J. Quantum Electron., **QE-25**, pp. 2297-2306, 1989.

54. P. B. Hansen, G. Raybon, M. D. Chien, U. Koren, M. G. Young, J. M. Verdiell, and C. A. Burrus, " A 1.54 μm monolithic semiconductor ring laser: CW and mode-locked operation", IEEE Photonics Technology Letters, **4**, pp. 411-413, 1992.

55. T. L. Koch, and U. Koren, "Semiconductor photonic integrated circuits", IEEE J. Quantum Electron., **27**, pp. 641-563, 1991.

56. P. B. Hansen, G. Raybon, and U. Koren, "5.5 mm long InGaAs monolithic extended cavity laser with an integrated Bragg-reflector for active mode-locking," IEEE Photonics Tech. Lett., **4**, pp. 215-217, 1992.

57. J. Herrmann, F. Weidner, and B. Wilhelmi, "Theory of passive mode-locking of CW dye lasers with contacted and non-contacted absorbers," Appl. Phys. B, **26**, pp. 197-202, 1981.

58. W. Dietel, "Transient absorber gratings shorten the pulses of a passively mode-locked CW dye laser," Optics Communications, **43**, pp. 69-71,1982.

59. M. S. Stix, and E. P. Ippen, "Pulse shaping in passively mode-locked ring dye lasers," IEEE J. Quantum Electronics, **QE-19**, pp. 520-525, 1983.

60. P. J. Delfyett, L. Florez, N. Stoffel, T. Gmitter, N. Andreadakis, and G. Alphonse, "Generation of femtosecond high-power optical pulses from a hybrid mode-locked semiconductor laser," 1991 Optical Society of America Annual Meeting, San Jose, CA, Paper MS3, 1991.

61. T. Okoshi, and K. Kikuchi, *Coherent Optical Fiber Communications*, KTK Scientific Publishers, Kluwer Academic Publishers, Tokyo, 1990.

62. W. B. Jiang, S. R. Friberg, H. Iwamura, Y. Yamamoto, "High powers and subpicosecond pulses from an exteranl cavity surace emitting InGaAs/InP MQW lasers", Appl. Phys. Lett., **58**, pp. 677-679, 1991.

63. W. B. Jiang, R. Mirin, and J. E. Bowers, "Mode-locked GaAs vertical cavity surface emitting lasers", Appl. Phys. Lett., **60**, pp. 677-679, 1992.

64. D. Welch et al., "Properties of broad area grating coupled surface emitting lasers" 1989 Optical Society of America Conference on Lasers and Electroopics.

65. D. Waarts, D. Mehuys, D. Nam, and D. Welch, "High power , CW, diffraction limited GaAlAs laser diode arrays in an external Talbot cavity," Appl. Phys. Lett., **58**, pp. 2586-2588, 1991.

66. D. Botez, and T. Holcomb, " Bloch function analysis of resonant arrays of anti-guided dode lasers", Appl. Phys. Lett., **60**, pp. 539-541, 1992.

67. M. L. Tilton, G. C. Dente, A. H. Paxton, J. Cser, R. K. DFreez, C.E. Moeller, and D. Depatie, "High power nearly diffraction limited output from a semiconductor laser with an unstable resonator", IEEE J. Quantum Electronics, **QE-27**, pp. 2098-2108, 1991.

68. G. Eisenstein, R. S. Tucker, U. Koren, and S. K. Korotky,"Active mode-locking characteristics of InGaAsP single mode fiber composite cavity lasers", IEEE J. Quantum Electron, **QE-22**, pp. 142-148, 1986.

69. K. L .Hall, J. Mark, E. P. Ippen, and G. Eisenstein, "Femtosecond gain dynamics in InGaAs optical amplifiers", Appl. Phys. Lett., **56**, pp. 1740-1742, 1990.

70. P. A. Morton, V. Mizrahi, S. G. Kosinski, L. F. Mollenauer, T. Tanbun-Ek, R. A. Logan, D. L. Coblentz, A. M. Sergent, nad K. W. Wecht, "Hybrid soliton pulse source with fiber Bragg reflector," 1992 Optical Society of America Conference on Laser and Electrooptics post-deadline paper, Paper CPD 25, San Jose, Ca. 1992.

71. D. J. Derickson, R. J. Helkey, A. Mar, J. G. Wasserbauer, and J. E. Bowers, "Microwave and millimeter wave signal generation using mode-locked semiconductor lasers with intrawaveguide saturable absorbers," IEEE International Microwave Theory and Technology Symposium, Albequerque, NM, Paper V-2, pp. 753-756, 1992.

72. D. J. Derickson, R. J. Helkey, A. Mar, and J. E. Bowers, "Muli-segment mode-locked semiconductor laser" IEEE J. Quantum Electron., **QE-28**, October 1992.

73. A. J. Taylor, J. M. Wiesenfeld, J. M. Eisenstein, and R. S. Tucker, " Timing jitter in mode-locked and gain switched InGaAsP injection lasers", Appl. Phys. Letts., **49**, pp 681-683, 1986.

74. R. Yuan, and H. F. Taylor, "Noise characteristics of repetitively pulsed semiconductor lasers", IEEE J. Quantum Electron., **QE-28**, pp. 109-117, 1992.

75. D. R. Hjelme, and A. R. Mickelson, "Theory of timing jitter in actively mode-locked lasers", IEEE J. Quantum Electron., **QE-28**, pp. 1594-1606, 1992.

76. M. J. W. Rodwell, D. M. Bloom, and K. J. Weingarten, "Sub-picosecond laser timing stabilization", IEEE J. Quantum Electron., **QE-25**, pp. 817-828, 1989.

77. D. Van Der Pol, " Characterization of the noise in continuously operating mode-locked lasers,", Appl. Phys. B, **25**, pp 1353-1361, 1989.

78. A. J. Lowry, "New time domain model for active mode-locking based on the transmission line laser model," IEE Proc. J., **136**, pp. 264-270, 1989.

79. W. P. Robbins, *Phase Noise in Signal Sources*, IEE Telecommunications series 9 (Peter Peregrinus LTD, London, 1984), p.53.

80. H. A. Haus, "Parameter ranges for CW passive mode-locking", IEEE J. Quantum Electron., **QE-12**, pp. 169-176, 1976.

81. K. Y. Lau and J. Paslaski, "Condition for short pulse generation in ultrahigh frequency mode-locking of semiconductor lasers," IEEE Photonics Tech. Lett., **3**, pp. 974-976, 1991.

82. P. A. Morton, R. J. Helkey, and J. E. Bowers, "Dynamic Detuning in actively mode-locked semiconductor lasers", IEEE J. Quantum Electron., **QE-25**, 1989.

83. G. P. Agrawal, *Nonlinear Fiber Optics*, San Diego, Academic Press, 1989.

84. K. Valhala, and A. Yariv, "Semi-classical theory of noise in semiconductor lasers-Part I", IEEE J. Quantum Electron., **QE-19**, pp. 1096-1101, 1983.

85. O. E. Martinez, " 3000 times grating compressor with positive group velocity dispersion : application to fiber compensation in the 1.3 μm - 1.6 μm region", IEEE J. Quatum Electron., **QE-23**, pp. 59-64, 1987.

86. M. Kuznetsov, J. M. Wiesenfeld, and L. R. Radzihovsky, "Compression of picosecond pulses from diode lasers using a modified grating-pair compressor", Optics Letters, **15**, pp.180-182, 1990.

87. M. Osinski, and Jens Buus, "Linewidth broadening factor in semiconductor lasers-An overview", IEEE J. Quantum Electon., **QE-23**, pp.9-29, 1987.

88. W. Rideout, B. Yu, J. LaCourse, P. K. York, K. J. Beernink, and J. J. Coleman,"Measurement of the carrier dendence of differential gain, refractive index, and linewidth enhancement factor in strained quantum well lasers", Applied Physics Letters, **56**, pp. 706-708, 1990.

89. G. P. Agrawal, "Effect of gain dispersion on ultrashort pulse propagation in semiconductor laser amplifiers," IEEE J. Quantum Electronics, **QE-27**, pp. 1843-1849, 1991.

90. S. Corzine, R. H. Yan, and L. A. Coldren, "Theoretical gain in strained quantum wells including valence band mixing effects," Appl. Phys. Lett., **57**, pp. 2835-2837, 1990.

91. H. Temkin, T. Tanbun-Ek, and R. A. Logan, " Strained InGaAs/InP quantum wells," Appl. Phys. Lett., **58**, 1991.

92. T. Fukushima, J. E. Bowers, R. Logan, T. Tanbun-Ek, and H. Temkin, " Effect if strain on the resonant frequency and damping factor in InGaAs/InP MQW lasers," Appl. Phys. Lett., **56**, pp. 1210-1212, 1990.

93. I. D. Henning and J. V. Collins, "Measurements of the semiconductor laser linewidth broadening factor," Electronics Lett., **19**, pp 927-929, 1983

94. T. Yamanaka, Y. Yoshikuni, W. Lui, K. Yokoyama, and S. Seki, "Potential chirpless lasers with InGaAs/InGaAsP strained quantum well" 1992 Optical Society of America Integrated Photonics Topical Meeting, Paper MD4-1, New Orleans, LA., 1992.

95. J. E. Bowers, U. Koren, B. I. Miller, C. Soccolich, and W. J. Jan, "High speed planar polyimide based buried heterostructures", Electronics Letters, **24**, p. 1263, 1987.

96. J. G. Wasserbauer, J. E. Bowers, M. J. Hafich, P. Silvestre, L. M. Woods, G. Y. Robinson, " Specific contact resistivity of InGaAs/InP p-isotype heterojuctions," 1992 InP and related materials conference, paper ThP27, Newport, RI., 1992.

97. R. Bruce, D. Clark, and S. Eicher, "Low resistance Pd/Zn/Pd Au ohmic contacts to P-type GaAs", Journal of Electronic Materials, **19**, pp. 225-229, 1990.

98. J. Kuhl, M. Serenyi, and E. O. Gobel, "Bandwidth-limited picosecond pulse generation in an actively mode-locked GaAs laser with intracavity chirp compensation," Optics Letters, **12**, pp. 334-336, 1987.